

**UFRRJ
INSTITUTO DE TECNOLOGIA
PROGRAMA DE PÓS-GRADUAÇÃO EM CIÊNCIA E
TECNOLOGIA DE ALIMENTOS**

TESE

**Obtenção de proteínas e amido de amaranto e sua
aplicação em cocervação complexa para carregamento de
compostos bioativos em produtos alimentícios**

AUGUSTO BENE TOMÉ CONSTANTINO

2022



**UNIVERSIDADE FEDERAL RURAL DO RIO DE JANEIRO
INSTITUTO DE TECNOLOGIA
PROGRAMA DE PÓS-GRADUAÇÃO EM CIÊNCIA E TECNOLOGIA
DE ALIMENTOS**

**OBTENÇÃO DE PROTEÍNAS E AMIDO DE AMARANTO E SUA
APLICAÇÃO EM COACERVAÇÃO COMPLEXA PARA
CARREAMENTO DE COMPOSTOS BIOATIVOS EM PRODUTOS
ALIMENTÍCIOS**

AUGUSTO BENE TOMÉ CONSTANTINO

Sob a Orientação do Professor
Dr. Edwin Elard Garcia Rojas

Tese submetida como requisito parcial
para obtenção do grau de **Doutor em
Ciência e Tecnologia de Alimentos**, no
Programa de Pós-Graduação em
Ciências e Tecnologia de Alimentos.

Seropédica
Julho de 2022

Universidade Federal Rural do Rio de Janeiro
Biblioteca Central / Seção de Processamento Técnico

Ficha catalográfica elaborada
com os dados fornecidos pelo(a) autor(a)

C 923o

Constantino, Augusto Bene Tomé, 1991-
Obtenção de proteínas e amido de Amarantho e sua
aplicação em coacervação complexa para carreamento de
compostos bioativos em produtos alimentícios / Augusto
Bene Tomé Constantino. - Chimoio, 2022.
158 f.: il.

Orientador: Edwin Elard Garcia-Rojas.
Tese (Doutorado). -- Universidade Federal Rural do Rio
de Janeiro, Pós-Graduação em Ciência e Tecnologia de
Alimentos, 2022.

1. coacervação complexa. 2. microencapsulação. 3.
fortificação de alimento. 4. filme comestível. I.
Garcia-Rojas, Edwin Elard, 1972-, orient. II
Universidade Federal Rural do Rio de Janeiro. Pós-
Graduação em Ciência e Tecnologia de Alimentos III.
Título.

**O presente trabalho foi realizado com apoio da Coordenação de Aperfeiçoamento de
Pessoal de Nível Superior - Brasil (CAPES) - Código de Financiamento 001.**



MINISTÉRIO DA EDUCAÇÃO
UNIVERSIDADE FEDERAL RURAL DO RIO DE JANEIRO
PROGRAMA DE PÓS-GRADUAÇÃO EM CIÊNCIA E TECNOLOGIA DE
ALIMENTOS



TERMO Nº 870/2022 - PPGCTA (12.28.01.00.00.00.41)

Nº do Protocolo: 23083.047004/2022-06

Seropédica-RJ, 02 de agosto de 2022.

UNIVERSIDADE FEDERAL RURAL DO RIO DE JANEIRO
INSTITUTO DE TECNOLOGIA
PROGRAMA DE PÓS-GRADUAÇÃO EM CIÊNCIA E TECNOLOGIA DE ALIMENTOS

AUGUSTO BENE TOMÉ CONSTANTINO

Tese submetida como requisito parcial para obtenção do grau de **Doutor em Ciência e Tecnologia de Alimentos**, no Curso de Pós-Graduação em Ciência e Tecnologia de Alimentos, área de Concentração em Ciência de Alimentos.

TESE APROVADA EM 28/07/2022

EDWIN ELARD GARCIA ROJAS (Dr) UFF (orientador)

EDUARDO BASILIO DE OLIVEIRA (Dr) UFV

RENATA CRISTINA FERREIRA BONOMO (Dra) UESB

LOUISE EMY KUROSZAWA (Dra) UNICAMP

LOURDES MARIA CORRÊA CABRAL (Dra) EMBRAPA

Documento não acessível publicamente

(Assinado digitalmente em 02/08/2022 16:39)

LOUISE EMY KUROSZAWA
ASSINANTE EXTERNO
CPF: 223.550.278-46

(Assinado digitalmente em 02/08/2022 09:37)

RENATA CRISTINA FERREIRA BONOMO
ASSINANTE EXTERNO
CPF: 002.289.356-36

(Assinado digitalmente em 02/08/2022 12:49)

EDUARDO BASÍLIO DE OLIVEIRA
ASSINANTE EXTERNO
CPF: 039.398.056-10

(Assinado digitalmente em 02/08/2022 09:40)

EDWIN ELARD GARCIA ROJAS
ASSINANTE EXTERNO
CPF: 014.548.996-54

(Assinado digitalmente em 02/08/2022 13:43)

LOURDES MARIA CORREA CABRAL
ASSINANTE EXTERNO
CPF: 628.646.967-20

Para verificar a autenticidade deste documento entre em <https://sipac.ufrrj.br/public/documentos/index.jsp> informando seu número: **870**, ano: **2022**, tipo: **TERMO**, data de emissão: **02/08/2022** e o código de verificação: **23c5d22698**

DEDICATÓRIA

Dedico esta tese aos meus pais, Constantino
(*in memoriam*) e Verónica.

AGRADECIMENTOS

Agradeço à Deus, pelo dom da vida, pelas oportunidades e por ter me dado saúde, força, vigor e sabedoria para prosseguir a jornada e concluir este trabalho.

À minha querida mãe, Verónica, pelo apoio incondicional e carinho.

Aos meus irmãos, Jilane, Eduarda, Clementino, Constantina, Clautino e Adelaide pelo, pelas orações, incentivo, paciência e amor demonstrados.

Ao meu amigo Lucas, pela inspiração na pesquisa, por me ajudar a chegar no Brasil e pela amizade. Também agradeço à Telma por ter me ajudado na minha instalação no Brasil, por me ajudar a alugar uma kitnet.

Ao meu amigo Sídio por ser companheiro e irmão durante todo momento em que estive no curso. Também agradeço ao meu amigo João de Matos, pela ajuda na resolução dos meus problemas pessoais em Moçambique enquanto eu estava ausente.

Aos meus amigos e colegas Moçambicanos, Adélio, Picardo, Xavier Maia e Tássio, por estarem presentes aqui no Brasil e terem proporcionado apoio e motivação.

Ao meu orientador, professor Edwin, por ser um exemplo de pessoa e de mestre, tendo sido muitas vezes um amigo ao me ensinar não só teorias, mas ensinamentos de vida.

À professora Maria Ivone por ter me ajudado a vir ao Brasil fazer o curso, por ter me recebido calorosamente e me ter ajudado a me inserir no PPGCTA.

Aos meus amigos Peruanos, Ronel e Raúl, por me terem ajudado a fazer as matrículas no PPGCTA, por terem me ajudado a tratar CPF e o registo nacional migratório junto a Polícia Federal.

Aos amigos do LETA-UFF, Ahmad, Monique, Bárbara, Bruno, Clyselen, Ianne, Jéssica e Lívia, que de alguma forma contribuíram para esse trabalho, obrigado pela amizade, carinho e companheirismo.

À UFRRJ em especial ao PPGCTA pela oportunidade e o aprendizado.

Ao Instituto de Bolsa de Moçambique pelo tratamento do visto e seguro de saúde

Ao Grupo Coimbra das Universidades Brasileiras pela facilitação da bolsa de estudos através do projeto Pro-Àfri.

RESUMO GERAL

CONSTANTINO, Augusto Bene Tomé. **Obtenção de proteínas e amido de amaranto e sua aplicação em coacervação complexa para carregamento de compostos bioativos em produtos alimentícios.** 2022. 158p. Tese de Doutorado (Doutor em Ciência e Tecnologia de Alimentos). Instituto de Tecnologia de Alimentos. Universidade Federal Rural do Rio de Janeiro, Seropédica, RJ, 2022.

Atualmente, há um aumento da busca por fontes naturais de polímeros para desenvolvimentos de diferentes produtos alimentícios devido aos seus benefícios à saúde. Dentre vários vegetais, o amaranto (*Amaranthus sp.*) pode ser destacado por conter concentrações relativamente altas de amido (até 69%) e proteínas (até 18%). Os benefícios do amaranto para a saúde são amplos, incluindo redução do colesterol sérico, propriedades antioxidantes e hipoglicêmicos. Amidos e proteínas do amaranto são biopolímeros que podem ter muitas aplicações tecnológicas, desde a produção de filmes e emulsões, até a microencapsulação de ingredientes ativos. O objetivo desta tese foi microencapsular compostos bioativos por coacervação complexa utilizando biopolímeros de amaranto e hidrocolóides. Inicialmente, o isolado proteico do amaranto (API) foi modificado com ultrassom de alta intensidade (HIUS). Os efeitos do HIUS no API foram pronunciados no aumento dos grupos sulfidrílicos, dos grupos hidrofóbicos e redução dos tamanhos de partículas. Essas modificações determinaram as melhoras da solubilidade em água e das propriedades emulsificantes do API. No pH 6.5, cerca de 90% da vitamina D₃ (VD₃) foi microencapsulada em complexos heteroprotéicos do API tratado com ultrassom (API-U) e a lactoferrina (LF). As microcápsulas protegeram a VD₃ da degradação durante o armazenamento e da degradação fotolítica. Também protegeram a VD₃ durante a simulação *in vitro* da digestão gastrointestinal, permitindo uma alta biacessibilidade ($B^* = 47\%$). Além disso, as microcápsulas também protegeram 86% da VD₃ durante a produção de pão, garantindo assim sua eficácia na fortificação deste alimento. Complexos coacervados formados por API-U e carboximetilcelulose sódica (CMC) foram utilizados para encapsular betanina no pH 3. Por betanina ser hidrossolúvel, formou-se uma emulsão dupla do tipo água-em-óleo-em-água. Foram obtidas microcápsulas de betanina com alta eficiência de encapsulação (EE = 87%), boa estabilidade térmica (50°C) e uma alta B^* (85%). As microcápsulas da betanina foram utilizadas na produção de filmes comestíveis de gelatina e aumentaram os valores da elongação até a ruptura, reduziram a transmissão da luz e melhoraram as propriedades antioxidantes. A liberação dos antioxidantes presente nos filmes foi governada pela cinética do Peppas-Sahlim. No final, microcápsulas de betacaroteno (β -C) foram produzidas utilizando complexos coacervados de amido de amaranto carboximetilado (CMS) e LF como material de parede. CMS com grau de substituição de 0.27 apresentou alta afinidade ao interagir eletrostaticamente com LF. Alta EE do β -C (98%) foi obtida no pH 5. As microcápsulas do β -C apresentaram boa estabilidade térmica e fotolítica. A liberação do β -C das microcápsulas foi baixa (19%) e lenta em matriz alimentar aquosa (50% etanol) comparada à matriz oleosa. Aplicação das microcápsulas β -C na fabricação de balas de goma foi viável, possibilitando uma B^* de 22% e redução da sua dureza e mastigação. Portanto, os resultados obtidos do presente trabalho abrem uma nova perspectiva do uso dos biopolímeros de amaranto na microencapsulação de compostos bioativos por coacervação complexa e mostram a possibilidade da aplicação dessas microcápsulas na fortificação de alimentos, como pão e balas de goma, e na produção de embalagens comestíveis biologicamente ativas.

Palavras-chave: coacervação complexa; microencapsulação; fortificação de alimento; filme comestível.

ABSTRACT GERAL

CONSTANTINO, Augusto Bene Tomé. **Obtention of proteins and starch from amaranth and its application in complex coacervation to carry bioactive compounds in food products**. 2022. 158p. Doctoral Thesis (Doctor in Food Science and Technology). Institute of Food Technology. Federal Rural University of Rio de Janeiro, Seropédica, RJ, 2022.

Currently, there is an increase in the search for natural sources of polymers for the development of different food products due to their health benefits. Among several vegetables, amaranth (*Amaranthus sp.*) can be highlighted for containing relatively high concentrations of starch (up to 69%) and proteins (up to 18%). The health benefits of amaranth are broad, including lowering serum cholesterol, and antioxidant and hypoglycemic properties. Amaranth starches and proteins are biopolymers that can have many technological applications, from the production of films and emulsions to the microencapsulation of active ingredients. The objective of this thesis was to microencapsulate bioactive compounds by complex coacervation using amaranth biopolymers and hydrocolloids. Initially, the amaranth protein isolate (API) was modified with high-intensity ultrasound (HIUS). The effects of HIUS on API were pronounced in the increase of sulfhydryl groups, hydrophobic groups, and reduction of particle sizes. These modifications determined improvements in the water solubility and emulsifying properties of the API. At pH 6.5, about 90% of the vitamin D₃ (VD₃) was microencapsulated in heteroprotein complexes of ultrasound-treated API (API-U) and lactoferrin (LF). The microcapsules protected VD₃ from degradation during storage and photolytic degradation. They also protected VD₃ during the *in vitro* simulation of gastrointestinal digestion, allowing high bioaccessibility ($B^* = 47\%$). In addition, the microcapsules also protected 86% of VD₃ during bread production, thus ensuring their effectiveness in fortifying this food. Complex coacervates formed by API-U and sodium carboxymethylcellulose (CMC) were used to encapsulate betanin at pH 3. Because betanin is water-soluble, a water-in-oil-in-water double emulsion was formed. Betanin microcapsules with high encapsulation efficiency ($EE = 87\%$), good thermal stability (50°C), and a high B^* (85%) were obtained. Betanin microcapsules were used to produce edible gelatine films and increased elongation at break values, reduced light transmission, and improved antioxidant properties. The release of antioxidants present in the films was governed by Peppas-Sahlim kinetic. In the end, beta-carotene (β -C) microcapsules were produced using complex coacervates of carboxymethylated amaranth starch (CMS) and LF as wall material. CMS with a degree of substitution of 0.27 showed high affinity when interacting electrostatically with LF. High EE of β -C (98%) was obtained at pH 5. The β -C microcapsules showed good thermal and photolytic stability. The release of β -C from microcapsules was low (19%) and slow in the aqueous food matrix (50% ethanol) compared to the oily matrix. Applying β -C microcapsules to manufacture gummy candies was feasible, allowing a B^* of 22% and reducing its hardness and chewing. Therefore, the results obtained from the present work open a new perspective on the use of amaranth biopolymers in the microencapsulation of bioactive compounds by complex coacervation and show the possibility of applying these microcapsules in the food fortification and the production of Biologically active edible packaging.

Keywords: complex coacervation; microencapsulation; food fortification; edible film.

LISTA DE FIGURAS

Figure 1. Representação esquemática do trabalho realizado no âmbito desta tese.	2
Figure 2. Morfologias das microcápsulas (A, B e C) e das microesferas (D e E).....	11
Figure 3. Valores de complexos formados entre Lisozima e Goma-Xantana na proporção de 1:1 de massa total do sistema com 0.1 mol/L NaCl.	14
Figure 4. Estrutura idealizada de carboximetilcelulose de sódio com um DS=1.....	16
Figure 5. (A) estrutura cristalina 3D da LF e (B) distribuição de carga superficial de LF bovina saturada de ferro (código de banco de dados de proteínas: 1BLF) na mesma orientação. N1, N2, C1 e C2 representam os quatro subdomínios da LF. As cores azul, branco e vermelho correspondem a cargas líquidas positivas, neutras e negativas, respetivamente. ...	17
Figure 6. Estrutura química da Vitamina D3 (A) e vitamina D2 (B).....	18
Figure 7. Estrutura química da betanina, R1 = R2 = H.	19
Figure 1.8. Representação esquemática da micela obtida depois da centrifugação da digesta intestinal de microcápsulas de betacaroteno.....	23
Figure 9. Changes in the physicochemical and techno-functional properties of pseudocereal proteins made by different chemical and physical methods.....	36
Figure 10. SDS-PAGE electrophoretic profiles of native and high-intensity ultrasound treated API. MWM) is the marker; Control) is the native API; A) 30%, 15 min; B) 60%, 15 min; C) 90%, 15 min; D) 30%, 30 min; E) 60%, 30 min; F) 90%, for 30 min.	58
Figure 11. Effect of ultrasound on surface free sulfhydryl groups of API. Control) is the native API; A) 30%, 15 min; B) 60%, 15 min; C) 90%, 15 min; D) 30%, 30 min; E) 60%, 30 min; F) 90%, for 30 min. The results are mean \pm standard deviation of 3 independent replicate experiments. Values followed by the same letter do not differ statistically from each other ($p < 0.05$).	60
Figure 3.12. Effect of ultrasound and pH on (A) the zeta potential and (B) solubility (%) of API. Control is the native API; A) 30%, 15 min; B) 60%, 15 min; C) 90%, 15 min; D) 30%, 30 min; E) 60%, 30 min; F) 90%, for 30 min. The results are mean \pm standard deviation of 3 technical repeats for Fig. A, and 3 independent replicate experiments for Fig. B.	61
Figure 13. The absolute value of Zeta potential (mV) of native and high-intensity ultrasound treated amaranth protein isolate at pH 7. Control) is the native API; A) 30%, 15 min; B) 60%, 15 min; C) 90%, 15 min; D) 30%, 30 min; E) 60%, 30 min; F) 90%, for 30 min. . The results are mean \pm standard deviation of 3 technical repeats. Values followed by the same letter in the columns do not differ statistically from each other ($p < 0.05$).	62
Figure 14. Solubility (%) of native and high-intensity ultrasound treated amaranth protein isolate at pH 7. Control) is the native API; A) 30%, 15 min; B) 60%, 15 min; C) 90%, 15 min; D) 30%, 30 min; E) 60%, 30 min; F) 90%, for 30 min. The results are mean \pm standard deviation of 3 independent replicate experiments. Values followed by the same letter in the columns do not differ statistically from each other ($p < 0.05$).	63
Figure 15. Picture of the bread and process of bread making fortified with VD ₃ microcapsules.	74

Figure 16. Zeta-potentials and Strength of Electrostatic Interaction (SEI) of API-U and Lf. The error bars represent \pm standard deviation, n = 3.	75
Figure 17. (A) Thermogram of heat flux ($\mu\text{cal/s}$) as a function of time (s), obtained during the titration of 0.10 mM of Lf in 0.00025 mM of API-U in MES-NaOH buffer at 10 mM (pH 6.5) at 25 °C. (B) Graphic representation of the integral of the areas of each peak (kcal/mol) as a function of the molar ratio of Lf/API-U ($p < 0.05$). (C) Zeta-potential of different proportions of API-U and Lf at pH = 6.5. The error bars of Fig. C represent \pm standard deviation, n = 3.	76
Figure 18. FTIR spectra of API-U, Lf, Coconut Oil (CO), VD ₃ , and VD ₃ – M.	78
Figure 19. Picture of the optical microscopy Vitamin D ₃ microcapsules (VD ₃ -M) microcapsules, with 10x of magnification.	79
Figure 20. (A) Release profile of encapsulated VD ₃ during in vitro gastrointestinal digestion. (B) Release profile of encapsulated VD ₃ and incorporated in simulated bread during in vitro intestinal digestion. C _t /C ₀ (%) is the percentage division of the concentration at time t (C _t) and at the beginning of the experiment (C ₀). The error bars represent \pm standard deviation, n = 3.	80
Figure 21. The stability of VD ₃ (64.29 $\mu\text{g/g}$ of water) at (A) ambient temperature (25 ± 1 °C), and (B) Ultraviolet radiation at 362 nm. C _t /C ₀ (%) is the percentage division of the concentration at time t (C _t) and at the beginning of the experiment (C ₀). The error bars represent \pm standard deviation, n = 3.	81
Figure 22. Stability of VD ₃ incorporated in bread, heated at 200 °C for 30 min. The error bars represent \pm standard deviation, n = 3. VD ₃ -M is the VD ₃ loaded in microcapsules. Different letters demonstrate statistical difference ($p < 0.05$).	82
Figure 23. Fitting models of VD ₃ release from bread in simulated <i>in vitro</i> of intestinal digestion. The error bars represent \pm standard deviation, n = 3.	82
Figure 24. (A) Zeta-potential and the strength of the electrostatic interaction (SEI) of carboxymethylcellulose (CMC) and ultrasonicated amaranth protein isolate (API-U) at a concentration of 0.1% (w/w). (B) Turbidity of CMC, API-U, and API-U/CMC mixture in a ratio of (1/1, w/w).	97
Figure 25 (A) amaranth protein isolate treated with ultrasound (API-U) and carboxymethylcellulose (CMC) solutions at pH 3. (B) API-U:CMC mixtures in different proportions (from left to right, 1:1, 2:1, 2.6:1, 5:1, 10:1 and 20:1), tested at pH 3 and total fixed concentration at 0.1%. (C) API-U:CMC mixtures ant 2.6: ratio, at different pHs. (D) 0.1% API-U solutions at different pHs. The images were captured 24 h after the phase equilibrium of the solutions (containing API-U and CMC in the mentioned ratios and pHs). (E) ζ -potential of API-U (red line), CMC (blue line) and mixtures of API-U:CMC in proportions 1:1 (purple line) and 2.6:1 (black line).	97
Figure 26. (A) Heat flow thermogram ($\mu\text{cal s}^{-1}$) as a function of time(s), obtained during the titration of 250 μL of 0.123 mmol L^{-1} of ultrasonicated amaranth protein isolate (API-U) in 1200 μL of 0.0154 mmol L^{-1} of carboxymethylcellulose (CMC), at 25 °C. The API-U and CMC concentrations was solubilized in solubilized in 10 mmol L^{-1} citrate buffer (pH 3.0). (B) Graphical representation of the integrated areas of each peak (kcal mol^{-1}) as a function of the molar ratio of API-U/CMC.	98
Figure 27. Phase diagram of encapsulation of betanin in complexes coacervates formed by of ultrasonicated amaranth protein isolate and sodium carboxymethylcellulose.	100

Figure 28. (A) Optical microscopy of emulsions after homogenization of the mixture of ultrasonicated Amaranth Protein Isolate (API-U), carboxymethylcellulose, and emulsion obtained with 10% (w/w) aqueous betanin solution and sachai inchi oil. (B) Microscopy of complex coacervates 24 h after the precipitation. The photographs were taken at the 10x magnification. The scale bars are of 1000µm.	101
Figure 5.29. Fourier Transform Infrared (FTIR) spectra of ultrasonicated Amaranth Protein Isolate (API-U), carboxymethylcellulose (CMC), sachai inchi oil (SIO), betanin, and betaine loaded microcapsules.....	102
Figure 30. (A) Stability of free and encapsulated betanin submitted to heat treatment of 50°C for 1 hour. (B) betanin release profile during the <i>in vitro</i> simulation of gastrointestinal digestion of microcapsules formed by complex coacervates of ultrasonicated amaranth protein isolate (API-U) and carboxymethylcellulose (CMC).....	103
Figure 31. Results of linear regression of the degradation of free and microencapsulated betanin.	103
Figure 32. (A) control gelatin film (GF), gelatin film with 1% of betanin microcapsules (MGF1), gelatin film with 2.5% of betanin microcapsules (MGF2.5), and gelatin film with 5% of betanin microcapsules (MGF5). (B) Images of GF, MGF1, MGF2.5 and MGF5.	105
Figure 33. UV-visible light spectra are transmitted through gelatin film (GF) and gelatin film with 1% microcapsule (MGF1), 2.5% microcapsule (MGF2.5), or 5% microcapsule (MGF5).	106
Figure 34. Mechanical properties of simple gelatin film (GF), gelatin films with 1% microcapsules (MGF1), 2.5% microcapsules (MGF2.5), and 5% microcapsules (MGF5). TS is tensile strength and EAB is elongation at break. The error bars represent the standard deviation of the results of three samples. The uppercase and lowercase letters are the results of the Tukey test and, when they are different, they indicate the statistical difference (p < 0.05).	106
Figure 35 Models of antioxidant activity released from gelatin film with 5% of betanin microcapsules. FRAP TE means ferric reducing antioxidant potential equivalent to Trolox.	107
Figure 36. (A) FTIR spectra of carboxymethyl (CMS) and native amaranth (AMS) starches. (B) Results of the ζ-potential and electrostatic interaction force (SEI) of lactoferrin (LF) and carboxymethyl amaranth starch (CMS).....	123
Figure 37. Zeta potentials of native amaranth starch (red) and carboxymethylated amaranth starch (green).	124
Figure 38. (A) State diagram of complexes formed by lactoferrin (LF) and carboxymethyl amaranth starch (CMS) in different proportions and total concentration of biopolymers (CT) at pH 4.5. (B) Visual representation of CMS/LF complexes formed after 24 h, □ represents cloudy solution with precipitate, ■ represents cloudy solution, ○ represents solution with lower volume precipitate, and ● represents solution with higher volume precipitate and slightly cloudy.	125
Figure 39. (A) Heat flow thermogram (µcal/s) as a function of time (s), obtained during the titration of 0.325 mmol/L of lactoferrin (LF) and 1.625 x 10 ⁻⁴ mmol/L of amaranth carboxymethyl starch (CMS) in citrate buffer (10 mmol/L, pH 4.5) at 25 °C. (B) Graphic representation of the integrated peak areas (kcal/mol) as a function of the molar ratio of LF/CMS (p <0.05).	126

Figure 40. Systems of beta-carotene microencapsulation by complex coacervation of amaranth carboxymethyl starch and lactoferin.....	127
Figure 41 Espectros FT-IR da lactoferrina (LF), amido nativo de amaranto (MAS) amido de carboximetilado (CMS), complexos coacervados CMS/LF (COM), betacaroteno (β -C), óleo de soja (SO) e microcápsulas de betacaroteno (MIC).	128
Figure 42. Imagens microscópicas das microcápsulas de betacaroteno tiradas pelas objetivas de 10x e 40x.....	129
Figure 43. (A) Estabilidade do betacaroteno (β -C) livre e microencapsulada a 50°C por 3 dias. (B) Estabilidade do β -C livre e microencapsulada na radiação ultravioleta por 8 horas. (C) Perfil de liberação do β -C microencapsulado no óleo de soja e em etanol 50%. (D) Perfil de liberação do β -C durante a simulação <i>in vitro</i> da digestão das microcápsulas de B-C.	130
Figure 44 Photographs of gummy candies with and without beta-carotene (β -C) microcapsules.	132

LISTA DE TABELAS

Table 1. Aplicações tecnológicas e tecnológicas de biopolímeros do amaranto.....	9
Table 2. Microencapsulação de ingredientes ativos por coacervação complexa.	13
Table 3. Proteínas e polissacarídeos frequentemente usados como materiais de parede	16
Table 4 Main methods used to modify pseudocereal proteins	39
Table 5.Effect of high-intensity ultrasound treatment on the hydrodynamic diameter of API expressed in volume (%).	59
Table 6. Effect of high-intensity ultrasound treatment on API surface hydrophobicity.	60
Table 7. Effects of high-intensity ultrasound treatment on the emulsifying activity index (EAI) and on the emulsion stability index (ESI) of API.....	64
Table 8. Encapsulation efficiency (EE), loading capacity (LC), and theoretical VD ₃ (OT) of VD ₃ microcapsules in different formulations.	77
Table 9. Particle sizes and polydispersity index (PDI) of Lf, API-U and VD ₃ -M.	79
Table 10. Constants of mathematical models were used to study the release profile of VD ₃ loaded in API-U: Lf matrices incorporated in the wheat bread, in simulated intestinal digestion conditions.....	83
Table 11. Percentage efficiency encapsulation (EE) of betanin at different concentrations in the nucleus of microcapsules (sample D).	94
Table 12. Encapsulation efficiency (EE) of betanin in complex coacervates formed by ultrasonicated amaranth protein (API-U) and carboxymethylcellulose (CMC).....	99
Table 13. Results of the physicochemical analyzes of the films	106
Table 14. Parameters of the mathematical models obtained after fitting the results of the release profile of antioxidants in the gelatin film with 5% microcapsules.....	108
Table 15. Electrolytes (1.25x of Concentrations) of fluids used during the in vitro simulated gastrointestinal digestion according to INFOGEST 2.0 protocol (Brodkorb et al., 2019)....	121
Table 16. Encapsulation efficiency (EE), loading capacity (LC), and initial β -C added (OT) of the microcapsules in different formulations.	127
Table 6.17. Fitting results of beta-carotene release in foods matrices	132
Table 18. Texture analysis of simple (GC) and beta-carotene microcapsules (GCM) candies gummy.....	133

SUMÁRIO

DEDICATÓRIA	iv
AGRADECIMENTOS	v
RESUMO GERAL	vi
ABSTRACT GERAL	vii
LISTA DE FIGURAS	viii
LISTA DE TABELAS	xii
SUMÁRIO	xiii
INTRODUÇÃO GERAL	1
OBJETIVO GERAL	3
OBJETIVOS ESPECÍFICOS	3
CAPÍTULO I. REVISÃO BIBLIOGRÁFICA	4
1 Amaranto.....	5
1.1 Amido do amaranto: propriedades físico-químicas	5
1.2 Proteína do amaranto.....	7
2 Aplicações tecnológicas do amido e da proteína do amaranto	8
3 Microencapsulação de ingrediente bioativos	10
3.1 Métodos de microencapsulação	11
3.2 Processo da coacervação complexa	11
4 Material de parede.....	15
4.1 Carboximetilcelulose.....	15
4.2 Lactoferrina	17
5 Ingredientes ativos	18
5.1 Vitamina D.....	18
5.2 Betanina.....	19
5.3 Carotenoides (β -caroteno).....	20
6 Liberação dos compostos bioativos encapsulados	20
6.1 Modelos matemáticos usados para estudo da cinética de liberação.....	21
6.2 Simulação <i>in vitro</i> da Digestão gastrointestinal e bioacessibilidade	23
7 Referências	24
CAPÍTULO II. PROTEINS FROM PSEUDOCEREAL SEEDS: SOLUBILITY, EXTRACTION, AND MODIFICATIONS OF THE PHYSICO-CHEMICAL AND TECHNO-FUNCTIONAL PROPERTIES	33
Abstract.....	34
1 Introduction	35
2 Solubility and extraction of the native amaranth, buckwheat, and quinoa seed proteins.....	36
3 Modifications of pseudocereal proteins	38
3.1 Heating	38

3.2	High-intensity ultrasound.....	42
3.3	Glycosylation technology.....	43
3.4	Biopolymers blends.....	44
3.5	High hydrostatic pressure.....	45
4	Conclusions and future perspectives.....	45
5	References.....	45
CAPÍTULO III. MODIFICATIONS OF PHYSICOCHEMICAL AND FUNCTIONAL PROPERTIES OF AMARANTH (<i>AMARANTHUS CRUENTUS</i> BRS ALEGRIA) PROTEIN ISOLATE TREATED WITH HIGH-INTENSITY ULTRASOUND.		
	52	
	Abstract.....	53
1	Introduction.....	54
2	Materials and methods.....	55
2.1	Materials.....	55
2.2	Preparation of amaranth protein isolate (API).....	55
2.3	Ultrasonic treatment of amaranth protein isolate (API).....	56
2.4	Physicochemical properties of the amaranth protein.....	56
2.5	Functional properties of the amaranth protein.....	57
2.6	Statistical analysis.....	58
3	Results and discussion.....	58
3.1	Effects of ultrasound on the physicochemical properties of amaranth protein isolate (API).....	58
3.2	Effects of ultrasound on the functional properties of amaranth protein isolates (API).....	62
4	Conclusion.....	64
5	References.....	64
CAPÍTULO IV. VITAMIN D₃ MICROCAPSULES FORMED BY HETEROPROTEIN COMPLEXES OBTAINED FROM AMARANTH PROTEIN ISOLATES AND LACTOFERRIN: FORMATION, CHARACTERIZATION, AND BREAD FORTIFICATION		
	67	
	Abstract.....	68
1	Introduction.....	69
2	Methodology.....	70
2.1	Materials.....	70
2.2	Obtention and modification of amaranth proteins.....	70
2.3	Formation of heteroprotein complex wall material.....	71
2.4	Encapsulation of vitamin D ₃	72
2.5	Incorporation of VD ₃ microcapsules in wheat bread.....	74
2.6	Statistical analysis.....	75
3	Results and discussion.....	75
3.1	Formation of API-U: Lf heteroprotein complexes: the wall material.....	75
3.2	Effects of pH on the formation of API-U: Lf heteroprotein complexes.....	75
3.3	Encapsulation efficiency of vitamin D ₃ in API-U: Lf complexes.....	77

3.4	Characterization of vitamin D ₃ microcapsules.....	78
3.5	Vitamin D ₃ microcapsules incorporated in bread	81
4	Conclusion.....	83
5	References	83

CAPÍTULO V. MICROENCAPSULATION OF BETANIN BY COMPLEX COACERVATION OF CARBOXYMETHYLCELLULOSE AND AMARANTH PROTEIN ISOLATE FOR APPLICATION IN EDIBLE GELATIN FILMS 88

Abstract.....		89
1	Introduction	90
2	Materials and methods	91
2.1	Materials.....	91
2.2	Study of wall material	91
2.3	Microencapsulation of betanin.....	92
2.4	Application of betanin microcapsules in production of gelatin the edible film ...	94
2.5	Statistical analysis	96
3	Results and discussion.....	96
3.1	Formation of ultrasonicated amaranth protein isolate / carboxymethylcellulose complex coacervates	96
3.2	Betanin microcapsules	99
3.3	Edible films prepared with gelatin and betanin microcapsules.....	104
4	Conclusion.....	108
5	References	108

CAPÍTULO VI. MICROENCAPSULATION OF BETA-CAROTENE BY COMPLEX COACERVATION USING AMARANTH CARBOXYMETHYL STARCH AND LACTOFERRIN FOR APPLICATION IN GUMMY CANDIES 114

Abstract.....		115
1	Introduction	116
2	Materials and methods	117
2.1	Materials.....	117
2.2	Isolation and carboxymethylation of amaranth starch	117
2.3	Study of the formation of complex coacervates of carboxymethyl amaranth starch and lactoferrin	118
2.4	Beta-carotene microencapsulation	119
2.5	Application of beta-carotene microcapsules in gummy candies formulation....	121
2.6	Statistical analysis	122
3	Results e Discussion.....	123
3.1	Synthesis of amaranth carboxymethyl starch.....	123
3.2	Formation of amaranth carboxymethyl starch and lactoferrin complex coacervates.	124
3.3	Isothermal titration calorimetry of lactoferrin in amaranth carboxymethyl starch.... ..	125
3.4	Beta-carotene microcapsules obtained by complex coacervates of amaranth carboxymethyl starch and lactoferrin.....	126

3.5	Gummy candies containing beta-carotene microcapsules	132
4	Conclusion.....	133
5	References	134
	CONCLUSÃO GERAL	138
	ANEXOS	139
	ANEXO A. Pedido de depósito de patente de filmes comestíveis composto por microcápsulas de betanina e gelatina	140
	ANEXO B. Pedido de depósito de patente de bala de goma de gelatina fortificada com microcápsulas de betacaroteno.....	141

INTRODUÇÃO GERAL

A atual tendência “verde” da indústria alimentar, motivada por aumento de consumidores de produtos naturais e com benefícios à saúde em detrimento dos sintéticos, tem motivado diversos pesquisadores a buscarem novas fontes de biopolímeros. Neste sentido, estudos de propriedades biológicas, físico-químicas e potencial aplicação em alimentos de biopolímeros obtidos de vegetais vêm aumentando nos últimos anos (QAMAR et al., 2020). É neste contexto que o amaranto é destacado devido ao seu alto teor de amido e proteínas, além de possuir características agrônômicas atraentes, como rápido crescimento, requerer pouca água e crescer em diferentes altitudes (FLETCHER, 2016). Os grãos de amaranto possuem cerca de 69% de amido, que é principalmente composto por amilopectina. Os grânulos do amido de amaranto são pequenos (0,8 a 2,5 μm de diâmetro), exibindo um padrão de raios-X do tipo A e baixos níveis de amilose. Apresentam-se ainda como sendo esféricos e poligonais, com isso podem apresentar propriedades funcionais únicas, como alta digestibilidade enzimática, baixa retrogradação e boa estabilidade térmica (BAKER; RAYAS-DUARTE, 1998; BELLO-PÉREZ et al., 2018; BET et al., 2018; CHANDLA; SAXENA; SINGH, 2017; XIA et al., 2015). No entanto, sua solubilidade em água e seu poder de intumescimento são limitados o que dificulta seu uso em algumas aplicações tecnológicas (FONSECA-FLORIDO et al., 2016; KONG et al., 2010; ZHU, 2017). Alternativamente, a carboximetilação introduz cargas negativas na estrutura do amido e pode melhorar sua solubilidade em água, suas propriedades gelificantes e, inclusive, pode proporcionar algumas atividades biológicas (antioxidantes, imunomoduladoras, antitumor, antibacteriana, entre outras) (XIE et al., 2021; ZHU, 2017).

Dependendo da espécie e local de cultivo, os grãos do amaranto podem conter até 18% de proteínas, que são compostas por cerca de 65% de albuminas, 17% de globulinas, 11% prolaminas e 7% de glutenina. A fração albumínica é rica em valina e lisina; já a fração globulínica é composta maioritariamente por valina, leucina, prolamina, treonina, fenilalanina, leucina, glutenina, histidina e pouca lisina (BARBA DE LA ROSA et al., 1992; BREENE, 1991; COELHO et al., 2018; MARCONE, 1999). Além desse valor nutricional, a proteína isolada do amaranto possui atividades biológicas, por exemplo os hidrolisados do isolado proteico de amaranto mostraram ter ação antitrombótica, através da inibição da fibrina (SABBIONE et al., 2016). Uma simulação da digestão gastrointestinal do isolado proteico do amaranto demonstrou o poder da eliminação dos radicais livres (MONTROYA-RODRÍGUEZ et al., 2014; ORSINI DELGADO et al., 2016; ORSINI DELGADO; TIRONI; AÑÓN, 2011). MONTROYA-RODRIGUEZ et al (2014) observaram atividades anti-inflamatórias dos peptídeos do amaranto, que abrangeu a inibição da enzima conversora da angiotensina e redução do fator alfa de necrose tumoral. Além desses efeitos, a proteína do amaranto pode reduzir os níveis de colesterol no sangue (MENDONÇA; ARÊAS, 2006).

Sob ponto de vista tecnológico, amidos e proteínas são polímeros que têm várias aplicações na indústria, incluindo a microencapsulação de compostos bioativos (SCHMITT; TURGEON, 2011; XIONG et al., 2017). A tecnologia da microencapsulação é utilizada para proteger os compostos bioativos de fatores que o degradam, incluindo a ação da luz, do calor, do pH, do oxigênio e da umidade. Desta forma a vida útil desses compostos é prolongada, além de favorecer sua adição segura no processamento de certos alimentos. Uma outra aplicação da microencapsulação é mascarar o sabor ou o cheiro de compostos bioativos com propriedades organolépticas não aceitáveis por consumidores. Por fim, a microencapsulação também pode ser usada para permitir a liberação controlada dos compostos bioativos, por exemplo, a proteção de compostos sensíveis à ação do suco gástrico para sua entrega nos

intestinos (COMUNIAN et al., 2013; MCCLEMENTS, 2015; YAN; ZHANG, 2014). Dentre várias técnicas empregadas para microencapsular compostos bioativos, podemos destacar o processo da coacervação complexa porque apresenta uma alta eficiência de encapsulação, alta integridade do material de parede e não usa condições drásticas como solventes orgânicos ou temperaturas altas (TIMILSENA et al., 2019; YAN; ZHANG, 2014). A encapsulação por coacervação complexa, como processo, compreende três fases: a formação de emulsões, a coacervação e a formação da parede e/ou endurecimento. Geralmente, a emulsão é formada pela mistura de óleo (contendo o composto bioativo) e proteína, usando um homogeneizador a alta velocidade (como ultraturrax), seguido da adição de um polissacarídeo. Depois disso, segue-se a complexação dos biopolímeros na solução homogeneizada, que pode ser iniciada pelo ajuste do pH para o ponto onde as cargas de ambos são opostas ao máximo, permitindo assim a atração electrostática dos mesmos. Em seguida, ocorre a formação de duas fases: precipitado e sobrenadante, onde o sobrenadante é descartado e o precipitado passa pelo processo de reticulação e posterior secagem (MCCLEMENTS, 2015; YAN; ZHANG, 2014).

Na presente tese, a proteína e o amido do amaranto foram modificados para seu uso, junto com outros biopolímeros, na microencapsulação de compostos bioativos por coacervação complexa (Figura 1). Os capítulos que compõem o presente trabalho são artigos publicados e submetidos em revistas científicas. Os assuntos abordados em cada capítulo são apresentados a seguir:

CAPÍTULO I compreende os fundamentos teóricos dos biopolímeros do amaranto, do processo da microencapsulação por coacervação complexa e da liberação de compostos microencapsulados. O CAPÍTULO II trata de uma revisão bibliográfica que abrange as modificações físico-químicas das proteínas dos principais pseudocereais (amaranto, quinoa e trigo sarraceno). Este capítulo descreve a composição e métodos de extração mais utilizados destas proteínas. No CAPÍTULO III descreve o efeito do tratamento ultrassônico de alta intensidade nas propriedades físico-químicas e tecno-funcionais das proteínas do amaranto.

O CAPÍTULO IV aborda o desenvolvimento de microcápsulas da vitamina D₃, utilizando complexos formados por proteína do amaranto modificada com ultrassom de alta intensidade e lactoferrina. No final, as microcápsulas foram adicionadas no pão. CAPÍTULO V trata da microencapsulação da betanina utilizando proteína do amaranto modificada por ultrassom de alta intensidade e carboximetilcelulose sódica, com a finalidade da sua aplicação na fabricação de filmes comestíveis de gelatina. Finalmente, no CAPÍTULO VI o amido de amaranto foi carboximetilado. Este amido modificado foi utilizado com a lactoferrina para microencapsular betacaroteno para fortificação de balas de goma.

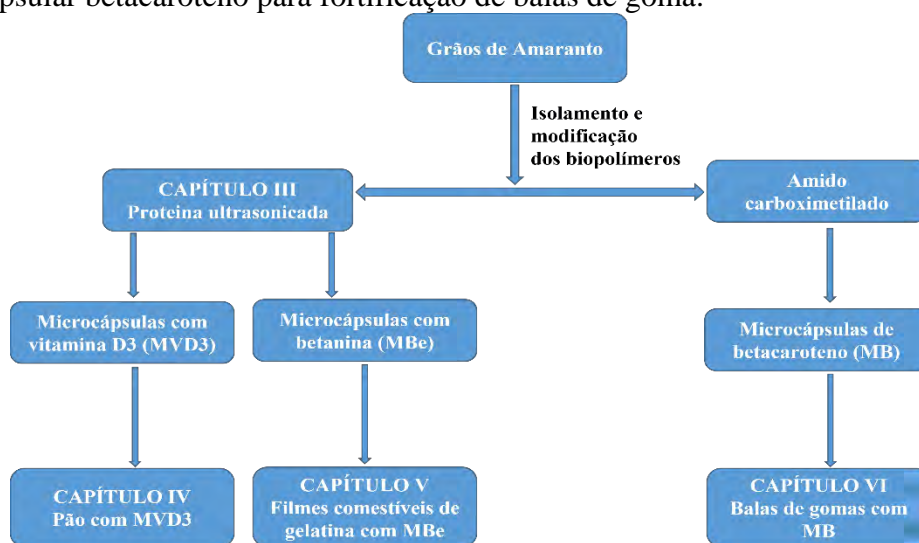


Figure 1. Representação esquemática do trabalho realizado no âmbito desta tese.

OBJETIVO GERAL

Microencapsular compostos bioativos pelo processo da coacervação complexa de biopolímeros isolados dos grãos de amaranto e hidrocolóides.

OBJETIVOS ESPECÍFICOS

- Descrever a solubilidade, extração e modificação das propriedades físico-químicas e tecnofuncionais de concentrados e isolados de proteínas de sementes de pseudocereais;
- Estudar os efeitos do tratamento ultrassônico de alta intensidade nas propriedades físico-químicas da proteína isolada do amaranto;
- Microencapsular a vitamina D₃ em complexos heteroproteico formado por isolado proteico de amaranto tratado com ultrassom de alta intensidade e lactoferrina para fortificação dos produtos de panificação;
- Microencapsular betanina por coacervação complexa do isolado proteico de amaranto tratado com ultrassom de alta intensidade e carboximetilcelulose sódica para aplicação em filmes comestível de gelatina;
- Microencapsular betacaroteno por coacervação complexa do amido carboximetilado de amaranto e lactoferrina para fortificação de balas de goma;

CAPÍTULO I. REVISÃO BIBLIOGRÁFICA

1 Amarantho

Amaranto é um pseudocereal que produz grãos amiláceos adequados para alimentação humana (FLETCHER, 2016). Diferentemente dos cereais verdadeiros que são monocotiledôneas, os pseudocereais são dicotiledôneas com grãos menores (JANSSEN et al., 2017). Sob ponto de vista agrônomo, este pseudocereal tem rápido crescimento, que pode ocorrer em qualquer altitude e em regiões com pouco nitrogênio (FLETCHER, 2016; LÓPEZ et al., 2018). O potencial do grão de amaranto como alimento foi reconhecido desde a antiguidade: os astecas e incas o usavam comumente até a era da colonização espanhola que, por razões ainda desconhecidas, foi substituída por outras culturas, como milho e feijão. Há alguns anos, este pseudocereal foi “redescoberto” como uma planta útil e promissora, principalmente pelo fato de poder ser uma alternativa para aliviar a crescente necessidade de alimentos nalguns países do em via de desenvolvimento (PAREDES-LOPEZ; LEHMANN, 1994).

Amaranto pertencente a família *Amaranthaceae*, constituída por cerca de 60 espécies (ALCARAZ; XAVIER, 2014; AMAYA-FARFAN; MARCÍLIO; SPEHAR, 2015; COELHO et al., 2018; YAMANI, 2015), onde as mais estudadas são *Amaranthus caudatus*, *A. cruentus* e *A. Hypochondriacus*; que podem facilmente ser confundidas com *A. hybridus*, *A. retroflexus*, *A. viridis* e *A. spinosus* que são espécies daninhas (SPEHAR, 2003). No Brasil, a Empresa Brasileira de Pesquisa Agropecuária (EMBRAPA) desenvolveu uma cultivar do *A. cruentus*, conhecida como *A. cruentus* BRS alegria, adaptada ao clima brasileiro e com semelhanças ao amaranto produzido no Peru e México (AMAYA-FARFAN; MARCÍLIO; SPEHAR, 2015; DANIELLY LEITE; SPEHAR; LUIZ AUGUSTO COPATI, 2003). O *A. Cruentus* BRS alegria apresenta uma estatura média de 180 cm, sendo que 48 cm pertencem a inflorescência. A planta demora secar após a sua maturação e esta acontece no período de seca, o que permite uma secagem adequada para a colheita dos grãos. Apresenta folhas grandes, alongadas; com caule ereto e coloração rósea. O fruto é pixídio, deiscente, que se prende aos ramos da panícula; a semente possui um diâmetro pequeno (entre 0,9 e 1,7 mm), é arredondada e de coloração bege (DANIELLY LEITE; SPEHAR; LUIZ AUGUSTO COPATI, 2003; YAMANI, 2015).

No geral, o amaranto possui alto teor de amido e proteína de alta qualidade. Dependendo do local de cultivo, o teor de proteína pode chegar a ser de 18%, enquanto do amido pode chegar a 69% (CHANDLA; SAXENA; SINGH, 2017; COELHO et al., 2018; GUERREIRO; MENEGALLI, 2007). Além desses polímeros, ele também possui lípidos, fibras, cinzas e minerais em quantidades mais altas do que alguns cereais comuns (ALCARAZ; XAVIER, 2014; MENDONÇA; ARÊAS, 2006). Neste sentido, em continuação passamos a descrever os biopolímeros dessa cultura.

1.1 Amido do amaranto: propriedades físico-químicas

Amido é um polissacarídeo composto principalmente pela amilopectina e pela amilose. A amilose é um polímero linear composta maioritariamente por glicoses (α -D-glicopiranosil) unidas por ligações (1 \rightarrow 4) e um pequeno número de ramos conectados por ligações α -D-(1 \rightarrow 6). O peso molecular da amilose varia de 10^5 a 10^6 Da. A amilopectina apresenta-se como sendo um polímero de alto peso molecular (10^7 a 10^9 Da) e bastante ramificada, principalmente por ligações α -D-(1 \rightarrow 6). O teor de amilose do amido é altamente dependente da origem botânica e pode variar de menos de 1% a 80%. Amidos com teor de amilose abaixo de 10% são denominados amidos cerosos (LIU et al., 2015). Conhecer os valores proporcionais da amilose e amilopectina de um amido é importante porque ela vai impactar nas propriedades físico-químicas do amido. Por exemplo, a quantidade de amilose,

bem como o entrelaçamento entre amilose/amilose e amilose/amilopectina afetam grandemente a capacidade de ligação à água, propriedades térmicas e suscetibilidade enzimática (BELITZ; GROSCH; SCHIEBERLE, 2009; ZHU, 2017; ZHU; XIE, 2018). No caso do amido de amaranto, o conteúdo da amilose pode variar de 0 a 14% e, portanto, sendo considerado em muitos casos amido ceroso. O peso molecular das amilopectinas de amaranto pode variar de aproximadamente 1 a 70×10^7 Da (MARFIL et al., 2018).

No geral, os grânulos do amido de amaranto são pequenos (0.8 a 2.5 μm de diâmetro), exibindo um padrão de raios-X do tipo A. Apresentam-se ainda como sendo esféricos e poligonais, com isso podem apresentar propriedades funcionais únicas, como alta digestibilidade enzimática, baixa retrogradação e boa estabilidade térmica (BAKER; RAYAS-DUARTE, 1998; BELLO-PÉREZ et al., 2018; BET et al., 2018; CHANDLA; SAXENA; SINGH, 2017; XIA et al., 2015).

Solubilidade. O amido pode inchar quando é aquecido com uma quantidade excessiva de água. As propriedades de retenção de água do amido são geralmente expressas como poder de expansão (SP) e índice solubilidade em água (WSI). O SP e o WSI tendem a aumentar com um aumento correspondente na temperatura. As altas temperaturas tendem a romper a estrutura cristalina do amido, o que promove a ligação de hidrogênio entre as moléculas de água e a amilose/amilopectina (ZHU; XIE, 2018). No geral, os amidos apresentam pobres SP e WSI a temperatura ambiente, os valores tendem a melhorar quando a temperatura atinge 50°C. Por exemplo, o *A. cruentus* pode apresentar um SP de 2 a 4 g/g a 50°C, podendo aumentar até cerca de 27 g/g a 80°C (PEREZ; BAHNASSEY; BREENE, 1993). Enquanto o WSI pode alcançar a 95% a temperatura de 80°C (ZHU, 2017). A análise de correlação de amidos de amaranto de três espécies mostrou que SP e WSI tiveram pouca correlação com a estrutura molecular da amilopectina (KONG et al., 2008). Além disso, parece que o tamanho granular está positivamente relacionado com o SP de amidos de diferentes fontes botânicas (ZHU, 2017).

Gelatinização e retrogradação. A gelatinização do amido pode ser definida como o inchamento e perda da estrutura cristalina dos seus grânulos. Isso pode ocorrer quando os grânulos de amido dispersos em água são aquecidos a uma temperatura específica (ZHU, 2017; ZHU; XIE, 2018). Por outro lado, retrogradação do amido é um fenômeno em que a estrutura do amido gelatinizado é parcialmente reordenada e recristalinizada durante um período de armazenamento. A relação amilose/amilopectina é um dos fatores mais importantes para a retrogradação do amido, pois a amilose retrograda muito mais rápido que a amilopectina (SINGH et al., 2003). A perda de estrutura cristalina dentro do grânulo de amido pode resultar em muitas mudanças em suas propriedades funcionais, incluindo inchamento, colagem e birrefringência do amido. Enquanto a retrogradação do amido pode afetar a viscosidade, digestibilidade e dureza (SINGH et al., 2003; ZHU; XIE, 2018). Estudos demonstraram que os amidos do amaranto apresentam temperatura de gelatinização acima de 60°C (CHANDLA; SAXENA; SINGH, 2017; VILLARREAL; ITURRIAGA, 2016). Os géis do amido de amaranto mostraram ter melhor resistência à retrogradação a temperaturas de armazenamento de -20, 4 e -25 °C (BAKER; RAYAS-DUARTE, 1998).

Reologia. Comparado com amidos de cereais normais, leguminosas, tubérculos e raízes, os amidos de amaranto tendem a ter menor viscosidade, menor decomposição e recuo com uma pasta mais estável em geral, e pode ser em grande parte devido ao seu pequeno tamanho granular e ao seu menor teor de amilose (ZHU, 2017). (KONG et al., 2010) reportaram que valores altos dos módulos de armazenamento e de perda foram relacionados a um maior teor de amilose com gel mais sólido. A formação de gel também é afetada pelo baixo teor da amilose nos amidos de amaranto e, por isso, esses amidos tendem a ter géis fracos e mais macios com maior adesividade, comparado com a maioria dos amidos de cereais e raízes e tubérculos (ZHU, 2017).

1.1.1 Amido modificado

A modificação do amido tem a finalidade de melhorar as suas propriedades físico-químicas, de tal modo que se estenda sua aplicação a nível industrial. Tais alterações ocorrem ao nível molecular, com pouca ou nenhuma mudança na aparência superficial do grânulo (ALCÁZAR-ALAY; MEIRELES, 2015; FENNEMA; DAMODARAN; PARKIN, 2010). A modificação do amido pode ocorrer na forma química ou física. A modificação física do amido pode aumentar a sua solubilidade em água e reduzir o tamanho dos seus grânulos. Os métodos físicos incluem combinações de temperatura, umidade, pressão, pH, cisalhamento e irradiação (ALCÁZAR-ALAY; MEIRELES, 2015); já os métodos químicos conhecidos são oxidação, reticulação, acetilação, hidroxipropilação e carboximetilação. Dentre eles destaca-se a carboximetilação pelo fato de ser relativamente barato, simples e de fácil reprodutividade industrial (GUERREIRO; MENEGALLI, 2007; SANGSEETHONG; KETSILP; SRIROTH, 2005; STOJANOVIĆ et al., 2005).

O amido carboximetilado (CMS), ou amido aniônico, é geralmente produzido pela reação de amido com ácido monocloroacético (SMCA). A reação se dá na presença de álcali (como hidróxido de sódio) para aumentar a nucleofilicidade do grupo hidroxila e para auxiliar o inchamento dos grânulos de amido. Contudo, é necessário otimizar a concentração do álcali porque, durante o processo, duas reações competitivas ocorrem. A primeira envolve a reação da hidroxila de amido com SMCA na presença de hidróxido de sódio para formar CMS, como mostrado na Equação 1. A segunda reação é a de hidróxido de sódio com SMCA para formar glicolato de sódio como na Equação 2 (BHATTACHARYYA; SINGHAL; KULKARNI, 1995b):



A carboximetilação pode ser feita em diferentes meios, incluindo água, álcool isopropílico, álcool etílico, álcool metílico, cicloexano e acetona. Mas, muitos trabalhos usam preferencialmente álcool isopropílico porque tem proporcionado um alto grau de substituição e, dependendo do tipo de amido, pode ser necessária a adição de certo teor de água para ajudar o inchamento do amido. Alguns autores sugerem uma proporção de água: álcool isopropílico de 20:80 (v/v). Portanto, é importante determinar o teor de umidade do amido antes de começar a reação (BHATTACHARYYA; SINGHAL; KULKARNI, 1995a; SANGSEETHONG et al., 2015).

O número médio de grupos carboximetil ligados por unidade de anidroglicose, ou seja, o grau de substituição (DS), afeta acentuadamente as propriedades físico-químicas do carboximetilamido, como a digestibilidade *in vitro*, a clareza da pasta e a viscosidade da pasta. Com isto, o DS foi estabelecido como um critério importante para o carboximetilamido e verificado rotineiramente na produção de amido modificado (LIU et al., 2012).

1.2 Proteína do amaranto

Proteína é definida como um peptídeo de aminoácidos, ligados entre si. A estrutura química de uma proteína pode variar de um simples peptídeo até uma forma complexa (estrutura quaternária ou oligomérica). A estrutura oligomérica resulta de interações específicas proteína-proteína, que podem ser interações não covalentes tais como ligação de hidrogênio, interações hidrofóbicas e eletrostáticas. As proteínas de muitos cereais são consideradas oligomérica apresentando pelo menos 30% de aminoácidos hidrofóbicos (BELITZ; GROSCH; SCHIEBERLE, 2009; FENNEMA; DAMODARAN; PARKIN, 2010).

A proteína isolada do amaranto é composta por cerca de 65% de albuminas, 17% de globulinas, 11% prolaminas e 7% de glutenina. A fração albumínica é rica em valina e lisina; já a fração globulínica é composta maioritariamente por valina, leucina, prolamina, treonina, fenilalanina, leucina, glutenina, histidina e pouca lisina (BARBA DE LA ROSA et al., 1992; BREENE, 1991; COELHO et al., 2018; MARCONE, 1999). Além desse valor nutricional, a proteína isolada do amaranto possui atividades biológicas, por exemplo os hidrolisados do isolado proteico de amaranto mostraram ter ação antitrombótica, através da inibição da fibrina (SABBIONE et al., 2016). Uma simulação da digestão gastrointestinal do isolado proteico do amaranto demonstrou o poder da eliminação dos radicais livres (MONTROYA-RODRÍGUEZ et al., 2014; ORSINI DELGADO et al., 2016; ORSINI DELGADO; TIRONI; AÑÓN, 2011). MONTROYA-RODRIGUEZ et al (2014) observaram atividades anti-inflamatórias dos peptídeos do amaranto, que abrangeu a inibição da enzima conversora da angiotensina e redução do fator alfa de necrose tumoral. Além desses efeitos, a proteína do amaranto pode reduzir os níveis de colesterol no sangue (MENDONÇA; ARÊAS, 2006).

No que consiste às propriedades tecno-funcionais, o isolado proteico do amaranto (IPA) demonstra ter algumas peculiaridades. O IPA tem uma solubilidade que aumenta com o pH, atingindo altas de solubilidades em pH entre 9 e 11 (MARTÍNEZ; AÑÓN, 1996; MENDONÇA; ARÊAS, 2006; SHEVKANI; SINGH, 2015) e o seu Ponto Isoelétrico pode variar de 4,5 a 5,7 (MARTÍNEZ; AÑÓN, 1996; MENDONÇA; ARÊAS, 2006). VENTUREIRA et al (2010) observaram que a espuma e a estabilidade de emulsões produzidas por proteínas do Amaranto têm uma alta *performance* no pH ácido (pH = 2), apesar das referidas emulsões terem pouca estabilidade.

2 Aplicações tecnológicas do amido e da proteína do amaranto

As propriedades tecno-funcionais particulares dos biopolímeros do amaranto têm vindo a ser estudadas para sua inserção na indústria alimentar, de modo que novos materiais e/ou produtos alimentares são sugeridos. Neste sentido, a partir do amido e da proteína do amaranto já foram desenvolvidos emulsões, filmes e microcápsulas (Tabela 1).

Filmes. O desenvolvimento de filmes é uma outra aplicação dos polissacarídeos e proteínas. Os filmes têm sido desenvolvidos para revestir ou cobrir alimentos (frescos ou processados), com o objetivo principal de estender a vida de prateleira. Com esse intuito, o amido e proteína do amaranto mostraram ter potencial para cobertura, proteção e aumento da vida útil de alimentos (CHANDLA; SAXENA; SINGH, 2017; CONDÉS; AÑÓN; MAURI, 2013). De acordo com CHANDLA et al (2017) os amidos de amaranto mostraram ser adequados para a formação de filmes comestíveis, com propriedades ótimas viscosidade-espessura, resistência à tração, solubilidade e permeabilidade ao vapor de água. Por outro lado, CONDÉS et al (2013) observaram que os filmes de isolados proteicos do amaranto mostraram ter baixa permeabilidade ao vapor de água, mas propriedades mecânicas pobres. De acordo com os mesmos autores, esta propriedade pode ser melhorada pelo tratamento térmico dos isolados, porém, apesar de conferir uma maior resistência à tração e menor solubilidade em água, também conferiram maior espessura e permeabilidade ao vapor de água.

Table 1. Aplicações tecnológicas e tecnológicas de biopolímeros do amaranto.

Biopolímero	Aplicação Tecnológica	Resultados	Referências
Proteína	Formação de filmes	A adição de nanocristais de amido de milho melhorou as propriedades mecânicas e de barreira dos filmes de proteína de amaranto.	(CONDÉS et al., 2015)
Proteína	Espumabilidade	Proteína do amaranto forma espumas estáveis em pH ácido.	(BOLONTRADE; SCILINGO; AÑÓN, 2016)
Proteína	Formação de filmes comestíveis por tratamento térmico	Obteve-se filmes comestíveis com interessantes propriedades de barreira ao vapor de água, ao utilizar proteínas parcialmente ou completamente desnaturadas	(CONDÉS; AÑÓN; MAURI, 2013)
Proteína	Capacidade emulsificante	Os isolados de proteína de amaranto são capazes de formar e estabilizar emulsões em pH ácido (2,0), porém sensíveis a formação de creme e à floculação.	(VENTUREIRA; MARTÍNEZ; AÑÓN, 2010)
Proteína	Capacidade emulsificante em soluções óleo em água	A estabilidade das emulsões aumenta com a concentração de proteína e com a diminuição do pH	(SUAREZ; AÑÓN, 2018)
Proteína	Formação de emulsões como sistemas de liberação controlada.	As emulsões mostraram ter estabilidade inferior a 8 dias, ser resistente ao suco gástrico e atividade inibitória da enzima conversora da angiotensina I.	(SUÁREZ; AÑÓN, 2019)
Amido	Modificação do amido como meio substituir o uso de gorduras	Os métodos de modificação do amido do amaranto afetaram os grupos funcionais, o que poderia levar a variações no desempenho quando usado como ingrediente alimentar. O amido oxidado foi identificado como o mais adequado como substituto de gordura.	(FASUAN; GBADAMOSI; AKANBI, 2018)
Amido	Formação de emulsões sólidas do amido modificado e não modificado	Os dois tipos de amidos foram adsorvidos na interface óleo-água formando uma barreira que atrasava a separação de fases. As emulsões preparadas usando 20 e 30% de peso produziram emulsões estáveis.	(LEAL-CASTAÑEDA et al., 2018)
Amido	Viscosidade do amido modificado por Carboximetilação	O amido modificado por Carboximetilação do amaranto mostrou melhor viscosidade em relação ao amido modificado do milho.	(BHATTACHARYYA; SINGHAL; KULKARNI, 1995a)
Amido	Formação de filmes comestíveis	Os filmes produzidos poderiam ajudar na eliminação de embalagens primárias excessivas e adicionar mais qualidade a alimentos integrais de uma maneira e outra.	(CHANDLA; SAXENA; SINGH, 2017)
Amido	Microencapsulação de beta – caroteno usando amido do amaranto como matrizes	O β -caroteno encapsulado em matrizes contendo o amido do amaranto mostrou uma estabilidade térmica.	(ROA et al., 2017)
Amido	Microencapsulação por extrusão termoplástica de próbiótico usando amido modificado de amaranto	O amido de amaranto modificado não ofereceu proteção completa aos probióticos durante o armazenamento aos 35 dias, o que foi explicado pelo aumento da atividade de água nas microcápsulas.	(CORTÉS et al., 2014)
Amido	Retrogradação do amido de amaranto	O amido de amaranto apresentou taxas de retrogradação de, aproximadamente, 2 a 9 vezes mais lentas que os amidos do milho, do trigo e do arroz a 4 e -20 °C.	(BAKER; RAYAS-DUARTE, 1998)
Amido	Emulsificação	O amido de amaranto lauroilado melhorou a capacidade emulsificante em comparação com o amido de amaranto nativo porque produziu menores tamanhos de gotas da emulsão, cremosidade mais lenta e uma melhor estabilização da emulsão de Pickering em comparação com emulsões preparadas com amido nativo.	(LEAL-CASTAÑEDA et al., 2018)
Amido	Extrusão para formação de emulsões	O amido de amaranto modificado apresentou um bom equilíbrio hidrofóbico-hidrofílico e valores de Tg para estabilização de emulsões. As emulsões tiveram tamanho e forma das partículas controláveis.	(GARCÍA-ARMENTA et al., 2021)
Amido	Modificação usando ácido octenil succínico (OSA) para formação de emulsão	O tratamento com OSA aumentou a capacidade de emulsificação, e o efeito é atribuído ao aumento das forças repulsivas refletidas pelo potencial zeta.	(SÁNCHEZ DE LA CONCHA et al., 2020)

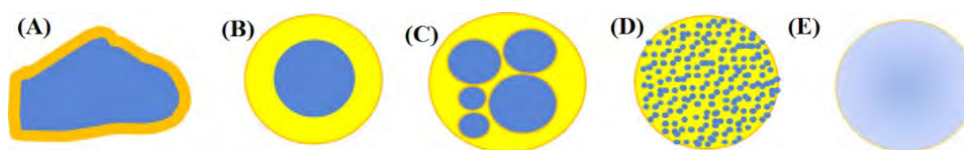
Emulsões. Emulsão pode ser definida como uma mistura de dois líquidos imiscíveis (óleo e água, por exemplo) em que um deles está disperso no outro em forma de pequenas gotículas. Geralmente essa mistura é efetuada à custa de um agente emulsificante, como proteínas, amidos modificados e certas gomas (BASTOS; DE CARVALHO; GARCIA-ROJAS, 2018; DONG et al., 2015; MCCLEMENTS, 2015). Muitas proteínas são macromoléculas anfifílicas com grupos polares e não polares em suas superfícies. Para ser um bom agente emulsificante, uma proteína deve ter um equilíbrio adequado de grupos polares e não polares em sua superfície, de modo a produzir boa solubilidade em água e boa interação com fase lipofílica. Se a superfície de uma proteína for muito apolar, ela não se dissolverá em água, mas se for muito polar, não terá atividade lipofílica. Normalmente, os emulsificantes à base de proteínas têm estruturas globular flexível ou em bobina, o que afeta as propriedades das interfaces formadas após a adsorção às superfícies das gotículas. Além disso, as propriedades elétricas das proteínas desempenham um papel importante na determinação da estabilidade física e química das emulsões (ver a seção 1.3.1). Normalmente, as cargas das proteínas movem-se de positivo, abaixo do ponto isoelétrico (onde a carga é zero), para negativo em pH alto (FENNEMA; DAMODARAN; PARKIN, 2010; MCCLEMENTS, 2015). No caso específico da proteína isolada do amarantho, a capacidade de formar tanto espuma quanto emulsão acontece com maior intensidade em pH baixo (2.0), talvez devido a desnaturação da proteína. Suas emulsões não são muito estáveis podendo se desfazer em até 8 dias, depois do seu preparo (BOLONTRADE; SCILINGO; AÑÓN, 2016; SUÁREZ; AÑÓN, 2019; VENTUREIRA; MARTÍNEZ; AÑÓN, 2010). Os amidos modificados de amarantho também apresentaram boas propriedades emulsificantes, principalmente o amido laurilado (LEAL-CASTAÑEDA et al., 2018), modificação utilizando ácido octenil succínico (SÁNCHEZ DE LA CONCHA et al., 2020) e amido extrusado (GARCÍA-ARMENTA et al., 2021).

Encapsulação. Os biopolímeros do amarantho mostraram ter potencial para encapsular ingredientes ativos. Apesar de não ter sucesso comprovado, o amido do amarantho mostra ter uma boa capacidade de formação de material de parede (CORTÉS et al., 2014; ROA et al., 2017). Por outro lado, a proteína do amarantho mostra ser resistente ao suco gástrico o que possibilita a sua aplicação como material de parede para liberação de ingredientes ativos nos intestinos (SUÁREZ; AÑÓN, 2019).

3 Microencapsulação de ingrediente bioativos

A microencapsulação pode ser definida como envolvimento dos ingredientes bioativos (núcleo) em um material polimérico (parede) com a finalidade de protegê-lo de fatores que o degradam, tais como luz, umidade, temperatura, oxigênio e agentes externos. Desta forma, microencapsulação permite uma vida útil prolongada do ingrediente (BALASSA; FANGER; WURZBURG, 1971; MCCLEMENTS, 2015; YAN; ZHANG, 2014). Além disso, o revestimento externo usado para microencapsular pode mascarar algumas propriedades organolépticas, como sabor, odor e, às vezes, a cor (YE; GEORGES; SELOMULYA, 2018). Geralmente, as cápsulas são classificadas de acordo com o seu tamanho, como sendo macrocápsulas (> 5,000 μm), microcápsulas (0,2 a 5000 μm) e nanocápsulas (< 0,2 μm). A sua morfologia é influenciada pela técnica usada, ingrediente a encapsular, bem como o material polimérico (ou material de parede) usado durante o processo de encapsulação. As cápsulas podem assumir duas morfologias: microcápsula e microesferas. Como se pode observar na Fig. 2., nas microcápsulas o núcleo é visto nitidamente concentrado na região central, circundado por um filme definido e contínuo do material de parede; enquanto nas microesferas o núcleo é uniformemente disperso em uma matriz. Apesar disso, o termo ‘encapsulação’ tem sido utilizado, em seu sentido amplo, englobando tanto a formação de

microcápsulas quanto de microesferas. As microcápsulas podem possuir ainda mais de um núcleo ou várias paredes para um mesmo núcleo (MARFIL et al., 2018; MATALANIS; MCCLEMENTS, 2013; YAN; ZHANG, 2014).



Fonte: (YAN; ZHANG, 2014)

Figure 2. Morfologias das microcápsulas (A, B e C) e das microesferas (D e E).

3.1 Métodos de microencapsulação

Os métodos de encapsulação podem ser químicos, físicos e físico-químicos. Os métodos físico-mecânicos são caracterizados pelo uso de temperatura e pressão para impulsionar a formação do material de parede que reveste o núcleo. Enquanto os químicos são definidos pela reatividade do material de parede externo que envolve o núcleo encapsulado (JINGYUAN WEN; GUANYU CHEN; ALANY, 2014; MCCLEMENTS, 2015). São métodos físico-mecânicos: *spray drying*, extrusão, emulsificação e inclusão em nanopartículas lipossomais. Os métodos físico-químicos são: a coacervação complexa e coacervação simples (JINGYUAN WEN; GUANYU CHEN; ALANY, 2014; LEE; WONG, 2014; MCCLEMENTS, 2015). Dentre esses métodos, o processo da coacervação complexa pode ser destacado, pois apresenta vantagem de não necessitar de altas temperaturas e solventes orgânicos (COMUNIAN et al., 2013), garante a integridade do material de parede, alta eficiência de encapsulação e permite a liberação de ingredientes ativos encapsulados (LEE; WONG, 2014; MCCLEMENTS, 2015).

3.2 Processo da coacervação complexa

O processo de encapsulação por coacervação complexa consiste em três etapas fundamentais, nomeadamente a emulsificação, a coacervação e a reticulação (*cross-linking*).

3.2.1 Formação de emulsões.

O preparo das emulsões pode ser efetuado seguindo um dos seguintes procedimentos: (i) triturar uma mistura de emulsificante e óleo com adição de água que formará a emulsão primária. Em seguida, a água é adicionada para diluir, com ajuda de uma mistura contínua até formar emulsão. (ii) Também pode ser produzida triturando inicialmente o óleo com água e um agente emulsificante. Em seguida, mais água deve ser adicionada misturando a solução até formar uma emulsão. Alternativamente (o mais usual), (iv) o óleo, a água e o emulsificante são misturados juntos e agitados em uma máquina formadora de emulsão (KALE; DEORE, 2016). Para se conseguir uma emulsão homogênea, um dos diferentes métodos pode ser utilizado, incluindo os que utilizam alta energia (como a ultrasonicação, misturadores de alto cisalhamento, homogeneizadores de alta pressão, moinhos coloidais, homogeneizadores ultrassônicos e homogeneizadores de membrana) e os que utilizam baixa energia (como métodos de inversão de fase e método de deslocamento de solvente) (MCCLEMENTS, 2015).

De acordo com a teoria da tensão superficial, os emulsificantes ou estabilizadores diminuem a tensão interfacial entre dois líquidos imiscíveis, reduz a força repelente entre eles e diminui a atração entre as moléculas do mesmo líquido. Também é possível que o agente emulsificante se oriente em torno de uma gota de líquido de uma maneira que reflete sua

solubilidade naquele líquido em particular. Uma outra possibilidade é que o agente emulsificante pode se encontrar localizado na fronteira entre a água e o óleo, formando um fino filme ao ser adsorvido na superfície das gotículas da fase interna. O filme evita o contato e posterior coalescência da fase dispersa; um filme mais resistente e maleável resultará em maior estabilidade física da emulsão (KALE; DEORE, 2016; MCCLEMENTS, 2015). O agente emulsificante também pode agir por meio de forças repulsivas, ou seja, o agente emulsificante forma um filme contendo glóbulos em uma das fases imiscíveis com capacidade de se repelirem. Assim, os glóbulos imiscíveis permanecem suspensos no meio de dispersão devido a essas forças repulsivas. Por fim, o agente emulsificante pode aumentar a viscosidade do meio e, assim, é formada uma suspensão viscosa miscível de glóbulos (KALE; DEORE, 2016).

As emulsões são termodinamicamente instáveis e, portanto, tendem a se decompor ao longo do tempo devido a vários mecanismos físico-químicos, incluindo separação gravitacional, floculação, coalescência, amadurecimento de Ostwald e separação de fases (MCCLEMENTS, 2015). Não abordaremos estes temas nesta tese, uma vez que as emulsões formadas para encapsulação por coacervação complexa são apenas uma etapa do processo e são utilizadas assim que são formadas. Na encapsulação por coacervação complexa, durante a emulsificação, o material do núcleo é adicionado a uma solução contendo um dos materiais de parede (geralmente uma proteína), sob agitação, com o intuito de se obter um tamanho desejado de gotícula de emulsão. Depois desse processo segue-se a coacervação complexa (YAN; ZHANG, 2014).

A Table 2 apresenta os principais biopolímeros, agentes reticulantes e o tipo de emulsão utilizados para encapsular ingredientes ativos por coacervação complexa. As emulsões alimentares do tipo óleo-em-água (O/A) - o que favorece a encapsulação de ingredientes ativos com características oleosas - são as mais utilizadas, provavelmente por serem mais simples de se produzirem ou porque a maioria dos compostos ativos de interesse nutracêutico, alimentar ou farmacêutico sejam de natureza lipofílica (JULIAN MCCLEMENTS; MAHDI JAFARI, 2017). Entretanto, em casos da existência de compostos ativos de natureza hidrofílica, a preferência óbvia do uso das emulsões múltiplas do tipo água-em-óleo-em-água (A/O/A) são preferíveis. Neste caso, a preparação de uma emulsão primária (do tipo água em óleo ou A/O) é necessária e depois, essa emulsão, é dispersa na fase aquosa. As emulsões A/O/A podem permitir a coencapsulação de dois compostos ativos: um hidrofílico e o outro lipofílico (KAIMAINEN et al., 2015; MCCLEMENTS, 2015; PAGANO et al., 2018). Em ambos os casos, a fase externa é aquosa onde necessariamente se encontram os biopolímeros ou material de parede utilizado para encapsular.

3.2.1 Coacervação

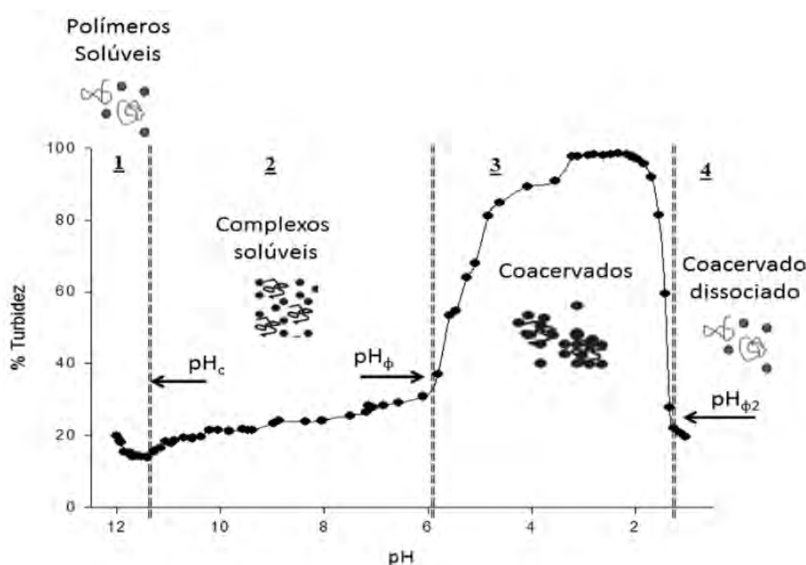
A coacervação é definida como sendo uma separação de sistemas coloidal em duas fases líquidas, em que uma delas está isenta de polímeros. Existem dois tipos de coacervação: a simples e a complexa. Na coacervação simples o sistema contém apenas um polímero e a separação de fases acontece por meio da ação de um agente externo, como sal ou pH. Por outro lado, na coacervação complexa o sistema contém pelo menos dois polímeros que interagem (de forma electroestática) entre si de tal modo que promove a separação de fases (BASTOS; DE CARVALHO; GARCIA-ROJAS, 2018; LEE; WONG, 2014; MCCLEMENTS, 2015; YAN; ZHANG, 2014).

Table 2. Microencapsulação de ingredientes ativos por coacervação complexa.

Polissacarídeo	Proteína	Ingrediente ativo (natureza)	Emulsão	Reticulante	Referência
Anidrido de octenilosuccínico Amido Dekudzu	Gelatina	Astaxantina (hidrossolúvel)	O/A	N/A	(ZHAO et al., 2019)
Amido modificado	Proteína de ervilha	Ácido docosahexaenóico (lipossolúvel)	O/A	N/A	(YILDIZ et al., 2018)
Goma arábica	Gelatina	Óleo de palma (lipossolúvel)	O/A	N/A	(MARFIL et al., 2018)
Carboximetilcelulose sódico	Gelatina	Ácido linoleico (lipossolúvel)			(DUHORANIMANA et al., 2018)
Goma arábica	Gelatina	Antocianinas de fambroesa preta (hidrossolúvel)	A/O/A	N/A	(SHADDEL et al., 2018)
Quitosana; Goma xantana e Pectina	N/A	Óleo de palma (lipossolúvel)	O/A	N/A	(RUTZ et al., 2017)
Goma de cajú	Gelatina	Astaxantina de resíduos de camarão (lipossolúvel)	O/A	N/A	(GOMEZ-ESTACA et al., 2016)
Goma isolada da chia	Pproteína isolada das sementes da chia	Óleo das sementes da chia (lipossolúvel)	O/A	Transglutami nase	(TIMILSENA et al., 2016)
Goma de linhaça	Proteína de linhaça	Óleo de linhaça (lipossolúvel)	O/A	Glutaraldeído	(KAUSHIK et al., 2016)
Goma tragacanta	Caseína	β -caroteno (lipossolúvel)	O/A	Genipina	(JAIN et al., 2016)
Goma acácia	Isolado proteico de soro de leite	β -caroteno (lipossolúvel)	O/A	Glutaraldeido	(JAIN et al., 2015)
Goma arábica	Proteína de soja	Óleo de linhaça (lipossolúvel)	O/A	N/A	(DONG et al., 2015)
Carboximetilce-lulose	Caseinato de sódio	β -pineno (lipossolúvel)	O/A	N/A	(KROUPANTZIS; PAVLIDOU; PARASKEVOPOULOU, 2014)
Quitosana e k-caragenina	N/A	Óleo essencial de pimenta (lipossolúvel)	O/A	Glutaraldeido	(DIMA et al., 2014)
Goma arábica	Gelatina	Óleo essencial de sementes de mostarda (lipossolúvel)	O/A	Genipina	(PENG et al., 2014)
Goma arábica	Gelatina	Ácido ascórbico (hidrossolúvel)	A/O/A	N/A	(COMUNIAN et al., 2013)
Pectina	Gelatina	Licopeno (lipossolúvel)	O/A	N/A	(SILVA et al., 2012)
Goma acácia	Gelatina	β -caroteno (lipossolúvel)	O/A	N/A	(NAKAGAWA; NAGAO, 2012)

Onde N/A significa não aplicável, O/A significa emulsão do tipo óleo em água, A/AO significa emulsão água-em-óleo-em-água.

A maioria dos complexos coacervados de utilidade na indústria alimentar são formados por proteína e polissacarídeo, já que esses materiais constituem parte integral de muitos alimentos, bem como a proteína pode agir como agente emulsificante (não necessitando de um emulsificante externo) e por proporcionarem boas características de encapsulamento devido às sinergias estruturais dos dois polímeros (SCHMITT; TURGEON, 2011; XIONG et al., 2017). Em geral, os complexos coacervados formam-se dentro de uma estreita faixa de pH, entre o pKa do polissacarídeo e o ponto isoelétrico da proteína. Uma das formas simples de explicar a ocorrência da formação do complexo coacervado é através da observação da turbidez (Figura 3): no princípio (pH 12) os biopolímeros encontram-se com cargas opostas e repelem-se. No entanto, quando se inicia a titulação (ajuste do pH), ocorre primeiramente a formação de complexos solúveis no pH crítico (pH_c) e observa-se aqui um ligeiro aumento na turbidez. Em seguida, a associação dos biopolímeros passa a ser mais forte em decorrência do aumento de densidade de cargas opostas, verificada com o rápido aumento da turbidez no pH_ϕ . Se a titulação continuar, a turbidez tenderá a um ponto máximo (pH_{max}) quando a equivalência elétrica for alcançada entre os biopolímeros. Imediatamente após ser atingido o pH_{max} os complexos insolúveis começam a dissociar-se devido à protonação de grupos aniônicos ou desprotonação de grupos catiônicos, atingindo completa dissociação ($pH_{\phi 2}$) quando os biopolímeros apresentarem a mesma carga (BASTOS; DE CARVALHO; GARCIA-ROJAS, 2018; MCCLEMENTS, 2015; SANTOS; DE CARVALHO; GARCIA-ROJAS, 2018; SOUZA, 2015).



Fonte: (SOUZA, 2015)

Figure 3. Valores de complexos formados entre Lisozima (ponto isoelétrico ao redor de 11) e Goma-Xantana na proporção de 1:1 de massa total do sistema com 0.1 mol/L NaCl.

A formação do complexo coacervado, além do pH, depende da proporção dos biopolímeros, concentração de sais e temperatura. A proporção de biopolímero no sistema altera o comportamento de formação dos complexos por influenciar no equilíbrio de carga dos complexos (MCCLEMENTS, 2015). A alteração na temperatura pode provocar modificações na conformação estrutural dos biopolímeros, além de facilitar a ocorrência de interações do tipo não eletrostáticas entre elas. Por exemplo, as ligações de hidrogênio são favorecidas a baixas temperaturas, enquanto altas temperaturas favorecem ligações hidrofóbicas (SCHMITT et al., 1998; TOLSTOGUZOV, 2002). A força iônica entre os biopolímeros pode ser afetada pela concentração de sais. Isso porque em altas concentrações de sais a densidade de íons

transportada pelos biopolímeros é reduzida pela interação com os íons presente no sal, resultando na diminuição da atração eletrostática entre as macromoléculas e, conseqüentemente, na diminuição ou supressão da formação de complexos coacervados (SOUZA; GARCIA-ROJAS, 2017; WEINBRECK et al., 2004; YE; FLANAGAN; SINGH, 2006).

3.2.2 Cross-link e secagem

Após o estudo prévio, a otimização e a formação do complexo coacervado, é usual a reticulação (ou *cross-link*) do material de parede. Uma das razões para tal é garantir uma maior estabilidade física das cápsulas, de tal modo que a eficiência da encapsulação seja a maior possível. Os compostos químicos que já foram utilizados para reticulação das cápsulas são aldeídos e ácido tânico; no entanto, esses compostos tendem a causar problemas de saúde. Por isso, alguns autores recorrem a *cross-link* usando a enzima transglutaminase (TGase) (AMJADI et al., 2018; CHEN et al., 2012; TIMILSENA et al., 2016; YAN; ZHANG, 2014). A TGase catalisa a formação de ligações peptídicas entre o grupo amino das cadeias laterais de resíduos das lisinas e o grupo carboxiamida das cadeias laterais de resíduos das glutaminas. É comestível e tem sido amplamente aplicado na fabricação de queijos, processamento de carnes e produção de filmes comestíveis. Outras formas de reticular consideradas seguras para a saúde humana são tratamento térmico (especialmente de proteínas globulares) e outras enzimas como genipina, lacase e ribose (YAN; ZHANG, 2014).

No final, pode ser necessária a secagem das microcápsulas sendo para isso necessário selecionar um processo que garanta a integridade dos ingredientes encapsulados. Neste sentido, o *spray dryer* e o *freeze dryer* (ou liofilização) têm sido os mais usados, por garantirem uma maior eficiência do encapsulado (TIMILSENA et al., 2016, 2019; YAN; ZHANG, 2014).

4 Material de parede

Material de parede é o polímero utilizado para envolver o ingrediente ativo, com a finalidade de evitar perdas, evitar interação com outros ingredientes do sistema alimentar; bem como, aumentar vida de prateleira e permitir a liberação controlada do ingrediente ativo nas condições desejadas. No entanto, muitos materiais de parede não possuem todas as propriedades desejadas para encapsular um determinado ingrediente ativo. Por isso, leva-se em conta o estudo da combinação de dois ou mais polímeros para que, por sinergia, se somem os atributos desejados. Para esse fim, proteínas e polissacarídeos têm sido a preferência e são largamente usados nas indústrias alimentar, têxtil e farmacêutica (JINGYUAN WEN; GUANYU CHEN; ALANY, 2014; MCCLEMENTS, 2015).

A Tabela 3 apresenta diversos biopolímeros que podem ser utilizados como materiais de parede na encapsulação por coacervação complexa.

4.1 Carboximetilcelulose

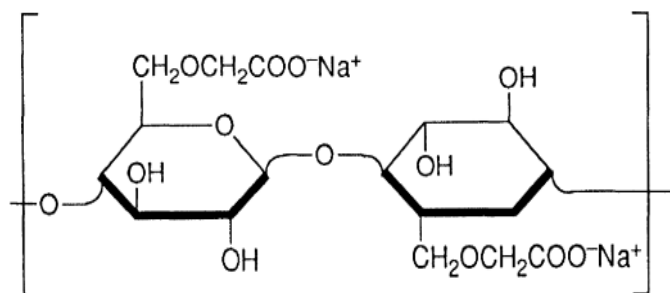
A carboximetilcelulose (CMC), geralmente usada como sal de sódio (NaCMC), é um produto derivado da celulose, produzido pela reação alcalina de celulose com o monocloroacetato de sódio (ver secção 1.1.1). A estrutura molecular do NaCMC é baseada no polímero β -(1 \rightarrow 4)-D-glucopiranosose de celulose (Fig. 4). Preparações de NaCMC podem ter diferentes graus de substituição (de 0 a 3), mas comercialmente é encontrado na faixa de 0.6 a 0.95. A solubilidade em água do NaCMC é aceita como uma função do grau de substituição, com NaCMC menos substituído (mais hidrofóbico) mostrando uma maior fração de agregados. No entanto, quando NaCMC se dissolve em água, ocorre um processo eletrolítico

para separar uma molécula de CMC em cátions de sódio e um ânion do polímero. Esses íons em solução interagem entre si por meio de forças eletrostáticas. Nesse sentido, o NaCMC pode ser considerado polieletrólito. Além disso, a molécula de água e os grupos OH na molécula de NaCMC exibem dipolo elétrico que realiza uma força de interação eletrostática considerável (a chamada ligação de hidrogênio) (FEDDERSEN; THORP, 1993; LOPEZ et al., 2015; YANG; ZHU, 2007).

Table 3. Proteínas e polissacarídeos frequentemente usados como materiais de parede

Polissacarídeos	Proteínas
Amido	Proteína isolada da Soja
Açúcar	Proteína Isolada do Trigo
Xarope de glicose	Proteína Isolada do Milho
Malto-dextrina	Gelatina
Goma-arábica	Caseína
Alginato	Concentrado proteico do soro de leite
Carragena	Isolado proteico do soro de leite
Pectina	Proteína Isolada da Linhaça
Dextrina	Proteína isolada da ervilha
Ciclo-dextrina	Lactoferrina
Octenilsucinato de amido	Ovalbumina
Carboximetilcelulose	β -lactoglobulina

Fonte: (YAN; ZHANG, 2014).



Fonte: (FEDDERSEN; THORP, 1993).

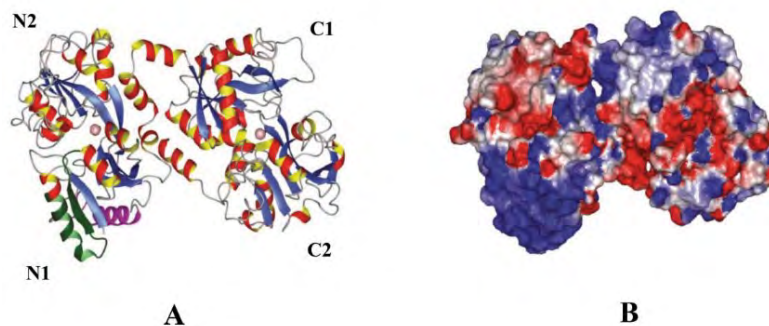
Figure 4. Estrutura idealizada de carboximetilcelulose de sódio com um DS=1.

NaCMC é versátil em sua capacidade de controlar a viscosidade de sistemas aquosos (estabilizar emulsões, por exemplo) e formar filmes fortes e resistentes. As viscosidades das soluções de CMC dependem da temperatura. Em condições normais, o efeito da temperatura é reversível, não exercendo um efeito permanente na viscosidade. No entanto, longos períodos de aquecimento em altas temperaturas tendem a despolimerizar e degradar o CMC. Além disso, soluções de NaCMC mantêm sua viscosidade em uma ampla faixa de pH. Em geral, as soluções apresentam viscosidade máxima e melhor estabilidade em pH ente 7-9. Acima do pH 10, observa-se alguma diminuição da viscosidade. Abaixo de pH 4, a viscosidade geralmente aumenta significativamente. Portanto, na preparação de soluções ácidas de NaCMC, é melhor dissolver o NaCMC em água neutra primeiro. Se uma solução é preparada antes da adição de ácido, uma viscosidade mais alta é obtida do que quando NaCMC seca é dissolvida em uma solução ácida. O NaCMC pode sofrer hidrólise catalisada por ácido em soluções ácidas, especialmente em temperaturas mais altas, resultando em perda permanente de viscosidade (FEDDERSEN; THORP, 1993; YANG; ZHU, 2007).

NaCMC foi usado pela primeira vez como um substituto para amido e gomas naturais, mas na atualidade seu uso e aplicação se estendeu grandemente, abrangendo indústria de papel, de processamento têxtil, de detergentes, de fluidos de perfuração, de revestimentos protetores, alimentícia, farmacêutica e cosmética (FEDDERSEN; THORP, 1993; LOPEZ et al., 2015).

4.2 Lactoferrina

A Lactoferrina (LF) é uma glicoproteína globular do leite com 700 resíduos de aminoácidos em sua estrutura e massa molar que pode variar de 80 – 84, com um ponto isoelétrico que varia de 8.0 a 8.5. A estrutura secundária da LF compreende 33-34% de hélices e 17-18% de folhas. As estruturas terciárias de LF (Fig. 5), conforme determinado por cristalografia de raios-X, consistem em dois lobos simétricos (N e C) unidos por uma curta a-hélice. Esses dois lobos são globulares e podem ser divididos em dois subdomínios de tamanhos semelhantes: N1 e N2; C1 e C2, respectivamente. Esses dois lobos podem se ligar a metais (como Fe^{2+} , Fe^{3+} , Cu^{2+} , Zn^{2+} e Mn^{2+}), através dos aminoácidos aspartato, tirosina e histidina (GONZÁLEZ-CHÁVEZ; ARÉVALO-GALLEGOS; RASCÓN-CRUZ, 2009; TOKLE; MCCLEMENTS, 2011; WANG et al., 2017). Uma das características mais notáveis da estrutura da LF é que sua superfície é carregada positivamente nos pHs tecnologicamente relevantes. Isso facilita a ligação de LF com biocompostos aniônicos. As porções carregadas positivamente de LF estão concentradas principalmente na região externa da primeira hélice do domínio N1 e no final do terminal C. Outro ponto, muito menor, mas intensamente carregado positivamente, existe na região interlobular, onde dois lobos são conectados por uma hélice (WANG et al., 2017).



Fonte: (WANG et al., 2017).

Figure 5. (A) estrutura cristalina 3D da LF e (B) distribuição de carga superficial de LF bovina saturada de ferro (código de banco de dados de proteínas: 1BLF) na mesma orientação. N1, N2, C1 e C2 representam os quatro subdomínios da LF. As cores azul, branco e vermelho correspondem a cargas líquidas positivas, neutras e negativas, respetivamente.

LFs de mamíferos têm sequência de aminoácidos semelhantes, o que sugere que ela desempenha funções biológicas idênticas em espécies diferentes. Vários estudos mostraram atividades biológicas da LF, que incluem ações antibacterianas, antivirais, antifúngicas, antiparasitárias, anticancerígenas e antiinflamatórias (GONZÁLEZ-CHÁVEZ; ARÉVALO-GALLEGOS; RASCÓN-CRUZ, 2009; VALENTI; ANTONINI, 2005). Portanto, a LF pode ser usada como um ingrediente ativo a ser encapsulada para ser entregue nos intestinos (DAVID-BIRMAN; MACKIE; LESMES, 2013). Além disso, a LF apresenta boas propriedades físico-químicas úteis para formar emulsões óleo em água, resistentes a agregação em pH abaixo de 6.0 (TOKLE; MCCLEMENTS, 2011). A LF, em combinação

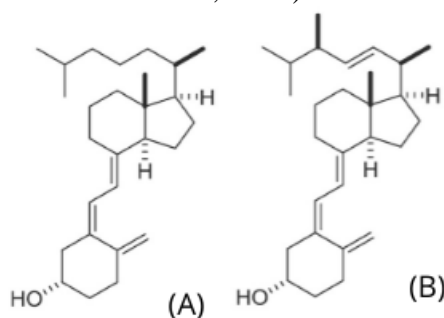
com outros biopolímeros, também mostrou ter uma ótima capacidade de encapsular óleos (BASTOS et al., 2020; SANTOS; GERALDO DE CARVALHO; GARCIA-ROJAS, 2021).

5 Ingredientes ativos

Os ingredientes ativos podem ser substâncias, compostos químicos e/ou microrganismos que podem ser microencapsulados. Na maioria das vezes, eles são instáveis quando expostos a luz, a umidade, ao oxigênio, a certas temperaturas (principalmente altas) e a certos pHs. Esses ingredientes devem, necessariamente, ter alguma vantagem quando ingerido, como é o caso da promoção do bem-estar e saúde Humana. Eles podem ser isolados e purificados a partir de fontes naturais, ou podem ser sintetizados quimicamente (MCCLEMENTS, 2015; ROA et al., 2017; SHAHIDI; HAN, 1993). Na natureza existem muitos ingredientes ativos passíveis de serem encapsulados, porém as suas propriedades moleculares, físico-químicas e biológicas podem determinar, de certa forma, a escolha do método ou técnica a usar, bem como material de parede. Dentre os ingredientes ativos que precisam ser encapsulados em alimentos e bebidas estão os pigmentos naturais, nutrientes como lípidos, proteínas, carboidratos, minerais e micro-organismos (FASUAN; GBADAMOSI; AKANBI, 2018; MCCLEMENTS, 2015; SILVA et al., 2012). Nesta tese, foram microencapsulados a vitamina D, a betanina e o betacaroteno, que são descritos nas seções a seguir.

5.1 Vitamina D

A vitamina D (Figura 6) é um composto lipossolúvel que pode ser encontrada em pelo menos duas formas: a vegetal conhecida como ergocalciferol (ou vitamina D₂) e a animal conhecida como colecalciferol (ou vitamina D₃). A vitamina D₃ é produzida na pele após a irradiação UV-B (290–315 nm) converter o precursor de colesterol conhecido como 7-desidrocolesterol em pré-vitamina D₃, que posteriormente se isomeriza em vitamina D₃; enquanto nas plantas e cogumelos a irradiação UV-B produz o isômero vitamina D₂ usando o ergosterol do esterol de membrana (GIUSTINA et al., 2019; MAESTRO; MOLNÁR; CARLBERG, 2019). Após a ingestão ou produção humana de uma destas formas da vitamina D, o fígado hidroxila na posição 25 para formar 25-hidroxivitamina D (a principal forma da vitamina D circulante no sangue) e, finalmente, os rins promovem hidroxilação na posição 1 para formar 1,25-dihidroxivitamina D (3). A mesma enzima responsável pela formação de 1,25-dihidroxivitamina D no rim, a CYP27B1, também é encontrada em muitos tecidos extrarrenais e é capaz de produzir 1,25-dihidroxivitamina D de forma para ou autócrina (GIUSTINA et al., 2019; PLUDOWSKI et al., 2018).



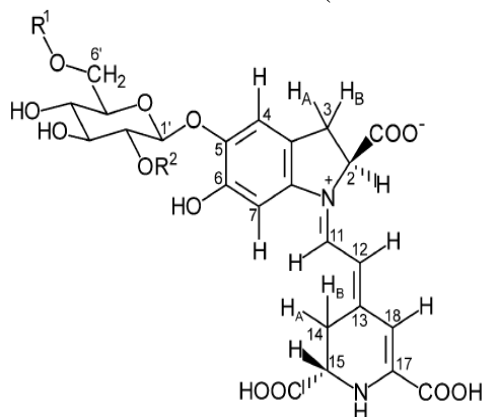
Fonte: (MAESTRO; MOLNÁR; CARLBERG, 2019)

Figure 6. Estrutura química da Vitamina D3 (A) e vitamina D2 (B).

No geral, a forma ativa da vitamina D desempenha um papel importante na regulação da homeostase do fosfato de cálcio e no controle da renovação óssea. Além disso, ela pode ter um efeito imunomodulador e pode estar relacionada a baixos níveis de inflamação no organismo (SASSI; TAMONE; D'AMELIO, 2018). Portanto, a deficiência da vitamina D pode estar associada a diferentes enfermidades crônicas e agudas, incluindo infecções, obesidade e cânceres (AMREIN et al., 2020). Podendo ser considerada um problema global de saúde, que chega a afetar bilhões de pessoas, incluindo crianças e idosos (HOLICK, 2017). A suplementação da vitamina D pode ser uma solução a esta situação. Ela é muitas vezes necessária porque a exposição à luz solar e a ingestão de alimentos naturais por si só podem não ser suficientes para maioria das pessoas (AMREIN et al., 2020). Uma das formas viáveis para a suplementação é a fortificação de alimentos, que pode estar condicionada devido à sua estabilidade durante o seu processamento ou armazenamento. No entanto, existem informações limitadas sobre a estabilidade da vitamina D ou dos compostos provitamina D e dos derivados ativos, embora esta vitamina tenha sido relatada como suscetível ao oxigênio, à luz e à temperatura (VILLOTA; HAWKES, 2018). Sobre essa estabilidade discutimos mais a posterior no CAPÍTULO IV.

5.2 Betanina.

A Fig 7 mostra a estrutura química da betanina, que é um pigmento natural hidrossolúvel pertencente à classe das betalainas, possui uma cor vermelha. Pode ser encontrada em *Beta vulgaris*, *Opuntiasp* e na família *Amarantheceae*. A sua cor não varia com o pH, sendo estável no intervalo de 3 - 7; ela tem sido aplicada em iogurtes, sorvetes, sopas, saladas, produtos farmacêuticos e cosméticos (ESATBEYOGLU et al., 2015).



Fonte: H (STRACK; VOGT; SCHLIEMANN, 2003).

Figure 7. Estrutura química da betanina, R1 = R2 = H.

Além da função de dar a cor, a betanina possui atividades biológicas. A atividade antioxidante desse pigmento é a que mais tem sido reportada na literatura e a partir desta foram estudados muitos efeitos benéficos e protetores de células, tecidos e órgãos. Ela protege a LDL (*LowDensityLipoprotein*) da oxidação (TESORIERE et al., 2004), pode estar envolvida na redução do dano ao ADN (ZIELIŃSKA-PRZYJEMSKA et al., 2012).

A atividade antioxidante da betanina é aproximadamente 3 a 4 vezes mais potente que o do ácido ascórbico, catequina e rutina. A atividade antioxidante foi relacionada com a eliminação dos radicais livres devido a presença do grupo hidroxilo e iminino, bem como a ligação 5-*O*-glicosilado (CAI; SUN; CORKE, 2003; ESATBEYOGLU et al., 2015). Embora a betanina possua essas características benéficas, ela é sensível a luz e a temperatura, o que limita a sua aplicação em alimentos. Como forma de resolver essa situação a encapsulação da

betanina mostra-se ser um método eficaz para protegê-la contra a ação da luz e de temperaturas elevadas.

As betalainas já foram microencapsuladas pela técnica *spraydryer* (VERGARA et al., 2014), por emulsificação A/O/A (PAGANO et al., 2018) e inclusão em nanopartículas lipossomais (AMJADI et al., 2018). Porém, não existem trabalhos que tratam da encapsulação da betanina usando a coacervação complexa e as técnicas referenciadas neste parágrafo apresentam alguns inconvenientes (como uso de altas temperaturas) que poderiam degradar a betanina, favorecendo a microencapsulação deste pigmento pela coacervação complexa.

5.3 Carotenoides (β -caroteno).

Os carotenoides são compostos químicos derivados de licopeno ($C_{40}H_{56}$) e apresentam oito (8) unidades de isoprenos. Suas estruturas moleculares absorvem comprimentos de onda na faixa de 400 a 550 nm, sendo responsáveis pelas cores vermelha, laranja e amarela de muitas frutas e vegetais. Mais de 600 carotenoides foram identificados na natureza e, de acordo com a presença ou não de oxigênio em sua estrutura, eles são classificados em xantofilas e carotenos, respectivamente (DELGADO-VARGAS; JIMÉNEZ; PAREDES-LÓPEZ, 2000). Os carotenoides mais comumente encontrados nos vegetais são: o β -caroteno, licopeno, xantofilas (como a zeaxantina e luteína) e a bixina. Dentre eles o β -caroteno foi mais largamente estudado, sendo achado nele atividades pró-vitamina A e antioxidante (DELGADO-VARGAS; JIMÉNEZ; PAREDES-LÓPEZ, 2000). A vitamina A é um nutriente importante para os olhos, sistema imunológico, função gastrointestinal e funcionamento dos sistemas reprodutivos. No que concerne a ação antioxidante do β -caroteno foi relacionada a prevenção de câncer e redução da sua incidência (GUL et al., 2015; OLSON, 1989).

Quanto as suas características físico-químicas o β -caroteno é lipossolúvel, possui uma estrutura linear, rígida e com ligações duplas conjugadas. A estrutura poliênica faz dele um composto químico altamente reativo, uma vez que é rica em elétrons e suscetível a ser atacada por reagentes eletrofílicos (como oxigênio) (DELGADO-VARGAS; JIMÉNEZ; PAREDES-LÓPEZ, 2000). Por fim, devido às características que ora mencionamos o β -caroteno tende a perder suas propriedades (antioxidante, pró-vitamina A e corante) durante o processamento e armazenamento, o que favorece sua encapsulação para que haja maior tempo de prateleira e preservação da integridade das suas propriedades.

6 Liberação dos compostos bioativos encapsulados

A liberação de compostos bioativos das matrizes na qual foram encapsulados são efetuados usando diferentes técnicas com o objetivo de compreender e/ou ajustar a taxa de liberação ou as concentrações do composto liberado em determinado meio que deve estar em contato ou disponível. Alguns exemplos de estudo de liberação de compostos microencapsulados incluem a simulação *in vitro* da digestão gastrointestinal e a liberação em matrizes alimentares, como água, óleo vegetal e 50% de etanol. Existem vários mecanismos pelos quais a liberação dos compostos microencapsulados pode ocorrer. Eles são dependentes da aplicação específica e podem atuar simultaneamente ou em diferentes etapas de um processo de entrega. No desenvolvimento e fabricação de sistemas de liberação controlada, é importante entender esses mecanismos (BRUSCHI, 2015; MCCLEMENTS, 2015; YAN; ZHANG, 2014).

Os principais mecanismos envolvidos na liberação do composto bioativo são difusão, erosão, fragmentação e inchamento. Na difusão a parede do encapsulado permanece intacta, no entanto o composto bioativo é liberado da matriz encapsulada por difusão molecular. Nestes casos, a taxa de liberação é determinada pelas propriedades químicas do núcleo

encapsulado e pelas propriedades físico-químicas do material de parede (JUG et al., 2018; KO; GUNASEKARAN, 2014; LEE; YEO, 2015; MCCLEMENTS, 2015). Geralmente, quando uma molécula atravessa a parede por uma difusão normal (ou Fickiana) é porque ela obedece a uma das duas leis de Fick: **(i)** a primeira lei de Fick estabelece que a difusão do soluto é feita do local onde a concentração é mais alta para onde a concentração é mais baixa através de um gradiente de concentração (SIEPMANN; SIEPMANN, 2008). **(ii)** A segunda lei de Fick tem como objetivo determinar a taxa de variação da concentração de difusão em um determinado ponto de um sistema, ou seja, essa lei é a equação do transporte de massa que enfatiza a variação da concentração em função do tempo em um determinado local (BRUSCHI, 2015).

Durante a erosão a matriz sofre degradação das suas moléculas, sendo que a temperatura, pH ou atividade enzimática podem determinar a velocidade na qual ocorre a erosão. Por outro lado, na fragmentação a liberação do composto bioativo ocorre após a quebra da partícula por uma ruptura física, química ou enzimática. No inchamento as partículas em solução e em condições ambientais específicas absorvem o solvente do meio envolvente resultando no aumento do tamanho do poro facilitando a liberação do composto bioativo (KO; GUNASEKARAN, 2014; LEE; YEO, 2015; MCCLEMENTS, 2015).

Os mecanismos de liberação de compostos bioativos podem ser melhor explicados através de modelos matemáticos, já que eles esses modelos permitem a medição de alguns parâmetros físicos importantes (por exemplo, coeficiente de difusão do fármaco) e recorrem ao ajuste do modelo em dados de liberação experimental (BRUSCHI, 2015). Á seguir procuramos descrever brevemente os principais modelos matemáticos mais usados por pesquisadores na área de alimentos.

6.1 Modelos matemáticos usados para estudo da cinética de liberação

Entre os diferentes modelos matemáticos usados para estudar a cinética de liberação podemos destacar ordem zero, primeira ordem, Higuchi, e Ritger–Peppas. Contudo, é importante lembrar que a liberação de um composto bioativo do seu invólucro é um processo complexo no qual intervêm diferentes fatores, que incluem a sua natureza (cristalinidade, solubilidade, dosagem, tamanho de partícula etc.), meio de dissolução, formulação (tipo de excipiente e quantidade relativa), tipo de forma farmacêutica e método de fabricação (AGUZZI et al., 2010).

Para cinética de ordem zero (equação 3), a liberação de um agente ativo é apenas uma função do tempo e o processo ocorre a uma taxa constante independente da concentração do agente ativo (BRUSCHI, 2015).

$$C_t = C_0 + K_0t \quad (3)$$

onde C_t representa a quantidade de agente ativo liberado durante o tempo t , C_0 é a concentração inicial de ativo liberado (geralmente, $C_0 = 0$) e K_0 é a constante de ordem zero.

O modelo da cinética de primeira ordem tem sido usado para descrever a absorção e/ou eliminação de uma variedade de agentes terapêuticos. No entanto, é difícil definir a cinética de primeira ordem usando uma teoria básica. Nesse sentido, a cinética de liberação de primeira ordem (equação 4) afirma que a mudança na concentração em relação à mudança no tempo depende apenas da concentração (BRUSCHI, 2015).

$$C_t = F(1 - e^{-K_1t}) \quad (4)$$

Onde o K_1 é a constante da primeira ordem, F é quantidade máxima da droga liberada no tempo t .

As relações matemáticas desenvolvidas por Higuchi estão relacionadas a partículas de ativos dispersos em matrizes homogêneas submetidas a um meio difusor. A equação de Higuchi (5) relaciona a concentração do agente ativo com a raiz quadrada do tempo, representando uma função linear (BRUSCHI, 2015).

$$C_t = K_H \sqrt{t} \quad (5)$$

Onde o K_H é a constante de Higuchi.

O modelo matemático desenvolvido por Ritger–Peppas (equação 6), também conhecido como lei de potência, é uma equação semi-empírica mais abrangente para descrever a liberação de compostos bioativos de sistemas poliméricos.

$$C_t/M_\infty = K t^n + b \quad (6)$$

onde M_∞ é a quantidade do composto bioativo no estado de equilíbrio, K é a constante de incorporação de modificações estruturais e características geométricas do sistema (também considerada a constante de velocidade de liberação), n é o expoente de liberação (relacionado ao mecanismo de liberação do fármaco) em função do tempo t . Quando o processo de liberação do composto bioativo é caracterizado por um aumento abrupto da liberação inicial do fármaco (efeito explosão) utiliza-se o valor b na equação (BRUSCHI, 2015; MCCLEMENTS, 2015; SIEPMANN; SIEPMANN, 2008).

Para determinar o expoente n , recomenda-se utilizar a porção da curva de liberação até o ponto onde $M_\infty/C_t < 0.60$ (ou 60%). Em todos os casos, assume-se que a liberação ocorre em apenas uma direção e que a relação entre a largura e a matriz é um máximo de 1:10. Dependendo do valor de n que melhor se ajuste ao perfil de liberação de um composto bioativo, é possível estabelecer uma classificação, de acordo com o tipo de comportamento observado (AGUZZI et al., 2010; BRUSCHI, 2015):

- a) **Caso I ou modelo Fickiano.** O valor de n é igual 0.5 e a liberação do composto bioativo é regida pela difusão. A difusão do solvente é muito maior do que o processo de relaxação da cadeia polimérica. O equilíbrio de absorção na superfície exposta do sistema polimérico ocorre rapidamente, levando a condições de ligações dependentes do tempo.
- b) **Caso II ou modelo não Fickiano** ($n = 1$), a taxa de liberação do composto bioativo corresponde à cinética de liberação de ordem zero e o mecanismo que conduz a liberação do fármaco é o inchaço ou relaxamento das cadeias poliméricas. A difusão do solvente através do sistema é muito rápida em comparação ao processo de relaxação na interface polimérica, que marca o limite interno de penetração ou dispersão do solvente em um determinado tempo. No final do transporte do Caso II, às vezes pode ser observado um rápido aumento da taxa de absorção do solvente. Nesta situação, o transporte caso II evoluiu para o transporte Super Caso II, devido à expansão das forças exercidas pelo gel inchado no núcleo vítreo. Além disso, quando $0.5 < n < 1$, o modelo é de transporte não Fickiano ou anômalo, e o mecanismo de liberação do composto bioativo é governado por difusão e inchaço. As taxas de difusão e inchaço são comparáveis. O rearranjo das cadeias poliméricas ocorrendo lentamente e o processo de difusão simultaneamente causam efeitos anômalos dependentes do tempo.
- c) Por fim, o **modelo Super Caso II** é caracterizado quando $n > 1$, constituindo uma forma extrema de transporte. Durante o processo de sorção, ocorre tensão e quebra do polímero.

6.2 Simulação *in vitro* da Digestão gastrointestinal e bioacessibilidade

Os sistemas de digestão *in vitro* são usados para testar a liberação controlada dos ingredientes ativos no trato digestivo. Esses sistemas, em comparação com os sistemas *in vivo*, tem a vantagem de um melhor custo-benefício, de serem mais rápidos e de natureza reprodutível, além de não envolver questões éticas pela não utilização de animais (MCCLEMENTS, 2015; TIMILSENA et al., 2019). A existência de muitos protocolos diferentes para a simulação *in vitro* da digestão gastrointestinal motivou vários cientistas a harmonizar e criar um único protocolo designado INFOGEST (BRODKORB et al., 2019). Este protocolo simula, sequencialmente, as 3 principais fases de digestão: oral (2 minutos), estomacal (2 horas) e intestino delgado (2 horas).

Na fase oral, as amostras líquidas ou sólidas são misturadas com fluído simulado oral (SSF) contendo a enzima α -amilase. Esta enzima deve estar na concentração final de 0.75 U/mL. As amostras sólidas são preferencialmente trituradas em partículas menores, para aumentar a área de contato com o SSF. Além disso, é importante que nesta fase, se a amostra for sólida, ela seja pastosa e, portanto, pode ser necessária a adição de água até que se atinja essa consistência. Na fase intestinal, a digesta proveniente da fase oral é misturada 1/1 com o fluído simulado gástrico (SGF) que deve conter na concentração final desta fase 2,000 U/mL de pepsina, o pH desse simulado deve ser ajustado para 3.0. Finalmente durante a fase intestinal, a digesta gástrica é misturada na proporção 1/1 com o fluído simulado intestinal (SIF) contendo 100 U/mL de pancreatina e 10 mmol/L de sais biliares, no simulado final. O pH nesta fase deve ser ajustado para 7.0. O SSF, SGF e o SIF com as enzimas devem ser pré-aquecidos e toda simulação deve ser feita a 37°C.

No final da digestão, é comum os pesquisadores determinarem a bioacessibilidade. Por definição, a bioacessibilidade é a fração de um composto que é liberada de sua matriz no trato gastrointestinal e assim fica disponível para absorção intestinal. A bioacessibilidade inclui toda a sequência de eventos que ocorrem durante a transformação digestiva do alimento em material que pode ser assimilado pelo organismo, a absorção/assimilação nas células do epitélio intestinal e, por último, o metabolismo pré-sistêmico (tanto intestinal quanto hepático) (FERNÁNDEZ-GARCÍA; CARVAJAL-LÉRIDA; PÉREZ-GÁLVEZ, 2009). A medição da bioacessibilidade costuma ser feita utilizando a concentração do composto bioativo na micela da digesta intestinal dividido pela concentração da digesta intestinal. Para se obter a concentração da micela (Figura 8), uma centrifugação (>14,000 rpm) por 30 minutos costuma ser efetuada e busca-se pegar uma alíquota entre a parte oleosa no sobrenadante e o precipitado. No corpo humano, micelas e outras partículas coloidais devem passar pela camada de muco que reveste o trato gastrointestinal antes da absorção para corrente sanguínea. Essa camada tem tamanho de poro em torno de 0.4 μm , o que obriga sua filtração para remoção de partículas maiores a esse diâmetro (OZTURK et al., 2015).



Figure 8. Representação esquemática da micela obtida depois da centrifugação da digesta intestinal de microcápsulas de betacaroteno.

7 Referências

AGUZZI, C. et al. Mathematical models describing drug release from biopolymeric delivery systems. **Materials Technology**, v. 25, n. 3–4, p. 205–211, 1 set. 2010.

ALCARAZ, A. PAULA B.; XAVIER, F. B. Amaranto e seus benefícios. **REVISTA UNINGÁ**, v. 40, n. 1, 20 jun. 2014.

ALCÁZAR-ALAY, S. C.; MEIRELES, M. A. A. Physicochemical properties, modifications and applications of starches from different botanical sources. **Food Science and Technology (Campinas)**, v. 35, n. 2, p. 215–236, jun. 2015.

AMAYA-FARFAN, J.; MARCÍLIO, R.; SPEHAR, C. R. Deveria o Brasil investir em novos grãos para a sua alimentação? A proposta do amaranto (*Amaranthus SP*). **Segurança Alimentar e Nutricional**, v. 12, n. 1, p. 47–56, 3 fev. 2015.

AMJADI, S. et al. Improvement in the stability of betanin by liposomal nanocarriers: Its application in gummy candy as a food model. **Food Chemistry**, v. 256, p. 156–162, 2018.

AMREIN, K. et al. Vitamin D deficiency 2.0: an update on the current status worldwide. **European Journal of Clinical Nutrition** 2020 **74:11**, v. 74, n. 11, p. 1498–1513, 20 jan. 2020.

BAKER, L. A.; RAYAS-DUARTE, P. Retrogradation of Amaranth Starch at Different Storage Temperatures and the Effects of Salt and Sugars. **Cereal Chemistry**, v. 75, n. 3, p. 308–314, 1998.

BALASSA, L. L.; FANGER, G. O.; WURZBURG, O. B. Microencapsulation in the food industry. **C R C Critical Reviews in Food Technology**, v. 2, n. 2, p. 245–265, 1971.

BARBA DE LA ROSA, A. P. et al. Fractionation procedures, electrophoretic characterization, and amino acid composition of amaranth seed proteins. **Journal of Agricultural and Food Chemistry**, v. 40, n. 6, p. 931–936, jun. 1992.

BASTOS, L. P. H. et al. Encapsulation of the black pepper (*Piper nigrum L.*) essential oil by lactoferrin-sodium alginate complex coacervates: Structural characterization and simulated gastrointestinal conditions. **Food Chemistry**, v. 316, p. 126345, 30 jun. 2020.

BASTOS, L. P. H.; DE CARVALHO, C. W. P.; GARCIA-ROJAS, E. E. Formation and characterization of the complex coacervates obtained between lactoferrin and sodium alginate. **International Journal of Biological Macromolecules**, v. 120, p. 332–338, dez. 2018.

BELITZ, H.-D.; GROSCH, W.; SCHIEBERLE, P. **Food Chemistry**. 4th ed. Berlin: Springer, 2009.

BELLO-PÉREZ, L. A. et al. Characteristics of Starch from Opaque and Translucent Perisperm of Amaranth (*A. hypochondriacus*) Grains. **Starch - Stärke**, v. 70, n. 11–12, p. 1700260, 2018.

BET, C. D. et al. Organic amaranth starch: A study of its technological properties after heat-moisture treatment. **Food Chemistry**, v. 264, p. 435–442, 2018.

BHATTACHARYYA, D.; SINGHAL, R. S.; KULKARNI, P. R. Physicochemical properties of carboxymethyl starch prepared from corn and waxy amaranth starch. **Carbohydrate Polymers**, v. 27, n. 3, p. 167–169, 1995a.

BHATTACHARYYA, D.; SINGHAL, R. S.; KULKARNI, P. R. A comparative account of conditions for synthesis of sodium carboxymethyl starch from corn and amaranth starch. **Carbohydrate Polymers**, v. 27, n. 4, p. 247–253, jan. 1995b.

BOLONTRADE, A. J.; SCILINGO, A. A.; AÑÓN, M. C. Amaranth proteins foaming properties: Film rheology and foam stability – Part 2. **Colloids and Surfaces B: Biointerfaces**, v. 141, p. 643–650, 2016.

BREENE, W. M. Food uses of grain Amaranth. **Cereal foods world.**, v. 36, n. 5, p. 426–430, 1991.

BRODKORB, A. et al. INFOGEST static in vitro simulation of gastrointestinal food digestion. **Nature Protocols**, v. 14, n. 4, p. 991–1014, 18 mar. 2019.

BRUSCHI, M. L. **Strategies to Modify the Drug Release from Pharmaceutical Systems**. [s.l.] Elsevier, 2015.

CAI, Y.; SUN, M.; CORKE, H. Antioxidant Activity of Betalains from Plants of the Amaranthaceae. **J Agric Food Chem**, v. 51, n. 8, p. 2288–2294, 2003.

CHANDLA, N. K.; SAXENA, D. C.; SINGH, S. Amaranth (*Amaranthus* spp.) starch isolation, characterization, and utilization in development of clear edible films. **Journal of Food Processing and Preservation**, v. 41, n. 6, p. e13217, 2017.

CHEN, B. et al. Formation and microstructural characterization of whey protein isolate/beet pectin coacervations by laccase catalyzed cross-linking. **LWT - Food Science and Technology**, v. 47, n. 1, p. 31–38, 2012.

COELHO, L. M. et al. Emerging opportunities in exploring the nutritional/functional value of amaranth. **Food & Function**, v. 9, n. 11, p. 5499–5512, 2018.

COMUNIAN, T. A. et al. Microencapsulation of ascorbic acid by complex coacervation: Protection and controlled release. **Food Research International**, v. 52, n. 1, p. 373–379, 2013.

CONDÉS, M. C. et al. Amaranth protein films reinforced with maize starch nanocrystals. **Food Hydrocolloids**, v. 47, p. 146–157, maio 2015.

CONDÉS, M. C.; AÑÓN, M. C.; MAURI, A. N. Amaranth protein films from thermally treated proteins. **Journal of Food Engineering**, v. 119, n. 3, p. 573–579, dez. 2013.

CORTÉS, R. N. F. et al. Evaluation of Modified Amaranth Starch as Shell Material for Encapsulation of Probiotics. **Cereal Chemistry**, v. 91, n. 3, p. 300–308, 2014.

DANIELLY LEITE, T.; SPEHAR, C.; LUIZ AUGUSTO COPATI, S. **Caracterização agrônômica de amaranto para cultivo na entressafra no Cerrado**. [s.l.: s.n.]. v. 38

DAVID-BIRMAN, T.; MACKIE, A.; LESMES, U. Impact of dietary fibers on the properties and proteolytic digestibility of lactoferrin nano-particles. **Food Hydrocolloids**, v. 31, n. 1, p. 33–41, 1 maio 2013.

DELGADO-VARGAS, F.; JIMÉNEZ, A. R.; PAREDES-LÓPEZ, O. Natural Pigments: Carotenoids, Anthocyanins, and Betalains — Characteristics, Biosynthesis, Processing, and Stability. **Crit Rev Food Sci Nutr**, v. 40, n. 3, p. 173–289, 2000.

DIMA, C. et al. Microencapsulation of essential oil of pimento [Pimenta dioica (L) Merr.] by chitosan/k-carrageenan complex coacervation method. **Innovative Food Science & Emerging Technologies**, v. 22, p. 203–211, 2014.

DONG, D. et al. Microencapsulation of flaxseed oil by soya proteins-gum arabic complex coacervation. **International Journal of Food Science and Technology**, v. 50, n. 8, p. 1785–1791, 2015.

DUHORANIMANA, E. et al. Thermodynamic characterization of Gelatin–Sodium carboxymethyl cellulose complex coacervation encapsulating Conjugated Linoleic Acid (CLA). **Food Hydrocolloids**, v. 80, p. 149–159, jul. 2018.

ESATBEYOGLU, T. et al. Betanin—A food colorant with biological activity. **Molecular Nutrition & Food Research**, v. 59, n. 1, p. 36–47, 2015.

FASUAN, T. O.; GBADAMOSI, S. O.; AKANBI, C. T. Modification of amaranth (Amaranthus viridis) starch, identification of functional groups, and its potentials as fat replacer. **Journal of Food Biochemistry**, v. 42, n. 5, p. e12537, 2018.

FEDDERSEN, R. L.; THORP, S. N. SODIUM CARBOXYMETHYLCELLULOSE. In: **Industrial Gums**. [s.l.] Elsevier, 1993. p. 537–578.

FENNEMA, O. R.; DAMODARAN, S.; PARKIN, K. L. **Química de Alimentos de Fennema**. IV ed. Porto Alegre: Artmed, 2010.

FERNÁNDEZ-GARCÍA, E.; CARVAJAL-LÉRIDA, I.; PÉREZ-GÁLVEZ, A. In vitro bioaccessibility assessment as a prediction tool of nutritional efficiency. **Nutrition Research**, v. 29, n. 11, p. 751–760, 1 nov. 2009.

FLETCHER, R. J. Pseudocereals: Overview. In: WRIGLEY, C. W. et al. (Eds.). **Encyclopedia of Food Grains**. 2nd. ed. [s.l.] Academic Press, 2016. v. 1p. 274–279.

FONSECA-FLORIDO, H. A. et al. Thermal study in the interactions of starches blends: Amaranth and achira. **Food Hydrocolloids**, v. 61, p. 640–648, 2016.

GARCÍA-ARMENTA, E. et al. Preparation of surfactant-free emulsions using amaranth starch modified by reactive extrusion. **Colloids and Surfaces A: Physicochemical and Engineering Aspects**, v. 608, p. 125550, 5 jan. 2021.

GIUSTINA, A. et al. Controversies in Vitamin D: Summary Statement From an International Conference. **The Journal of Clinical Endocrinology & Metabolism**, v. 104, n. 2, p. 234–240, 1 fev. 2019.

GOMEZ-ESTACA, J. et al. Encapsulation of an astaxanthin-containing lipid extract from shrimp waste by complex coacervation using a novel gelatin–cashew gum complex. **Food Hydrocolloids**, v. 61, p. 155–162, dez. 2016.

GONZÁLEZ-CHÁVEZ, S. A.; ARÉVALO-GALLEGOS, S.; RASCÓN-CRUZ, Q. **Lactoferrin: structure, function and applications**. **International Journal of Antimicrobial Agents** Elsevier, , 1 abr. 2009.

GUERREIRO, L. M. R.; MENEGALLI, F. C. **Estudo reológico dos amidos de amaranto, de mandioca e de suas mistura, sob condições de acidez e tratamento térmico**. Campinas - SP: Universidade Estadual de Campinas, 2007.

GUL, K. et al. Chemistry, encapsulation, and health benefits of β -carotene - A review. **Cogent Food & Agriculture**, v. 1, n. 1, p. 1018696, 2015.

HOLICK, M. F. The vitamin D deficiency pandemic: Approaches for diagnosis, treatment and prevention. **Reviews in Endocrine and Metabolic Disorders** 2017 **18:2**, v. 18, n. 2, p. 153–165, 17 maio 2017.

JAIN, A. et al. Microencapsulation by Complex Coacervation Using Whey Protein Isolates and Gum Acacia: An Approach to Preserve the Functionality and Controlled Release of β -Carotene. **Food and Bioprocess Technology**, v. 8, n. 8, p. 1635–1644, 2015.

JAIN, A. et al. Characterization of microcapsulated β -carotene formed by complex coacervation using casein and gum tragacanth. **International Journal of Biological Macromolecules**, v. 87, p. 101–113, 2016.

JANSSEN, F. et al. Proteins of Amaranth (*Amaranthus* spp.), Buckwheat (*Fagopyrum* spp.), and Quinoa (*Chenopodium* spp.): A Food Science and Technology Perspective. **Comprehensive Reviews in Food Science and Food Safety**, v. 16, n. 1, p. 39–58, 1 jan. 2017.

JINGYUAN WEN; GUANYU CHEN; ALANY, R. G. Theories and Concepts of Nano Materials, Nano- and microencapsulation. In: KWAK, H.-S. (Ed.). **Nano- and Microencapsulation for Foods**, 1^a ed ed. Oxford: John Wiley & Sons, Ltd, 2014. p. 17–42.

JUG, M. et al. An overview of in vitro dissolution/release methods for novel mucosal drug delivery systems. **Journal of Pharmaceutical and Biomedical Analysis**, v. 147, p. 350–366, 2018.

JULIAN MCCLEMENTS, D.; MAHDI JAFARI, S. Improving Emulsion Formation, Stability and Performance using Mixed Emulsifiers: A Review. 2017.

KAIMAINEN, M. et al. Encapsulation of betalain into w/o/w double emulsion and release during in vitro intestinal lipid digestion. **LWT - Food Science and Technology**, v. 60, n. 2, Part 1, p. 899–904, 2015.

KALE, S. N.; DEORE, S. L. Emulsion Micro Emulsion and Nano Emulsion: A Review. **Systematic Reviews in Pharmacy**, v. 8, n. 1, p. 39–47, 19 nov. 2016.

KAUSHIK, P. et al. Microencapsulation of flaxseed oil in flaxseed protein and flaxseed gum complex coacervates. **Food Research International**, v. 86, p. 1–8, 2016.

KO, S.; GUNASEKARAN, S. Controlled Release of Food Ingredients. In: KWAK, H.-S. (Ed.). **Nano- and microencapsulation for foods**. 1 ed ed. Oxford: John Wiley & Sons, Ltd, 2014. p. 327–343.

KONG, X. et al. Rheological properties of starches from grain amaranth and their relationship to starch structure. **Starch - Stärke**, v. 62, n. 6, p. 302–308, 2010.

KOUPANTSIS, T.; PAVLIDOU, E.; PARASKEVOPOULOU, A. Flavour encapsulation in milk proteins – CMC coacervate-type complexes. **Food Hydrocolloids**, v. 37, p. 134–142, 2014.

LEAL-CASTAÑEDA, E. J. et al. Pickering emulsions stabilized with native and lauroylated amaranth starch. **Food Hydrocolloids**, v. 80, p. 177–185, 2018.

LEE, J. H.; YEO, Y. Controlled drug release from pharmaceutical nanocarriers. **Chemical Engineering Science**, v. 125, p. 75–84, 2015.

LEE, S. J.; WONG, M. Nano- and Microencapsulation of Phytochemicals. In: KWAK, H.-S. (Ed.). **Nano- and Microencapsulation for Foods**, 1^a ed ed. Oxford: John Wiley & Sons, Ltd, 2014. p. 119–165.

LIU, H. et al. Physicochemical and textural properties of tartary buckwheat starch after heat-moisture treatment at different moisture levels. **Starch - Stärke**, v. 67, n. 3–4, p. 276–284, 1 mar. 2015.

LIU, J. et al. Determination of degree of substitution of carboxymethyl starch by Fourier transform mid-infrared spectroscopy coupled with partial least squares. **Food Chemistry**, v. 132, n. 4, p. 2224–2230, 2012.

LOPEZ, C. G. et al. Structure of sodium carboxymethyl cellulose aqueous solutions: A SANS and rheology study. **Journal of Polymer Science, Part B: Polymer Physics**, v. 53, n. 7, p. 492–501, 1 abr. 2015.

LÓPEZ, D. N. et al. Amaranth, quinoa and chia protein isolates: Physicochemical and structural properties. **International Journal of Biological Macromolecules**, v. 109, p. 152–159, 1 abr. 2018.

MAESTRO, M. A.; MOLNÁR, F.; CARLBERG, C. Vitamin D and its synthetic analogs. **Journal of Medicinal Chemistry**, v. 62, n. 15, p. 6854–6875, 8 ago. 2019.

MARCONI, M. F. Possible nutritional implications of varietal influence on the 7S/11S seed globulin ratios in Amaranth. **Plant Foods for Human Nutrition**, v. 54, n. 4, p. 375–380, 1999.

MARFIL, P. H. M. et al. Production and characterization of palm oil microcapsules obtained by complex coacervation in gelatin/gum Arabic. **Journal of Food Process Engineering**, v. 41, n. 4, 2018.

MARTÍNEZ, E. N.; AÑÓN, M. C. Composition and Structural Characterization of Amaranth Protein Isolates. An Electrophoretic and Calorimetric Study. **J Agric Food Chem**, v. 44, n. 9, p. 2523–2530, 1996.

MATALANIS, A.; MCCLEMENTS, D. J. Hydrogel microspheres for encapsulation of lipophilic components: Optimization of fabrication & performance. **Food Hydrocolloids**, v. 31, n. 1, p. 15–25, 2013.

MCCLEMENTS, D. J. **Nanoparticle- and microparticle-based delivery systems: Encapsulation, protection and release of active compounds**. [s.l.] CRC Press, 2015.

MENDONÇA, S.; ARÊAS, J. A. G. **Efeito hipocolesterolemizante da proteína de amaranto (Amaranthus cruentus BRS-Alegria) em Hamsters**. São Paulo: Universidade de São Paulo, 2006.

MONTOYA-RODRÍGUEZ, A. et al. Extrusion improved the anti-inflammatory effect of amaranth (*Amaranthus hypochondriacus*) hydrolysates in LPS-induced human THP-1 macrophage-like and mouse RAW 264.7 macrophages by preventing activation of NF- κ B signaling. **Molecular Nutrition & Food Research**, v. 58, n. 5, p. 1028–1041, 2014.

NAKAGAWA, K.; NAGAO, H. Microencapsulation of oil droplets using freezing-induced gelatin–acacia complex coacervation. **Colloids and Surfaces A: Physicochemical and Engineering Aspects**, v. 411, p. 129–139, 2012.

OLSON, J. A. Provitamin A Function of Carotenoids: The Conversion of β -Carotene into Vitamin A. **The Journal of Nutrition**, v. 119, n. 1, p. 105–108, 1989.

ORSINI DELGADO, M. C. et al. Identification and characterization of antioxidant peptides obtained by gastrointestinal digestion of amaranth proteins. **Food Chemistry**, v. 197, p. 1160–1167, abr. 2016.

ORSINI DELGADO, M. C.; TIRONI, V. A.; AÑÓN, M. C. Antioxidant activity of amaranth protein or their hydrolysates under simulated gastrointestinal digestion. **LWT - Food Science and Technology**, v. 44, n. 8, p. 1752–1760, 2011.

OZTURK, B. et al. Nanoemulsion delivery systems for oil-soluble vitamins: Influence of carrier oil type on lipid digestion and vitamin D3 bioaccessibility. **Food Chemistry**, v. 187, p. 499–506, 15 nov. 2015.

PAGANO, A. P. E. et al. Microencapsulation of betanin in monodisperse W/O/W emulsions. **Food Res Int**, v. 109, p. 489–496, 2018.

PAREDES-LOPEZ, O.; LEHMANN, J. W. Amaranth: Commercialization and Industrialization. In: **Amaranth Biology, Chemistry, and Technology**. [s.l.] CRC Press, 1994. p. 207–217.

PENG, C. et al. Chemical composition, antimicrobial property and microencapsulation of Mustard (*Sinapis alba*) seed essential oil by complex coacervation. **Food Chemistry**, v. 165, p. 560–568, 2014.

PEREZ, E.; BAHNASSEY, Y. A.; BREENE, W. M. Some Chemical, Physical, and Functional Properties of Native and Modified Starches of *Amaranthus hypochondriacus* and *Amaranthus cruentus*. **Starch - Stärke**, v. 45, n. 6, p. 215–220, 1 jan. 1993.

PLUDOWSKI, P. et al. Vitamin D supplementation guidelines. **Journal of Steroid Biochemistry and Molecular Biology**, v. 175, p. 125–135, 1 jan. 2018.

QAMAR, S. et al. Nuts, cereals, seeds and legumes proteins derived emulsifiers as a source of plant protein beverages: A review. **Critical Reviews in Food Science and Nutrition**, v. 60, n. 16, p. 2742–2762, 7 set. 2020.

ROA, D. F. et al. Encapsulation and Stabilization of β -Carotene in Amaranth Matrices Obtained by Dry and Wet Assisted Ball Milling. **Food and Bioprocess Technology**, v. 10, n. 3, p. 512–521, 2 mar. 2017.

RUTZ, J. K. et al. Microencapsulation of palm oil by complex coacervation for application in food systems. **Food Chemistry**, v. 220, p. 59–66, abr. 2017.

SABBIONE, A. C. et al. Amaranth peptides with antithrombotic activity released by simulated gastrointestinal digestion. **Journal of Functional Foods**, v. 20, p. 204–214, jan. 2016.

SÁNCHEZ DE LA CONCHA, B. B. et al. OSA Esterification of Amaranth and Maize Starch Nanocrystals and Their Use in “Pickering” Emulsions. **Starch - Stärke**, v. 72, n. 7–8, p. 1900271, 1 jul. 2020.

SANGSEETHONG, K. et al. Influence of reaction parameters on carboxymethylation of rice starches with varying amylose contents. **Carbohydrate Polymers**, v. 115, p. 186–192, 2015.

SANGSEETHONG, K.; KETSILP, S.; SRIROTH, K. The Role of Reaction Parameters on the Preparation and Properties of Carboxymethyl Cassava Starch. **Starch - Stärke**, v. 57, n. 2, p. 84–93, 2005.

SANTOS, M. B.; DE CARVALHO, C. W. P.; GARCIA-ROJAS, E. E. Heteroprotein complex formation of bovine serum albumin and lysozyme: Structure and thermal stability. **Food Hydrocolloids**, v. 74, p. 267–274, 2018.

SANTOS, M. B.; GERALDO DE CARVALHO, M.; GARCIA-ROJAS, E. E. Carboxymethyl tara gum-lactoferrin complex coacervates as carriers for vitamin D3: Encapsulation and controlled release. **Food Hydrocolloids**, v. 112, p. 106347, mar. 2021.

SASSI, F.; TAMONE, C.; D'AMELIO, P. Vitamin D: Nutrient, Hormone, and Immunomodulator. **Nutrients** **2018**, Vol. 10, Page 1656, v. 10, n. 11, p. 1656, 3 nov. 2018.

SCHMITT, C. et al. Structure and technofunctional properties of protein-polysaccharide complexes: a review. **Crit Rev Food Sci Nutr**, v. 38, n. 8, p. 689–753, 1998.

SCHMITT, C.; TURGEON, S. L. Protein/polysaccharide complexes and coacervates in food systems. **Advances in Colloid and Interface Science**, v. 167, n. 1–2, p. 63–70, 14 set. 2011.

SHADDEL, R. et al. Use of gelatin and gum Arabic for encapsulation of black raspberry anthocyanins by complex coacervation. **International Journal of Biological Macromolecules**, v. 107, p. 1800–1810, 2018.

SHAHIDI, F.; HAN, X. Q. Encapsulation of food ingredients. **Crit Rev Food Sci Nutr**, v. 33, n. 6, p. 501–547, 1993.

SHEVKANI, K.; SINGH, N. Relationship between protein characteristics and film-forming properties of kidney bean, field pea and amaranth protein isolates. **International Journal of Food Science & Technology**, v. 50, n. 4, p. 1033–1043, abr. 2015.

SIEPMANN, J.; SIEPMANN, F. Mathematical modeling of drug delivery. **International Journal of Pharmaceutics**, v. 364, n. 2, p. 328–343, 8 dez. 2008.

SILVA, D. F. et al. MICROENCAPSULATION OF LYCOPENE BY GELATIN–PECTIN COMPLEX COACERVATION. **Journal of Food Processing and Preservation**, v. 36, n. 2, p. 185–190, 2012.

SINGH, N. et al. Morphological, thermal and rheological properties of starches from different botanical sources. **Food Chemistry**, v. 81, n. 2, p. 219–231, 1 maio 2003.

SOUZA, C. J. F. **Formação de Complexos Coacervados a Partir das Proteínas da Clara de Ovo e Polissacarídeos**. Seropédica: UFRRJ, 2015.

SOUZA, C. J. F.; GARCIA-ROJAS, E. E. Interpolymeric complexing between egg white proteins and xanthan gum: Effect of salt and protein/polysaccharide ratio. **Food Hydrocolloids**, v. 66, p. 268–275, maio 2017.

SPEHAR, C. R. Diferenças morfológicas entre *Amaranthus cruentus*, cv. BRS Alegria, e as plantas daninhas *A. hybridus*, *A. retroflexus*, *A. viridis* e *A. spinosus*. **Planta Daninha**, v. 21, p. 481–485, 2003.

STOJANOVIĆ, Ž. et al. A Comparison of Some Methods for the Determination of the Degree of Substitution of Carboxymethyl Starch. **Starch - Stärke**, v. 57, n. 2, p. 79–83, 2005.

STRACK, D.; VOGT, T.; SCHLIEMANN, W. Recent advances in betalain research. **Phytochemistry**, v. 62, n. 3, p. 247–269, 2003.

SUÁREZ, S.; AÑÓN, M. C. Amaranth proteins emulsions as delivery system of Angiotensin-I converting enzyme inhibitory peptides. **Food Hydrocolloids**, v. 90, p. 154–161, 2019.

SUAREZ, S. E.; AÑÓN, M. C. Comparative behaviour of solutions and dispersions of amaranth proteins on their emulsifying properties. **Food Hydrocolloids**, v. 74, p. 115–123, 2018.

TESORIERE, L. et al. Absorption, excretion, and distribution of dietary antioxidant betalains in LDLs: potential health effects of betalains in humans. **The American Journal of Clinical Nutrition**, v. 80, n. 4, p. 941–945, 2004.

TIMILSENA, Y. P. et al. Microencapsulation of chia seed oil using chia seed protein isolate–chia seed gum complex coacervates. **International Journal of Biological Macromolecules**, v. 91, p. 347–357, out. 2016.

TIMILSENA, Y. P. et al. Complex coacervation: Principles, mechanisms and applications in microencapsulation. **International Journal of Biological Macromolecules**, v. 121, p. 1276–1286, jan. 2019.

TOKLE, T.; MCCLEMENTS, D. J. Physicochemical properties of lactoferrin stabilized oil-in-water emulsions: Effects of pH, salt and heating. **Food Hydrocolloids**, v. 25, n. 5, p. 976–982, 1 jul. 2011.

TOLSTOGUZOV, V. Thermodynamic Aspects of Biopolymer Functionality in Biological Systems, Foods, and Beverages. **Critical Reviews in Biotechnology**, v. 22, n. 2, p. 89–174, 2002.

VALENTI, P.; ANTONINI, G. Lactoferrin: an important host defence against microbial and viral attack. **Cell. Mol. Life Sci**, v. 62, p. 2576–2587, 2005.

VENTUREIRA, J.; MARTÍNEZ, E. N.; AÑÓN, M. C. Stability of oil: Water emulsions of amaranth proteins. Effect of hydrolysis and pH. **Food Hydrocolloids**, v. 24, n. 6, p. 551–559, 2010.

VERGARA, C. et al. Microencapsulation of pulp and ultrafiltered cactus pear (*Opuntia ficus-indica*) extracts and betanin stability during storage. **Food Chem**, v. 157, p. 246–251, 2014.

VILLARREAL, M. E.; ITURRIAGA, L. B. Viscoelastic properties of amaranth starch gels and pastes. Creep compliance modeling with Maxwell model. **Starch - Stärke**, v. 68, n. 11–12, p. 1073–1083, 2016.

VILLOTA, R.; HAWKES, J. G. Reaction Kinetics in Food Systems. In: **Handbook of Food Engineering**. [s.l.] CRC Press, 2018. p. 225–484.

WANG, B. et al. Lactoferrin: Structure, function, denaturation and digestion. <https://doi-org.ez30.periodicos.capes.gov.br/10.1080/10408398.2017.1381583>, v. 59, n. 4, p. 580–596, 21 fev. 2017.

WEINBRECK, F. et al. Complexation of whey proteins with carrageenan. **J Agric Food Chem**, v. 52, n. 11, p. 3550–3555, 2004.

XIA, X. et al. Granular Structure and Physicochemical Properties of Starches from Amaranth Grain. **International Journal of Food Properties**, v. 18, n. 5, p. 1029–1037, 2015.

XIE, L. et al. Structure, function and food applications of carboxymethylated polysaccharides: A comprehensive review. **Trends in Food Science & Technology**, v. 118, p. 539–557, 1 dez. 2021.

XIONG, W. et al. Complex coacervation of ovalbumin-carboxymethylcellulose assessed by isothermal titration calorimeter and rheology: Effect of ionic strength and charge density of polysaccharide. **Food Hydrocolloids**, v. 73, p. 41–50, 1 dez. 2017.

YAMANI, B. V. **Substituição parcial de farinha de trigo por farinha de amarantoo (*Amaranthus cruentus* L.), quinoa (*Chenopodium quinoa* W.) e maçã (*Lepidium meyenii* W.) na elaboração de panetone**. São Paulo: Universidade de São Paulo, 2015.

YAN, C.; ZHANG, W. Coacervation Processes. In: GAONKAR, A. G. et al. (Eds.). **Microencapsulation in the Food Industry**. Boston: Elsevier, 2014. p. 125–137.

YANG, X. H.; ZHU, W. L. Viscosity properties of sodium carboxymethylcellulose solutions. **Cellulose**, v. 14, n. 5, p. 409–417, 29 out. 2007.

YE, A.; FLANAGAN, J.; SINGH, H. Formation of stable nanoparticles via electrostatic complexation between sodium caseinate and gum arabic. **Biopolymers**, v. 82, n. 2, p. 121–133, 2006.

YE, Q.; GEORGES, N.; SELOMULYA, C. Microencapsulation of active ingredients in functional foods: From research stage to commercial food products. **Trends in Food Science & Technology**, v. 78, p. 167–179, ago. 2018.

YILDIZ, G. et al. Microencapsulation of docosahexaenoic acid (DHA) with four wall materials including pea protein-modified starch complex. **International Journal of Biological Macromolecules**, v. 114, p. 935–941, 2018.

ZHAO, Y. et al. Complex coacervates from gelatin and octenyl succinic anhydride modified kudzu starch: Insights of formulation and characterization. **Food Hydrocolloids**, v. 86, p. 70–77, 2019.

ZHU, F. Structures, physicochemical properties, and applications of amaranth starch. **Critical Reviews in Food Science and Nutrition**, v. 57, n. 2, p. 313–325, 22 jan. 2017.

ZHU, F.; XIE, Q. Structure and Physicochemical Properties of Starch. In: **Physical Modifications of Starch**. Singapore: Springer Singapore, 2018. p. 1–14.

ZHU, Z. et al. Effects of sonication on the physicochemical and functional properties of walnut protein isolate. **Food Research International**, v. 106, n. November 2017, p. 853–861, 2018.

ZIELIŃSKA-PRZYJEMSKA, M. et al. The Beetroot Component Betanin Modulates ROS Production, DNA Damage and Apoptosis in Human Polymorphonuclear Neutrophils. **Phytotherapy Research**, v. 26, n. 6, p. 845–852, 2012.

**CAPÍTULO II. PROTEINS FROM PSEUDOCEREAL SEEDS:
SOLUBILITY, EXTRACTION, AND MODIFICATIONS OF THE
PHYSICOCHEMICAL AND TECHNO-FUNCTIONAL PROPERTIES**

Abstract

Pseudocereals (amaranth, buckwheat, and quinoa) are emerging as popular gluten-free crops. This may be attributed to their wide-ranging health benefits, including antioxidant, hypoglycemic and serum-cholesterol reducing properties. Proteins of these crops have a high nutritional quality due to the presence of essential amino acids. Additionally, amaranth, buckwheat and quinoa proteins (AP, BP and QP, respectively) have physicochemical properties that are useful for the manufacture of different types of food. However, native pseudocereal proteins demonstrate low solubility in water, mainly due to their composition. The major components of these proteins are albumins (water-soluble) and globulins (salt-soluble), although some proportions of glutelin (alkali-soluble) and prolamins (alcohol-soluble) are also found. The most commonly used method for extracting pseudocereal proteins is the alkaline extraction method, which may contribute to the low solubility of pseudocereal protein. Fortunately, different methods for modifying physicochemical (or techno-functional) properties have been proposed to extend their industrial application. For example, high-intensity ultrasound (HIUS) proved useful for improving the solubility of API and QP. Heating can allow for the formation of soluble aggregates of QP. The combination of heating and HIUS can improve the digestibility, solubility, and foam properties of AP. Conjugation through the Maillard reaction can improve BPI and QP interfacial properties. Thus, the aim of this work was to provide a review of the solubility, extraction and modification of the techno-functional properties of AP, BP, and QP.

Keywords: Molecular modification, physical modification, pseudocereal protein, biopolymers interactions.

1 Introduction

The growing use of plant-based proteins is currently trending due to their sustainability, relatively low cost, and health advantages compared to animal-based proteins. This fact is correlative to the current “green” trend in the pharmaceutical, cosmetic, and food industries ¹. Among several important vegetables, pseudocereals (mainly amaranth, buckwheat, and quinoa) are outstanding because they are fast-growing crops, require little water and are capable of growing at different altitudes ². The level of production of these crops has increased, which indicates greater demand and, probably, greater consumption. For example, in Peru and Bolivia, the general growth of “amaranth products” showed an increase between 2007 and 2012, with export values per ton that ranged from US \$360 in 2009 to US \$640 in 2011 ³. In the case of quinoa in Peru, although approximately 80% of exports were in grains without added value, the export value has increased during the last 5 years from US\$ 82.206.357 in 2013 to US\$ 125 430 720 in 2018 ⁴. The average worldwide production of buckwheat is 2.4 million tons, with France producing the most buckwheat at a production rate of 3,735 kg/ha ⁵.

The economic importance of pseudocereals is related to their phytochemical components, such as flavonoids, as well as their exceptional nutritional characteristics. These crops have a high content of essential amino acids, such as arginine, aspartate and lysine, which are considered to be lacking in some economically important cereals. Amaranth, buckwheat and quinoa are considered gluten-free crops that can be consumed by people with celiac disease ². Moreover, their health benefits are wide-ranging, including serum cholesterol reduction, antioxidant properties, and anti-hypoglycemic agents, so consumption of these crops can be beneficial for people with diabetes, dyslipidemia, and obesity ⁵⁻¹⁰. Recently, there has been an increasing amount of interest in the identification and characterization of bioactive peptides from pseudocereal protein hydrolysates, and discoveries regarding these exceptional proteins have already been made, including antioxidant activities, and effects on enzymes, offensive microorganisms and normal human flora ^{5,11}.

Amaranth, buckwheat, and quinoa have high protein contents (up to 180 g kg⁻¹) compared to cereals such as rice (70 g kg⁻¹) and wheat (100 g kg⁻¹) ^{2,3,12}. This may have aroused interest in its isolation and subsequent studies for possible industrial application. Many researchers have used pseudocereal protein isolates for the formation of edible films, stabilization of emulsions, and encapsulation of bioactive compounds or microorganisms ¹³⁻¹⁷. These applications are possible because of the physicochemical properties of proteins, which arise from the qualities of protein purity, size, hydration, flexibility, structural conformation, surface activity, and level of distribution of ionic charges ¹⁸. The extraction and drying methods play an important role in these properties. For example, extraction through use of an isoelectric precipitation method and drying through use of a heating method can favor protein denaturation, thus exposing the interior regions of the protein structure, such as hydrophobic regions, and leading to the formation of insoluble protein aggregates ^{19,20}. On the other hand, before isolation, pretreatment can be useful to improve or maintain the physicochemical properties of the proteins. Therefore, the protein extraction process must be well selected to avoid undesirable outcomes.

However, even after adequate extraction or drying, protein isolates may have certain limitations. For example, pseudocereal proteins have been reported to have low water solubility ¹². These limitations can curtail the use of pseudocereal proteins in the food industry, which is very complex due to the many different types of food production. Therefore, modifications are necessary to extend the application of pseudocereal protein isolates. Modifications of biopolymers can be performed through physical, chemical, and enzymatic methods. Physical modifications involve the use of pressure, irradiation, heat, and

moisture¹⁸. Chemical modifications usually occur with the introduction of functional groups into the molecule through derivatization reactions (e.g., etherification, esterification, crosslinking) or decomposition reactions (e.g., hydrolysis and oxidation)²¹. In the end, these modifications may affect the structure of the native protein, leading to protein breakdown, formation, or breakdown of aggregates. These changes may be useful for some applications, as shown in Figure 9.

This review aims to describe the solubility, extraction, and modification of the physicochemical and techno-functional properties of pseudocereal seed protein concentrates and isolates.

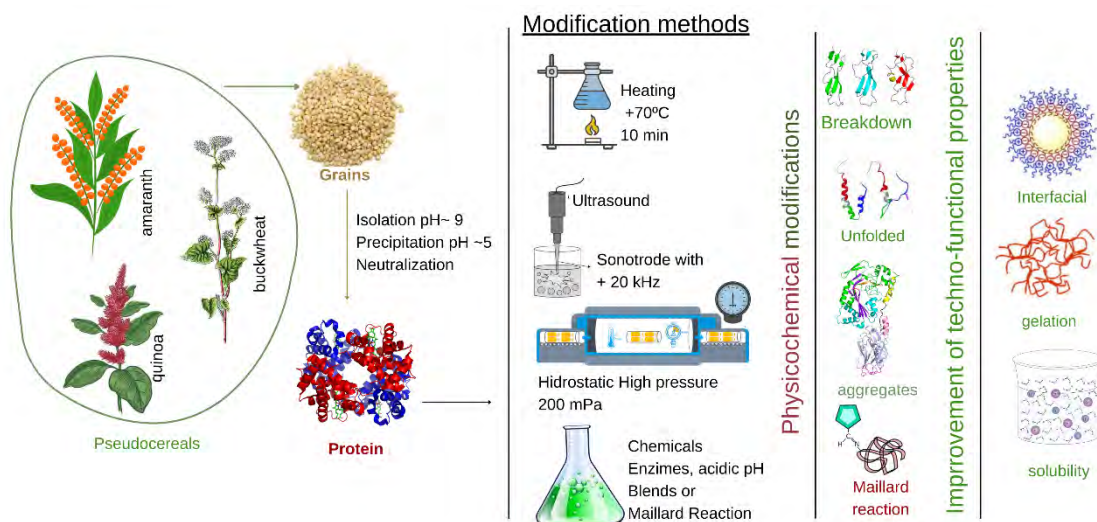


Figure 9. Changes in the physicochemical and techno-functional properties of pseudocereal proteins made by different chemical and physical methods.

2 Solubility and extraction of the native amaranth, buckwheat, and quinoa seed proteins

Among several techno-functional properties, protein solubility is outstanding due to its significant influence on other properties; that is, good emulsion, foam, and gelling properties, for example, are often associated with good solubility. However, the solubility of proteins is influenced by several factors, including composition (or presence of other components), concentration, pH, ionic strength, and temperatures²². Typically, pseudocereal proteins present pH-dependent solubility in the form of U. Maximum solubility is achieved below or above pH 4 or 7, respectively. At pH values between 4 and 7, the solubility tends to be less than or close to 50%; this is most likely due this pH range containing the isoelectric point of the protein, which is related to its composition. For example, according to Condés et al.²³, the low solubility at neutral pH (or in water) observed in amaranth protein isolate (API) can be related to the presence of globulin-P and 11S-globulin. The main fraction of API is albumin (650 g kg⁻¹ of protein), followed by globulin (170 g kg⁻¹), prolamin (110 g kg⁻¹), and glutelin (70 g kg⁻¹). The globulins of amaranth are amarantnine (11S) and globulin, similar to vicilin (7S). The 11S subunit is represented in the major fraction of globulin in amaranth and can be glycosylated and/or phosphorylated^{12,24}. Compared to API, quinoa protein isolate (QPI) and buckwheat protein isolate (BPI) have a similar solubility in neutral pH due to their composition²⁵⁻²⁸. Quinoa protein isolates (QPI) have fractions of 2S albumin (350 g kg⁻¹) and 11S globulin (370 g kg⁻¹)²⁹, while the protein isolates from tartaric buckwheat seeds have albumin as the predominant fraction (438 g kg⁻¹), followed by glutelin (146 g kg⁻¹), prolamin (105 g kg⁻¹), and globulin (78.2 g kg⁻¹)^{30,31}. It is important to remember that the water soluble fraction contains albumin, whereas globulin is soluble in the aqueous salt-

containing fraction (such as 0.4 M of NaCl). Prolamins can be soluble in water upon the addition of alcohol (such as 60% v/v ethanol), and glutelins are the most difficult fraction to solubilize, being generally extractable in alkaline or weak acid media or media containing detergent^{31–33}.

Despite these properties, it is possible to obtain good solubility in pseudocereal protein fractionation. For example, Wu et al.³¹ extracted approximately 910 g kg⁻¹ of buckwheat albumins using water, thus obtaining high solubility (approximately 90%) at neutral pH. However, it may be necessary to obtain the maximum protein yield from pseudocereals. This may be the reason why many researchers prefer to use the alkaline extraction method when trying to obtain an isolate or concentrate with maximum protein content. This method is carried out at a pH ranging from 8 to 11 before precipitation at an isoelectric point, which occurs in pH ranges from 4 to 6.5^{24,31,34,35}. One of the negative effects of this extraction method is the use of extremely alkaline pH values, as the protein tends to denature³⁶. Therefore, during precipitation, there may be an association of previously exposed hydrophobic groups of polypeptides, leading to the formation of insoluble protein aggregates. Reversible association reactions of amaranthine molecules, which have molecular weights (Mw) between 300 and 350 kDa, have been reported¹⁹. Furthermore, other negative effects of the extremely alkaline pH include the formation of disulfide bonds (S-S) due to sulfhydryl (SH, pKa of 8.5) oxidation, the formation of undesirable compounds (such as lysinoalanine), an increase in Maillard reactions (due to high pH) resulting in dark colored (i.e., melanoidin-based) products, and, at the time of precipitation, the coprecipitation of other compounds, thus leading to coextraction of impurities^{37–39}.

To avoid most of these problems, many researchers choose to use a pH less than or equal to 9, since proteins isolated at these pH values have excellent physicochemical characteristics, including purity, techno-functional and thermal properties^{40–42}. Alternatively, choosing other extraction methods, such as enzymatic or physical methods, may provide other advantages. For example, enzymatic extraction can often result in products with a high protein content, obtained by processing flour with enzymes (such as α -amylase, glucoamylase and pullulanase) that hydrolyze starch⁴³ (the main constituent of the endosperm of pseudocereal seeds). However, the cost of enzymes is high, which can raise sustainability issues for the use of this protein in the food industry. Furthermore, little is known about the effectiveness of different enzymes in extracting proteins from pseudocereals. One of the few works, carried out by Chen et al.³⁹, demonstrated that the synergistic effect of α -amylase and amyloglucosidase does not show an improvement in the extracted buckwheat protein content compared to alkaline or salt extraction methods. In addition, the proteins extracted by these enzymes contained a higher content of polyphenols that caused low protein solubility.

Physical methods can include wet (including freeze–thaw, high-speed blending, sonication, hydrothermal cooking, micro fluidization and the use of subcritical water) or dry fractionation. Chen et al.⁴⁴ showed that it was possible to obtain flours with high protein content (approximately 36%) using dry fractionation of surface abrasion. Despite the low protein content in the final product, the proteins did not change their properties during processing. Currently, there is a growing trend in the consumption of "natural" or "green" products, although there is, on the other hand, the concern about whether the final product is an isolate or a protein concentrate. However, it is possible to emphasize that the researchers will preferably seek to explore the techno-functional properties of the most preferred (by the consumers) protein products.

Additionally, a pretreatment using one or more wet or dry methods can improve the extraction yield. For example, Grossman, Rao and Da Silva⁴⁵ saw encouraging results when they used pectinase and hemicellulase concomitantly as a pretreatment of buckwheat bran. The extraction percentage was improved from 37% (with the alkaline extraction only) to

67.5%. In another study, Olivera-Montenegro, Best, and Gil-Saldarriaga⁴ studied the effect of pretreatments (supercritical CO₂ and ethanol cosolvent) on antioxidant activity in quinoa protein hydrolysate. However, this pretreatment had no significant effect on the protein content or protein solubility, but the antioxidant activity was improved.

After extraction, the drying method of proteins is another factor that influences solubility. Freeze-drying is the method of choice for protein drying because it results in less protein denaturation during the process. According to Shen et al.²⁰, freeze-drying can remove approximately 90% of water through vaporization, resulting in minimum salt or carbohydrate migration to the drying surface; thus, the interactions between components can be reduced. Additionally, an alternative explanation for the low solubility of pseudocereal proteins is the balance of comprised hydrophobic/hydrophilic amino acids and the thermodynamics of their association with the solvent⁴⁶. It is estimated that pseudocereal proteins contain more than 30% hydrophobic amino acids⁴⁷, which can interfere with water solubility due to a reduction of hydrophilic interactions (with water) and increase hydrophobic interactions. However, this property can be beneficial for other applications, including the formation and stabilization of emulsions and foams²².

3 Modifications of pseudocereal proteins

In recent years, the most commonly used methods for modifications of AP, QP, and BP were hydrolysis (enzymatic and acidic), heating, ultrasound, high pressures, Millard reactions, and mixing with other polymers (Table 4). Below, we discuss the most common modifications resulting from these treatments on these proteins.

3.1 Heating

Heating is a well-known treatment used for protein modification. Protein structure is normally unchanged at temperatures between 0-50 °C. However, when the temperature is raised sufficiently for a certain amount of time, the protein can denature (or unfold). Temperature influences the noncovalent bonds (such as hydrogen, electrostatic and hydrophobic bonds) that stabilize secondary and tertiary structures. When these structures are unfolded, hydrophobic groups can interact, reducing water solubility or even inducing the formation of aggregates, and subsequently coagulation and precipitation. Depending on the protein, this phenomenon may not be reversible when heating ceases and the original temperature is restored. An increase in the surface hydrophobicity and the formation of insoluble aggregates was observed for API when heated at 70 or 90 °C for 15 min⁴⁸. The 7S and 11S polypeptides were involved in the formation of these aggregates. However, these effects of the heating process occur to a greater extent at 90 °C and to a lesser extent at 70 °C for a duration under 10 min^{48,49}. Even though this phenomenon occurs, the different electrophoretic profiles of API may not incur notable changes⁵⁰. Even though the heated API presented low water solubility, Condés et al.⁴⁹ applied these proteins to form edible films. These authors observed that utilization of the heated API in the edible films can reduce the water vapor permeability and tensile strength due to crosslinking.

Table 4 Main methods used to modify pseudocereal proteins

Pseudocereal	Methods	Mw*	Native structure	Functional proprieties	References
Amaranth	HIUS (100 W, 30 kHz)	No significant changes observed	S ₀ was increased when the time of treatment was prolonged The free SH was increased	Improvement of solubility at pH 7-9. Improvement of EAI e ESI	12
	HP (200, 400 and 600 MPa)	The disappearance of polypeptides for 1 and 5% of the API treated with 400 and 600 MPa	S ₀ increased Free SH was increased for API of 1%, and for 5% API was increased at 200 MPa, but reduced at 400 and 600 MPa	Reduction of solubility, except for API concentration of 5 and 10%, treated with 200 MPa	24
	Heating (70 and 90°C, for 3, 5, 10, 15, and 30 min)	No differences were observed, although a significant number of polypeptides below 20 kDa were identified and high Mw bands were observed on top of the gel for treatment at 90°C	API heated at 70 °C: S ₀ reduced for treatment below 10 min ↑ S ₀ increased for treatment above 10 min API heated at 90 °C: S ₀ reduced for treatment above 15 min for API isolated at pH 11. S ₀ heated was higher than the native API only after 30 min of heating at 90 °C	Reduction of solubility	48
	Enzymatic hydrolysis (Cucurbita and papain) and heating for 10 min at 90 °C	Heating did not change Mw. The hydrolysates did not show bands of ~ 56 kDa	N/A	Heating did not significantly change the solubility The solubility was improved for protein hydrolyzed with or not heating	50
	Acid hydrolysis (pH 2) and Mixing (1: 1) with SPI	Disappearance of ~ 56 kDa (pH 2) bands. Presence of aspartic protease. The blends presented characteristic bands of API and SPI	Hydrolysates API presented S ₀ reduced	Reduction of solubility for hydrolysates. Improved blends solubility. Improved foamability and half-time of foam	68
	pH-shifting (2 and 12) for 1 h and HIUS (500/750W, 50% of amplitude) for 10 min	Difficulty detecting 11S globulin bands, likely formation of aggregates. The treatment did not affect albumins (Mw ~18kDa)	There was a reduction in exposed SH, mainly for the simultaneous treatment of pH 12 and HIUS. There was a reduction in particle size. HIUS promoted a certain level of reduction in API negative charges at various pH's, while pH-shifting and its combination with HIUS promoted a slight increase in negative charges	Increased solubility, highlighting the combination of pH 12 and HIUS. Both treatments improved foaming ability, except for the pH 2 treatment;	36

Table 4. Continuação.

Pseudocereal	Methods	Mw*	Native structure	Functional proprieties	References
Amaranth	Enzymatic hydrolysis (alkalase and trypsin)	The hydrolysates showed polypeptides of lower Mw compared to native API **	N/A	Solubility was reduced by hydrolysis, except at pH 6.3 for treatment with trypsin and a high degree of hydrolyses of alkalase; the same occurred for trypsin treatment at pH 7. Low degree Trypsin hydrolysates emulsions presented sensibility to the cream formation and flocculation	77
Quinoa	Heating (3 min 560W microwave, 15 min steaming at 100°C, 15 min boiling at 100°C, 5 min roasting at 160 ° C)	Without modification. Some proteins did not enter the gel (possible insoluble aggregates) for steaming and baking.	S ₀ was reduced, except for boiling were increased SH reduced	Only Boiling and microwave improved solubility at pH 7. EAI was improved at alkaline and neutral pH, notably for microwave and boiling. Steaming and roasting had negative impacts on the stability of the QPI emulsion	52
	Heating at pH 8.5 and 10.5 (100°C, 15 min)	Heating at pH 8.5 did not show the bands of the basic peptides Heating at pH 10.5 showed both acidic and basic bands. There were aggregates at the top of the gel	Total SH reduced Free SH reduced only for heating at pH 8.5 S ₀ increased only for heating at pH 8.5	heating at pH 10.5 increased solubility at low and high pH by 30-40%, while heating at pH 8.5 decreased slightly at high pH	51
	Heating (30, 60, 90, and 120 ° C) for 1 h	The disappearance of bands as an increase in temperature, especially for the treatment of 120°C	N/A	N/A	55
	HIUS (20 kHz, 700W) for 5, 10, 15, 20 and 30 min	The appearance of 190 kDa bands in non-reduced conditions	Increase of fluorescence intensity, indicating unfolding of the QPI	Solubility was improved	29
	Heating (90°C, 1h) Freezing (-40°C, 24h)	N/A	N/A	Freezing improved solubility at pH 10. Freezing reduced solubility at pH 4. Heating did not improve the solubility. Freezing improved the emulsifying capacity at pH 4 Heating and freezing reduced foam capacity, except at pH 10 where freezing did not differ with native QPI	54

Table 4. Continuação.

Pseudocereal	Methods	Mw*	Native structure	Functional proprieties	References
Quinoa	Maillard reaction of 5% QPI and 1-3g of mannose or xylose, heated at 60°C for 4 h	The electrophoretic bands of the QPI-monosaccharide complex became lighter (mainly with xylose), meaning that the free amino groups were reduced after the Maillard reaction.	N/A	Solubility, EAI, ESI, water and fat absorption capacities were significantly improved, mainly with 3g monosaccharide.	64
	HIUS (20 kHz, 500W, 25% amplitudes) for 15, 25, 35 min	There was no division of bands	There was a reduction in the fluorescence intensity after HIUS, indicating an unfolding of the QPI	EAI and ESI was improved	25
Buckwheat	Heating 100°C in boiling water bath	The soluble aggregates showed decreases in the intensity of the protein bands at 34–36 kDa and the disappearance of a component at 21–22 kDa	Reduction in disulfide bonds and increase SH group in insoluble aggregates, but increase in soluble aggregates	N/A	58
	HIUS (20 kHz) for 5, 10, 15, 20, and 30 min	N/A	increased the surface hydrophobicity, intrinsic fluorescence intensity, and total sulfhydryl contents	N/A	62
	Conjugation (xylose, fructose, glucose, dextran, and maltodextrin) by Millard reaction Heating at 60°C 12, 24, and 48h	The disappearance of bands with MW of 21 and 45 kDa The appearance of bands with 200 kDa for the conjugates	Heating increased the intensity of fluorescence	The conjugate with dextran showed better EAI and ESI. Solubility was improved in the conjugates and the sample heated to 12h. There was a general reduction in solubility after 48 hours of treatment	65

* The analyzes listed are electrophoresis on sodium dodecyl sulfate-polyacrylamide gel (SDS-PAGE) under reduced conditions.

** Analysis done through gel filtration chromatography

Where: API is the amaranth protein isolate, SPI is the soy protein isolate, QPI is the protein isolate from quinoa, BPI is the protein isolate from buckwheat, Mw is molecular weight, HIUS is high-intensity ultrasonic treatment, HP - high pressures, S₀ is surface hydrophobicity, SH is sulfhydryl group, N/A means that the work does not present data/no analysis was performed, EAI is an index of emulsifying activity, ESI is an index of emulsion.

The solubility of QPI was improved after different heat treatments. Mäkinen et al.⁵¹ verified a 30-40% increase in the solubility of QPI at pH 8-11 after heating at 100 °C (pH 8.5 and 10.5). Wang et al.⁵² observed that cooking and microwave heating improved QPI solubility at neutral pH. Moreover, a temperature of 80 °C and a duration of 30 min were considered to be the best conditions for improving the techno-functional properties of QPI⁵³. However, Cerdán-Leal et al.⁵⁴ found no significant differences in the QPI solubility index (pH 10) after heating at 90 °C for 1 h. These observations may be related to the formation of aggregates. The formation of QPI aggregates was attributed to the extensive increase in the formation of new S-S bonds, increase in particle sizes and reduction of the free SH groups⁵¹⁻⁵⁵. Additionally, heating QPI can promote an increase in surface hydrophobicity⁵¹. This observation proves that changes in protein conformation can result from protein denaturation or unfolding, which can contribute to the formation of aggregates. However, Wang et al.⁵² observed a significant reduction in the surface hydrophobicity of heated QPI (microwave, steam, and bread-making). Therefore, the surface hydrophobicity cannot conclusively explain the changes in solubility of QPI. Another contradictory observation concerns the particle sizes: Mir, Riar, and Singh⁵³ observed a decrease in the particle sizes of all heated QPIs. These differences may be due to treatment conditions, specifically protein concentration and pH. If the proteins are at a pH in which they are more soluble and at a lower concentration, the extent of denaturation will likely be greater, which may contribute to the formation of larger aggregates. Mir, Riar, and Singh⁵³ used 8% QPI concentration and the pH of water (near 7) to treat their QPI. It should also be noted that steaming and baking significantly reduced the solubility of QPIs, due to the recombination and polymerization of protein subunits during these processes⁵².

Studies dealing with the modifications of BPI are very limited. This may be associated with the limited use of buckwheat as food because this pseudocereal has several antinutritional factors, such as protease inhibitors, tannins, and saponins, which impair the digestion of starch and protein and affect the use of minerals⁵⁶. However, in the few works that exist, heating was applied to buckwheat globulin. According to Siu-Mei and Ching-Yung⁵⁷, globulin from common buckwheat can initiate aggregate formation at 90 °C. Therefore, the heating of these proteins at 100 °C can promote the formation of intermolecular disulfide linkages and small aggregates and large compact globular soluble macroaggregates⁵⁸. Therefore, more research is needed to better understand how heating can influence the physicochemical and techno-functional properties of BPIs.

3.2 High-intensity ultrasound

High-intensity ultrasound (HIUS) can cause significant changes in the structure and functional properties of proteins. HIUS is widely used to modify different products. This technology uses low frequencies (between 20-100 kHz) that can produce high intensities over 1 W/cm². These frequencies can produce cavitation, bubble formation, and bubble collapse. Cavitation occurs quickly and mainly in an aqueous medium and can promote different phenomena, such as intense shear forces, free radical formation, and increased pressures (up to 100 MPa), and temperatures (up to 5000 K). As with heating, the HIUS method ultimately results in the breakdown of the noncovalent bonds that stabilize secondary and tertiary structures of proteins. However, other factors can affect the state of denaturation, including ionic strength and pH. For example, Constantino and Garcia-Rojas¹² applied HIUS (30 kHz with a power of 100 W, at 30, 60, and 90% amplitudes) to API (10% in water) and observed improvements in the water solubility and emulsification properties of these proteins. The best treatment was the moderate HIUS treatment (60% and 30 min). These improvements were attributed to the reduced API particle size and increased surface hydrophobicity and free SH groups. In another study, Figueroa-González et al.³⁶ observed that the combination of HIUS at 50%

amplitude for 10 min and pH 12 for 1 h improved solubility and foam properties. HIUS caused a significant reduction in the exposed SH groups and presented difficulties in the detection of 11S globulin fractions, which may be due to the formation of aggregates with higher Mw. However, Constantino and Garcia-Rojas¹² did not observe any change in electrophoretic profiles. However, HIUS has a great impact on the unfolding of the native API structure, as both studies observed changes in the content of SH groups.

HIUS has significantly improved the solubility of QPI and has been related to conformational changes and the formation of soluble protein aggregates through S-S interactions^{25,59}, similar to the heating process. Additionally, HIUS can promote an increase in the surface hydrophobicity and particle size of QPI⁵⁹. HIUS (43 W/cm²) for 25 min seems to be ideal for improving both the QPI emulsifying activity index (EAI) and emulsifying stability index (ESI)²⁵. Qin et al.⁶⁰ demonstrated that QPI nanoparticles treated with ultrasound showed better emulsifying and interfacial properties for the production of Pickering emulsions. In addition to these applications, HIUS modification of QPI has shown promising results in the improvement of antioxidant activity. According to Li et al.⁶¹, the ultrasonic pretreatment of QPI (105.86 W/cm²) has the potential to significantly improve the degree of enzymatic hydrolysis (alkalase) of QPI and to increase the antioxidant activity of these hydrolysates.

Jin et al.⁶² studied the effect of HIUS (20 kHz and intensities between 55 and 105 W/cm²) on the physicochemical properties and in vitro digestion of BPI. These authors found that HIUS broke intramolecular bonds because of increased surface hydrophobicity and intrinsic fluorescence, decreased presence of β -turns and β -sheets, and decreased disulfide content. Additionally, HIUS promoted the formation of aggregates with a size of 2130.8 and a corresponding decrease in the polydispersity index. However, to date, we have not found studies that have studied the effects of HIUS on the techno-functional properties of these proteins. In another study, Xue et al.⁶³ applied HIUS (544.59 W/cm²) and heating (90 °C) to form a conjugate of BPI and dextrin. These authors observed that HIUS significantly improved the interfacial properties of BPI when compared to heating. This may be related to the fact that the cavitations induced by HIUS tend to cause many modifications, including the reduction of particle size, which can increase the area of contact with the two liquids involved in the emulsification.

3.3 Glycosylation technology

Glycosylation technology is widely used in research within the protein modification, and a clear example is the Maillard reaction. These reactions occur through the covalent interactions between the amino groups of proteins and the carbonyl group of carbohydrates, leading to the production of conjugates. These can be prepared using both conventional (dry and wet heating) and new techniques (e.g., pulsed field gradient, sonication, extrusion, high pressure, and electrospinning). Often, after the protein is modified by polysaccharide grafting, its fundamental properties, such as solubility, are improved. Teng et al. grafted⁶⁴ samples and reacted them with different proportions of mannose, xylose and QPI at 65 °C. The authors observed structural changes through SDS-PAGE analysis, in which color changes and small displacements of protein bands were observed, indicating the occurrence of a Maillard reaction. In the end, the modified QPIs showed improvements in solubility, emulsifying properties, water absorption capacities, fat absorption and biological activities. These properties were more prominent because the proportion of quinoa and monosaccharide protein isolates was 2:1.

Guo and Xiong⁶⁵ produced BPI-sugar (xylose, fructose, glucose, dextran, and maltodextrin) conjugates with improved techno-functional solubility that stabilized the oil-in-water emulsion through Millard's reaction. The cross-linking of sugars and BPI was

confirmed by the disappearance of the bands which represent the basic (21 kDa) and acidic (45 kDa) subunit. In addition, the authors observed several polymers of approximately 200 kDa and a reduction in the surface hydrophobicity of these proteins. However, the improvement of these techno-functional properties may depend on the duration of the reaction. It appears that 12 h is ideal for solubility improvement.

3.4 Biopolymers blends

Blends or mixtures of polymers, such as protein–protein or protein-polysaccharide, can produce thermodynamic incompatibility or compatibility, and if the polymers interact, they can favor the formation of complexes, coacervates, or other structures^{34,66,67}. Often, these additions are made to improve some property, including flow behavior, viscosity, and texture, and to control the stability and quality of food products. For example, Ventureira, Martínez, and Añón⁶⁸ studied the effect of acid treatment on the structural and foaming properties of soy protein (SPI)/API mixtures. These authors observed that hydrolyzed API promoted SPI hydrolysis due to the presence of proteases that were activated at acidic pH. The results of the SPI/API mixtures showed an improvement in the water-solubility and foaming properties. In another study, Condés et al.⁶⁹ produced API films by adding normal and waxy corn nanocrystals. This addition improved the overall behavior of the films. According to the authors, the hydrogen bonding of the API with the normal corn nanocrystals induced a greater reinforcement effect in the API films, resulting in a lower crystallinity. Cortez-Trejo et al.³⁴ evaluated the potential of API and bean isolates to form gels mixed with xanthan gum (XG) in aqueous solutions. These authors observed electrostatic attraction at pH values from 7 to 9, and the gel formed with API/XG mixtures did not need a crosslinking agent, and it was not as necessary to undergo heating.

Escamilla-García et al.⁷⁰ evaluated the effects of transglutaminase (TG) on chitosan (CT)/QPI mixture films. The authors observed that the cross-linking promoted by TG primarily occurred through the amino acid lysine and enhanced edible film properties. Additionally, the presence of CT and TG was favorable for the formation of films with good stability. The CT/QPI interaction was thought to be induced by electrostatic attraction because the films were manufactured at pH 11⁷¹. In addition, it is possible that the effect of TG on crosslinking was the predominant factor, although it has been reported in the literature that hydrogen bonds are the most important factor in the interaction between CT and QPI^{71,72}. In addition, interaction with polysaccharides can modify the secondary and tertiary structure of the proteins and enhance some properties, such as the thermal stability of QPI⁷¹. In another study, it was found that QPI can interact with alginate through noncovalent (hydrophobic interactions and hydrogen bonds) and weak electrostatic interactions to form soluble complexes. Another change in QPI techno-functional properties was observed when carrageenan (carr) was added to solutions containing QPI. According to Duran et al.⁷³, carr improved the solubility of QPI near the isoelectric point (from pH 2.5 to 5.5), while the opposite occurred at the pH where the protein is most soluble. In addition, carr can induce minor conformational changes in QPI and can also protect these proteins from thermal denaturation. Another consideration is the complex coacervates formed by the interaction between QPI and Gum Arabic, formed at pH 4 and in a 4:1 ratio (wt/wt). These complexes can encapsulate a high content (up to 88.60%) of eugenol, a natural and safe compound mainly extracted from *Myrtaceae*, which has broad-spectrum and strong inhibition against bacteria, yeast, and molds, as well as the ability of suppressing lipid peroxidation. In this way, the microcapsules could be applied to protect pork meat stored for 9 days at 4°C⁷⁸.

BPI can also form films. According to Wang et al.⁷⁴, films composed of BPI and bacterial cellulose presented low permeability to water vapor and excellent mechanical

properties (tensile strength). The authors reported that the main interaction mechanism involved hydrogen bonding.

3.5 High hydrostatic pressure

High hydrostatic pressure (HP) is another physically innovative technology that can promote reversible (such as dissociation of polymers) and nonreversible effects (such as denaturation, which includes the unfolding of monomeric proteins, aggregation, and gelation phenomena). The water solubility of the API treated with HP was reduced as the pressure was increased from 200 to 600 MPa; on the other hand, the high concentrations of API can result in protection from the shear effects caused by HP in aqueous dispersions of API. However, this phenomenon occurs only at low pressures (200 MPa, for example)^{24,75}. As the case of heating, HP affected the API solubility due to the denaturation and formation of insoluble aggregates. Condés et al.²⁴ hypothesized this occurrence when they observed the disappearance of the 45 kDa polypeptide due to its susceptibility to aggregate formation after denaturation. Furthermore, HP (at 400 and 600 MPa) resulted in a significant increase in the free SH group and surface hydrophobicity, suggesting the occurrence of protein unfolding and denaturation, which can also contribute to the formation of protein aggregates^{24,75}. In the end, these modifications were applied to the formation of films with better techno-functionality, due to the API becoming reassociated as a result of higher crosslinking or matrices⁷⁵.

Although BPIs have excellent nutritional properties, there are many reports of IgE-mediated allergies, which are associated with severe anaphylaxis. To reduce this negative attribute of BPIs, Lee et al.⁷⁶ treated these proteins with HP at 600 MPa for 30 min and then hydrolyzed them with alkaline protease for 240 min. Their results clearly showed that the method of hydrolysis with alkaline protease after treatment with HP could be applied to reduce the binding of IgE to BPI, up to 100%.

4 Conclusions and future perspectives

The increased demand for pseudocereals can promote important economic and social growth in some producing countries. Moreover, food products based on protein isolates from amaranth, buckwheat and quinoa can be an agreeable alternative to animal protein derivatives due to their nutritional properties and various health benefits. Although there are some limitations to their use, such as low water solubility, several researchers have shown that it is possible to use these proteins by applying inexpensive modifications, such as the use of high-intensity ultrasound and glycosylation. In addition to these technologies, blending or synergy with other biopolymers or compounds can be a relatively inexpensive alternative for the manufacture of products with interesting characteristics, for example, for the formation of edible films, coacervate complexes and emulsions. Therefore, the search for new renewable sources of proteins should focus on animal protein substitutes and the potential for various applications, especially in food.

5 References

- 1 Qamar S, Manrique YJ, Parekh H, and Falconer JR. Nuts, cereals, seeds and legumes proteins derived emulsifiers as a source of plant protein beverages: A review. *Crit Rev Food Sci Nutr* 60:2742–2762 (2020).
- 2 Fletcher RJ. Pseudocereals: Overview. In: Wrigley CW, Corke H, Seetharaman K, Faubion J, eds. *Encyclopedia of Food Grains* 2nd ed. Academic Press; p. 274–279 2016.

- 3 Fabio A Di and Parraga G. Origin, Production and Utilization of Pseudocereals. *Pseudocereals* Chichester, UK: John Wiley & Sons, Ltd; p. 1–27 2017.
- 4 Olivera-Montenegro L, Best I, and Gil-Saldarriaga A. Effect of pretreatment by supercritical fluids on antioxidant activity of protein hydrolyzate from quinoa (*Chenopodium quinoa* Willd.). *Food Sci Nutr* **9**:574–582 (2021).
- 5 Singh M, Malhotra N, and Sharma K. Buckwheat (*Fagopyrum* sp.) genetic resources: What can they contribute towards nutritional security of changing world? *Genet Resour Crop Evol* **67**:1639–1658 (2020).
- 6 Galante M, Flaviis R De, Boeris V, and Spelzini D. Effects of the enzymatic hydrolysis treatment on functional and antioxidant properties of quinoa protein acid-induced gels. *LWT* **118**:108845 (2020).
- 7 Navruz-Varli S and Sanlier N. Nutritional and health benefits of quinoa (*Chenopodium quinoa* Willd.). *J Cereal Sci Academic Press*; **69**:371–376 (2016).
- 8 Giménez-Bastida JA and Zieliński H. Buckwheat as a Functional Food and Its Effects on Health. *J Agric Food Chem* **63**:7896–7913 (2015).
- 9 Sabbione AC, Nardo AE, Añón MC, and Scilingo A. Amaranth peptides with antithrombotic activity released by simulated gastrointestinal digestion. *J Funct Foods* **20**:204–214 (2016).
- 10 Orsini Delgado MC, Nardo A, Pavlovic M, Rogniaux H, Añón MC, and Tironi VA. Identification and characterization of antioxidant peptides obtained by gastrointestinal digestion of amaranth proteins. *Food Chem* **197**:1160–1167 (2016).
- 11 Mudgil P, Omar LS, Kamal H, Kilari BP, and Maqsood S. Multi-functional bioactive properties of intact and enzymatically hydrolysed quinoa and amaranth proteins. *LWT* **110**:207–213 (2019).
- 12 Tomé Constantino AB and Garcia-Rojas EE. Modifications of physicochemical and functional properties of amaranth protein isolate (*Amaranthus cruentus* BRS Alegria) treated with high-intensity ultrasound. *J Cereal Sci* **95**:103076 (2020).
- 13 Roa DF, Buera MP, Tolaba MP, and Santagapita PR. Encapsulation and Stabilization of β -Carotene in Amaranth Matrices Obtained by Dry and Wet Assisted Ball Milling. *Food Bioprocess Technol* **10**:512–521 (2017).
- 14 Yu C, Cha Y, Wu F, Xu X, Qin Y, Li X, and Du M. Effects of high-pressure homogenisation on structural and functional properties of mussel (*Mytilus edulis*) protein isolate. *Int J Food Sci Technol* **53**:1157–1165 (2018).
- 15 Kierulf A, Whaley J, Liu W, Enayati M, Tan C, Perez-Herrera M, You Z, and Abbaspourrad A. Protein content of amaranth and quinoa starch plays a key role in their ability as Pickering emulsifiers. *Food Chem* **315**:126246 (2020).
- 16 Martínez JH, Velázquez F, Burrieza HP, Martínez KD, Paula Domínguez Rubio A, Santos Ferreira C dos, Pilar Buera M del, and Pérez OE. Betanin loaded nanocarriers based on quinoa seed 11S globulin. Impact on the protein structure and antioxidant activity. *Food Hydrocoll* **87**:880–890 (2019).
- 17 Condés MC, Añón MC, Mauri AN, and Dufresne A. Amaranth protein films reinforced with maize starch nanocrystals. *Food Hydrocoll* **47**:146–157 (2015).

- 18 Mirmoghtadaie L, Shojaee Aliabadi S, and Hosseini SM. Recent approaches in physical modification of protein functionality. *Food Chem Elsevier Ltd*; **199**:619–627 (2016).
- 19 Cordero-de-los-Santos MY, Osuna-Castro JA, Borodanenko A, and Paredes-López O. Physicochemical and Functional Characterisation of Amaranth (*Amaranthus hypochondriacus*) Protein Isolates Obtained by Isoelectric Precipitation and Micellisation. *Food Sci Technol Int* **11**:269–280 (2005).
- 20 Shen Y, Tang X, and Li Y. Drying methods affect physicochemical and functional properties of quinoa protein isolate. *Food Chem Elsevier Ltd*; **339**:127823 (2021).
- 21 Boutureira O and Bernardes GJL. Advances in chemical protein modification. *Chem Rev* **115**:2174–2195 (2015).
- 22 Vojdani F. Solubility. In: Hall GM, ed. *Methods of testing protein functionality* 1 ed. London: Blackie Academic & Professional; p. 11–60 1996.
- 23 Condés MC, Scilingo AA, and Añón MC. Characterization of amaranth proteins modified by trypsin proteolysis. Structural and functional changes. *LWT - Food Sci Technol Academic Press*; **42**:963–970 (2009).
- 24 Condés MC, Speroni F, Mauri A, and Añón MC. Physicochemical and structural properties of amaranth protein isolates treated with high pressure. *Innov Food Sci Emerg Technol* **14**:11–17 (2012).
- 25 Mir NA, Riar CS, and Singh S. Structural modification of quinoa seed protein isolates (QPIs) by variable time sonification for improving its physicochemical and functional characteristics. *Ultrason Sonochem* **58**:104700 (2019).
- 26 Tang C-H. Functional properties and in vitro digestibility of buckwheat protein products: Influence of processing. *J Food Eng Elsevier*; **82**:568–576 (2007).
- 27 Tomotake H, Shimaoka I, Kayashita J, Nakajoh M, and Kato N. Physicochemical and Functional Properties of Buckwheat Protein Product. *J Agric Food Chem American Chemical Society*; **50**:2125–2129 (2002).
- 28 López-Castejón ML, Bengoechea C, Díaz-Franco J, and Carrera C. Interfacial and Emulsifying Properties of Quinoa Protein Concentrates. *Food Biophys* **15**:122–132 (2020).
- 29 Vera A, Valenzuela MA, Yazdani-Pedram M, Tapia C, and Abugoch L. Conformational and physicochemical properties of quinoa proteins affected by different conditions of high-intensity ultrasound treatments. *Ultrason Sonochem* **51**:186–196 (2019).
- 30 GUO X and YAO H. Fractionation and characterization of tartary buckwheat flour proteins. *Food Chem* **98**:90–94 (2006).
- 31 Wu L, Li J, Wu W, Wang L, Qin F, and Xie W. Effect of extraction pH on functional properties, structural properties, and in vitro gastrointestinal digestion of tartary buckwheat protein isolates. *J Cereal Sci Academic Press*; **101**:103314 (2021).
- 32 Vondel J Van de, Lambrecht MA, and Delcour JA. Osborne extractability and chromatographic separation of protein from quinoa (*Chenopodium quinoa* Willd.) wholemeal. *LWT* **126** (2020).

- 33 Osborne TB. The proteins of the wheat kernel. Washington, D.C.: Carnegie Institution of Washington,; 1907.
- 34 Cortez-Trejo MC, Mendoza S, Loarca-Piña G, and Figueroa-Cárdenas JD. Physicochemical characterization of protein isolates of amaranth and common bean and a study of their compatibility with xanthan gum. *Int J Biol Macromol Elsevier B.V.*; **166**:861–868 (2021).
- 35 Mir NA, Riar CS, and Singh S. Effect of pH and holding time on the characteristics of protein isolates from Chenopodium seeds and study of their amino acid profile and scoring. *Food Chem Elsevier Ltd*; **272**:165–173 (2019).
- 36 Figueroa-González JJ, Lobato-Calleros C, Vernon-Carter EJ, Aguirre-Mandujano E, Alvarez-Ramirez J, and Martínez-Velasco A. Modifying the structure, physicochemical properties, and foaming ability of amaranth protein by dual pH-shifting and ultrasound treatments. *LWT Academic Press*; **153**:112561 (2022).
- 37 Deleu LJ, Lambrecht MA, Vondel J Van de, and Delcour JA. The impact of alkaline conditions on storage proteins of cereals and pseudo-cereals. *Curr Opin Food Sci Elsevier Ltd*; **25**:98–103 (2019).
- 38 Ayala-Niño A, Rodríguez-Serrano GM, González-Olivares LG, Contreras-López E, Regal-López P, and Cepeda-Saez A. Sequence Identification of Bioactive Peptides from Amaranth Seed Proteins (*Amaranthus hypochondriacus* spp.). *Molecules MDPI AG*; **24**:3033 (2019).
- 39 Chen X, Chen Y, Li J, Wang Y, and Yang X. Enzyme-assisted development of biofunctional polyphenol-enriched buckwheat protein: physicochemical properties, in vitro digestibility, and antioxidant activity. *J Sci Food Agric John Wiley and Sons Ltd*; **99**:3176–3185 (2019).
- 40 Das D, Mir NA, Chandla NK, and Singh S. Combined effect of pH treatment and the extraction pH on the physicochemical, functional and rheological characteristics of amaranth (*Amaranthus hypochondriacus*) seed protein isolates. *Food Chem Elsevier Ltd*; **353**:129466 (2021).
- 41 Ruiz GA, Xiao W, Boekel M van, Minor M, and Stieger M. Effect of extraction pH on heat-induced aggregation, gelation and microstructure of protein isolate from quinoa (*Chenopodium quinoa* Willd). *Food Chem* **209**:203–210 (2016).
- 42 Abugoch LE, Romero N, Tapia CA, Silva J, and Rivera M. Study of Some Physicochemical and Functional Properties of Quinoa (*Chenopodium Quinoa* Willd) Protein Isolates. *J Agric Food Chem American Chemical Society*; **56**:4745–4750 (2008).
- 43 Baker PW and Charlton A. A comparison in protein extraction from four major crop residues in Europe using chemical and enzymatic processes-a review. *Innov Food Sci Emerg Technol Elsevier*; **59**:102239 (2020).
- 44 Chen XW, Luo DY, Chen YJ, Wang JM, Guo J, and Yang XQ. Dry fractionation of surface abrasion for polyphenol-enriched buckwheat protein combined with hydrothermal treatment. *Food Chem Elsevier Ltd*; **285**:414–422 (2019).
- 45 GROSSMAN M V., RAO CS, and SILVA RSF DA. EXTRACTION OF PROTEINS FROM BUCKWHEAT BRAN. *J Food Biochem John Wiley & Sons, Ltd*; **4**:181–188 (1980).

- 46 Ghumman A, Mudgal S, Singh N, Ranjan B, Kaur A, and Rana JC. Physicochemical, functional and structural characteristics of grains, flour and protein isolates of Indian quinoa lines. *Food Res Int* Elsevier Ltd; **140**:109982 (2021).
- 47 Mota C, Santos M, Mauro R, Samman N, Matos AS, Torres D, and Castanheira I. Protein content and amino acids profile of pseudocereals. *Food Chem* Elsevier Ltd; **193**:55–61 (2016).
- 48 Avanza MV and Añón MC. Effect of thermal treatment on the proteins of amaranth isolates. *J Sci Food Agric* **87**:616–623 (2007).
- 49 Condés MC, Añón MC, and Mauri AN. Amaranth protein films from thermally treated proteins. *J Food Eng* **119**:573–579 (2013).
- 50 Scilingo AA, Molina Ortiz SE, Martínez EN, and Añón MC. Amaranth protein isolates modified by hydrolytic and thermal treatments. Relationship between structure and solubility. *Food Res Int* **35**:855–862 (2002).
- 51 Mäkinen OE, Zannini E, and Arendt EK. Modifying the Cold Gelation Properties of Quinoa Protein Isolate: Influence of Heat-Denaturation pH in the Alkaline Range. *Plant Foods Hum Nutr* **70**:250–256 (2015).
- 52 Wang L, Dong J, Zhu Y, Shen R, Wu L, and Zhang K. Effects of microwave heating, steaming, boiling and baking on the structure and functional properties of quinoa (*Chenopodium quinoa* Willd.) protein isolates. *Int J Food Sci Technol* Blackwell Publishing Ltd; **56**:709–720 (2021).
- 53 Mir NA, Riar CS, and Singh S. Improvement in the functional properties of quinoa (*Chenopodium quinoa*) protein isolates after the application of controlled heat-treatment: Effect on structural properties. *Food Struct* Elsevier Ltd; **28**:100189 (2021).
- 54 Cerdán-Leal MA, López-Alarcón CA, Ortiz-Basurto RI, Luna-Solano G, and Jiménez-Fernández M. Influence of heat denaturation and freezing–lyophilization on physicochemical and functional properties of quinoa protein isolate. *Cereal Chem* Wiley-Blackwell; **97**:373–381 (2020).
- 55 Ruiz GA, Opazo-Navarrete M, Meurs M, Minor M, Sala G, Boekel M van, Stieger M, and Janssen AEM. Denaturation and in Vitro Gastric Digestion of Heat-Treated Quinoa Protein Isolates Obtained at Various Extraction pH. *Food Biophys* **11**:184–197 (2016).
- 56 Deng Y, Padilla-Zakour O, Zhao Y, and Tao S. Influences of High Hydrostatic Pressure, Microwave Heating, and Boiling on Chemical Compositions, Antinutritional Factors, Fatty Acids, In Vitro Protein Digestibility, and Microstructure of Buckwheat. *Food Bioprocess Technol* **8**:2235–2245 (2015).
- 57 Choi S-M and Ma C-Y. Conformational Study of Globulin from Common Buckwheat (*Fagopyrum esculentum* Moench) by Fourier Transform Infrared Spectroscopy and Differential Scanning Calorimetry. *J Agric Food Chem* American Chemical Society; **53**:8046–8053 (2005).
- 58 Choi S-M, Mine Y, and Ma C-Y. Characterization of heat-induced aggregates of globulin from common buckwheat (*Fagopyrum esculentum* Moench). *Int J Biol Macromol* Elsevier; **39**:201–209 (2006).
- 59 Vera A, Valenzuela MA, Yazdani-Pedram M, Tapia C, and Abugoch L. Conformational and physicochemical properties of quinoa proteins affected by

- different conditions of high-intensity ultrasound treatments. *Ultrason Sonochem* **51**:186–196 (2019).
- 60 Qin X-S, Luo Z-G, and Peng X-C. Fabrication and Characterization of Quinoa Protein Nanoparticle-Stabilized Food-Grade Pickering Emulsions with Ultrasound Treatment: Interfacial Adsorption/Arrangement Properties. *J Agric Food Chem* **66**:4449–4457 (2018).
 - 61 Li X, Da S, Li C, Xue F, and Zang T. Effects of high-intensity ultrasound pretreatment with different levels of power output on the antioxidant properties of alcalase hydrolyzates from Quinoa (*Chenopodium quinoa* Willd.) protein isolate. *Cereal Chem Wiley-Blackwell*; **95**:518–526 (2018).
 - 62 Jin J, Okagu OD, Yagoub AEA, and Udenigwe CC. Effects of sonication on the in vitro digestibility and structural properties of buckwheat protein isolates. *Ultrason Sonochem Elsevier B.V.*; **70**:105348 (2021).
 - 63 Xue F, Wu Z, Tong J, Zheng J, and Li C. Effect of combination of high-intensity ultrasound treatment and dextran glycosylation on structural and interfacial properties of buckwheat protein isolates. *Biosci Biotechnol Biochem* **81**:1891–1898 (2017).
 - 64 Teng C, Xing B, Fan X, Zhang B, Li Y, and Ren G. Effects of Maillard reaction on the properties and anti-inflammatory, anti-proliferative activity in vitro of quinoa protein isolates. *Ind Crops Prod Elsevier*; **174**:114165 (2021).
 - 65 Guo X and Xiong YL. Characteristics and functional properties of buckwheat protein–sugar Schiff base complexes. *LWT - Food Sci Technol* **51**:397–404 (2013).
 - 66 BeMiller JN. Pasting, paste, and gel properties of starch–hydrocolloid combinations. *Carbohydr Polym* **86**:386–423 (2011).
 - 67 Yang C, Zhong F, Douglas Goff H, and Li Y. Study on starch-protein interactions and their effects on physicochemical and digestible properties of the blends. *Food Chem* **280**:51–58 (2019).
 - 68 Ventureira JL, Martínez EN, and Añón MC. Effect of acid treatment on structural and foaming properties of soy amaranth protein mixtures. *Food Hydrocoll* **29**:272–279 (2012).
 - 69 Condés MC, Añón MC, Mauri AN, and Dufresne A. Amaranth protein films reinforced with maize starch nanocrystals. *Food Hydrocoll* **47**:146–157 (2015).
 - 70 Escamilla-García M, Delgado-Sánchez LF, Ríos-Romo RA, García-Almendárez BE, Calderón-Domínguez G, Méndez-Méndez JV, Amaro-Reyes A, Pierro P Di, and Regalado-González C. Effect of Transglutaminase Cross-Linking in Protein Isolates from a Mixture of Two Quinoa Varieties with Chitosan on the Physicochemical Properties of Edible Films. *Coatings MDPI AG*; **9**:736 (2019).
 - 71 Romo I, Abugoch L, and Tapia C. Soluble complexes between chenopodins and alginate/chitosan: Intermolecular interactions and structural-physicochemical properties. *Carbohydr Polym Elsevier Ltd*; **227**:115334 (2020).
 - 72 Abugoch LE, Tapia C, Villamán MC, Yazdani-Pedram M, and Díaz-Dosque M. Characterization of quinoa protein–chitosan blend edible films. *Food Hydrocoll* **25**:879–886 (2011).
 - 73 Montellano Duran N, Galante M, Spelzini D, and Boeris V. The effect of carrageenan

- on the acid-induced aggregation and gelation conditions of quinoa proteins. *Food Res Int* **107**:683–690 (2018).
- 74 Wang X, Ullah N, Sun X, Guo Y, Chen L, Li Z, and Feng X. Development and characterization of bacterial cellulose reinforced biocomposite films based on protein from buckwheat distiller's dried grains. *Int J Biol Macromol* **96**:353–360 (2017).
- 75 Condés MC, Añón MC, and Mauri AN. Amaranth protein films prepared with high-pressure treated proteins. *J Food Eng* **166**:38–44 (2015).
- 76 Lee C, Lee W, Han Y, and Oh S. Effect of Proteolysis with Alkaline Protease Following High Hydrostatic Pressure Treatment on IgE Binding of Buckwheat Protein. *J Food Sci* Blackwell Publishing Inc.; **82**:834–839 (2017).
- 77 Ventureira J, Martínez EN, and Añón MC. Stability of oil: Water emulsions of amaranth proteins. Effect of hydrolysis and pH. *Food Hydrocoll* **24**:551–559 (2010).
- 78 Chen K, Zhang M, Mujumdar A S, and Wang H. Quinoa protein-gum Arabic complex coacervates as a novel carrier for eugenol: Preparation, characterization and application for minced pork preservation. *Food Hydrocoll* **120**: 106915 (2021).

**CAPÍTULO III. MODIFICATIONS OF PHYSICOCHEMICAL AND
FUNCTIONAL PROPERTIES OF AMARANTH (*AMARANTHUS
CRUENTUS* BRS ALEGRIA) PROTEIN ISOLATE TREATED WITH
HIGH-INTENSITY ULTRASOUND.**

Published in 2020 at Journal of Cereal Science 95 (2020) 103076.
DOI: <https://doi.org/10.1016/j.jcs.2020.103076>

Abstract

The present study investigated the effects of high-intensity ultrasound (HIUS) on the physicochemical and functional properties of amaranth protein isolates (API). Aqueous dispersions of API (10%) were continuously treated for 15 or 30 min with ultrasound equipment (100 W, 30 kHz) at 30, 60, and 90% amplitudes. The electrophoresis technique demonstrated no changes in the molar masses of the proteins. However, HIUS significantly increased the surface free sulfhydryl groups (SH) and changed the surface hydrophobicity, indicating a breakdown of internal links that maintained the native API structure. Ultrasound reduced the size of the particles in the aqueous dispersions of API, suggesting the dissociation of aggregates from API. The results showed that the solubility in most HIUS-treated API was significantly ($p < 0.05$) higher than that of the native proteins at pH 7. The energy density of 50 J/cm^3 provided the best-combined properties of emulsion formation and stability. These results suggest that HIUS is a useful technology to improve the functional properties of amaranth proteins.

Keywords: Pseudocereal; Solubility; Emulsifying properties; High-intensity ultrasound.

1 Introduction

Amaranth (*Amaranthus cruentus* BRS Alegria) is a pseudocereal with a relatively short life cycle that requires little water, and it is capable of growing at a wide range of altitudes. These advantages, including its low cost, are responsible for its current growing use and application in food production (Fabio and Parraga, 2017). Amaranth has a high protein content (~ 14%) compared to many common cereals, such as wheat (~ 10%) and rice (~ 7%) (Acosta et al., 2016; Janssen et al., 2017; Vilcacundo et al., 2018). It also contains a considerable amount of hydrophobic amino acids (~34%) (Mota et al., 2016), and essential amino acids, such as methionine and lysine, which are rare in other cereals (Condés et al., 2012; Janssen et al., 2017). Amaranth is a useful and promising crop primarily because it is an alternative to alleviate the growing need for food in some developing countries (Fabio and Parraga, 2017). This pseudocereal has several health benefits, such as antithrombotic (Sabbione et al., 2016), and antioxidant (Orsini Delgado et al., 2016) activities. Amaranth does not contain gluten, and therefore, it is suitable for people with gluten allergies (Janssen et al., 2017).

The protein fractions of amaranth are primarily composed of albumin (~ 65%) and globulin (~ 17%), but prolamin (~ 11%) and glutelin (~ 7%) are also present (Janssen et al., 2017). The globulins of amaranth are amarantin (11S) and vicilin-like globulin (7S). The 11S subunit is the main globulin fraction in amaranth, and it is glycosylated and phosphorylated. Under reduced and denaturation conditions for electrophoresis (SDS-PAGE), it produces three main polypeptides with molar masses that vary between 50 and 64 kDa, 33 and 37 kDa, and 18 and 25 kDa. The hetero-oligomer globulin (the 7S) is in minor proportion in amaranth protein and presents 8 subunits with molar masses of 90, 71, 40, 37, 35, 31, 24, and 16 kDa (Condés et al., 2012; Janssen et al., 2017). The 11S, prolamin, and glutelin fractions have poor solubility in water (Janssen et al., 2017), which makes its application difficult in certain food systems. Therefore, some authors tried to improve this poor solubility via physical changes. For example, Scilingo et al. (2002) studied the effects of enzymatic hydrolysis and heating on amaranth protein isolate (API) and observed that hydrolysis with papain and heating of these hydrolysates were the only conditions that offered high solubility. Condés et al. (2012) observed a reduction in solubility when evaluating the effect of high pressures on API. Avanza and Añón (2007) also observed a decrease in water solubility when they subjected API to heat treatment. These results show the difficulty of inserting these proteins in water-based food systems. The use of enzymes is also relatively expensive and makes it even more difficult to apply API. Therefore, it is necessary to examine other methods of modification.

High-intensity ultrasound treatment (HIUS), with frequencies between 20 - 100 kHz and intensities over 1 W/cm², is a relatively new technology in the food industry, but it is widely used to produce changes in different products or in the processes in which they are used (Ozuna et al., 2015). The effects of HIUS on food structures are attributed to ultrasonic cavitation, rapid bubble formation, and collapse (O'Sullivan et al., 2017). Cavitation occurs in a short span of time in an aqueous medium via turbulent movement, intense hydrodynamic shear forces, likely free radical formation and increased pressures (up to 100 MPa) and temperature (up to 5000 K) (O'Sullivan et al., 2017; Zhu et al., 2018). The large shear forces generated can break inter and intramolecular bonds, mainly the noncovalent and, in some cases, covalent bonds (disulfide), which in turn may lead to fragmentation of aggregates (Chandrapala et al., 2011; Jambrak et al., 2014).

Many authors applied HIUS on plant-based proteins to understand its effect on physicochemical properties and functionalities. Vera et al. (2019) observed an increase in solubility of quinoa proteins after HIUS treatment and related this improvement to the formation of soluble protein aggregates, and the increases in α -helix and fluorescence

intensity. In addition to quinoa, studies of effects of HIUS on pseudocereal proteins are limited in the literature. However, there are works on other proteins such as that reported by Zhu et al. (2018), who applied HIUS (25 kHz) for 15 and 30 min in walnut protein isolate and finding a 22% of increase of water-solubility. In another study, Jiang et al. (2014) reported an increase of solubility of black beans protein isolate when HIUS (20 kHz, 300W) was applied for 12 min. Similarly, several authors applied HIUS to soy protein isolate and observed an improvement in their functional properties (O'Sullivan et al., 2017). Many times these improvements can be related to the changes in the protein secondary structure (such as the increase in α -helix or β -sheet), as well as the changes in the tertiary structure which can be observed, for example, by an increase of free surface sulfhydryl groups or surface hydrophobicity, and finally can be attributed to physical changes such as reduction on particle sizes. However, no studies demonstrated the effects of ultrasonic treatment on the physicochemical and functional properties of API.

Therefore, the present work studied the effects of HIUS on the physicochemical properties of API to determine the ideal HIUS parameters and evaluate its effects on solubility and emulsifying properties.

2 Materials and methods

2.1 Materials

Amaranth grains (*Amaranthus cruentus* BRS alegria) were purchased from Relva Verde Alimentos EIRELI (São Paulo, Brazil), and soybean oil was purchased from the local market (Volta Redonda, Brazil). Bromophenol blue (BPB), Coomassie G-250 and low-range standard proteins for electrophoresis [phosphorylase b (97.5 kDa), bovine serum albumin (66.2 kDa), ovalbumin (45 kDa), carbonic anhydrase (31.5 kDa), soybean trypsin inhibitor (21.5 kDa) and lysozyme (14.4 kDa)] were purchased from Bio-Rad Laboratories (California, USA). Sodium dodecyl sulphate (SDS), Tris base and glycine were acquired from Vetec Química Fina (Rio de Janeiro, Brazil). 5,5-Dithiobis-2-nitrobenzoic acid (DTNB) was purchased from Sigma-Aldrich (St. Louis, USA). Ultrapure water with a conductivity of 0.05 μ S/cm (Gehaka-Master P&D, Brazil) and reagents of analytical grade were used for all analyses.

2.2 Preparation of amaranth protein isolate (API)

API was obtained according to the methodology of Martínez and Añón (1996), with some modifications. Once obtained, the amaranth flour was defatted with 95% ethanol (in a proportion of 1:10 w/v) for 24 h and dried at room temperature. The defatted flour was suspended in water, and the pH was adjusted to 9 using 2 mol/L NaOH. After mixing and stirring for 30 min, the suspension was centrifuged (Digicen 21 R, Orto Alresa, Spain) at 9000 g for 20 min. The supernatant was adjusted to pH 5.0 using 2 mol/L HCl, and the solution was centrifuged again at 4000 g for 10 min at 4 °C. The precipitate was resuspended in water, neutralized, and lyophilized (Enterprise I, Terroni, Brazil).

The proximate characterization of the final product was performed according to (AOAC, 2005) methods, namely, 920.87, 927.43, 920.85, and 945.15 for total proteins (micro-Kjeldahl), ash, crude fat, and moisture, respectively. The results were $84.12 \pm 2.15\%$ ($N \times 6.25$) of total proteins, $3.7 \pm 0.01\%$ of total ash, $3.89 \pm 0.10\%$ crude fat, and $4.50 \pm 0.01\%$ moisture.

2.3 Ultrasonic treatment of amaranth protein isolate (API)

Aqueous solutions (20 mL) containing 10% of API were submitted to ultrasonic treatment (UP 100H, Hielschier, Germany). The device had a titanium sonotrode probe (MS2, 2 mm in diameter) that provided continuous waves of 30 kHz and a power of 100 W. The ultrasound probe was submerged in the sample to a depth of 0.5 cm, and HIUS was performed for 15 or 30 min at amplitudes of 30%, 60%, and 90%. During HIUS, the temperatures of all solutions were maintained at 3.0 ± 1 °C in an ice bath. The energy densities applied to the solutions were calculated as 25, 35 or 51 J/cm³ and 29, 50 or 66 J/cm³ (ZHU et al., 2018) were used for the amplitude conditions 30, 60 or 90% for 15 and 30 min, respectively. The samples were lyophilized and kept at 4 °C in airtight containers until analyzed.

2.4 Physicochemical properties of the amaranth protein

2.4.1 Sodium dodecyl sulfate-polyacrylamide gel electrophoresis (SDS-PAGE)

The analyses of the molecular structures of the API (control and HIUS-treated) were performed according to the methodology described by Zhu et al. (2018), with some modifications, using a 15% separation gel and 5% packaging gel. Therefore, 180 µL of protein sample solutions (5 mg/mL) were mixed with 420 µL of buffer solution (2% SDS, 25% glycerol, 50 mM Tris-HCl (pH = 6.8), 0.1% BPB and 0.5% mercaptoethanol). The mixtures were heated for 5 min at 95 °C and cooled. Eight microliters of each mixture were loaded into gel wells mounted in electrophoresis equipment (SE 260, Hoefer, USA). The gel was stained with Coomassie G-250.

2.4.2 Surface hydrophobicity

The surface hydrophobicity of the samples was determined using the methodology described by Girard et al. (2018). For this procedure, 200 µL of BPB (1 mg/mL) was added to 1 mL of a protein solution (5 mg/mL) and mixed well. Deionized water was used instead of the protein solution as a control. The mixture was stirred for 10 min and centrifuged at 5590 g for 15 min. The absorbance of the supernatant was recorded at 595 nm using a UV-VIS spectrophotometer (Biomate 3S, Thermo Scientific, USA). The analyses were performed in 3 independent replicate experiments, and the hydrophobicity was calculated as:

$$BPB \text{ bond} = 200 \mu\text{g} \times (A \text{ control} - A \text{ sample}) / A \text{ control} \quad (1)$$

2.4.3 Free surface sulfhydryl groups

The free surface sulfhydryl group (SH) of the samples was determined according to the methodology described by Hu et al. (2013b), with minor modifications. Ellman's reagent was prepared with the addition of 4 mg DTNB to 1 mL of a buffer solution (0.086 M Tris, 0.09 M glycine, 4 mM EDTA, pH 8). This reagent (0.05 mL) was added to 5 mL of the protein solution (0.15%) previously prepared in the above buffer. The mixtures were incubated for 1 h at 25 ± 1 °C with shaking (TE-424, Tecnal, Brazil) at 200 rpm and centrifuged at 10,000 g for 15 min at room temperature. The supernatant was used to read the absorbance at a wavelength of 412 nm. The buffer with Ellman's reagent without protein samples served as the blank. To calculate SH micromoles per gram of protein, the molar extinction coefficient of 13600 M⁻¹ cm⁻¹ was used. The analyses were performed in 3 independent replicate experiments.

2.4.4 Particle size

For measurements of the hydrodynamic diameters of the samples, protein solutions (0.1%, w/v) were prepared via solubilization in ultrapure water. The pH was adjusted to 9.0 using 0.1 mol/L NaOH. The samples were filtered (0.45 μ m) before a determination using DLS (dynamic light scattering) in a Zetasizer Nano ZS90 (Malvern Instruments, United Kingdom) equipped with an He-Ne laser at a wavelength of 632.8 nm. The angle of detection was set at 90°. The measurements were performed with 3 technical repeats at 25 °C.

2.4.5 Zeta potential

The zeta potential was measured in a Zetasizer Nano ZS90. Protein solutions (0.1%) were prepared in ultrapure water. Determinations were made at different pH values (from 10 to 3), adjusted using 0.1 mol/L HCl or NaOH solutions. The downward variation in pH was 0.5 ± 0.05 units. The measurements were performed with 3 technical repeats at 25 °C.

2.5 Functional properties of the amaranth protein

2.5.1 Solubility

Analyses of the solubility of the protein samples were performed as described by Vojdani (1996). A 2.0% (w/v) API aqueous solution was prepared, and the solubility was evaluated at different pH values (11 to 2), adjusted using 0.1 mol/L HCl or NaOH. The downward variation in pH was 1.0 ± 0.05 units. The samples were left under slight agitation at the adjusted pH for 15 min and centrifuged at 8,000 g for 10 min at room temperature. Protein solubility was determined in 3 independent replicate experiments, and the results were expressed as a percentage, according to equation 2:

$$\text{Solubility (\%)} = 100 \times C_2/C_1 \quad (2)$$

where C_1 and C_2 are the concentrations of proteins in the samples before centrifugation and in the supernatant after centrifugation, respectively. Protein concentration was determined using the Biuret method (Pinckney, 1961) with bovine serum albumin (BSA, Sigma-Aldrich, USA) as the standard, and absorbance was read at 550 nm ($Y = 0.0507X$; $R^2 = 0.99$).

2.5.2 Emulsifying properties

Emulsifying properties were evaluated using the emulsifying activity index (EAI) and the emulsion stability index (ESI) as described by Zhu et al. (2018), with some modifications. Ten milliliters of aqueous API solutions (10 mg/mL) was added to 3.3 mL of soybean oil. The mixture was homogenized using an ultraturax (T25D, IKA, Germany) at 24,000 rpm for 2 min. A sample of 0.05 mL was taken from the bottom of the falcon tube and diluted in a solution of 4.95 ml of 0.1% (w/v) SDS. The mixture was vortexed for 5 seconds, and the absorbance was read at 500 nm against the blank of the SDS solution and water without sample. EAI and ESI were determined in 3 independent replicate experiments, and calculated according to equations 3 and 4, respectively:

$$EAI (m^2/g) = (4.604 \times DF \times A_0)/(C \times \theta \times \square \times 10000) \quad (3)$$

$$ESI (min) = (A_0 \times 10)/(A_0 - A_{10}) \quad (4)$$

where DF is the emulsion dilution factor (100), A_0 is the absorbance at minute 0 after the formation of the emulsion, A_{10} is the absorbance at minute 10, 10 is the variation of time between the two absorbance readings, C is the concentration of the initial sample (0.1 g/mL),

θ is the length of the light path in the cuvette (0.01 m), and \square is the fraction of oil in the initial emulsion (0.25).

2.6 Statistical analysis

One-way analysis of variance (ANOVA) and Tukey's test was used to establish the significance of differences among the mean values at the 0.05 significance level. Statistical analysis was performed with the software Origin[®] 8.5 (OriginLab Corporation, USA).

3 Results and discussion

3.1 Effects of ultrasound on the physicochemical properties of amaranth protein isolate (API)

3.1.1 SDS-PAGE

Figure 10 shows the electrophoretic profiles of API (native and HIUS). The native API showed the typical pattern for amaranth proteins (Condés et al., 2012; Janssen et al., 2017; Martínez and Añón, 1996), with the presence of polypeptides corresponding to the subunits of 7S globulin [\sim 72.2 kDa (a)] and 11S globulins [\sim 50.9 kDa (b), \sim 35.9 kDa (c) and \sim 28.2 kDa (d)]. Compared with the control, none of the treatments produced significant changes in the electrophoretic patterns. This result suggests that HIUS did not alter the molar masses of API. These findings are consistent with O'Sullivan et al. (2016), who found no significant differences in the molecular structures of wheat or soy proteins after ultrasound treatment (\sim 34 W/cm²). Jiang et al. (2014) also applied high intensities (72 to 120 W/cm²) to black bean protein isolate and did not observe any molecular alterations. In contrast, some researchers observed a decrease of molar masses of protein after ultrasonic treatment, such as jackfruit protein isolate (Resendiz-Vazquez et al., 2017). Also, in some cases, it is possible to observe an increase in molar masses as observed for quinoa proteins (Vera et al., 2019). These differences may be attributed to several factors, including the nature of the protein, ultrasonication conditions, and solution conditions (Zhu et al., 2018).

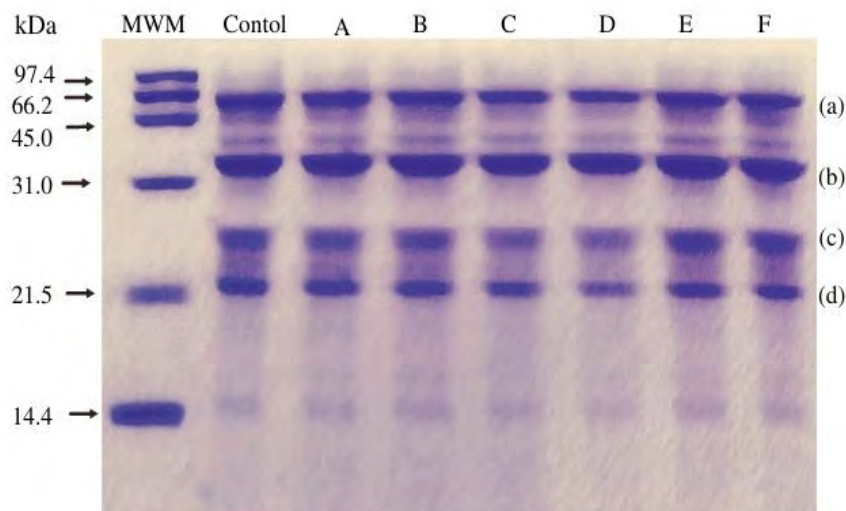


Figure 10. SDS-PAGE electrophoretic profiles of native and high-intensity ultrasound treated API. MWM) is the marker; Control) is the native API; A) 30%, 15 min; B) 60%, 15 min; C) 90%, 15 min; D) 30%, 30 min; E) 60%, 30 min; F) 90%, for 30 min.

3.1.1 Particle size

Table 5 presents the results of particle sizes of API treated and untreated by HIUS. The results show that HIUS increased particle sizes of API from 414.40 ± 32.35 to 478.67 ± 15.02 d nm (hydrodynamic diameter in nanometer) at 30% of amplitude and 15 min. After that, the particle sizes decreased considerably in all treatments, where treatment D presented the smallest value (38.96 d nm with 92.7% of volume fraction). Furthermore, an increase in HIUS time to 30 min favored reduction of particle sizes for low (30%) amplitude, while the treatments of 60 and 90% of amplitudes not presented considerable changes. According to Jiang et al (2014), the low-power of HIUS may cause turbulent forces and micro-streaming which can increase the speed of collision and aggregation, resulting in the formation of some unstable aggregates and an increase in the particles sizes. Then, when the power of HIUS is increased these unstable aggregates are violently broken up into smaller soluble protein aggregates. This may explain what occurred in the present study, where treatment A presented larger sizes and then reduced in subsequent treatments where the amplitude was increased. The reduction in particle sizes after HIUS has also been reported for other proteins, such as nut protein isolate (Zhu et al., 2018), soy protein isolate, wheat protein isolate (O’Sullivan et al., 2016), and whey protein isolate (Jambrak et al., 2014). However, very-intense HIUS and/or his application for prolonged periods can promote extensive protein denaturation and favor the formation of aggregates, trough noncovalent bonds such as hydrophobic interactions of exposed regions during the process (Chandrapala et al., 2011; Zhu et al., 2018). This phenomenon can explain the results of treatments of 30 min, where considerably larger particle sizes were observed in treatments E and F compared to treatment D. Similarly, Zhu et al. (2018) observed that the mean particle size of walnut protein isolate was higher when the samples were treated at 600W for 30 min than at 600W for 15 min. Thus, the sonication conditions should be optimized to ensure efficient protein aggregate disruption, without promoting excessive protein denaturation.

Table 5. Effect of high-intensity ultrasound treatment on the hydrodynamic diameter of API expressed in volume (%).

Treatment (Amplitude, time)	Size 1 (dnm)	Size 2 (dnm)	Size 3 (dnm)	Size 1 (%)	Size 2 (%)	Size 3 (%)
Control (native API)	414.40 ± 32.35	53.32 ± 30.72	0	81.43	18.57	0
A (30%, 15 min)	478.67 ± 15.02	143.44 ± 35.63	0	93.40	6.60	0
B (60%, 15 min)	345.06 ± 18.18	39.11 ± 19.09	0	96.10	3.90	0
C (90%, 15 min)	221.30 ± 09.53	204.15 ± 35.63	0	86.40	13.23	0
D (30%, 30 min)	318.27 ± 11.64	198.73 ± 6.26	38.96 ± 19.09	1.30	6.00	92.7
E (60%, 30 min)	325.77 ± 18.91	150.63 ± 57.96	0	95.76	4.24	0
F (90%, 30 min)	216.78 ± 09.33	159.27 ± 2.33	0	94.33	5.67	0

The data are the means \pm standard of 3 technical repeats, d nm is the hydrodynamic diameter of API in nanometre and sizes 1, 2, and 3 are the different peaks of averages sizes in volume fraction measured by DLS.

3.1.2 Free surface sulfhydryl (SH) group

HIUS significantly increased the free SH group in the surface of API (Figure 11) and reached $\sim 66\%$ for treatment E (50 J/cm^3). The results indicate that increasing the HIUS time from 15 to 30 min show a significant presence of the free SH group. These results suggest that HIUS promoted small changes in the tertiary structure. Many studies (Hu et al., 2013a; Xiong et al.,

2018; Zhu et al., 2018) showed the same result, and the possible explanations are attributed to cavitation caused by ultrasound that lead to the breaking of some S - S bonds, which allows for the formation of new hydrogen bonds. This process may also be one of the causes of the decrease in particle sizes if intermolecular disulfide bonds were broken (Hu et al., 2013a). Additionally, the increase in the free SH group may be due to the partial unfolding of proteins caused by disruptive forces generated during ultrasonic treatment, which may allow some of the SH groups originally present inside the protein molecules to be exposed on their surfaces (Zhu et al., 2018). Besides, as observed in treatment F (66 J/cm³), when HIUS is more intense and prolonged can generate hydrogen peroxide that may oxidize susceptible functional groups, such as the SH thus allowing its decrease. The same phenomenon was observed for walnut proteins (Zhu et al., 2018).

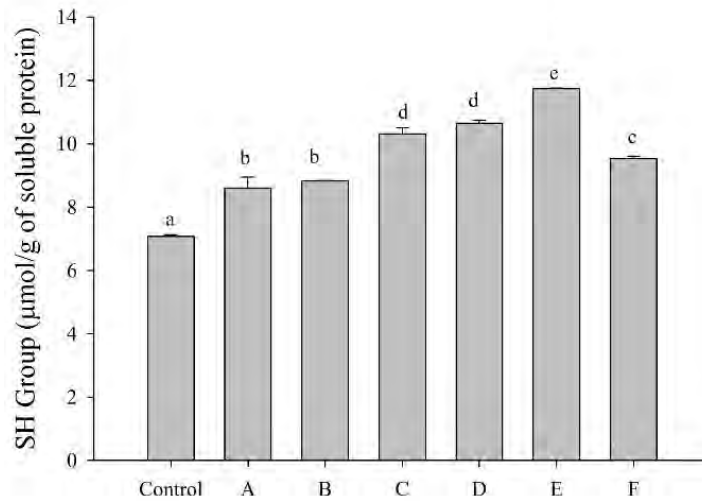


Figure 11. Effect of ultrasound on surface free sulfhydryl groups of API. Control) is the native API; A) 30%, 15 min; B) 60%, 15 min; C) 90%, 15 min; D) 30%, 30 min; E) 60%, 30 min; F) 90%, for 30 min. The results are mean \pm standard deviation of 3 independent replicate experiments. Values followed by the same letter do not differ statistically from each other ($p < 0.05$).

Table 6. Effect of high-intensity ultrasound treatment on API surface hydrophobicity.

Treatment (Amplitude, time)	Surface hydrophobicity (BPB bond, μg)
Control (native API)	110.78 \pm 0.16 ^{b c}
A (30%, 15 min)	112.95 \pm 0.32 ^{c d}
B (60%, 15 min)	108.80 \pm 0.55 ^{b c}
C (90%, 15 min)	103.54 \pm 0.23 ^a
D (30%, 30 min)	116.57 \pm 0.26 ^d
E (60%, 30 min)	121.05 \pm 2.35 ^e
F (90%, 30 min)	107.84 \pm 1.16 ^b

The data are shown as mean \pm standard deviation of 3 independent replicate experiments. Values followed by the same letter in the same columns do not differ statistically from each other ($p < 0.05$).

3.1.3 Surface hydrophobicity

The results of the surface hydrophobicity of native API and HIUS-treated are presented in Table 6. Surface hydrophobicity increased when HIUS time was increased from 15 min to 30 min, and the highest values were observed for the treatments D and E (116.57 ± 0.26 and $121.05 \pm 2.35 \mu\text{g}$ of BPB bonds, respectively). When compared the results of different HIUS amplitudes (30 to 60%), we observed an increase in surface hydrophobicity, but not the 90% amplitude decreased significantly. Presumably, HIUS caused changes in the API tertiary structure, which altered the local environment of hydrophobic amino acids. In consistence with particle size results, increases in surface hydrophobicity observed in treatment D and E are related to the denaturation of proteins due to prolonged time of HIUS. Increases in surface hydrophobicity were also reported for proteins isolated from black beans (Jiang et al., 2014), soybeans (Hu et al., 2013a), and peas (Xiong et al., 2018). Moreover, the surface hydrophobicity of protein treated with high-amplitudes of HIUS tends to decrease due to the formation of protein aggregates, which can protect the hydrophobic regions. Also, in these treatments the extensions of non-covalent bonds may be increased, leading to a reduction in surface hydrophobicity (Chandrapala et al., 2011; Jiang et al., 2014).

3.1.4 Zeta potential

Figure 12A shows the results of zeta potentials of native and HIUS-treated API. All samples showed positive charges at pH values below ~ 4.7 , and the opposite result occurred at pH values above ~ 4.7 . The isoelectric point (pI) of native API was 4.61 ± 0.01 and was slightly modified by the ultrasound treatment, with the highest value observed in treatment B (35 J/cm^3 , $\text{pI} = 4.80$). These results are consistent with the mean isoelectric points reported in the literature, which were between 4.5 and 6.5 for different amaranth protein fractions (Ventureira et al., 2012). At neutral pH (Figure 13), we observed that the ultrasonic treatment slightly increased the negative value of the zeta potential of all samples, with the highest value found in treatment B (from -21.67 ± 0.71 to $-26.33 \pm 0.38 \text{ mV}$). The phenomenon observed at $\text{pH} = 7$ was similar at $\text{pH} = 3.5$ and pH values between 6.5 to 8.5. The increase in these negative charges confirms that HIUS promoted partial changes of the API tertiary structure, in agreement with the free SH group and surface hydrophobicity results. Therefore, HIUS reinforced the electrostatic repulsion in such a way that it prevented further aggregations of API at the end of treatments. The literature reported that the stability of colloidal solutions was achieved with absolute values of zeta potential greater than 20 mV (Shen et al., 2017). Jiang et al. (2014) had similar results in their study with black bean protein isolate.

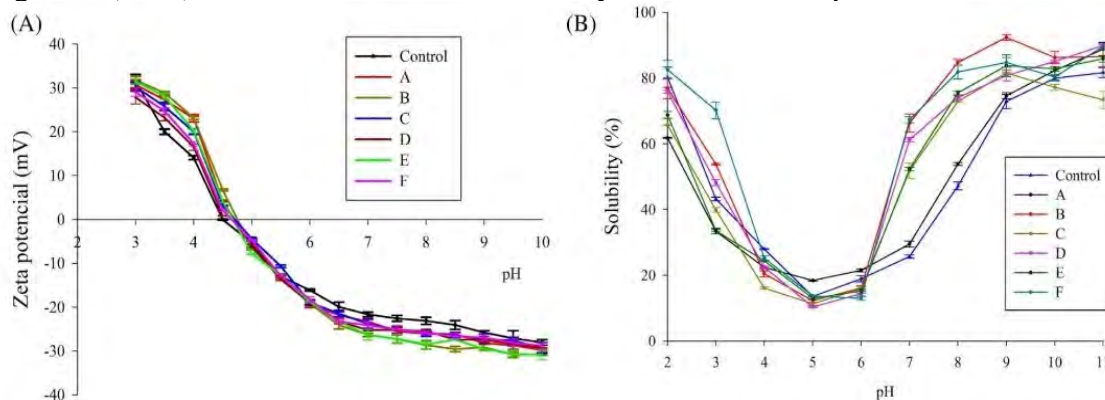


Figure 12. Effect of ultrasound and pH on (A) the zeta potential and (B) solubility (%) of API. Control is the native API; A) 30%, 15 min; B) 60%, 15 min; C) 90%, 15 min; D) 30%, 30 min; E) 60%, 30 min; F) 90%, for 30 min. The results are mean \pm standard deviation of 3 technical repeats for Fig. A, and 3 independent replicate experiments for Fig. B.

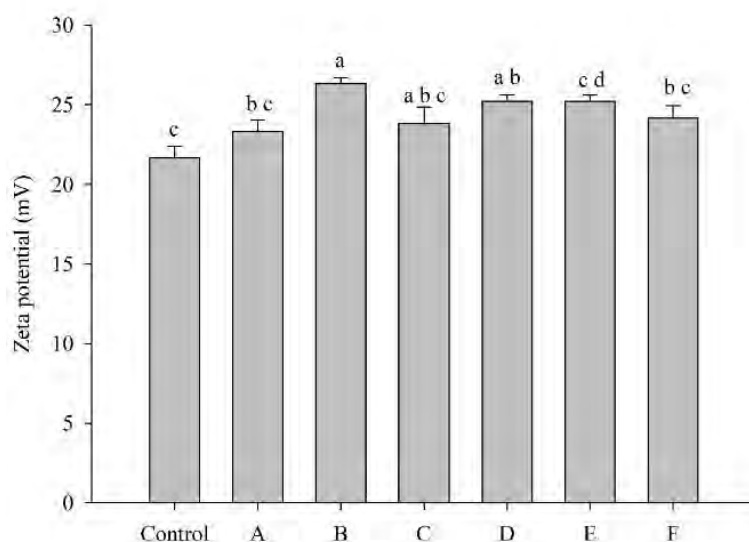


Figure 13. The absolute value of Zeta potential (mV) of native and high-intensity ultrasound treated amaranth protein isolate at pH 7. Control) is the native API; A) 30%, 15 min; B) 60%, 15 min; C) 90%, 15 min; D) 30%, 30 min; E) 60%, 30 min; F) 90%, for 30 min. . The results are mean \pm standard deviation of 3 technical repeats. Values followed by the same letter in the columns do not differ statistically from each other ($p < 0.05$).

3.2 Effects of ultrasound on the functional properties of amaranth protein isolates (API)

3.2.1 Solubility

Figure 12B shows the results of API solubility (%) as a function of pH variation (2.0 to 11.0) and HIUS. Most improvements of solubility were observed at pH values between 7.0 and 9.0. The highest solubility was observed at pH 7 for treatments B and F (Figure 14.). The API of treatment A (25 J/cm^3) showed a similar solubility as native proteins, and all pH values were equal to or greater than 5. The increases in solubility after HIUS were attributed to the reduction in the particle sizes of API and the consequent increase in the area of contact with water (Arzeni et al., 2012). This hypothesis was confirmed in the results of treatment A, in which most of the particles in solution had a larger hydrodynamic diameter compared to other HIUS-treated APIs and thus their solubility was similar to the native API. An increase of solubility in water after HIUS was also reported for nut protein isolate (Zhu et al., 2018), soy protein isolate (Hu et al., 2013b), and black bean protein isolate (Jiang et al., 2014). In most cases, these phenomena are related to the ability of HIUS to cause alteration of the surface chemistry, which can be observed by increases in free SH group and surface hydrophobicity, and changes of surface amino acid content which increased the absolute zeta potential values (Zhu et al., 2018). We refer to the solubility of sample E (50 J/cm^3), which was relatively low compared to other samples (D and F) with the same duration of HIUS (30 min). In this case, the protein showed higher surface hydrophobicity, which also coincided with the relative increase in particle size and/or formation of small aggregates upon sonication (Table 6), which may precipitate during the centrifugation of solutions (Arzeni et al., 2012).

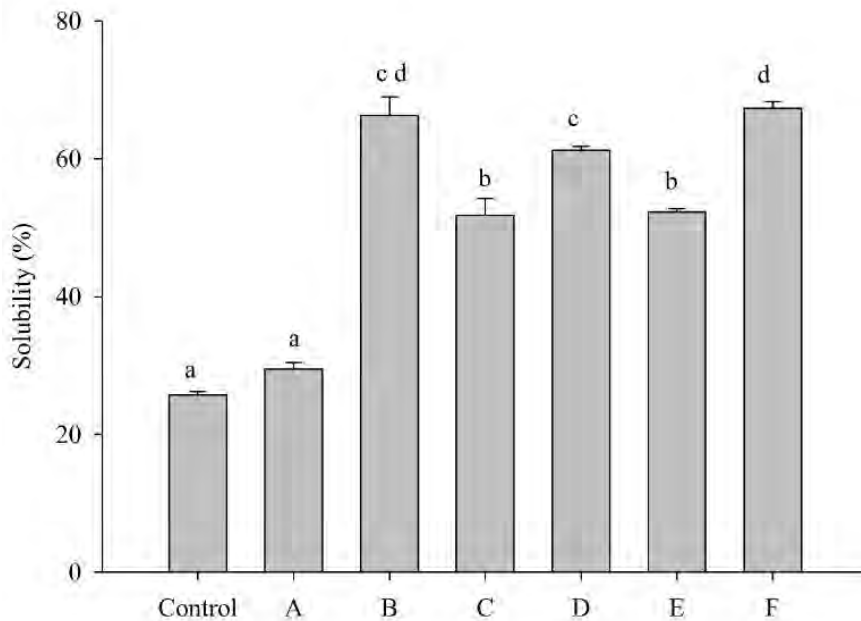


Figure 14. Solubility (%) of native and high-intensity ultrasound treated amaranth protein isolate at pH 7. Control) is the native API; A) 30%, 15 min; B) 60%, 15 min; C) 90%, 15 min; D) 30%, 30 min; E) 60%, 30 min; F) 90%, for 30 min. The results are mean \pm standard deviation of 3 independent replicate experiments. Values followed by the same letter in the columns do not differ statistically from each other ($p < 0.05$).

3.2.2 Emulsion formation and stability properties

Table 7 shows that the ultrasonic treatment increased the index of emulsifying activity from 136.95 ± 1.54 to 158.63 ± 2.33 m^2/g . This improvement also occurred with an increase in amplitudes and time of HIUS. These results may be explained by the fact that HIUS increased solubility and reduced the hydrodynamic diameter of the API. Additionally, as discussed in hydrophobicity and the free SH, HIUS promoted the partial unfolding of these globular proteins, which allowed exposure to the surrounding aqueous phase of some nonpolar groups that were originally present in the hydrophobic interiors, which increased their surface activity. Similar results were reported for proteins isolated from nuts (Zhu et al., 2018). Table 3 also shows that time and HIUS power affected the emulsion stability index (ESI), with the highest ESI value (28.12 ± 0.72 min) observed in treatment E. Similar results were found for walnut protein (Zhu et al., 2018), and proteins isolated from wheat and soy (O'Sullivan et al., 2016). In these cases, the improvement in ESI was attributed to changes in the surface chemistry of lipid droplets that altered the attractive or repulsive interactions between the droplets, or even small changes in the structure of proteins. For example, the emulsifying properties of proteins are closely related to their hydrophobicity in the surface (O'Sullivan et al., 2017), which was observed for treatment E because it showed a higher surface hydrophobicity compared to other treatments. However, the ESI of amaranth proteins decreased when the most intense HIUS (treatment F) conditions were used, which may have occurred because the overprocessing promoted extensive protein aggregation, as we discussed earlier.

Table 7. Effects of high-intensity ultrasound treatment on the emulsifying activity index (EAI) and on the emulsion stability index (ESI) of API.

Treatment (Amplitude, time)	EAI (m ² /g)	ESI (min)
Control (native API)	136.95 ± 2.54 ^a	17.87 ± 0.64 ^a
A (30%, 15 min)	144.94 ± 1.56 ^{ab}	19.06 ± 0.48 ^{ab}
B (60%, 15 min)	142.61 ± 1.47 ^{ab}	21.09 ± 1.43 ^{bc}
C (90%, 15 min)	155.31 ± 3.19 ^{cd}	22.18 ± 0.55 ^c
D (30%, 30 min)	145.30 ± 1.88 ^{ab}	23.75 ± 0.21 ^c
E (60%, 30 min)	146.96 ± 2.90 ^{bc}	28.12 ± 0.72 ^d
F (90%, 30 min)	158.63 ± 2.33 ^d	18.72 ± 0.43 ^{ab}

The data are mean ± standard deviation of 3 independent replicate experiments. The results values followed by the same letter in the same columns do not differ statistically from each other ($p < 0.05$).

4 Conclusion

The present work investigated the effects of the level and duration of HIUS on the structure and functional properties of API. HIUS did not change the API molar masses, but the tertiary structure was partially modified, with a significant increase of the free SH group. It was possible to observe that prolonged time promoted a decrease in particle sizes and an increase in surface hydrophobicity, very notorious at 30 min of treatment, and 30 or 60% of amplitudes, respectively. These physicochemical changes influenced the functional properties of proteins. For example, several HIUS-treated APIs presented higher water-solubility, except treatment A (25 J/cm³) where their particle size was increased by ultrasound. Moreover, HIUS with 30 min of treatment and 60% of amplitude (treatment E, 50 J/cm³) presented the best emulsifying properties attributed to the increased surface hydrophobicity. Therefore, HIUS may be used to improve the functional properties of amaranth proteins. These results may be important to increase their use as natural functional herbal ingredients in foods and beverages.

5 References

- Acosta, C., Carpió, C., Vilcacundo Chamorro, R., Carrillo Terán, W., 2016. Identification of proteins isolate from amaranth (*Amaranthus caudatus*) by sodium dodecyl sulfate-polyacrylamide gel electrophoresis with water and NaCl 0.1 M solvents. *Asian J. Pharm. Clin. Res.* 9.
- AOAC, 2005. Official method of Analysis, 18th ed. Association of Officiating Analytical Chemists, Washington DC.
- Arzeni, C., Martínez, K., Zema, P., Arias, A., Pérez, O.E., Pilosof, A.M.R., 2012. Comparative study of high intensity ultrasound effects on food proteins functionality. *J. Food Eng.* 108, 463–472. <https://doi.org/https://doi.org/10.1016/j.jfoodeng.2011.08.018>
- Avanza, M.V., Añón, M.C., 2007. Effect of thermal treatment on the proteins of amaranth isolates. *J. Sci. Food Agric.* 87, 616–623. <https://doi.org/doi:10.1002/jsfa.2751>
- Chandrapala, J., Zisu, B., Palmer, M., Kentish, S., Ashokkumar, M., 2011. Effects of ultrasound on the thermal and structural characteristics of proteins in reconstituted

- whey protein concentrate. *Ultrason. Sonochem.* 18, 951–957.
<https://doi.org/https://doi.org/10.1016/j.ultsonch.2010.12.016>
- Condés, M.C., Speroni, F., Mauri, A., Añón, M.C., 2012. Physicochemical and structural properties of amaranth protein isolates treated with high pressure. *Innov. Food Sci. Emerg. Technol.* 14, 11–17. <https://doi.org/https://doi.org/10.1016/j.ifset.2011.12.006>
- Fabio, A. Di, Parraga, G., 2017. Origin, Production and Utilization of Pseudocereals, in: *Pseudocereals*. John Wiley & Sons, Ltd, Chichester, UK, pp. 1–27.
<https://doi.org/10.1002/9781118938256.ch1>
- Girard, A.L., Bean, S.R., Tilley, M., Adrianos, S.L., Awika, J.M., 2018. Interaction mechanisms of condensed tannins (proanthocyanidins) with wheat gluten proteins. *Food Chem.* 245, 1154–1162.
<https://doi.org/https://doi.org/10.1016/j.foodchem.2017.11.054>
- Hu, H., Li-Chan, E.C.Y., Wan, L., Tian, M., Pan, S., 2013a. The effect of high intensity ultrasonic pre-treatment on the properties of soybean protein isolate gel induced by calcium sulfate. *Food Hydrocoll.* 32, 303–311.
<https://doi.org/https://doi.org/10.1016/j.foodhyd.2013.01.016>
- Hu, H., Wu, J., Li-Chan, E.C.Y., Zhu, L., Zhang, F., Xu, X., Fan, G., Wang, L., Huang, X., Pan, S., 2013b. Effects of ultrasound on structural and physical properties of soy protein isolate (SPI) dispersions. *Food Hydrocoll.* 30, 647–655.
<https://doi.org/https://doi.org/10.1016/j.foodhyd.2012.08.001>
- Jambrak, A.R., Mason, T.J., Lelas, V., Paniwnyk, L., Herceg, Z., 2014. Effect of ultrasound treatment on particle size and molecular weight of whey proteins. *J. Food Eng.* 121, 15–23. <https://doi.org/https://doi.org/10.1016/j.jfoodeng.2013.08.012>
- Janssen, F., Pauly, A., Rombouts, I., Jansens, K.J.A., Deleu, L.J., Delcour, J.A., 2017. Proteins of Amaranth (*Amaranthus* spp.), Buckwheat (*Fagopyrum* spp.), and Quinoa (*Chenopodium* spp.): A Food Science and Technology Perspective. *Compr. Rev. Food Sci. Food Saf.* 16, 39–58. <https://doi.org/10.1111/1541-4337.12240>
- Jiang, L., Wang, J., Li, Y., Wang, Z., Liang, J., Wang, R., Chen, Y., Ma, W., Qi, B., Zhang, M., 2014. Effects of ultrasound on the structure and physical properties of black bean protein isolates. *Food Res. Int.* 62, 595–601.
<https://doi.org/https://doi.org/10.1016/j.foodres.2014.04.022>
- Martínez, E.N., Añón, M.C., 1996. Composition and Structural Characterization of Amaranth Protein Isolates. An Electrophoretic and Calorimetric Study. *J Agric Food Chem* 44, 2523–2530. <https://doi.org/10.1021/jf960169p>
- Mota, C., Santos, M., Mauro, R., Samman, N., Matos, A.S., Torres, D., Castanheira, I., 2016. Protein content and amino acids profile of pseudocereals. *Food Chem.* 193, 55–61.
<https://doi.org/10.1016/j.foodchem.2014.11.043>
- O’Sullivan, J., Park, M., Beevers, J., 2016. The effect of ultrasound upon the physicochemical and emulsifying properties of wheat and soy protein isolates. *J. Cereal Sci.* 69, 77–84.
<https://doi.org/https://doi.org/10.1016/j.jcs.2016.02.013>
- O’Sullivan, J.J., Park, M., Beevers, J., Greenwood, R.W., Norton, I.T., 2017. Applications of ultrasound for the functional modification of proteins and nanoemulsion formation: A review. *Food Hydrocoll.* 71, 299–310.
<https://doi.org/https://doi.org/10.1016/j.foodhyd.2016.12.037>
- Orsini Delgado, M.C., Nardo, A., Pavlovic, M., Rogniaux, H., Añón, M.C., Tironi, V.A., 2016. Identification and characterization of antioxidant peptides obtained by

- gastrointestinal digestion of amaranth proteins. *Food Chem.* 197, 1160–1167. <https://doi.org/https://doi.org/10.1016/j.foodchem.2015.11.092>
- Ozuna, C., Paniagua-Martínez, I., Castaño-Tostado, E., Ozimek, L., Amaya-Llano, S.L., 2015. Innovative applications of high-intensity ultrasound in the development of functional food ingredients: Production of protein hydrolysates and bioactive peptides. *Food Res. Int.* 77, 685–696. <https://doi.org/https://doi.org/10.1016/j.foodres.2015.10.015>
- Pinckney, A.J., 1961. The biuret test as applied to the estimation of wheat protein. *Cereal Chem.* 38, 501–506.
- Resendiz-Vazquez, J.A., Ulloa, J.A., Urías-Silvas, J.E., Bautista-Rosales, P.U., Ramírez-Ramírez, J.C., Rosas-Ulloa, P., González-Torres, L., 2017. Effect of high-intensity ultrasound on the technofunctional properties and structure of jackfruit (*Artocarpus heterophyllus*) seed protein isolate. *Ultrason. Sonochem.* 37, 436–444. <https://doi.org/https://doi.org/10.1016/j.ultsonch.2017.01.042>
- Sabbione, A.C., Nardo, A.E., Añón, M.C., Scilingo, A., 2016. Amaranth peptides with antithrombotic activity released by simulated gastrointestinal digestion. *J. Funct. Foods* 20, 204–214. <https://doi.org/https://doi.org/10.1016/j.jff.2015.10.015>
- Scilingo, A.A., Molina Ortiz, S.E., Martínez, E.N., Aón, M.C., 2002. Amaranth protein isolates modified by hydrolytic and thermal treatments. Relationship between structure and solubility. *Food Res. Int.* 35, 855–862. [https://doi.org/10.1016/S0963-9969\(02\)00089-3](https://doi.org/10.1016/S0963-9969(02)00089-3)
- Shen, X., Fang, T., Gao, F., Guo, M., 2017. Effects of ultrasound treatment on physicochemical and emulsifying properties of whey proteins pre- and post-thermal aggregation. *Food Hydrocoll.* 63, 668–676. <https://doi.org/https://doi.org/10.1016/j.foodhyd.2016.10.003>
- Ventureira, J.L., Bolontrade, A.J., Speroni, F., David-Briand, E., Scilingo, A.A., Ropers, M.-H., Boury, F., Añón, M.C., Anton, M., 2012. Interfacial and emulsifying properties of amaranth (*Amaranthus hypochondriacus*) protein isolates under different conditions of pH. *LWT - Food Sci. Technol.* 45, 1–7. <https://doi.org/https://doi.org/10.1016/j.lwt.2011.07.024>
- Vera, A., Valenzuela, M.A., Yazdani-Pedram, M., Tapia, C., Abugoch, L., 2019. Conformational and physicochemical properties of quinoa proteins affected by different conditions of high-intensity ultrasound treatments. *Ultrason. Sonochem.* 51, 186–196. <https://doi.org/10.1016/j.ultsonch.2018.10.026>
- Vilcacundo, R., Barrio, D.A., Piñuel, L., Boeri, P., Tombari, A., Pinto, A., Welbaum, J., Hernández-Ledesma, B., Carrillo, W., 2018. Inhibition of Lipid Peroxidation of Kiwicha (*Amaranthus caudatus*) Hydrolyzed Protein Using Zebrafish Larvae and Embryos. *Plants*. <https://doi.org/10.3390/plants7030069>
- Vojdani, F., 1996. Solubility, in: Hall, G.M. (Ed.), *Methods of Testing Protein Functionality*. Blackie Academic & Professional, London, pp. 11–60.
- Xiong, T., Xiong, W., Ge, M., Xia, J., Li, B., Chen, Y., 2018. Effect of high intensity ultrasound on structure and foaming properties of pea protein isolate. *Food Res. Int.* 109, 260–267. <https://doi.org/https://doi.org/10.1016/j.foodres.2018.04.044>
- Zhu, Z., Zhu, W., Yi, J., Liu, N., Cao, Y., Lu, J., Decker, E.A., McClements, D.J., 2018. Effects of sonication on the physicochemical and functional properties of walnut protein isolate. *Food Res. Int.* 106, 853–861. <https://doi.org/https://doi.org/10.1016/j.foodres.2018.01.060>

**CAPÍTULO IV. VITAMIN D₃ MICROCAPSULES FORMED BY
HETEROPROTEIN COMPLEXES OBTAINED FROM AMARANTH
PROTEIN ISOLATES AND LACTOFERRIN: FORMATION,
CHARACTERIZATION, AND BREAD FORTIFICATION**

Published at Food Hydrocolloids, volume 129, August 2022, 107636.
DOI: <https://doi.org/10.1016/j.foodhyd.2022.107636>

Abstract

Vitamin D₃ (VD₃) is a fat-soluble compound important for human health but is unstable in the presence of environmental factors such as light and hot temperature. The present work aimed to microencapsulate VD₃ in complexes formed by Amaranth protein isolates (APIs) and lactoferrin (Lf). The encapsulation was conducted at pH 6.5 and a ratio of 1:3 (API:Lf, w/w) after confirming these complexes affinity with zeta potential and isothermal titration calorimetry analysis. The microcapsules showed a spherical morphology with sizes below 600 nm and high encapsulation efficiency (up to 90%). Fourier transform infrared spectroscopy data confirmed the encapsulation of VD₃. During simulated gastrointestinal digestion of the microcapsules, the highest percentage (70%) of VD₃ release was observed in the intestinal phase, with a high bioaccessibility (approximately 46%). Compared to unencapsulated VD₃, microencapsulation protected VD₃ from degradation under stress conditions (ultraviolet radiation and storage at room temperature) by a factor of up to three times. Furthermore, API:Lf heteroprotein complexes also protected (86%) VD₃ during a simulation of bread production. Microcapsules added to bread showed release profile kinetics of the first order when exposed to simulated intestinal fluid. These results suggest that VD₃ microcapsules formed as API:Lf complexes can be applied successfully for food fortification and baking.

Key-words: Amaranth protein isolate; Lactoferrin; Cholecalciferol; Whey protein; Baking

1 Introduction

Vitamin D₃, or cholecalciferol, is a fat-soluble precursor of calcitriol (1,25-dihydroxy-vitamin D), an active form of vitamin D that is critical to the regulation of phosphorus and calcium homeostasis. Additionally, calcitriol may have immunomodulatory effects that are associated with protecting of the body from infections and some inflammatory processes (Bilezikian et al., 2020; Santos, Geraldo De Carvalho, & Garcia-Rojas, 2021; Sassi, Tamone, & D'Amelio, 2018, p. 1656). Therefore, a vitamin D deficiency can cause or be associated with different chronic and acute illnesses, including osteoporosis, rickets, obesity, and cancers (Amrein et al., 2020). Vitamin D deficiency has affected billions of people worldwide, increasing the need for vitamin D supplementation (Holick, 2017). Food fortification is a viable method for supplementation. However, vitamin D is unstable in various conditions of food processing and storage (including hot temperatures, light, oxygen, and humidity), thus requiring protection through technical procedures such as microencapsulation (Luo, Teng, & Wang, 2012).

Several methods for vitamin D encapsulation have been reported in the literature, including emulsification, nanoparticle formation, spray drying, and complex coacervation (Bajaj, Marathe, & Singhal, 2021; Diarrassouba et al., 2015; Jannasari, Fathi, Moshtaghian, & Abbaspourrad, 2019; Lamsen et al., 2020; Luo et al., 2012; Santos, de Carvalho, & Garcia-Rojas, 2021; Santos, Geraldo De Carvalho, & Garcia-Rojas, 2021). Among these methods, microencapsulation by complex coacervation is worth highlighting because it yields a wall material of high integrity, high encapsulation efficiency, and excellent controlled release characteristics (Gaonkar, Vasisht, Khare, & Sobel, 2014; Santos, Geraldo De Carvalho, & Garcia-Rojas, 2021). As a process, microencapsulation by complex coacervation comprises emulsification, complex formation, and crosslinking. The formation of complexes occurs mainly through the electrostatic attraction of two polymers (such as polysaccharide-polysaccharide, polysaccharide-protein, or protein-protein), although other factors can affect complex-formation, including pH, temperature, ionic strength, and the concentration and ratio of polymers. Two phases form during complex coacervation, with one phase rich in polymers (precipitated phase), and the other containing fewer polymer molecules. Encapsulation of the bioactive compound occurs in the polymer-rich phase, which is collected for specific applications (Devi, Sarmah, Khatun, & Maji, 2017; Santos, Costa, & Garcia-Rojas, 2018).

Recently, several reports proposed the use of proteins to form complex coacervates (or heteroprotein complexes) (Santos, de Carvalho, & Garcia-Rojas, 2018; Wei, Cheng, & Huang, 2019; Zheng et al., 2021; Zheng, Gao, et al., 2020; Zheng, Tang, Ge, Zhao, & Sun, 2020). This suggestion can be attributed to the nutritional and structural properties (including texture and stability) that proteins impart to foods (Chapeau et al., 2017). However, most published works on encapsulation employing heteroprotein complexes have used animal-based rather than plant proteins (Chapeau et al., 2017; Diarrassouba et al., 2015; J. Zhu, Li, Xu, & Wang, 2019). It is worthwhile understanding that use of plant proteins could reduce consumer acceptability due to uninviting “plant flavors”. However, this can be resolved with treatments to reduce plant odor compounds like controlling germination conditions (such as germination substrates, reducing environmental stress, and adding antioxidants), using alkaline extraction-isoelectric precipitation, and defatting (Xu, Jin, Gu, Rao, & Chen, 2020; Yue et al., 2021). Moreover, numerous advantages would result from using plant proteins, such as increased sustainability, lowered cost, advanced nutritional properties, and biological properties which encourages continued research on their physical, chemical, technological, and functional properties (Lan, Ohm, Chen, & Rao, 2021; Luo et al., 2012; Yuan, Kong, Sun, Zeng, & Yang, 2017). In this work, amaranth protein isolate (API) is proposed because it presents high nutritional quality compared with rice and wheat proteins. Additionally, it

presents several biological activities, including antithrombotic, antioxidant, and hypocholesterolemic activities (Orsini Delgado et al., 2016; Sabbione, Nardo, Añón, & Scilingo, 2016; Tomé Constantino & Garcia-Rojas, 2020). API is composed principally of albumin (~65%) and globulin (~17%), with smaller amounts of prolamine (~11%) and glutelin (~7%) (Tomé Constantino & Garcia-Rojas, 2020). Furthermore, API can be used to encapsulate bioactive compounds for targeted release in the intestine, as it can resist the action of gastric juice to a certain degree (Suárez & Añón, 2019). To better understand how API can form heteroprotein complexes, we proposed using lactoferrin (Lf), because this widely known milk protein has excellent emulsion forming capabilities and has been applied to complex formation with other polymers (El Ghazzaoui Barbosa et al., 2022). Lf has a molar mass that can vary between 80 and 84 kDa, and its isoelectric point (pI) can vary between 8 and 8.5. It consists of a single polypeptide chain folded into two symmetrical globular lobes (N and C lobes). Each lobe is capable of binding strongly to Fe^{+3} with a small affinity for Fe^{+2} , although also it has been reported to bind to Cu^{+2} , Zn^{+2} , and Mn^{+2} (Bastos, de Carvalho, & Garcia-Rojas, 2018). These properties give Lf many beneficial biological effects, including iron delivery and potential activities against different microorganisms (Wang, Timilsena, Blanch, & Adhikari, 2017).

Therefore, the aim of this research was to study the formation of API: Lf heteroprotein complexes for VD_3 encapsulation and fortification of bakery products. First, the complexes were studied using zeta potential and isothermal titration analysis. Subsequently, VD_3 was encapsulated and we evaluated the *in vitro* gastrointestinal digestion and stability of the microcapsules against intestinal stress conditions. Finally, we added microcapsules to bread and studied the controlled release of VD_3 under conditions of *in vitro* intestinal simulation.

2 Methodology

2.1 Materials

Amaranth seeds (*Amaranthus cruentus* BRS Alegre) were purchased from Relva Verde Alimentos EIRELI (São Paulo, Brazil), and coconut oil was purchased in the local market (Volta Redonda, Brazil). Lactoferrin 95% (Vivinal® Lactoferrin) was donated by Friesland Campina (Amersfoort, Netherlands). Vitamin D_3 (code C9756-5G), α -amylase (code A3403), porcine pepsin (code P6887), porcine pancreatin (code P7545), and porcine biliary extract (code B3883) were purchased from Sigma–Aldrich (St. Louis, USA). Transglutaminase from *Streptomyces mobaraensis* (85–121 U/g) was donated by Ajinomoto (São Paulo, Brazil). Ultrapure water with a conductivity of 0.05 $\mu\text{S}/\text{cm}$ (Master System R&D, Gehaka, Brazil) and analytical grade reagents were used for all analyses.

2.2 Obtention and modification of amaranth proteins

Amaranth protein isolate (API) was obtained according to a previously reported methodology (Tomé Constantino & Garcia-Rojas, 2020). Defatted (ethanol 95%, v/v) amaranth flour was suspended in water at a ratio of 1:10 (w/v), and the pH of the mixture was adjusted to 9 using 2 mol/L NaOH. The suspension was stirred for 30 min and then centrifuged (Digicen 21 R, Orto Alresa, Spain) at 9,000 g for 20 min. Then, the supernatant was adjusted to pH 5 with 2 mol/L HCl and centrifuged at 4,000 g for 10 min at 4 °C. The precipitate was resuspended in water, neutralized, and lyophilized (Terroni, Enterprise I, Brazil). The lyophilized API (10% in water, w/v) was treated with ultrasound UP100H (Hielscher, Germany) at 100 W and 30 kHz at 60% amplitude for 30 min and then lyophilized again, packaged, and stored at -20 °C for further analysis. The proteins thus obtained were named API-U.

2.3 Formation of heteroprotein complex wall material

2.3.1 Solutions of amaranth protein isolate and lactoferrin

The biopolymers (API-U and Lf) were weighed on an analytical balance (Shimadzu, AY220, Philippines) to prepare solutions containing a fixed concentration of 0.1% (w/w). The dispersions containing Lf were stirred (NT101, Nova Técnica, Brazil) for 30 min at room temperature. API-U dispersions were adjusted to pH 9.0 and stirred for 30 min to ensure complete solubilization.

2.3.2 Zeta potential

The zeta potentials of API-U and Lf were determined using a Zetasizer Nano ZS90 (Malvern Instruments, UK). Analyses were conducted as a function of pH (8.5–5.0) in the range of 0.5 ± 0.05 units. The pH was adjusted with the aid of 0.25 mol/L HCl or 0.25 mol/L NaOH. The strength of the electrostatic interaction (SEI) between API-U and Lf was estimated according to Equation (1) (Bastos, de Sá Costa et al., 2020):

$$\text{SEI (mV}^2\text{)} = |\text{ZP}_1| \times |\text{ZP}_2| \quad (1)$$

where ZP_1 and ZP_2 are the measured zeta potentials of API-U and Lf, respectively, at each pH.

2.3.3 Determination of the molecular weight of amaranth protein isolate and lactoferrin

The determination of the average molecular weight (M_w) of API-U and Lf was performed by the static light scattering (SLS) technique using the Zetasizer Nano ZS90. For this, 100 mg of API-U was dissolved overnight in 40 mL of 35 mM potassium phosphate buffer (pH 7.50) with 0.4 M NaCl; 50 mg of Lf was dissolved for 1 h in 30 mL of 100 mM citrate buffer (pH 5.0) containing 0.1 M NaCl. Solutions, including buffers, were filtered at 0.22 μm . Samples were then serially diluted: 0–1 mg/mL for API-U and 0–1.6 mg/mL for Lf. Their concentrations were determined by the biuret method through a standard curve ($y = 0.0507X$, $R^2 = 0.99$) previously constructed with bovine serum albumin (BSA) using a UV–VIS spectrophotometer (Biomate 3S, Thermo Scientific, USA) at a wavelength of 550 nm. In addition, the specific increment of the refractive index ($d\tilde{n}/dC$) of 0.185 was considered. M_w was obtained by measuring the scattered light intensity (KC/RoP) compared to the scattered light of acetone (the standard used as a reference).

2.3.4 Isothermal titration calorimetry

Isothermal titration calorimetry (ITC) was performed using Nano-ITC equipment (TA Instruments, New Castle, USA). The analysis was performed at pH 6.5 using 10 mM MES-NaOH buffer. The Lf solution was 0.1 mM, and the API-U was 2.5×10^{-4} mM. After dissolving the biopolymers, the solutions were dialyzed for 3 h using 3.5 kDa membranes (Sigma–Aldrich, Midi 3500, USA) to balance ionic strength and pH. The solutions were filtered (0.45 μm) and degassed. During the ITC, 10 μL of Lf was injected into the sample cell within 150 s. In total, 250 μL of the Lf solution was titrated in a sample cell containing 1200 μL of API-U solution under agitation at 250 rpm. Thermodynamic parameters were obtained using the TA Nano Analyze[®] program, and the results were expressed at a significance level of 0.05.

2.4 Encapsulation of vitamin D₃

Several encapsulation systems were evaluated to identify the best conditions for the encapsulation of vitamin D₃ (VD₃). To this end, solutions with 0.5, 0.75 and 1.0% (w/w) wall material and varied proportions (1:1, 1:2 and 1:3) of core/wall were used. First, an emulsion was produced using Lf and coconut oil containing VD₃ (1%, w/w). The process was conducted in an Ultra-Turrax (T25D, IKA, Germany) at 10,000 rpm for 3 min. The mixtures and all solutions were kept at 25 ± 1 °C. Once the emulsion was formed, the API-U solution was added, and the pH was adjusted to 6.5 using 10% (v/v) acetic acid or 0.1 M NaOH, with gentle mechanical stirring. After that, the mixtures were stirred for 3 min to allow the electrostatic attraction of the biopolymers. To induce crosslinking, 5 mL of transglutaminase (TG, 30 U/g of protein) was added to the microcapsules, followed by stirring (60 rpm) in a shaker (Tecnal, model TE-424, Brazil) for 4 h at 25 °C. The microcapsules were then placed in an ice bath for 30 min and kept at 4 °C for 48 h. Finally, VD₃ microcapsules were frozen in liquid nitrogen and lyophilized for 48 h.

2.4.1 Encapsulation efficiency

The encapsulation efficiency (EE%) of VD₃ was determined according to the methodology previously described by Santos, Geraldo De Carvalho, and Garcia-Rojas (2021), with some modifications. A 5 mL aliquot of hexane was added to 0.05 g of the lyophilized microcapsules and then placed for 20 min in an ultrasound bath (Branson 2510 DTH, Sonitech, Brazil) set at 42 kHz frequency and 235 W power. The samples were centrifuged (Digicen 21 R, Orto Alresa, Spain) at 4,000 rpm for 15 min, and the supernatant was collected and measured in a spectrophotometer at 264 nm to quantify VD₃. The theoretical value of VD₃ (OT%) was given by Equation (2), and the content of loaded VD₃ (LC%) was given by Equation (3). EE (%) was calculated according to Equation (4).

$$OT (\%) = 100x(WId/WIc) \quad (2)$$

$$LC (\%) = 100x(WFd/WFc) \quad (3)$$

$$EE (\%) = 100x(LC (\%)/OT (\%)) \quad (4)$$

where WId is the initial mass of VD₃ added to the system, WIc is the initial mass of VD₃ carried in the API-U: Lf complexes, WFd is the content of VD₃ (g) after encapsulation and WFc is the final mass of VD₃ used in the analysis as carried in the API-U: Lf complexes after lyophilization.

To determine the concentration of encapsulated VD₃, a calibration curve ($y = 0.0479x + 0.0164$, $R^2=0.9987$) was constructed with VD₃ dissolved in hexane (0-30 µg/mL), and the absorption of the standard solutions was measured in a spectrophotometer at a wavelength of 264 nm.

2.4.2 Fourier transform infrared spectroscopy

Biopolymers, coconut oil, VD₃, and lyophilized microcapsules containing VD₃ (VD₃-M) were analyzed with an FTIR (Fourier transform infrared) spectrophotometer (Bruker, Vertex 70, Germany), and the spectra were obtained at wavelengths from 4,000 to 400 cm⁻¹ (Bastos et al., 2018).

2.4.3 Particle size

The particle size distributions of API-U and Lf in the buffers described in Section 2.2.3 and VD₃-M (before freeze-drying) were monitored by dynamic light scattering (DLS) using the Zetasizer Nano ZS90. The detection angle was set at 90°. Measurements were performed at 25 °C (Bastos, de Sá Costa et al., 2020).

2.4.4 Study of microcapsule stability

To evaluate the stability of the microcapsules, studies of photolytic degradation and storage at ambient temperature were conducted. Therefore, 10 mL of VD₃-M (before lyophilization) and 10 mL of free VD₃ were exposed to ultraviolet light (UV) irradiation at 362 nm for 22 h using UV darkroom equipment (AG-DC-02, ACS Gold, Brazil). Free VD₃ was prepared under similar conditions to microcapsule production; that is, 0.225 g of VD₃ solution (1%, w/w) was dissolved in absolute ethanol, and then deionized water was added to 35 g. To assess the stability of VD₃ at room temperature (25 ± 1 °C), 10 mL of VD₃-M (before lyophilization) or free VD₃ was placed in the dark for 5 days. Microcapsules and free VD₃ were prepared using 0.02% (w/w) sodium azide to prevent microorganism growth. The concentrations of VD₃ remaining in each specific period were determined using a calibration curve ($y = 0.051116x + 0.014689$, $R^2 = 0.99853$) of VD₃ dissolved in absolute ethanol at the same concentrations and wavelengths described in Section 2.4.2.

2.4.5 Simulation of in vitro gastrointestinal digestion of microcapsules

The in vitro digestion of VD₃-M was simulated in three steps: oral (2 min), gastric (2 h), and intestinal (2 h), as described by INFOGEST 2.0 (Brodkorb et al., 2019). The oral phase was conducted at a pH of 7.0 by adding 0.70 g of lyophilized VD₃-M (1/1) to prewarmed (37 °C) simulated salivary fluid (SSF) containing alpha-amylase (75 U/mL in the final oral solution). The gastric phase was performed with 1.4 mL of prewarmed simulated gastric fluid (SGF) containing 0.07 mL of pepsin solution (2,000 U/mL in the final gastric solution), which was added to the oral digestion mixture. The entire gastric mixture was adjusted to a pH of 3.0 with 6 M HCl. At the end of the gastric digestion, 2.8 mL of prewarmed simulated intestinal fluid (SIF) was added to the mixture, along with 0.7 mL of pancreatin solution (100 U/mL of final intestinal solution volume), 0.5 mL of extract of bile solution (10 mM) and 5.6 µL of 0.3 M CaCl₂. The pH of the complete intestinal mixture was then adjusted to 7.0 with 6 mol/L NaOH. All simulations were performed under agitation (95 rpm) in a shaker at 37 °C.

During the in vitro digestion procedure, 0.2 mL sample aliquots were taken for analysis at the end of the oral phase and at 5, 15, 30, 60, and 120 min into the gastric phase and at the same times during the intestinal phase; as each sample was removed during the digestion procedure, it was replaced with 0.2 mL of SSF, SGF, and SIF in the respective phases. The amount of VD₃ released was calculated from the absorbance as described in section (2.4.4), and a blank microcapsules (with coconut oil and complexes) was used throughout the simulation.

2.4.6 Bioaccessibility of encapsulated VD₃

The bioaccessibility of the encapsulated VD₃ was determined according to the methodology reported by Santos, Geraldo De Carvalho, and Garcia-Rojas (2021), with modification. Briefly, after intestinal simulation, the digestion samples were collected and centrifuged at 9,000 g for 30 min at 4 °C. The micellar phase (between the supernatant and the precipitate)

was collected and filtered (0.2 μm) to quantify VD_3 using absorbance as described in Section 2.4.4. Bioaccessibility (B^*) was determined by Equation (5):

$$B^* = (C_{\text{micelle}}/C_{\text{digeste}}) \times 100 \quad (5)$$

where C_{micelle} is the VD_3 concentration in micelle and C_{digeste} is the VD_3 digest concentration determined in the end (120 min) of intestinal digestion.

2.5 Incorporation of VD_3 microcapsules in wheat bread

Wheat bread was chosen for testing vitamin D nutritional fortification by incorporating VD_3 microcapsules into the food matrix. For the preparation, 20 g (100%) of wheat flour was mixed with 0.4 g (2%) of dry yeast, 0.4 g (2%) NaCl, and 11.6 g (58%) of water, which was $\text{VD}_3\text{-M}$ (nonlyophilized) or free VD_3 solutions (as described in Section 2.4.4.) (Cauvain, 2015). The dough was prepared manually for 10 min and then heated in an LAB 1,000 oven (Bravac, Brazil) at 200 $^\circ\text{C}$ for 30 min (Jakobsen & Knuthsen, 2014; H.; Zhu, Mettu, Cavalieri, & Ashokkumar, 2021). The physical appearance of the bread during the process can be seen in Fig. 15.

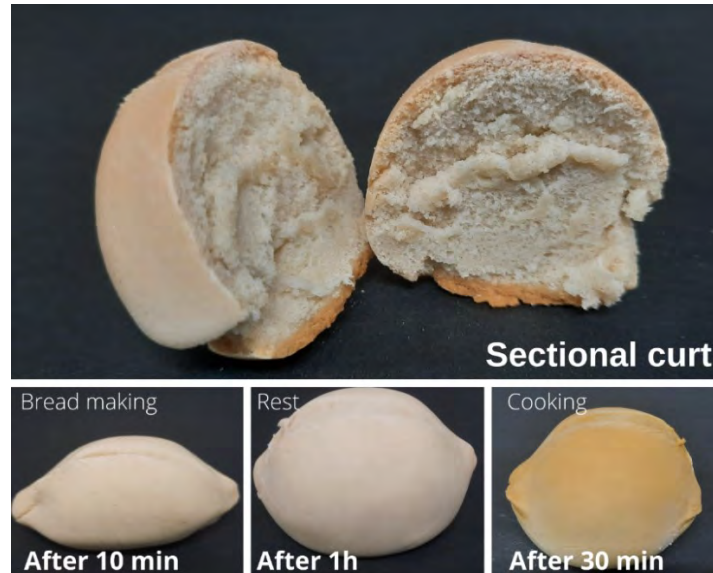


Figure 15. Picture of the bread and process of bread making fortified with VD_3 microcapsules.

2.5.1 Stability of VD_3 during the baking process

The stability of VD_3 during the baking process was measured by determining the amount of VD_3 recovered after the process. Each bread specimen was crushed in a blender, and then 5 g was weighed and mixed with 20 mL of ethanol (96%). The mixture was then stirred for 1 h and centrifuged at 9,000 g for 10 min at 10 $^\circ\text{C}$. The supernatant was collected for determination of VD_3 according to the ethanol calibration curve described in Section 2.4.4.

2.5.2 Simulation of the in vitro release kinetics of encapsulated VD_3 incorporated in food matrices

To quantify the release of VD_3 added to the food, an in vitro release study was conducted in SIF. Five grams of ground bread was added to the SIF at a ratio of 1:3 (w/w). Then, 2.7 mL of 96% ethanol was added to 0.3 mL aliquots of the simulated intestinal digesta taken at 5, 10, 15, 20, 25, 30, 40, 50, 60, 100, 120, and 180 min. The concentrations of VD_3 were determined

according to the previous methodology (Section 2.5.1.). Plain bread was used as a control. Furthermore, to explain the controlled release mechanism, mathematical models of zero order, first order, Higuchi and Ritger-Peppas were used (Table 10).

2.6 Statistical analysis

All experiments were conducted in triplicate. One-way analysis of variance (ANOVA) and Tukey's test were used to establish the differences between means at the 0.05 significance level for EE, ambient temperature, and photolytic stability analyses. Statistical analysis was performed using Origin® 8.0 software (OriginLab Corporation, USA).

3 Results and discussion

3.1 Formation of API-U: Lf heteroprotein complexes: the wall material

3.2 Effects of pH on the formation of API-U: Lf heteroprotein complexes

Fig. 16 shows the zeta potentials and SEIs of API-U and Lf. The analyses were conducted in the pH range between 5.0 and 8.5, due to the isoelectric points (pI) of the studied proteins being close to 5.0 and 8.5 for API-U and Lf, respectively. This region is favorable for the formation of complexes through electrostatic interactions. Therefore, we investigated the pH at which the interaction would be greater. As shown in Fig. 16, the highest SEI was $442.36 \pm 10.94 \text{ mV}^2$ at pH 6.5, followed by pH 6.0 ($397.29 \pm 7.60 \text{ mV}^2$) and pH 7.0 ($392.85 \pm 6.46 \text{ mV}^2$). These results indicated that pH 6.5 was ideal for the formation of complex coacervates between Lf and APIU-U. However, as reported in previous works, the pI of API can vary between pH 4 and 6.5 due to the presence of different protein species and their concentrations in the isolates (Tomé Constantino & Garcia-Rojas, 2020). However, pH levels close to the pIs are not ideal for the formation of complexes since solubility is reduced due to protein self-aggregation. The zeta potential results show that at pH 6.5, API-U was soluble with negative charges of $-23 \pm 0.49 \text{ mV}$, which may have contributed to the stability of the solution due to electrostatic repulsions. Zheng, Gao, et al. (2020) obtained a similar result when studying the formation of complexes between Lf and soybean protein isolate (SPI). These authors reported that in pH ranges above 6, the SPI did not self-aggregate. Thus, we focused the present study on pH 6.5.

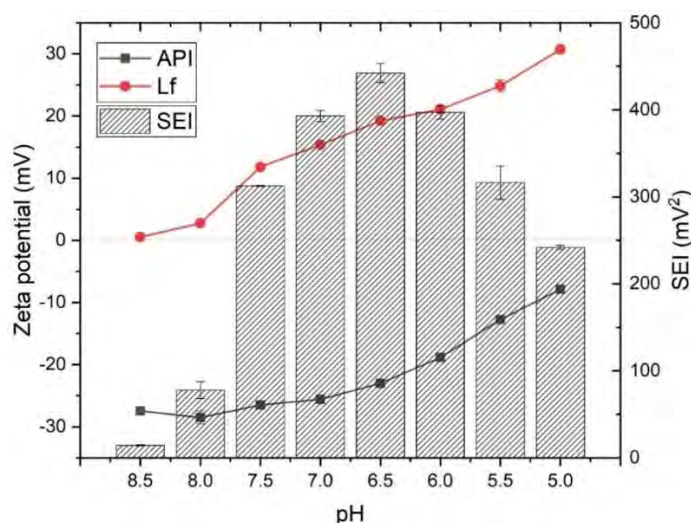


Figure 16. Zeta-potentials and Strength of Electrostatic Interaction (SEI) of API-U and Lf. The error bars represent \pm standard deviation, $n = 3$.

3.2.1 The average molecular weight of API-U and Lf

The Mw values of Lf and API-U obtained by SLS were 85.1 ± 0.0477 and 723 ± 12.9 kDa, respectively. The Mw of Lf was measured to confirm the suitability of the method used, as it is known and reported that values are usually between 80 and 84 kDa (Bastos, dos Santos, de Carvalho, & Garcia-Rojas, 2020). In this work, the difference in Mw that Lf presented can be explained by the presence of oligomers in the solution that contributed to the estimated values. These data can be seen in Table 9, where particles with a diameter of 42 nm (d.nm) were 0.30% of the volume. In the case of API-U, the high Mw agrees with the literature. For example, Cordero-delos-Santos et al. (2005) used gel filtration chromatography and observed peaks at 1380 kDa for API. In another work, Bejarano-Luján and Netto (2010) using chromatographic methods, also observed the presence of peaks at 754.7 kDa. One of the explanations for this occurrence is the extraction and precipitation pH values, which were related to association and disassociation reactions of polypeptide species, leading to the formation of large protein aggregates. Reversible association reactions of amaranthine molecules, which have Mw between 300 and 350 kDa, have been reported (Cordero-delos-Santos et al., 2005).

3.2.2 Isothermal titration calorimetry

Through the thermograms (Fig. 17A), we can see an exothermic titration profile of Lf in API-U at 25 °C. On the other hand, Fig. 17 (B) shows the binding isotherm of the API-U: Lf complex. The ITC data were best fitted using the independent binding model provided by TA Nano Analyze[®] software. Therefore, the following values were obtained: 24.85, 4.36×10^6 M⁻¹, -4.99 kcal/mol, 13.63 cal/mol, and -9.06 kcal/mol for the reaction stoichiometry (N), binding constant (K), enthalpy (ΔH), entropy change (ΔS), and Gibbs free energy change (ΔG), respectively. ΔG was calculated from the equation $\Delta G = \Delta H - T\Delta S$, where T is the temperature in degrees Kelvin (298,15).

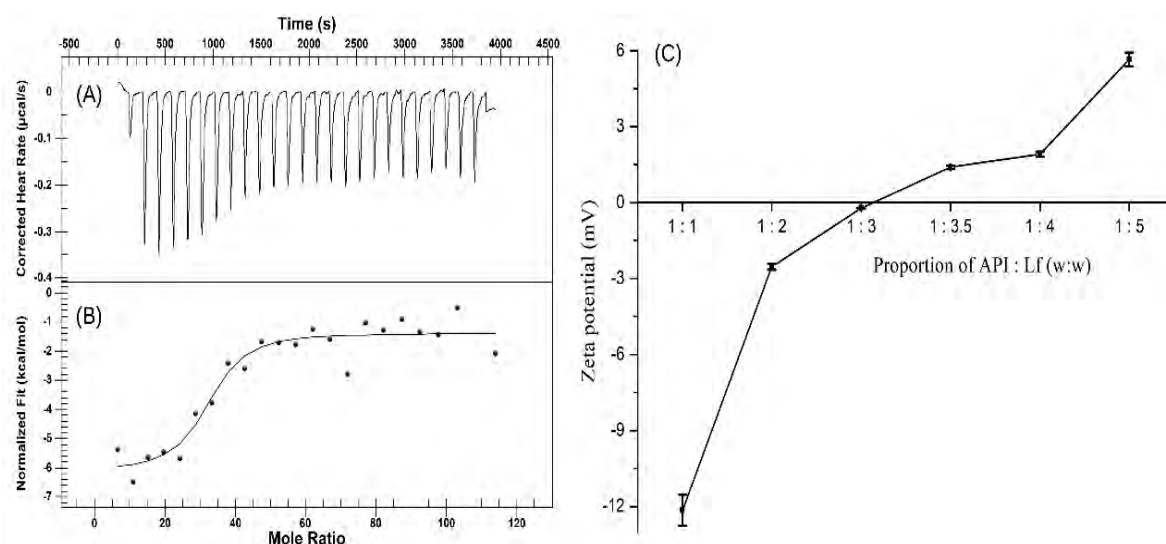


Figure 17. (A) Thermogram of heat flux ($\mu\text{cal/s}$) as a function of time (s), obtained during the titration of 0.10 mM of Lf in 0.00025 mM of API-U in MES-NaOH buffer at 10 mM (pH 6.5) at 25 °C. (B) Graphic representation of the integral of the areas of each peak (kcal/mol) as a function of the molar ratio of Lf/API-U ($p < 0.05$). (C) Zeta-potential of different proportions of API-U and Lf at pH = 6.5. The error bars of Fig. C represent \pm standard deviation, $n = 3$.

These data show that the formation of the API-U: Lf complex was enthalpically and entropically favorable. The negative value of ΔH can be associated with electrostatic interactions (Gao et al., 2021). A positive ΔS suggests that other interactions (such hydrophobic) and conformational changes of API-U may have occurred, although there is a possibility that the electrostatic attraction was strong enough to result in the expulsion of water and the transfer of hydrogen bonds (Zheng, Tang, et al., 2020). A negative ΔG indicates that the reaction was spontaneous.

The results also show that Lf and API-U have high interaction affinity at pH 6.5, as they present a K_a value about 10^6 M^{-1} (Ferstl et al., 2013). However, it took approximately 25 mol of Lf to interact with 1 mol of API-U. In terms of mass, calculated from the molecular weight described in the previous section (3.1.2), approximately 2.92 g of Lf would be needed to form a complex with 1.0 g of API-U. Fig. 2C confirms that the 3:1 ratio (Lf: APIU, w/w) is ideal for complex formation since it presented a zeta potential value closer to zero ($-0.33 \pm 0.03 \text{ mV}$) than the other proportions analyzed (1/1, 2/1, 3.5/1, and 4/1). Zheng, Gao, et al. (2020) found comparable results when studying the complex between SPI/Lf, with a 1/3 ratio observed at pH 6.25 and a 1:4 ratio at pH 6.60. In this sense, a 1:3 ratio was used to encapsulate VD_3 .

3.3 Encapsulation efficiency of vitamin D_3 in API-U: Lf complexes

The results of the encapsulation efficiency (EE) of VD_3 in API-U: Lf complexes can be seen in Table 8. The wall material formed by the heteroprotein complexes API-U: Lf was shown to have an excellent ability to encapsulate VD_3 , with values greater than 60%. Sample 4, although not significantly different from sample 9, had the highest EE ($90.94 \pm 2.09\%$). This sample was constituted with a wall: core ratio of 1:1 (w/w) and 0.75% (w/w) of the total concentration of biopolymers (TC). Additionally, we can see that the TC and the load capacity (LC) of VD_3 were the most determining factors for higher EE. Systems with higher TC had higher EE. This means that the amount of biopolymer was enough to be able to encapsulate and protect VD_3 . Santos, Geraldo De Carvalho, and Garcia-Rojas (2021) also noted that it is important to have sufficient wall material content to encapsulate VD_3 . On the other hand, the LC values were between 0.17 and 0.45%. The sample with the highest EE (sample 4) had the highest LC. According to Jannasari et al. (2019), the larger amount of the core (VD_3) considerably influences the encapsulation load due to the sufficient capacity of the wall material to trap the core. Additionally, according to Lamsen et al. (2020), LC values below 0.57% present VD_3 EE above 90%, while extremely high LC values are not as favorable.

Table 8. Encapsulation efficiency (EE), loading capacity (LC), and theoretical VD_3 (OT) of VD_3 microcapsules in different formulations.

Sample	Wall:Core	API	Lf	Wall	TC (%)	Core	OT (%)	LC (%)	EE (%)
1	01:01	0.0375	0.1125	0.1500	0.5	0.1500	0.50	0.31	61.95 ± 1.50^a
2	02:01	0.0375	0.1125	0.1500	0.5	0.0750	0.33	0.22	65.47 ± 1.33^{ab}
3	03:01	0.0375	0.1125	0.1500	0.5	0.0500	0.25	0.17	68.50 ± 0.43^b
4	01:01	0.0563	0.1688	0.2250	0.75	0.2250	0.50	0.45	90.94 ± 2.09^e
5	02:01	0.0563	0.1688	0.2250	0.75	0.1125	0.33	0.27	80.63 ± 1.16^d
6	03:01	0.0563	0.1688	0.2250	0.75	0.0750	0.25	0.17	69.36 ± 1.55^{bc}
7	01:01	0.0750	0.2250	0.3000	1.0	0.3000	0.50	0.37	74.15 ± 1.31^c
8	02:01	0.0750	0.2250	0.3000	1.0	0.1500	0.33	0.25	73.97 ± 2.07^c
9	03:01	0.0750	0.2250	0.3000	1.0	0.1000	0.25	0.22	87.02 ± 1.71^e

EE (%) and LC (%) were calculated from Equation (4) and Equation (3), respectively. TC (%) is the total concentration of biopolymer in the system. LC (%) represents the amount of VD₃ loaded in each capsule mass. The same letters in the same column do not differ significantly by Tukey's test with a probability of 5%. The symbol ± is the standard deviation, n = 3.

3.4 Characterization of vitamin D₃ microcapsules

3.4.1 Fourier transform infrared spectroscopy

Fig. 18 shows the FTIR spectra of VD₃-M (sample 4), VD₃, coconut oil, Lf, and API-U. In the protein spectra, the most important bands are those corresponding to amide I (1625–1750 cm⁻¹), amide II (1475–1575 cm⁻¹), and amide III (1225–1425 cm⁻¹). In the figure, we can see that Lf presented bands at 1637, 1518, and 1382 cm⁻¹. A similar result was observed by Santos, Geraldo De Carvalho, and Garcia-Rojas (2021). In the case of API-U, the amide I, II, and III bands can be visualized at 1632, 1536, and 1395 cm⁻¹, respectively. Shevkani, Singh, Rana, and Kaur (2014) observed a similar spectrum when studying the protein of amaranth (*Amaranthus hypochondriacus*), although these authors identified the peak of amide III at 1237 cm⁻¹. These differences can be attributed to the amaranth species. Furthermore, we identified the free amino acid O–H group (band between 3300 and 3170 cm⁻¹) at 3278 and 3278 cm⁻¹ for Lf and API-U, respectively (Bastos, dos Santos et al., 2020).

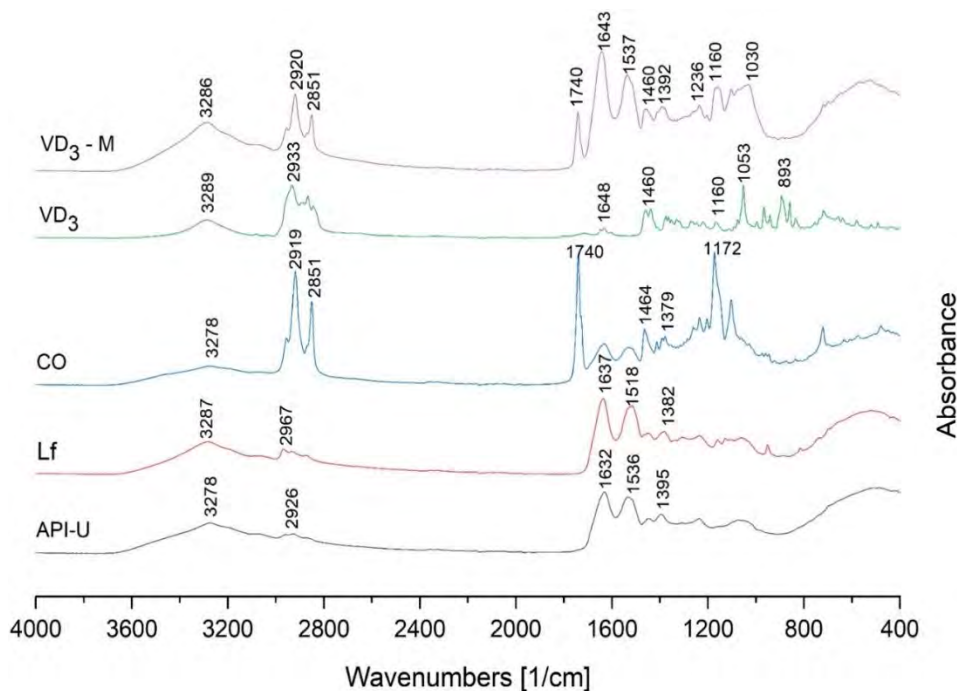


Figure 18. FTIR spectra of API-U, Lf, Coconut Oil (CO), VD₃, and VD₃ – M.

In the spectra of VD₃, like the work published by Santos, de Carvalho, and Garcia-Rojas (2021), we identified peaks corresponding to the elongation vibration of hydrogen in the ring substituent group, aromatic elongation vibration C–O, elongation vibration –CH₃, elongation vibration Cdouble bondO, elongation vibration = CH and hydrogen bonds, which were close to 893, 1053, 1460, 1648, 2933 and 3289 cm⁻¹, respectively. For the coconut oil spectrum, we can see CH elongation at 2933 cm⁻¹. Additionally, we can observe two alkane peaks that are attributed to the flexural absorption of the methylene (CH₂) and methyl (CH₃) groups at 1464 and 1379 cm⁻¹, respectively. The two peaks observed at 1740 and 1172 cm⁻¹ are attributed to the elongation of the absorption of aldehydes (C = O) and esters (C–O),

respectively. The elongation of (O–H) observed at 3278 cm^{-1} corresponds to hydrogen bonding (Amit et al., 2020).

The spectrum of VD₃-M (sample 4) observed in Fig. 18 is a combination of the spectra of biopolymers (Lf and API-U), VD₃, and coconut oil. Although there may be overlapping bands, it is possible to identify the presence of Lf and API-U through the absorbances at 1644, 1537, and 1392 cm^{-1} . The formation of complexes through electrostatic interactions between the $-\text{COO}^-$ (C = O) groups of one protein and the $-\text{NH}_3^+$ (NH) groups of the other justify the changes observed in the bands corresponding to the amides (Santos, de Carvalho, & Garcia-Rojas, 2018). We can confirm the presence of oil through the bands at 2920, 2851, and 1740 cm^{-1} , while VD₃ can be verified through the bands at 1460 and 1160 cm^{-1} . Furthermore, the increase in intensity verified at 3288 cm^{-1} could indicate the formation of hydrogen bonds between biopolymers in the formation of complexes or between protein and VD₃ (Santos, Geraldo De Carvalho, & Garcia-Rojas, 2021).

3.4.2 Particle size and morphology of the microcapsules

As we can see in Table 9, VD₃-M (sample 4) presented different particle sizes (PDI greater than 0.1) observable by the presence of two peaks at 59.82 ± 13.46 and 512.1 ± 87.46 nm of hydrodynamic diameter (d.nm), which occupied volumes of 8.4% and 91.6%, respectively. On the other hand, Lf and API-U were mostly composed of particles with 9.109 ± 1.314 and 192.2 ± 48.02 d nm, respectively. We can see that VD₃-M had larger particles than Lf and API-U together; that is, the particles were larger due to the formation of the complexes of these biopolymers and particles (from coconut oil containing VD₃) formed during emulsification. The microstructure of VD₃-M can be seen in Fig. 19. The images were captured with a 10x objective, and VD₃-M presented a well-defined spherical aspect, with a nucleus and an extremely limited wall. These results indicate the presence of microcapsules (Gaonkar et al., 2014). The literature has reported the formation of spherical complexes with sizes on the nanometer scale when using proteins (Wei et al., 2019; Zheng et al., 2021).

Table 9. Particle sizes and polydispersity index (PDI) of Lf, API-U and VD₃-M.

Sample	Peak 1		Peak 2		PDI
	d.nm	%	d.nm	%	
Lf	9.109 ± 1.314	99.7 %	49.01 ± 11.41	0.3%	0.363 ± 0.003
U-API	192.2 ± 48.02	67.2%	373.1 ± 75.22	32.8%	0.263 ± 0.013
VD ₃ -M	512.1 ± 87.46	91.6%	59.82 ± 13.46	8.4%	0.398 ± 0.103

The symbol \pm is the standard deviation, n = 3.

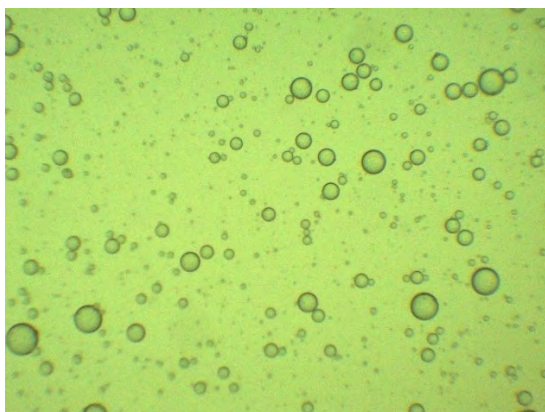


Figure 19. Picture of the optical microscopy Vitamin D₃ microcapsules (VD₃-M) microcapsules, with 10x of magnification.

3.4.3 In vitro digestion and bioaccessibility

Fig. 20 (A) presents the release profile of VD₃ loaded in API-U: Lf complexes during the in vitro digestion. As we can see, only $10.68 \pm 1.06\%$ of VD₃ was released during oral digestion. This low release may be related to the pH (6.50) used for encapsulation since in this region Lf and API-U had opposite charges and possibly some electrostatic interaction between them still occurred. During gastric digestion, it was possible to observe a release of $26.10 \pm 1.60\%$ of VD₃ in the first 15 min. In the phase of gastric digestion, the pH was 3.0, and both proteins had positive charges and repelled each other, thus reducing their main interaction strength. In addition, the action of pepsin on proteins can favor the breakdown of microcapsule integrity and facilitate the release of VD₃. However, the release was not complete because the API has a certain degree of resistance to gastric digestion; thus, it may protect Lf and retain VD₃ (Suárez & Añón, 2019; Wang et al., 2017). However, during intestinal digestion, approximately $71.87 \pm 2.02\%$ of VD₃ was released after 60 min. At this stage, pancreatin and the bile salts present may have digested API-U, Lf, and coconut oil, thus allowing the release of VD₃. Santos, Geraldo De Carvalho, and Garcia-Rojas (2021) also obtained a high (80%) intestinal release of VD₃ after encapsulation by complex coacervation using carboxymethyl tara gum and Lf.

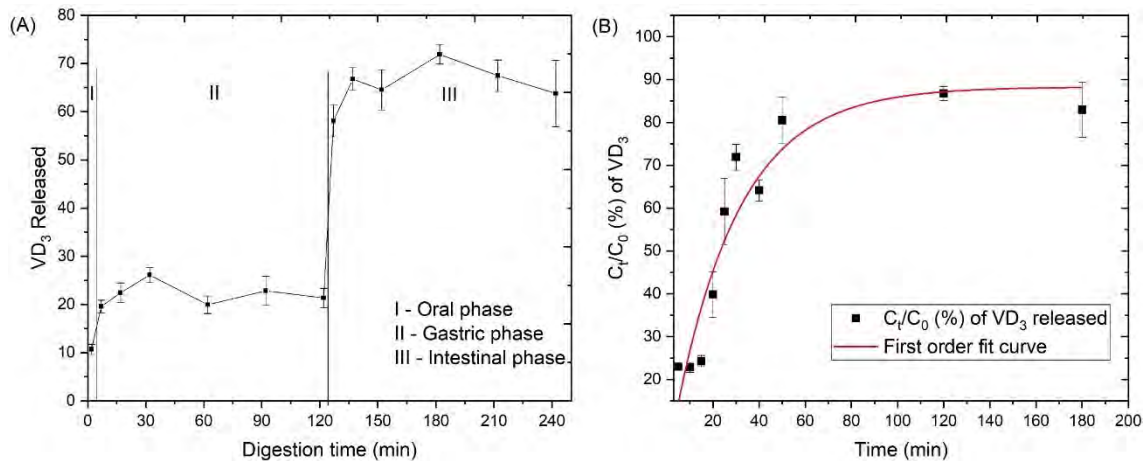


Figure 20. (A) Release profile of encapsulated VD₃ during in vitro gastrointestinal digestion. (B) Release profile of encapsulated VD₃ and incorporated in simulated bread during in vitro intestinal digestion. C_t/C_0 (%) is the percentage division of the concentration at time t (C_t) and at the beginning of the experiment (C_0). The error bars represent \pm standard deviation, $n = 3$.

4.3.3.2. Stability of microcapsules

The stability results for free VD₃ and VD₃-M (sample 4) are shown in Fig. 21. In all cases, microencapsulated VD₃ was protected significantly ($p < 0.05$). For UV radiation, the exposure of free VD₃ and VD₃-M presented a slow trend in the first 2 h (Fig. 21B). However, in the third hour, the degradation of free VD₃ started to be faster until 22 h, from which its degradation started to be slow, reaching $20.89 \pm 1.23\%$ of recovered VD₃. Therefore, the study of the degradation of VD₃-M was conducted for up to 22 h. We observed that $87.40 \pm 1.65\%$ of the VD₃ encapsulated in the API-U: Lf heteroprotein complex was protected from the action of UV radiation after the exposure period. Similarly, Luo et al. (2012) obtained high stability (more than 70%) of VD₃ encapsulated in matrices formed by zein and carboxymethyl chitosan. In another study, Jiang et al. (2019) observed that 74.22 and 65.3% of VD₃ encapsulated in nano emulsion and nano complexes formed by pea protein isolate were protected from degradation by UV after 180 min of exposure. Zhang et al. (2019)

observed that soy protein isolates protected VD₃, probably due to the absorption of ultraviolet light by aromatic hydroxyl groups and double bonds in the soy protein, thus reducing UV intensity and protecting VD₃.

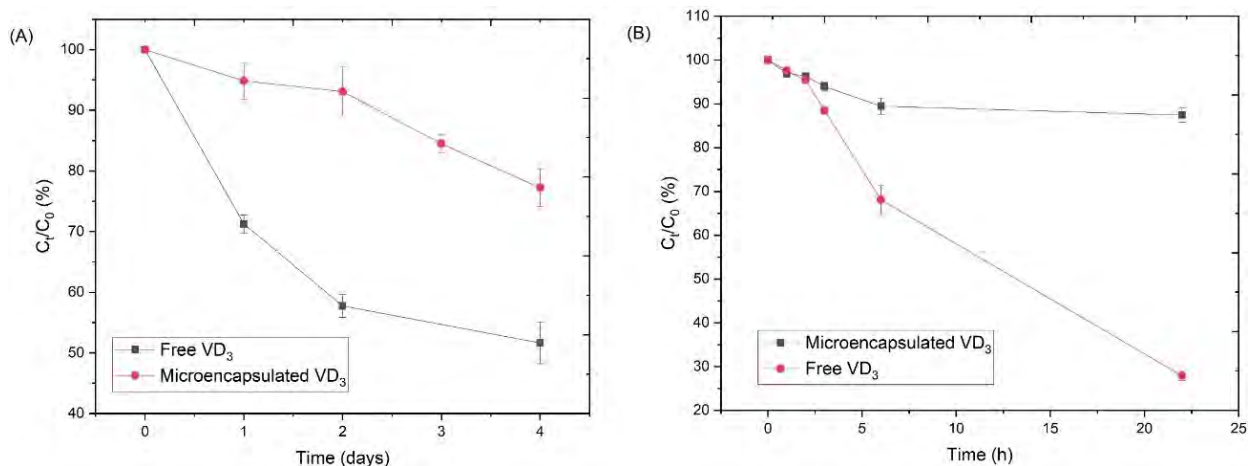


Figure 21. The stability of VD₃ (64.29 µg/g of water) at (A) ambient temperature (25 ± 1 °C), and (B) Ultraviolet radiation at 362 nm. C_t/C₀ (%) is the percentage division of the concentration at time t (C_t) and at the beginning of the experiment (C₀). The error bars represent ± standard deviation, n = 3.

At room temperature, free VD₃ showed a high degradation trend, where approximately 29% of VD₃ was degraded during the first day, reaching 49% on the fourth day, from which the variation in degradation was not significant until the fifth day of the experiment (Fig. 21A). In the case of microencapsulated VD₃, on the first day, degradation was only 5%, and by the fourth day, it was only 23%. These results show the ability of microcapsules to protect VD₃ at room temperature. Many authors have shown that VD₃ has some resistance to heat degradation, which may explain the slow degradation of free VD₃ that we observed in this study. For example, Zareie, Abbasi, and Faghieh (2019) fortified canola oil with different concentrations of VD₃ subjected to different temperatures, and they observed that, at a concentration of 5.625 µg/mL, approximately 95% of VD₃ resisted degradation upon heating at 100 °C for 30 min. It was also estimated that the time to maximum rate under isothermal conditions of VD₃ exceeded 100 days for approximately 70.91 °C (Tsai, Lin, Hong, & Lin, 2017). However, this situation depends on the medium in which VD₃ is dissolved. Like our study, Temova Rakuša et al. (2021) observed that VD₃ at 25 °C in an aqueous medium can undergo high degradation (90%) in 24 h. However, this depends on the concentration of VD₃, with slower degradation at high concentrations, which justifies the difference between these authors' results and ours. Because they used 10 µg/mL VD₃, the concentrations in our study were approximately 64.29 µg/mL.

3.5 Vitamin D₃ microcapsules incorporated in bread

The need for food fortification with vitamin D has been urgent for many countries. Among various products, orange juice, baked products, milks, and their derivatives are seriously considered for vitamin D fortification (Villota & Hawkes, 2018). Therefore, in the present study, bread was chosen as the food model for the incorporation of microencapsulated VD₃. According to the results presents in Fig. 22, approximately 88.65 ± 2.08% of microencapsulated VD₃ in API-U: Lf heteroprotein complexes was protected during the bakery process, while only 64.63 ± 1.80% of free VD₃ was recovered. The high stability of VD₃ during cooking was expected, as we reported earlier (Section 3.3.4.). H. Zhu et al. (2021) also verified high (81%) VD₃ recovery after simulated bread fortification with microcapsules

formed with hen egg white and green tea. Fig. 20 (B) shows the profile of the release kinetics of the microencapsulated VD₃ incorporated in the bread under intestinal simulation conditions. Approximately $22.98 \pm 0.33\%$ of VD₃ was released in the first 5 min, and at the end of 180 min, $82.96 \pm 6.44\%$ of VD₃ was released. Data obtained during digestion were analyzed using zero-order, first-order, Higuchi, and Ritger-Peppas mathematical models (Fig. 23). Our results (Table 10) were better fitted ($R^2 = 0.85$) in the first-order model, meaning that the release of VD₃ occurred by molecular diffusion (Fickian) due to concentration gradients. Generally, this diffusion can occur when the solvent fills the matrix pores with sizes between 20 and 50 nm, or the solute (encapsulated bioactive substance) can pass through small “pores” existing in the matrices to fluid where its concentration is lower (Bruschi, 2015; Peppas, 1984). As discussed in the gastrointestinal digestion simulation (Section 3.3.3.), the entire structure of VD₃-M was completely disrupted due to the action of enzymes and bile salts present in the intestinal fluid, which may explain the possible diffusion inside the food matrices to the surrounding solvent. Our results are in line with the findings by Luo et al. (2012) that encapsulated VD₃ using nanocomplexes of carboxymethyl chitosan and zein.

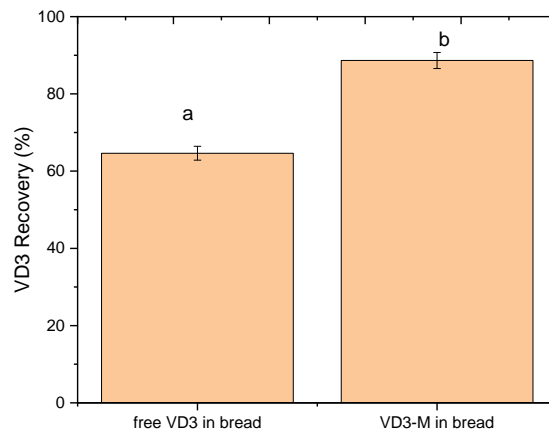


Figure 22. Stability of VD₃ incorporated in bread, heated at 200 °C for 30 min. The error bars represent \pm standard deviation, $n = 3$. VD₃-M is the VD₃ loaded in microcapsules. Different letters demonstrate statistical difference ($p < 0.05$).

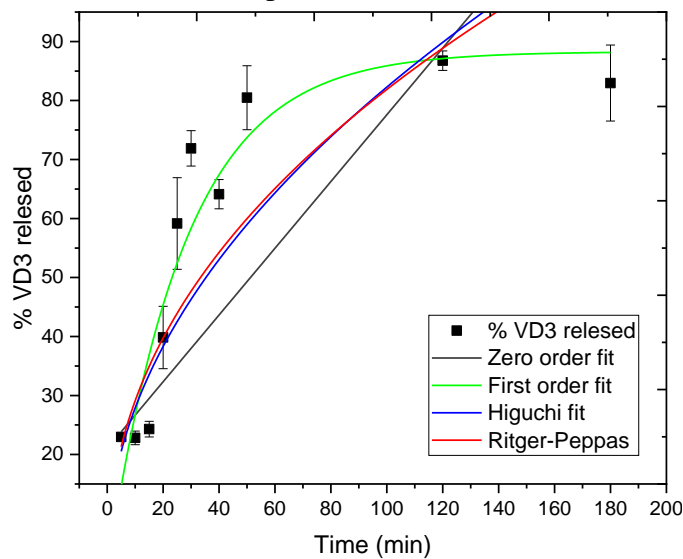


Figure 23. Fitting models of VD₃ release from bread in simulated *in vitro* of intestinal digestion. The error bars represent \pm standard deviation, $n = 3$.

Table 10. Constants of mathematical models were used to study the release profile of VD₃ loaded in API-U: Lf matrices incorporated in the wheat bread, in simulated intestinal digestion conditions.

Model	Higuchi			First Order			Ritger-Peppas				Zero Order		
	$Y = k_h t^{0.5} + F_0$			$Y = F_{max}[1 - \exp(-k_1 t)]$			$Y = F_0 + k t^n$				$Y = F_0 + k_0 t$		
Constants	k_h	R^2	F_0	k_1	R^2	F_{max}	k	n	R^2	F_0	K_0	R^2	F_0
Values	6.15	0.65	5.63	0.03	0.85	91.00	5.20	0.59	0.40	9.13	0.33	0.47	38.98

k, kh, k1, and k0 is the model constant, F0 is the release fraction in time zero, Fmax is the release maxim fraction, R² is the adjusted chi-square, t is the time.

4 Conclusion

In the present study, VD₃ was microencapsulated using heteroprotein complexes (API-U and Lf) as a wall material at pH 6.5 and in a ratio of 1:3 (w/w). The high affinity of API-U and Lf observed through ITC made it possible to obtain a high VD₃ encapsulation efficiency (up to 90%) such that the microcapsules were protected from thermal and photolytic degradation. During the simulation of the in vitro gastrointestinal digestion, the greatest amount of microencapsulated VD₃ was released in the intestinal phase. In the bread production simulation, the microcapsules protected 86% of VD₃ from thermal degradation (200 °C), and the intestinal digestion showed that approximately 90% of VD₃ was released by diffusion, obeying first-order kinetics. Thus, we conclude that VD₃ encapsulated by API-U: Lf complexes can be used for food fortification in the bakery industry.

5 References

- Amit, Jamwal, R., Kumari, S., Dhaulaniya, A. S., Balan, B., & Singh, D. K. (2020). Application of ATR-FTIR spectroscopy along with regression modelling for the detection of adulteration of virgin coconut oil with paraffin oil. *LWT- Food Science and Technology*, 118, 108754. <https://doi.org/10.1016/j.lwt.2019.108754>
- Amrein, K., Scherkl, M., Hoffmann, M., Neuwersch-Sommeregger, S., Köstenberger, M., Tmava Berisha, A., Martucci, G., Pilz, S., & Malle, O. (2020). Vitamin D deficiency 2.0: an update on the current status worldwide. *European Journal of Clinical Nutrition* 2020 74:11, 74(11), 1498–1513. <https://doi.org/10.1038/S41430-020-0558-Y>
- Bajaj, S. R., Marathe, S. J., & Singhal, R. S. (2021). Co-encapsulation of vitamins B12 and D3 using spray drying: Wall material optimization, product characterization, and release kinetics. *Food Chemistry*, 335, 127642. <https://doi.org/10.1016/j.foodchem.2020.127642>
- Bastos, L. P. H., de Carvalho, C. W. P., & Garcia-Rojas, E. E. (2018). Formation and characterization of the complex coacervates obtained between lactoferrin and sodium alginate. *International Journal of Biological Macromolecules*, 120, 332–338. <https://doi.org/10.1016/j.ijbiomac.2018.08.050>
- Bastos, L. P. H., de Sá Costa, B., Siqueira, R. P., & Garcia-Rojas, E. E. (2020). Complex coacervates of β-lactoglobulin/sodium alginate for the microencapsulation of black pepper (*Piper nigrum* L.) essential oil: Simulated gastrointestinal conditions and modeling release kinetics. *International Journal of Biological Macromolecules*, 160, 861–870. <https://doi.org/10.1016/j.ijbiomac.2020.05.265>
- Bastos, L. P. H., dos Santos, C. H. C., de Carvalho, M. G., & Garcia-Rojas, E. E. (2020). Encapsulation of the black pepper (*Piper nigrum* L.) essential oil by lactoferrin-sodium alginate complex coacervates: Structural characterization and simulated gastrointestinal conditions. *Food Chemistry*, 316, 126345. <https://doi.org/10.1016/j.foodchem.2020.126345>

- Bejarano-Luján, D. L., & Netto, F. M. (2010). Effect of alternative processes on the yield and physicochemical characterization of protein concentrates from *Amaranthus cruentus*. *LWT - Food Science and Technology*, *43*(5), 736–743. <https://doi.org/10.1016/j.lwt.2009.11.013>
- Bilezikian, J. P., Bikle, D., Hewison, M., Lazaretti-Castro, M., Formenti, A. M., Gupta, A., Madhavan, M. V, Nair, N., Babalyan, V., Hutchings, N., Napoli, N., Accili, D., Binkley, N., Landry, D. W., & Giustina, A. (2020). MECHANISMS IN ENDOCRINOLOGY: Vitamin D and COVID-19. *European Journal of Endocrinology*, *183*(5), R133–R147. <https://doi.org/10.1530/EJE-20-0665>
- Brodkorb, A., Egger, L., Alminger, M., Alvito, P., Assunção, R., Ballance, S., Bohn, T., Bourlieu-Lacanal, C., Boutrou, R., Carrière, F., Clemente, A., Corredig, M., Dupont, D., Dufour, C., Edwards, C., Golding, M., Karakaya, S., Kirkhus, B., Le Feunteun, S., ... Recio, I. (2019). INFOGEST static in vitro simulation of gastrointestinal food digestion. *Nature Protocols*, *14*(4), 991–1014. <https://doi.org/10.1038/s41596-018-0119-1>
- Bruschi, M. L. (2015). *Strategies to Modify the Drug Release from Pharmaceutical Systems*. Elsevier. <https://doi.org/10.1016/C2014-0-02342-8>
- Cauvain, S. P. (2015). Breadmaking Processes. In *Technology of Breadmaking* (pp. 23–55). Springer International Publishing. https://doi.org/10.1007/978-3-319-14687-4_2
- Chapeau, A. L., Hamon, P., Rousseau, F., Croguennec, T., Poncelet, D., & Bouhallab, S. (2017). Scale-up production of vitamin loaded heteroprotein coacervates and their protective property. *Journal of Food Engineering*, *206*, 67–76. <https://doi.org/10.1016/J.JFOODENG.2017.03.005>
- Cordero-de-los-Santos, M. Y., Osuna-Castro, J. A., Borodanenko, A., & Paredes-López, O. (2005). Physicochemical and Functional Characterisation of Amaranth (*Amaranthus hypochondriacus*) Protein Isolates Obtained by Isoelectric Precipitation and Micellisation. *Food Science and Technology International*, *11*(4), 269–280. <https://doi.org/10.1177/1082013205056491>
- Devi, N., Sarmah, M., Khatun, B., & Maji, T. K. (2017). Encapsulation of active ingredients in polysaccharide–protein complex coacervates. In *Advances in Colloid and Interface Science* (Vol. 239, pp. 136–145). Elsevier B.V. <https://doi.org/10.1016/j.cis.2016.05.009>
- Diarrassouba, F., Remondetto, G., Garrait, G., Alvarez, P., Beyssac, E., & Subirade, M. (2015). Self-assembly of β -lactoglobulin and egg white lysozyme as a potential carrier for nutraceuticals. *Food Chemistry*, *173*, 203–209. <https://doi.org/10.1016/j.foodchem.2014.10.009>
- El Ghazzaqui Barbosa, A., Constantino, A. B. T., Bastos, L. P. H., & Garcia-Rojas, E. E. (2022). Encapsulation of sacha inchi oil in complex coacervates formed by carboxymethylcellulose and lactoferrin for controlled release of β -carotene. *Food Hydrocolloids for Health*, *2*, 100047. <https://doi.org/10.1016/j.fhfh.2021.100047>
- Ferstl, M., Drechsler, M., Rachel, R., Rischer, M., Engel, J., Backofen, M., & Goepferich, A. (2013). The impact of polyelectrolyte structure on the shape of nanoassemblies with cationic peptides. *Journal of Pharmaceutical Sciences*, *102*(8), 2599–2607. <https://doi.org/10.1002/jps.23619>
- Gao, J., Liu, C., Shi, J., Ni, F., Shen, Q., Xie, H., Wang, K., Lei, Q., Fang, W., & Ren, G. (2021). The regulation of sodium alginate on the stability of ovalbumin-pectin complexes for VD3 encapsulation and in vitro simulated gastrointestinal digestion study. *Food Research International*, *140*, 110011. <https://doi.org/10.1016/j.foodres.2020.110011>
- Gaonkar, A. G., Vasisht, N., Khare, A. R., & Sobel, R. (2014). *Microencapsulation in the*

- Food Industry*. Elsevier. <https://doi.org/10.1016/C2012-0-00852-6>
- Holick, M. F. (2017). The vitamin D deficiency pandemic: Approaches for diagnosis, treatment and prevention. *Reviews in Endocrine and Metabolic Disorders* 2017 18:2, 18(2), 153–165. <https://doi.org/10.1007/S11154-017-9424-1>
- Jakobsen, J., & Knuthsen, P. (2014). Stability of vitamin D in foodstuffs during cooking. *Food Chemistry*, 148, 170–175. <https://doi.org/10.1016/j.foodchem.2013.10.043>
- Jannasari, N., Fathi, M., Moshtaghian, S. J., & Abbaspourrad, A. (2019). Microencapsulation of vitamin D using gelatin and cress seed mucilage: Production, characterization and in vivo study. *International Journal of Biological Macromolecules*, 129, 972–979. <https://doi.org/10.1016/J.IJBIOMAC.2019.02.096>
- Jiang, S., Yildiz, G., Ding, J., Andrade, J., Rababah, T. M., Almajwal, A., Abulmeatyc, M. M., & Feng, H. (2019). Pea Protein Nanoemulsion and Nanocomplex as Carriers for Protection of Cholecalciferol (Vitamin D3). *Food and Bioprocess Technology* 2019 12:6, 12(6), 1031–1040. <https://doi.org/10.1007/S11947-019-02276-0>
- Lamsen, M. R. L., Wang, T., D'Souza, D., Dia, V., Chen, G., & Zhong, Q. (2020). Encapsulation of vitamin D 3 in gum arabic to enhance bioavailability and stability for beverage applications. *Journal of Food Science*, 85(8), 2368–2379. <https://doi.org/10.1111/1750-3841.15340>
- Lan, Y., Ohm, J. B., Chen, B., & Rao, J. (2021). Microencapsulation of hemp seed oil by pea protein isolate–sugar beet pectin complex coacervation: Influence of coacervation pH and wall/core ratio. *Food Hydrocolloids*, 113, 106423. <https://doi.org/10.1016/J.FOODHYD.2020.106423>
- Luo, Y., Teng, Z., & Wang, Q. (2012). Development of Zein Nanoparticles Coated with Carboxymethyl Chitosan for Encapsulation and Controlled Release of Vitamin D3. *Journal of Agricultural and Food Chemistry*, 60(3), 836–843. <https://doi.org/10.1021/jf204194z>
- Orsini Delgado, M. C., Nardo, A., Pavlovic, M., Rogniaux, H., Añón, M. C., & Tironi, V. A. (2016). Identification and characterization of antioxidant peptides obtained by gastrointestinal digestion of amaranth proteins. *Food Chemistry*, 197, 1160–1167. <https://doi.org/10.1016/j.foodchem.2015.11.092>
- Peppas, N. A. (1984). Mathematical Models for Controlled Release Kinetics. In R. S. Langer & D. L. Wise (Eds.), *Medical Applications of Controlled Release* (1st ed., pp. 169–188). CRC Press. <https://doi.org/10.1201/9780429276620-10>
- Sabbione, A. C., Nardo, A. E., Añón, M. C., & Scilingo, A. (2016). Amaranth peptides with antithrombotic activity released by simulated gastrointestinal digestion. *Journal of Functional Foods*, 20, 204–214. <https://doi.org/10.1016/j.jff.2015.10.015>
- Santos, M. B., Costa, N. R. da, & Garcia-Rojas, E. E. (2018). Interpolymeric Complexes Formed Between Whey Proteins and Biopolymers: Delivery Systems of Bioactive Ingredients. *Comprehensive Reviews in Food Science and Food Safety*, 17(3), 792–805. <https://doi.org/10.1111/1541-4337.12350>
- Santos, M. B., de Carvalho, C. W. P., & Garcia-Rojas, E. E. (2018). Heteroprotein complex formation of bovine serum albumin and lysozyme: Structure and thermal stability. *Food Hydrocolloids*, 74, 267–274. <https://doi.org/https://doi.org/10.1016/j.foodhyd.2017.08.016>
- Santos, M. B., de Carvalho, C. W. P., & Garcia-Rojas, E. E. (2021). Microencapsulation of vitamin D3 by complex coacervation using carboxymethyl tara gum (*Caesalpinia spinosa*) and gelatin A. *Food Chemistry*, 343, 128529.

- <https://doi.org/10.1016/j.foodchem.2020.128529>
- Santos, M. B., Geraldo De Carvalho, M., & Garcia-Rojas, E. E. (2021). Carboxymethyl tara gum-lactoferrin complex coacervates as carriers for vitamin D 3 : Encapsulation and controlled release. *Food Hydrocolloids*, 112. <https://doi.org/10.1016/j.foodhyd.2020.106347>
- Sassi, F., Tamone, C., & D'Amelio, P. (2018). Vitamin D: Nutrient, Hormone, and Immunomodulator. *Nutrients* 2018, Vol. 10, Page 1656, 10(11), 1656. <https://doi.org/10.3390/NU10111656>
- Shevkani, K., Singh, N., Rana, J. C., & Kaur, A. (2014). Relationship between physicochemical and functional properties of amaranth (*Amaranthus hypochondriacus*) protein isolates. *International Journal of Food Science & Technology*, 49(2), 541–550. <https://doi.org/10.1111/ijfs.12335>
- Suárez, S., & Añón, M. C. (2019). Amaranth proteins emulsions as delivery system of Angiotensin-I converting enzyme inhibitory peptides. *Food Hydrocolloids*, 90, 154–161. <https://doi.org/10.1016/j.foodhyd.2018.11.046>
- Temova Rakuša, Ž., Pišlar, M., Kristl, A., & Roškar, R. (2021). Comprehensive Stability Study of Vitamin D3 in Aqueous Solutions and Liquid Commercial Products. *Pharmaceutics*, 13(5), 617. <https://doi.org/10.3390/pharmaceutics13050617>
- Tomé Constantino, A. B., & Garcia-Rojas, E. E. (2020). Modifications of physicochemical and functional properties of amaranth protein isolate (*Amaranthus cruentus* BRS Alegria) treated with high-intensity ultrasound. *Journal of Cereal Science*, 95, 103076. <https://doi.org/10.1016/j.jcs.2020.103076>
- Tsai, S. Y., Lin, H. Y., Hong, W. P., & Lin, C. P. (2017). Evaluation of preliminary causes for vitamin D series degradation via DSC and HPLC analyses. *Journal of Thermal Analysis and Calorimetry*, 130(3), 1357–1369. <https://doi.org/10.1007/S10973-017-6209-4/FIGURES/11>
- Villota, R., & Hawkes, J. G. (2018). Reaction Kinetics in Food Systems. In *Handbook of Food Engineering* (pp. 225–484). CRC Press. <https://doi.org/10.1201/9780429449734-3>
- Wang, B., Timilsena, Y. P., Blanch, E., & Adhikari, B. (2017). Lactoferrin: Structure, function, denaturation and digestion. *Critical Reviews in Food Science and Nutrition*, 59:4, 580-596. <https://doi.org/10.1080/10408398.2017.1381583>
- Wei, Z., Cheng, Y., & Huang, Q. (2019). Heteroprotein complex formation of ovotransferrin and lysozyme: Fabrication of food-grade particles to stabilize Pickering emulsions. *Food Hydrocolloids*, 96, 190–200. <https://doi.org/10.1016/j.foodhyd.2019.05.024>
- Xu, M., Jin, Z., Gu, Z., Rao, J., & Chen, B. (2020). Changes in odor characteristics of pulse protein isolates from germinated chickpea, lentil, and yellow pea: Role of lipoxygenase and free radicals. *Food Chemistry*, 314, 126184. <https://doi.org/10.1016/J.FOODCHEM.2020.126184>
- Yuan, Y., Kong, Z. Y., Sun, Y. E., Zeng, Q. Z., & Yang, X. Q. (2017). Complex coacervation of soy protein with chitosan: Constructing antioxidant microcapsule for algal oil delivery. *LWT- Food Science and Technology*, 75, 171–179. <https://doi.org/10.1016/j.lwt.2016.08.045>
- Yue, J., Gu, Z., Zhu, Z., Yi, J., Ohm, J. B., Chen, B., & Rao, J. (2021). Impact of defatting treatment and oat varieties on structural, functional properties, and aromatic profile of oat protein. *Food Hydrocolloids*, 112, 106368. <https://doi.org/10.1016/J.FOODHYD.2020.106368>
- Zareie, M., Abbasi, A., & Faghieh, S. (2019). Thermal Stability and Kinetic Study on Thermal

- Degradation of Vitamin D3 in Fortified Canola Oil. *Journal of Food Science*, 84(9), 2475–2481. <https://doi.org/10.1111/1750-3841.14764>
- Zhang, A., Chen, S., Wang, Y., Zhou, G., Wang, L., Wang, X., & Xu, N. (2019). Effect of different homogenization pressure on soy protein isolate-vitamin D3 complex. *Process Biochemistry*, 87, 145–150. <https://doi.org/10.1016/j.procbio.2019.09.011>
- Zheng, J., Gao, Q., Ge, G., Wu, J., Tang, C., Zhao, M., & Sun, W. (2021). Heteroprotein Complex Coacervate Based on β -Conglycinin and Lysozyme: Dynamic Protein Exchange, Thermodynamic Mechanism, and Lysozyme Activity. *Journal of Agricultural and Food Chemistry*, 69(28), 7948–7959. <https://doi.org/10.1021/acs.jafc.1c02204>
- Zheng, J., Gao, Q., Tang, C., Ge, G., Zhao, M., & Sun, W. (2020). Heteroprotein complex formation of soy protein isolate and lactoferrin: Thermodynamic formation mechanism and morphologic structure. *Food Hydrocolloids*, 100, 105415. <https://doi.org/10.1016/j.foodhyd.2019.105415>
- Zheng, J., Tang, C., Ge, G., Zhao, M., & Sun, W. (2020). Heteroprotein complex of soy protein isolate and lysozyme: Formation mechanism and thermodynamic characterization. *Food Hydrocolloids*, 101, 105571. <https://doi.org/10.1016/j.foodhyd.2019.105571>
- Zhu, H., Mettu, S., Cavalieri, F., & Ashokkumar, M. (2021). Ultrasonic microencapsulation of oil-soluble vitamins by hen egg white and green tea for fortification of food. *Food Chemistry*, 353, 129432. <https://doi.org/10.1016/j.foodchem.2021.129432>
- Zhu, J., Li, H., Xu, Y., & Wang, D. (2019). Construction of Fucoxanthin Vector Based on Binding of Whey Protein Isolate and Its Subsequent Complex Coacervation with Lysozyme. *Journal of Agricultural and Food Chemistry*, 67(10), 2980–2990. <https://doi.org/10.1021/ACS.JAFC.8B06679>

**CAPÍTULO V. MICROENCAPSULATION OF BETANIN BY
COMPLEX COACERVATION OF CARBOXYMETHYLCELLULOSE
AND AMARANTH PROTEIN ISOLATE FOR APPLICATION IN
EDIBLE GELATIN FILMS**

Aceito para publicação na Food Hydrocolloids em 05 de julho de 2022

Abstract

Betanin is a natural pigment with a hydrophilic nature, a red color, and high antioxidant power but is unstable in the presence of heat and light and stable at pH values between 3 and 7. The present research aimed to microencapsulate betanin by complex coacervation using ultrasound-treated amaranth protein isolate (API-U) and sodium carboxymethyl cellulose (CMC) for application in edible gelatin films. The study of the formation of the wall material was carried out by zeta potential, turbidity, and isothermal titration calorimetry analysis. Betanin was encapsulated using the formation of a double emulsion in different core/wall ratios. Finally, the microcapsules were used to manufacture gelatin films. The results showed that API-U and CMC can form complexes at pH 3.0, through electrostatic attraction with high affinity. The encapsulation efficiency of betanin was high, ranging from 61 to 87%. The microcapsules protected betanin from thermal degradation (50 °C), increasing its half-life by approximately 2.92-fold. After gastrointestinal digestion, the bioaccessibility of encapsulated betanin was approximately 84%. Betanin microcapsules were added to edible gelatin films, which resulted in reduced light transmission and higher antioxidant activity (FRAP and ABTS⁺). The controlled release of antioxidants from the films was driven by diffusion and case II relaxation. Therefore, betanin-containing microcapsules formed by API-U/CMC complex coacervates can be used in the production of edible gelatin films with reduced light transmission and good antioxidant activity properties.

Keywords: Amaranth protein isolate, carboxymethylcellulose, microencapsulation, biocomposite film, betanin.

1 Introduction

Betanin is a natural red pigment that belongs to the betalains class and can be extracted from *Beta vulgaris*, *Opuntia* sp., and the Amaranthaceae family. Betanin is water-soluble and stable at pH values between 3 and 7 (Esatbeyoglu et al., 2015). In addition to coloring, betanin has biological activity as an antioxidant that is approximately 3 to 4 times higher than those of ascorbic acid, catechin, or rutin (Cai et al., 2003; Esatbeyoglu et al., 2015). Also, betanin can be highlighted as a compound with potential for the protection of cells, tissues, and organs of the human organism. For example, betanin has been proven to protect blood LDL (low-density lipoprotein) from oxidation and may be involved in reducing damage to the body's DNA (Tesoriere et al., 2004; Zielińska-Przyjemska et al., 2012). Although betanin has these beneficial properties, it is sensitive to light and high temperatures, which limits its application in the food industry. To address this situation, encapsulation has been demonstrated to be an effective method of preserving its properties (Amjadi et al., 2018; Pagano et al., 2018; Vergara et al., 2014).

Among several encapsulation methods, the complex coacervation process can be highlighted because it presents a high encapsulation efficiency, high integrity of the wall material, and does not use harsh conditions such as organic solvents or high temperatures (Yan & Zhang, 2014; Timilsena et al., 2019). The complex coacervation process consists of three basic steps: emulsification, coacervation, and formation and/or crosslinking. At the emulsion formation stage, hydrophobic bioactive compounds are encapsulated using oil-in-water (O/W) emulsions. In the case of water-soluble compounds (such as betanin), double emulsions such as water-in-oil-in-water (W/O/W) are used. These emulsions may allow coencapsulation with enriched oils or even with oils that have biological properties (Comunian et al., 2013; Kanha et al., 2020). In the second stage, complex coacervation occurs by the electrostatic interaction of the polymers that form the wall material of the microcapsule, which can be initiated by changes in environmental conditions (such as pH adjustment) that can affect the solubility of polymers in the aqueous phase. However, this depends on many parameters, including the load density of polymers, their conformation or proportion, total solid content, and pH (Yan & Zhang, 2014; Gomez-Estaca et al., 2016; Lan et al., 2021; Timilsena et al., 2019; Vicente et al., 2017). Finally, in the third step, due to the ionic nature of the interaction between the layers of biopolymers, the walls of the microcapsules formed by complex coacervates are generally unstable and have low mechanical strength, making it necessary to use crosslinkers to harden them (Yan & Zhang, 2014).

The use of protein-polysaccharide complex coacervates as wall material appears to be viable, as they are integral parts of many foods, as well as the fact that they do not need an external emulsifying agent and provide good encapsulation characteristics due to the structural synergies of the two polymers (Schmitt & Turgeon, 2011; Xiong et al., 2017). Thus, in this work, sodium carboxymethylcellulose (CMC) and amaranth protein isolate (API) were studied as encapsulation wall materials. CMC is an anionic biodegradable linear polymer that has negative charges at practically all pH values due to ionized carboxylic groups (Barbucci et al., 2000). CMC in combination with other polymers, including lactoferrin, gelatin, or chitosan, proved to be a good wall material due to its high interaction affinity in the formation of complex coacervates, which provided a high encapsulation efficiency of different compounds (Duhoranimana et al., 2018; El Ghazzaqui Barbosa et al., 2022; Kanha et al., 2020). Corroborating the current trend in the use of vegetable proteins, the API is a promising protein due to the presence of essential amino acids, including tryptophan, methionine, lysine, histidine, phenylalanine, valine, and isoleucine (Coelho et al., 2018). It originates from a relatively inexpensive source with attractive agronomic characteristics because it grows at

different altitudes. The API is composed of different polypeptide fractions, which include globulins, albumins, glutelins, and prolamins (Constantino & Garcia-Rojas, 2022a). In addition to this nutritional value, the API has biological activities that include antithrombotic action and the elimination of free radicals (Montoya-Rodríguez et al., 2014; Orsini Delgado et al., 2016; Sabbione et al., 2016).

The microcapsules obtained by complex coacervation showed potential for applications in the food industry, such as in the production of yogurt, bread, and biodegradable and edible films (Rutz et al., 2017; H. Wang et al., 2021). Edible and biodegradable films are an alternative to plastic packaging due to safety issues and environmental concerns (H. Wang et al., 2021). Generally, these films are composed of proteins, polysaccharides, and lipids. Among proteins, gelatin has been commonly used because it is a renewable, biodegradable, and edible material; films produced from gelatin provide a good barrier to vapor exchange and have durable mechanical properties (S. Wang et al., 2019). Different studies have shown that it is possible to add free or microencapsulated bioactive compounds to gelatin films, making them functional with antibacterial and antioxidant properties (Amjadi et al., 2020; Kowalczyk et al., 2021; H. Wang et al., 2021; S. Wang et al., 2019).

In this context, the present work aimed to manufacture betanin microcapsules using CMC and ultrasound-treated amaranth protein isolate (API-U) complex coacervates for use in edible gelatin film. First, through turbidity, zeta potential, and isothermal titration calorimetry, the optimal pH and ratio for the formation of CMC/API-U complex coacervates were studied. Then, we evaluated the best conditions for betanin encapsulation in complex coacervates formed by CMC/API-U. Finally, the microcapsules were added to edible gelatin films, and their antioxidant and physicochemical properties were evaluated.

2 Materials and methods

2.1 Materials

Amaranth grains were purchased from Relva Verde Alimentos EIRELI (São Paulo, Brazil). Sacha inchi (*Plukenetia volubilis* L.) oil (SIO) was purchased from Peruvian Functional Foods (Lima, Perú). Betanin (ref. 901266), α -amylase (ref. A3403), porcine pepsin (ref. P6887), porcine pancreatin (ref. P7545), porcine bile extract (ref. B3883), 2,4,6-tris(2-pyridyl)-s-triazine (TPTZ) (ref 93285), 2,2 azino bis (3-ethylbenzothiazoline-6-sulfonic acid) diammonium salt (ABTS) (ref A1888), 6-hydroxy-2,5,7,8-tetramethylchroman-2-carboxylic acid (Trolox) (ref. 238813), and sodium carboxymethyl cellulose (CMC) with a degree of substitution of 0.9 and a molecular weight of 250 kDa (ref. 419303) were purchased from Sigma–Aldrich (St. Louis, USA). Polyglycerol (PGPR 90) was purchased from SGS (Brazil). Ultrapure water (Master System R&D, Gehaka, Brazil) with 0.05 $\mu\text{S}/\text{cm}$ and P.A. reagents were used in all assays.

2.2 Study of wall material

2.2.1 Isolation and ultrasound treatment of amaranth protein

The API-U was obtained according to the methodology described by Constantino & Garcia-Rojas (2022a). Briefly, defatted amaranth grain flour was suspended in water (1/10, w/v), and the pH was adjusted to 9.0 with 2.0 mol L⁻¹ NaOH. The suspension was magnetically stirred (NT101, Nova técnica, Brazil) for 30 min and then centrifuged (Digicen 21 R, Orto Alresa, Spain) at 9,000 $\times g$ for 20 min. The supernatant was collected, and its pH was adjusted to 5.0 using 2.0 mol L⁻¹ HCl, followed by centrifugation at 4,000 $\times g$ for 10 min at 4 °C. The

precipitate was collected, resuspended in water, neutralized, and freeze-dried (Terroni, Enterprise I, Brazil) for 48 h. Then, a 20 mL aqueous solution of the obtained proteins (10%, w/v) was treated with a UP100H ultrasound (Hilscher, Germany) at 60% amplitude for 30 min, lyophilized, packaged, and stored at -20 °C for further analysis. The API-U average molecular weight (723 ± 12.9 kDa) was determined in our previous study (Constantino & Garcia-Rojas, 2022a).

2.2.2 Preparation of solutions

The biopolymers (API-U and CMC) were weighed on an analytical balance (Shimadzu, AY220, Philippines) to prepare an aqueous solution at 0.1% (w/w). The biopolymers were magnetically stirred (Fisatom, São Paulo, Brazil) at room temperature. API-U was homogenized for 30 minutes at pH 9.0, while CMC was homogenized overnight.

2.2.3 Zeta-potential and turbidity of ultrasonicated amaranth protein isolate and carboxymethylcellulose

A Zetasizer Nano ZS90 (Malvern Instruments, UK) was used to determine the zeta (ζ)-potential of CMC and API-U solutions. To identify the best conditions for the formation of complex coacervates, the strength of electrostatic interaction (SEI) was calculated according to Equation (1). The turbidity analysis of CMC, API-U, and 1/1 (w/w) solutions was performed by reading the transmittance (T%) on a UV-vis spectrophotometer (Biomate 3S, Thermo Scientific, USA) at 400 nm, using water as a blank. Turbidity was calculated as $100 - T\%$. The pH of the solutions was adjusted from 5 to 2 (in the range of 0.5 ± 0.05 units) with the aid of 0.1 mol L^{-1} NaOH and 0.1 mol L^{-1} HCl.

$$\text{SEI (mV}^2) = |ZP_1| \times |ZP_2| \quad (1)$$

where: ZP_1 and ZP_2 is the measured ζ -potential at each pH for API-U and CMC solutions, respectively.

2.2.4 Isothermal titration calorimetry

Isothermal titration calorimetry (ITC) was performed in Nano-ITC equipment (TA Instruments, USA). The API-U ($0.123 \text{ mmol L}^{-1}$) and CMC ($0.0154 \text{ mmol L}^{-1}$) solutions were prepared in citrate buffer (10 mmol L^{-1} , pH 3.0) at 25 °C. After solubilization, API-U and CMC solutions were dialyzed using 3.5 kDa membranes (Sigma-Aldrich, Midi 3500, USA) and then degassed. In total, 250 μL of API-U was injected into the sample cell containing 1200 μL of CMC. Ten microliters were injected into the sample cell every 150 seconds with agitation at 250 rpm. The thermodynamic parameters (reaction stoichiometry, binding constant, enthalpy, change in entropy, and change in free Gibbs energy) were obtained through the TA Nano Analyze program[®].

2.3 Microencapsulation of betanin

Betanin microencapsulation was performed for 0.5, 1.0, 2.0, and 4.0% (w/w) wall material concentrations and 1/1, 1/2, and 1/4 (w/w) core (betanin aqueous solution)/wall ratios. CMC was solubilized in water overnight, while API-U was solubilized in water for 1 h at pH 9.0 with the aid of 0.1 mol L^{-1} NaOH. Then, the pH was adjusted to 7.0 with the aid of 0.1 mol L^{-1} HCl. Since betanin is a water-soluble compound, encapsulation was performed through a water-in-oil-in-water (W/O/W) double emulsion. The primary emulsion (water-in-oil, W/O) was formed using 33.0% aqueous solution containing betanin (10.0%, w/w) and 67.0% SIO

containing 2.0% PGPR 90. The mixture was homogenized with Ultraturax T25D (IKA, Germany) at 13,500 rpm for 5 min. Then, the W/O emulsion was added to the aqueous solution containing API-U and CMC, according to the proportions mentioned in Table 12. The second emulsion (W/O/W) was formed by homogenizing the suspensions with the Ultraturax T25D at 10,000 rpm for 2 min. The pH was then adjusted to 3.0, and then the microcapsules were magnetically stirred for 4 min. The microcapsules were then left to rest at 4 °C for 24 h. The supernatant was collected for determination of encapsulation efficiency, and the precipitated microcapsules were frozen in liquid nitrogen, lyophilized for 48 h, and stored in a desiccator until further analysis.

2.3.1 Betanin microencapsulation efficiency

The concentration of unencapsulated betanin was determined using a UV–vis spectrophotometer at 531 nm and a calibration curve ($Y=0.1986X$, $R^2=0.9989$) obtained from aqueous solutions of betanin at concentrations ranging from 0.5 to 5 mg mL⁻¹. The encapsulation efficiency of betanin was determined by Equation (2):

$$EE (\%) = 100 \times (TB - UB)/TB \quad (2)$$

where EE (%) is the percentage of encapsulation efficiency, UB is the concentration of unencapsulated betanin present in the supernatant after filtration (0.2 μm), and TB is the theoretical concentration of betanin initially added to the system.

2.3.2 Optical microscopy of emulsions and betanin microcapsules

An aliquot of emulsions and microcapsules (before lyophilization) was observed under a K220 optical microscope (Kasvi, Brazil) coupled to a 5 MP Moticom camera (Kasvi, Brazil) for image capture at 10x magnification with the help of immersion oil.

2.3.3 Simulation of the in vitro gastrointestinal digestion and bioaccessibility of betanin microcapsules

The in vitro simulation of gastrointestinal digestion was performed based on the model proposed by INFOGEST[®] 2.0 (Brodkorb et al., 2019). Briefly, 1 g of lyophilized microcapsules was mixed with 0.8 mL of salivary simulated fluid (SSF) and 0.1 mL of salivary amylase solution (0.75 U mL⁻¹), 0.005 mL of 0.3 mol L⁻¹ CaCl₂ and 0.095 mL of water at pH 7.0. For digestion of the gastric phase, 1.6 mL of gastric simulated solution (SGF), 0.1 mL of pepsin solution (2,000 U mL⁻¹), 0.001 mL of 0.3 mol L⁻¹ CaCl₂, and 0.199 mL of water were mixed with 2 mL of suspension originating from the oral phase. This mixture was adjusted to pH 3.0 with 6 mol L⁻¹ HCl (approximately 0.1 mL). Then, 4 mL originating from gastric digestion was used for intestinal digestion with 1.7 mL of intestinal fluid simulated (SIF), 1 mL of pancreatin solution (100 U mL⁻¹), 0.5 mL of bile solution (10 mmol L⁻¹), 0.008 mL of 0.3 mol L⁻¹ CaCl₂ and 0.592 mL of water, and approximately 0.2 mL of 6 mol L⁻¹ NaOH was added to adjust the pH to 7.0. The entire gastrointestinal simulation was performed under agitation in a shaker at 95 rpm and 37 °C for 2 min for the oral phase and 2 h for each of the gastric and intestinal phases. Aliquots of 0.2 mL of the solutions of each phase were taken at certain times to determine betanin concentrations, and the same amount of each fluid was added.

Bioaccessibility (B*) was determined according to the methodology described by Constantino & Garcia-Rojas (2022b) and calculated using Equation (3):

$$B^* = C_{micela}/C_{digest} \times 100 \quad (3)$$

where C_{micela} and C_{digest} are the concentrations of betanin in the micellar phase and beginning of the digest phase, respectively.

2.3.4 Thermal stability of microencapsulated betanin

The study of the thermal stability of the microcapsules (before lyophilization) and free betanin was performed following the methodology of Aztatzi-Ruggerio et al. (2019), with minor modifications. Five milliliters of the samples containing approximately 1 mg mL^{-1} of betanin were placed in an oven with air circulation (SSDr, Mylbor, Brazil) at $50 \text{ }^\circ\text{C}$ for 1 h. Samples were taken every 10 min, diluted 2 times in phosphate buffer solution (0.1 mol L^{-1} , pH 7.4), shaken in a vortex for 1 min, left to rest for 5 min, and centrifuged at 4,000 rpm for 10 min, and the absorbances of the supernatants were read as described in Section 2.3.1. The percentage of betanin degradation (D) and the half-time ($T_{1/2}$) life were calculated by Equations 4 and 5:

$$D (\%) = 100 * C_t/C_i \quad (4)$$

$$T_{1/2} = \ln(2)/k \quad (5)$$

where C_t and C_i correspond to the concentrations of betanin at time t and the beginning (i) of the experiment, respectively; k is the constant of the velocity of betanin degradation, which is the value of a of the linear regression equation given by plotting the results of $\ln(C_t/C_i)$ and time (y and x , respectively).

2.4 Application of betanin microcapsules in production of gelatin the edible film

2.4.1 Concentration of betanin in microcapsules used for edible film formation

To ensure a higher concentration of betanin in microcapsules, several concentrations of betanin in the core were evaluated, as shown in Table 11. As there was no significant difference ($p < 0.05$) in the results obtained, the system with the highest concentration of betanin (40%, w/w) was chosen for the preparation of the films.

Table 11. Percentage efficiency encapsulation (EE) of betanin at different concentrations in the nucleus of microcapsules (sample D).

Biopolymers				Betanine (%)	EE (%)
TC (%)	API-U (g)	CMC (g)	Total Wall (g)		
1.00	0.072	0.028	0.100	10.0	85.80 ± 1.43^a
1.00	0.072	0.028	0.100	20.0	83.65 ± 3.64^a
1.00	0.072	0.028	0.100	30.0	86.84 ± 0.98^a
1.00	0.072	0.028	0.100	40.0	86.62 ± 0.44^a

TC (%) is the total concentrations of biopolymer in percentage, API-U is ultrasonicated amaranth protein isolate, CMC is carboxymethylcellulose. The results are means \pm the standard deviation and the superscript letters are the results of Tukey's statistic test and the difference between them means that the samples differ statistically ($p < 0.05$).

2.4.2 Preparation of edible film composed with gelatin and betanin microcapsules

Edible films were produced by the casting method based on the methodology of Amjadi et al. (2020), with minor modifications. Therefore, 4.0% (w/w) gelatin, 1.5% (w/w) glycerol, and 0.0, 1.0, 2.5 or 5.0% (w/w) lyophilized microcapsules were used in the final film-forming

solution. Gelatin was solubilized for 30 min at 40 °C, and then the glycerol previously solubilized in water and the microcapsules were added to the solution, followed by homogenization in an Ultraturrax T25D at 4,000 rpm for 4 min. The obtained filmogenic solution was left to rest for 10 min for the removal of air bubbles, and then 34 g of the filmogenic solution was placed in glass Petri dishes 12 cm in diameter (i.e., 0.30 g cm⁻² in area) and dried at 25 °C in an SL 222 incubator shaker (Solab, Brazil) for 24 h. Before the analyses, the films were manually removed from the Petri dishes and left in a desiccator containing saturated magnesium nitrate solution (50% humidity) for two days at room temperature (25 ± 1 °C).

2.4.3 Fourier transform infrared spectrophotometry

Biopolymers, SIO, betanin, lyophilized microcapsules, and edible gelatin films were analyzed by Fourier Transform Infrared Spectrophotometry (FT-IR) (Bruker, Vertex 70, Germany), and spectra were recorded in the wavelength range of 4000 to 400 cm⁻¹.

2.4.4 Light transmission and opacity of the films

Analyses of light transmission and opacity of the films were made following the methodology described by S. Wang et al. (2019). The transparency of the films (4 cm × 0.5 cm) was measured using a Biomate 3S UV–vis spectrophotometer at wavelengths between 190 and 800 nm. In the case of opacity, absorbance at 600 nm (A₆₀₀) was recorded and was calculated according to Equation 6:

$$O_p = A_{600}/E_s \quad (6)$$

where O_p is the opacity of the film and E_s is the thickness of the film, which was analyzed using an MDC-SX digital micrometer (Mitutoyo, Kawasaki, Japan) at fifteen different points, and the average was used.

2.4.5 Mechanical properties of films

Mechanical properties, including tensile strength (TS) and elongation at break (EAB), were measured by a TA.XTPlus texture analyzer (Stable Micro Systems, Surrey, UK) according to the standard ASTM D882–02 method (ASTM Standard, 2002). Strips of films (10 x 100 mm) were fixed to the claws and subjected to extensional deformation with the application of a displacement rate of 50 mm/min until rupture. Five repetitions were performed.

2.4.6 Antioxidant activities of films

The antioxidant activities of the films were studied using radical scavenging methods (ABTS^{•+}) and the antioxidant potential for ferric reduction (FRAP). For the evaluations, 10 mL of 95% ethanol was added to 0.2 g (2 x 2 cm²) of the films and shaken (100 rpm) in an SL 222 incubator shaker for 4 h at 30 °C. Then, the supernatant was collected for the following antioxidant analyses:

- a) **ABTS.** An aliquot of 0.03 mL of film extract was mixed with 3 mL of ABTS^{•+} radical solution, vortexed, and left to react for 6 min, after which the absorbance was recorded at 734 nm. The results were compared with a Trolox standard curve ($y = -0.0003x + 0.648$, $R^2 = 0.9995$) and expressed as equivalent to Trolox (TE) $\mu\text{mol g}^{-1}$ of the film. The ABTS^{•+} radical was prepared by reacting 0.088 mL of 140 mmol L⁻¹ persulfate of potassium and 5 mL of 7 mmol L⁻¹ ABTS for 16 h in the dark. Then, the sample was diluted to an absorbance reading of 0.70 ± 0.05 at 734 nm (M. do S. Rufino et al., 2007).

- b) **FRAP.** An aliquot of 0.09 mL of film extract was added to 0.27 mL of water and 2.7 mL of FRAP reagent (0.83 mmol L⁻¹ TPTZ, 1.67 mmol L⁻¹ FeCl₃, and 250 mmol L⁻¹ sodium acetate buffer). The sample was incubated in an SL 222 shaker for 30 min at 37 °C and then cooled in an ice bath, and the absorbance was read at 595 nm. The results were compared with a Trolox standard curve ($y = 0.0013x + 0.0047$, $R^2 = 0.9997$) and expressed as TE μmol g⁻¹ of the film (M. do S.M. Rufino et al., 2006).

2.4.7 Release kinetics of the antioxidants present in films

A study of the controlled-release kinetics was performed to evaluate the release of antioxidants present in films with 5.0% betanin microcapsules. The extract of the films and the analysis of the concentration of released antioxidants (FRAP) were made according to the methodology described in Section 2.4.3. Aliquots were withdrawn after 10, 20, 30, 40, 50, 60, 80, 100, 120, 180 and 240 min. To evaluate the release mechanism, first-order (Equation 7), Higuchi (Equation 8), Ritger-Peppas (Equation 9), and Peppas-Sahlim (Equation 10) equations were used. The data were modeled in Origin 8.0 software to obtain the adjusted R² and were also analyzed by the DDSolve Excel add-in (Zhang et al., 2010) to obtain the value of the model selection criterion (MSC, Equation 11).

$$y = y_{max} * (1 - \exp(-kt)) \quad (7)$$

$$y = y_0 + kt^{0.5} \quad (8)$$

$$y = y_0 + kt^n \quad (9)$$

$$y = k_1t^m + k_2t^{2m} \quad (10)$$

where k , k_1 , and k_2 are the constants of the models; y_0 is the initial fraction (concentration of antioxidants at time t divided by the total concentration of antioxidants), usually zero; y_{max} is the maximum fraction of antioxidants, and n and m are the exponents of release (related to the mechanism of release of the compound under study) as a function of time t .

$$MSC = \ln \left(\frac{\sum_{i=1}^n W_i (Y_i - Y_m)^2}{\sum_{i=1}^n w_i (Y_i - Y_z)^2} \right) - (2p/n) \quad (11)$$

where W_i is the weighting factor, which is usually equal to 1 to fit the dissolution data, Y_i is the i -th observed Y -value, Y_z is the i -th predicted Y -value, Y_m is the average of all points of observed Y data, p is the number of parameters in the model and n is the number of data points.

2.5 Statistical analysis

All experimental measurements were performed in three independent repetitions, and the data are expressed as the mean ± standard deviation. One-way variance analyses (ANOVA) were performed in Origin[®] 8.0 software, and Tukey's test was used to determine the existence of a significant difference at the level of $\alpha = 0.5$.

3 Results and discussion

3.1 Formation of ultrasonicated amaranth protein isolate / carboxymethylcellulose complex coacervates

Fig. 24 presents the results of the analyses of the ζ-potential, SEI, and turbidity of CMC and API-U. As shown in Fig. 24A, in the range of the pH values studied (2.0 to 5.0), the two biopolymers presented opposite charges, being positive for API-U and negative for CMC. SEI

values were significantly high ($p < 0.05$) at pH 3.5 and 4.0, followed by pH 3.0. According to Fig. 24B, the values of CMC turbidity in this pH range were low (approximately 3%), indicating that it was practically soluble. The turbidity of API-U increased from 18.03 ± 0.05 (pH 2.5) to 71.67 ± 0.34 (pH 5.0). Although this suggests self-aggregation, the ζ -potential values above +20 mV of API-U demonstrate that the solutions were stable due to repulsive forces. This behavior was confirmed after allowing a 0.1% (w/w) solution of API-U at pHs 2.0 - 3.0 to equilibrate the phases for 24 h, in which no phase separation was observed (Fig 25). Additionally, the 1/1 (API-U/CMC) proportion showed a decreasing trend of turbidity, mainly from pH 3.0 to 5.0, indicating the presence of soluble complexes and/or stability of the system due to the increase in the density of negative charges of the CMC. These results indicate that the optimal pH values for API-U/CMC complex coacervates formation were between 2.0 and 3.0. Therefore, to avoid API-U self-aggregation and to ensure betanin stability during its encapsulation, pH 3.0 was chosen.

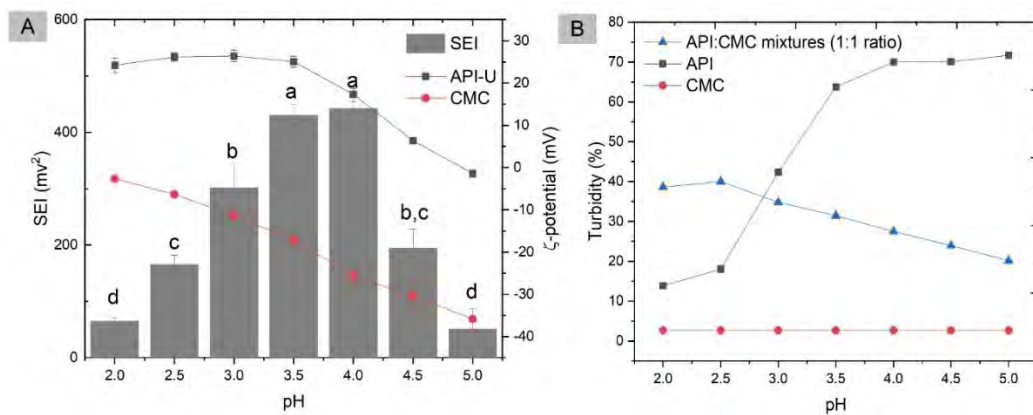


Figure 24. (A) Zeta-potential and the strength of the electrostatic interaction (SEI) of carboxymethylcellulose (CMC) and ultrasonicated amaranth protein isolate (API-U) at a concentration of 0.1% (w/w). (B) Turbidity of CMC, API-U, and API-U/CMC mixture in a ratio of (1/1, w/w).

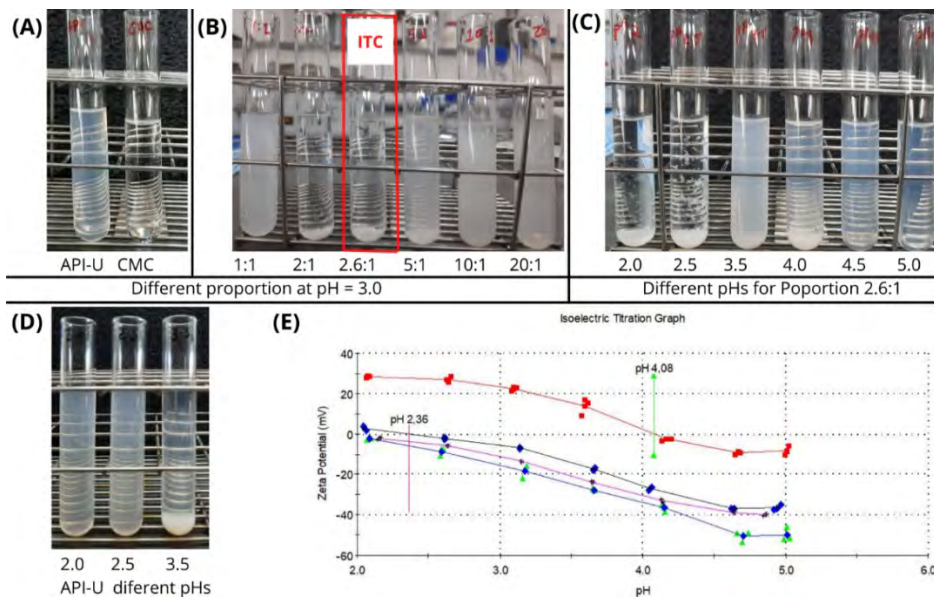


Figure 25 (A) amaranth protein isolate treated with ultrasound (API-U) and carboxymethylcellulose (CMC) solutions at pH 3. (B) API-U:CMC mixtures in different proportions (from left to right, 1:1, 2:1, 2.6:1, 5:1, 10:1 and 20:1), tested at pH 3 and total fixed concentration at 0.1%. (C) API-U:CMC mixtures ant 2.6: ratio, at different pHs. (D) API-U different pHs. (E) Isoelectric Titration Graph showing Zeta Potential (mV) vs pH for API-U and CMC.

0.1% API-U solutions at different pHs. The images were captured 24 h after the phase equilibrium of the solutions (containing API-U and CMC in the mentioned ratios and pHs). (E) ζ -potential of API-U (red line), CMC (blue line) and mixtures of API-U:CMC in proportions 1:1 (purple line) and 2.6:1 (black line).

Fig. 26 presents the results of the interaction of API-U and CMC obtained by ITC at 25 °C and pH 3. As shown in Fig. 26A, the titration had an exothermic profile over time. Moreover, as shown in Fig. 26B, the binding isotherm of the API-U/CMC complex was better adjusted to the independent model. In addition, the data obtained by the model, including reaction stoichiometry (N, 0.898 ± 0.01), binding constant (Kd, $2.04 \times 10^{-8} \pm 9.72 \times 10^{-9}$ M), enthalpy (ΔH , -173.20 ± 3.71 kcal mol⁻¹), the change in entropy (ΔS , -546.1 kcal mol⁻¹ K⁻¹) and the change in free Gibbs energy (ΔG , -10.39 kcal mol⁻¹), indicate that the process of formation of API-U/CMC complexes is spontaneous. Meanwhile, negative ΔH and ΔS values indicate that the reaction is enthalpically favorable and entropically unfavorable, respectively. This means that the electrostatic interaction between API-U and CMC was predominant throughout the titration (El Ghazzaqui Barbosa et al., 2022) since the two polyelectrolytes had opposite charges, although the hydrogen bonds and hydrophobic interaction may also have contributed to the formation of complexes. This same phenomenon has been reported for the formation of coacervated ovalbumin-CMC complexes (Xiong et al., 2017) and CMC gelatin (Duhoranimana et al., 2018). In addition, API-U and CMC had high interaction affinity (Kd). It took approximately 0.898 moles (N) of API-U to saturate all available sites in 1 mol of CMC. In terms of mass, 2.597 g of API-U was required to interact with 1 g of CMC. This proportion was used for the formation of complex coacervates (as shown in Fig. 24) and in the manufacture of betanin microcapsules.

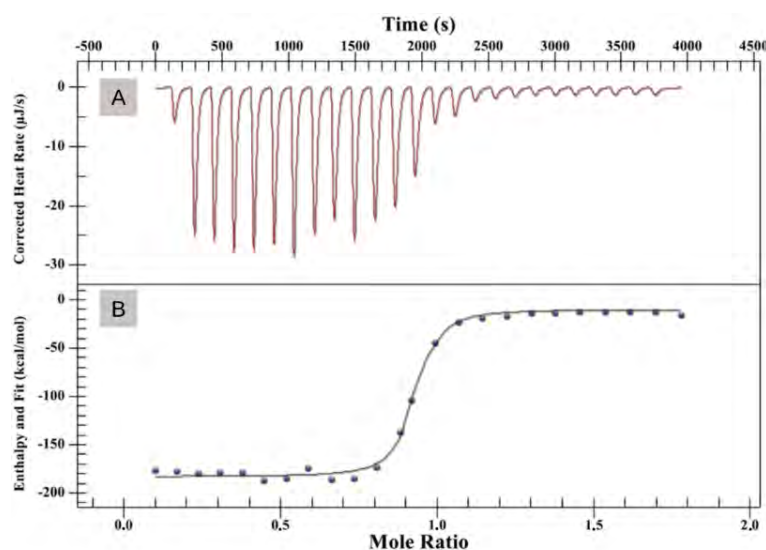


Figure 26. (A) Heat flow thermogram ($\mu\text{cal s}^{-1}$) as a function of time(s), obtained during the titration of 250 μL of 0.123 mmol L^{-1} of ultrasonicated amaranth protein isolate (API-U) in 1200 μL of 0.0154 mmol L^{-1} of carboxymethylcellulose (CMC), at 25 °C. The API-U and CMC concentrations was solubilized in solubilized in 10 mmol L^{-1} citrate buffer (pH 3.0). (B) Graphical representation of the integrated areas of each peak (kcal mol^{-1}) as a function of the molar ratio of API-U/CMC.

3.2 Betanin microcapsules

3.2.1 Encapsulation efficiency

According to the results presented in Table 12, the EE (%) of betanin varied from 61 to 87%. The systems with a 1% total content of biopolymer (TC) showed higher EE (%), mainly for samples D and E (approximately 85 and 87%, respectively). EE (%) did not differ in any of the systems with 0.5% TC, while in systems with 2% TC, the samples with lower core content presented high EE (%), ranging from 73 (system C) to 61% (system A). This last case can be explained by the fact that they presented a higher content of wall material compared to the core. In this table, it is also observed that systems with less dense complex coacervates (Fig. 27) presented low EE (%), which can be attributed to the structure that coacervates may present. According to Lan et al. (2021), complex coacervates that have a less condensed characteristic have a greater ability to encapsulate oils because their structure is more organized and tends to trap the encapsulated oil more effectively. In the present work, encapsulation was performed using a W/O/W emulsion that has lower stability than O/W emulsions, which may be associated with the formation of larger W/O/W droplets (Shaddel et al., 2018). This situation may have contributed to higher volume formation, especially in systems with higher TC and higher core ratio/wall proportion. Consequently, it may have allowed a partial loss of betanin and thus a lower EE (%) compared to more compact systems. Other authors reported results of EE (%), such as those observed in the present study. For example, Kanha et al. (2020) obtained 62-73% EE (%) by encapsulating anthocyanins using acacia gum-gelatin and chitosan-CMC. Shaddel et al. (2018) obtained EE (%) values of approximately 90 and 81% for black raspberry anthocyanins using gelatin-arabic gum at pH 5.0 and 4.0, respectively. However, some studies showed EE(%) below 60%, while others were above 90%, which can be attributed to different factors, including wall material (Comunian et al., 2013).

Table 12. Encapsulation efficiency (EE) of betanin in complex coacervates formed by ultrasonicated amaranth protein (API-U) and carboxymethylcellulose (CMC)

Sample	Wall/core	Biopolymers				SIO (g)	Betanin (mg)	EE (%)	Tukey's test
		TC (%)	API-U (g)	CMC (g)	Wall (g)				
A	1/1	2.00	0.144	0.056	0.200	0.396	20.0	61.16 ± 1.08	a
B	2/1	2.00	0.144	0.056	0.200	0.198	10.0	67.94 ± 3.20	b
C	4/1	2.00	0.144	0.056	0.200	0.099	05.0	73.21 ± 1.35	b, c
D	1/1	1.00	0.072	0.028	0.100	0.270	10.0	85.80 ± 1.43	e
E	2/1	1.00	0.072	0.028	0.100	0.099	05.0	87.38 ± 1.12	e
F	4/1	1.00	0.072	0.028	0.100	0.050	2.50	78.96 ± 1.065	d
G	1/1	0.50	0.036	0.014	0.050	0.099	05.0	70.76 ± 0.45	b, c
H	2/1	0.50	0.036	0.014	0.050	0.050	2.50	70.44 ± 0.91	b, c
I	4/1	0.50	0.036	0.014	0.050	0.025	1.25	75.58 ± 1.82	c, d

SIO is the sachal inchi oil. The results of the EE (%) are the means ± the standard deviation. The letters in the Tukey's test column statistical results and the difference between them means that the samples differ statistically (p<0.05).

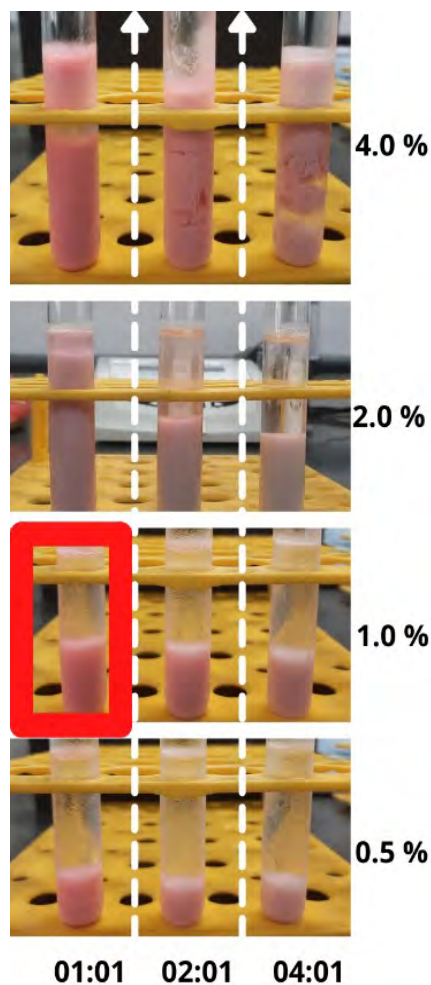


Figure 27. Phase diagram of encapsulation of betanin in complexes coacervates formed by of ultrasonicated amaranth protein isolate and sodium carboxymethylcellulose.

3.2.2 Optical microscopy

Fig. 28 shows the morphology of the particles (sample D) formed during the betanin microencapsulation. It is possible to verify the presence of a double emulsion (Fig. 28A), where a larger droplet (SIO) is filled by other smaller droplets (solution containing betanin). In the larger droplet, one can observe a denser interface (circle-shaped) that was probably formed by the studied wall material (API-U and CMC). Other authors who encapsulated hydrophilic compounds using W/O/W emulsions have reported images similar to those observed in the present study (Shaddel et al., 2018). However, in Fig. 28B, we can observe an agglomerate of particles and a material deposited around it. This can be explained by the formation of a solid bond of microcapsules due to the formation of complex coacervates (Rocha-Selmi et al., 2013).

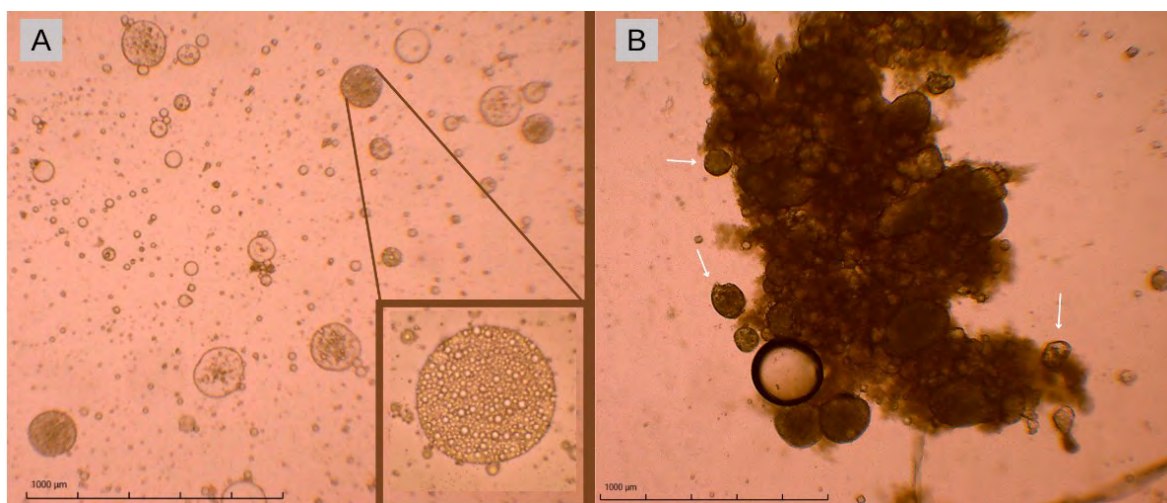


Figure 28. (A) Optical microscopy of emulsions after homogenization of the mixture of ultrasonicated Amaranth Protein Isolate (API-U), carboxymethylcellulose, and emulsion obtained with 10% (w/w) aqueous betanin solution and sacha inchi oil. (B) Microscopy of complex coacervates 24 h after the precipitation. The photographs were taken at the 10x magnification. The scale bars are of 1000µm.

3.2.3 Fourier transform infrared spectroscopy

Fig. 29 shows the FTIR spectra of CMC, API-U, betanin microcapsules (sample D), SIO, and betanin. The CMC spectra exhibited absorption bands typical of polysaccharides at 3224 cm^{-1} (broad -OH band), a vibration of C-H elongation at 2920 cm^{-1} , and vibration of asymmetric -COONa group elongation in CMC at 1582 cm^{-1} . The band at 1411 cm^{-1} was attributed to the symmetrical elongation of the -COO^- groups, while C-O elongation was observed at 1022 cm^{-1} . These results are similar to the data reported by El Ghazzaqui Barbosa et al. (2022) and Seki et al. (2014). In the API-U spectra, amide I, II, and III bands were observed at 1633 , 1537 , and 1396 cm^{-1} , respectively. The -OH of the free amino acid group was observed at 3280 cm^{-1} .

In the SIO spectrum, the vibrational stretching of the cis-olefinic double bands ($=\text{CH}$) can be observed at 3008 cm^{-1} . The bands corresponding to -CH stretching can be observed at 2923 and 2854 cm^{-1} . The C=O vibration of polyunsaturated fatty acids can be seen at 1743 cm^{-1} , while C-O elongation can be observed at 1155 and 721 cm^{-1} . Similar results were previously reported by El Ghazzaqui Barbosa et al. (2022). Betanin was identified through the presence of broadband, referring to the elongation of OH connected to the aromatic ring (peaking at 3294 cm^{-1}), C-H binding at 2923 cm^{-1} , elongation of C=O at 1743 cm^{-1} , elongation of the C=N bond at 1635 cm^{-1} , elongation of the length of the C-H bond at 1367 cm^{-1} , the frequency of elongation of C-O-C in the bands between 1184 and 881 cm^{-1} , and finally C-H at 848 cm^{-1} (Aztatzi-Ruggerio et al., 2019; Cai et al., 1998; Sengupta et al., 2015).

The spectra of the betanin microcapsules revealed the presence of SIO at 3008 , 2923 , 2854 , 1743 , and 1151 cm^{-1} . In the case of betanin, many bands overlapped, which can be explained by the fact that during encapsulation, betanin was in the internal phase of the first emulsion. In addition, there were changes in the peaks corresponding to the amides and the COO^- group for API-U and CMC, respectively; that is, it was only possible to observe peaks at 1648 and 1537 cm^{-1} , while the peak at 1411 cm^{-1} shifted to 1454 cm^{-1} . These changes are attributed to the electrostatic interactions between the amino groups of API-U (-NH_3^+) and the carboxylic groups of CMC (-COO^-). Changes in the peaks corresponding to the bands of -NH_3^+ and -COO^- were also observed in the formation of complex coacervates of pea protein

and beet pectin (Lan et al., 2020), as well as for egg white protein and xanthan gum (Souza & Garcia-Rojas, 2017).

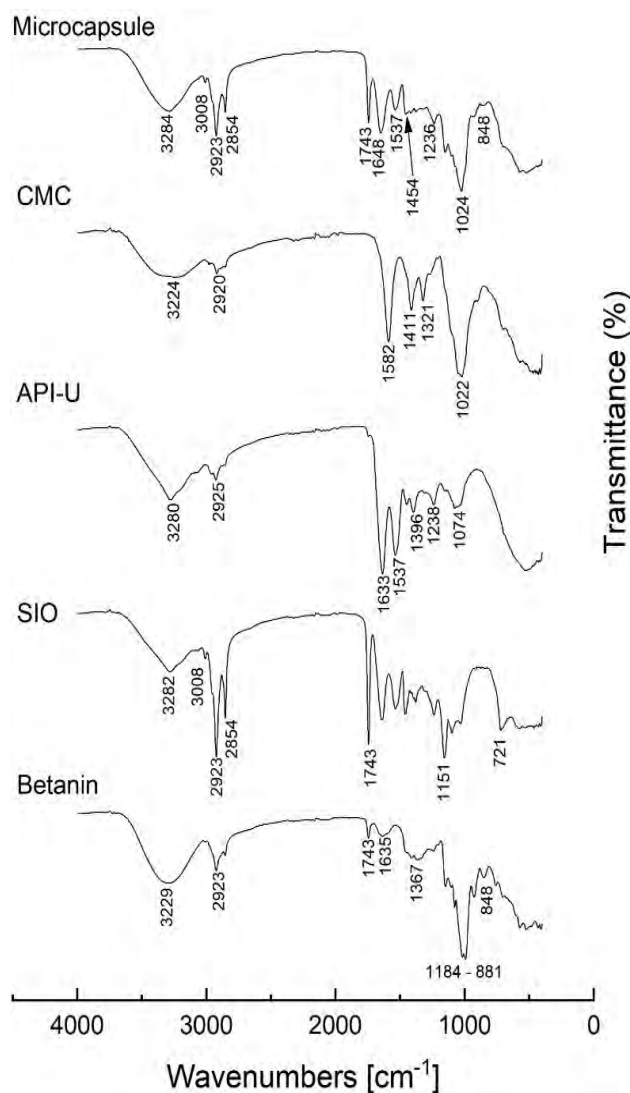


Figure 29. Fourier Transform Infrared (FTIR) spectra of ultrasonicated Amaranth Protein Isolate (API-U), carboxymethylcellulose (CMC), sachal inchi oil (SIO), betanin, and betaine loaded microcapsules.

3.2.4 Thermal stability of encapsulated betanin

Fig. 30A presents the results of the thermal stability of free and encapsulated betanin. In the first 10 min, approximately 10% of free betanin was degraded, reaching 53% at the end of the experiment. Conversely, encapsulated betanin took approximately 30 min to begin to be significantly degraded, and by the end of 60 min, only 21% of betanin had been lost. The $T_{1/2}$ of free betanin was lower (54.90 ± 1.30 min) than that of encapsulated betanin (159.98 ± 2.12 min). In this study, the degradation of betanin followed first-order kinetics (adjusted $R^2 = 0.99$, Fig. 31), as has been reported in the literature (Aztatzi-Ruggerio et al., 2019). The high $T_{1/2}$ value of encapsulated betanin compared with free betanin shows the protective effect of microcapsules formed by the API-U/CMC complex coacervates at 50 °C.

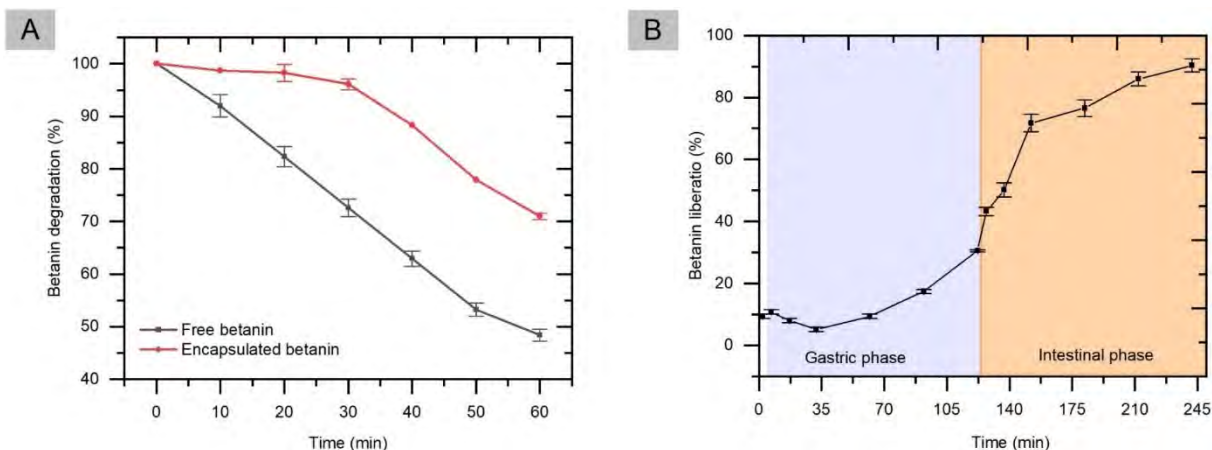


Figure 30. (A) Stability of free and encapsulated betanin submitted to heat treatment of 50°C for 1 hour. (B) betanin release profile during the *in vitro* simulation of gastrointestinal digestion of microcapsules formed by complex coacervates of ultrasonicated amaranth protein isolate (API-U) and carboxymethylcellulose (CMC).

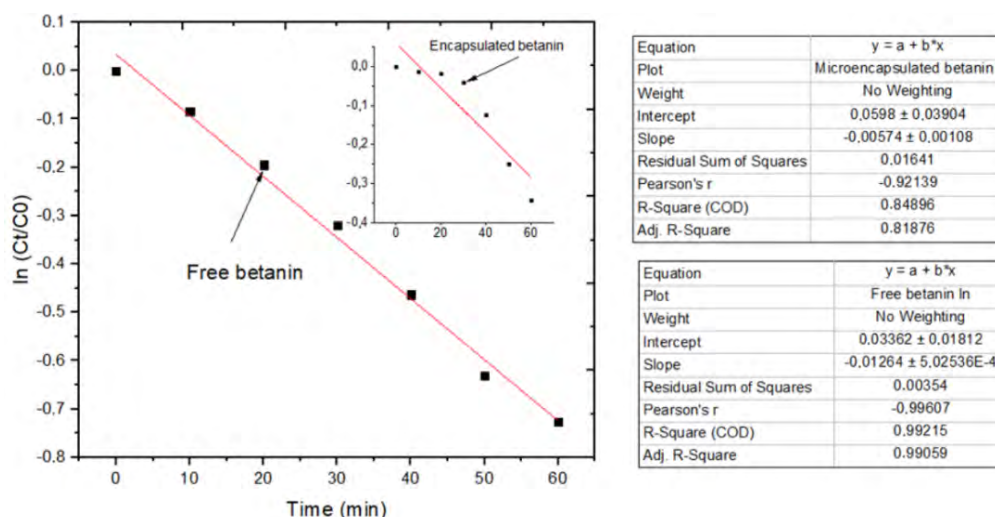


Figure 31. Results of linear regression of the degradation of free and microencapsulated betanin.

3.2.5 Simulation of the *in vitro* of gastrointestinal digestion of betanin microcapsules

Fig. 30B presents the betanin release profile during the *in vitro* simulation of microcapsule digestion (sample D). At the end of the oral phase, approximately 9% of betanin was released. Although pH 7 was far from the pH value of 3 used to microencapsulate betanin, the oral digestion time was not sufficient for the complete disintegration of microcapsules. In the gastric phase, the content of betanin released remained the same during the first 60 minutes of gastric digestion, thus resisting its degradation in the SGF. This is due to at least two factors: first, the pH of the complex formation favored the delayed release of betanin since the pH (3.0) of the SGF was similar to the pH used for the formation of microcapsules. Afterward, the protective effects of biopolymers were also prominent. Many researchers have demonstrated that CMC resists gastric conditions (El Ghazzaqui Barbosa et al., 2022), and a certain resistance of amaranth protein to gastric juice has been reported (Suárez & Añón, 2019). In the intestinal phase, the action of pH and SIF constituent enzymes affected the release of 90% betanin.

After the *in vitro* simulation of the gastrointestinal digestion of microcapsules, betanin bioaccessibility showed high values ($84.99 \pm 2.84\%$). This means that the complex coacervates preserved betanin throughout the digestion process, thus ensuring the high availability of betanin, which can be absorbed by the body. Encapsulations that use W/O/W emulsions have shown high bioaccessibility compared to O/W emulsions. For example, Chen et al. (2018) verified an increase of 30.5 (O/W) to 48.5% (W/O/W) in the bioaccessibility of (-)-epigallocatechin-3-gallate after encapsulation in W/O/W emulsions. Similarly, Huang et al. (2021) observed an increase from 20.15 (O/W) to 40.72% (W/O/W) in the bioaccessibility of grape seed proanthocyanidin.

3.3 Edible films prepared with gelatin and betanin microcapsules

3.3.1 Thicknesses, FTIR, transparency, light transmission, and mechanical properties

As shown in Fig. 32A, the films formed exclusively with gelatin (GF) presented a transparent appearance, while the edible films composed of gelatin and 1% microcapsule (MGF1), 2.5% microcapsule (MGF2.5), and 5% microcapsule (MGF5) presented reddish colorations, with the most color noted for MGF5. As presented in Table 13, the film thicknesses of GF, MGF1, MGF2.5 and MGF5 were 0.16 ± 0.01 , 0.17 ± 0.01 , 0.22 ± 0.02 and 0.27 ± 0.03 mm, respectively. These results indicate that the addition of a smaller amount (up to 1.0%) of microcapsules in the production of gelatin films may not affect the thickness. Similar results were reported for edible gelatin films and anthocyanin nanocomplexes (S. Wang et al., 2019). However, by increasing the concentrations of microcapsules to 2.5% or even 5.0%, the film thickness was significantly affected. This is probably related to the increase in total solids in the filmogenic solution.).

Fig. 32B presents the FTIR results of GF, MGF1, MGF2.5, and MGF5. Some spectral differences were observed between the FTIR spectra of GF and films containing microcapsules. The peak at 1542 cm^{-1} (NH stretch of amide II) was shifted to higher peaks. The gelatin $-\text{NH}_2$ group is capable of interacting with CMC $-\text{COOH}$ groups through electrostatic attraction. Thus, the changes observed in the bands corresponding to the amide groups can confirm the possible interaction of gelatin with the betanin microcapsules. In addition, we noted the presence of SIO in MGFs through the peak at 1743 cm^{-1} (the elongation of $\text{C}=\text{O}$, as discussed in Section 3.2.3).

The addition of microcapsules significantly increased ($p < 0.05$) the opacity of the film (Table 13), and the results were 0.23 ± 0.01 , 1.06 ± 0.05 , 1.87 ± 0.01 and 2.11 ± 0.06 for GF, MGF1, MGF2.5 and MGF5, respectively. Light transmission analyses showed that both films had a good ability to absorb ultraviolet radiation (at wavelengths between 190 and 290 nm, Fig. 33). For example, the transmittance at 200 nm was zero (0) for all films, while at 250 nm, it was 9.1 for GF, 1.0 for MGF1, and zero for MGF2.5 and MGF5. In the visible bands, GFs showed higher light transmittance (with 92% at 800 nm), while MGFs showed reduced transmittance (mainly for MGF5, with 34% at 800 nm). In addition, it was verified that the higher the opacity of the film is, the lower the transmittance at practically all wavelengths. According to Kowalczyk et al. (2021), the reduction of transmittance is related to the presence of proteins (gelatin) that have a good absorption capacity for ultraviolet radiation. For the visible regions, this phenomenon may be directly related to the color of the films, which was deepened due to betanin, which showed maximum absorbance at approximately 531 nm. Therefore, these results indicate that the incorporation of microcapsules in the production of gelatin films has a positive effect on the protection of light passage, which is beneficial for the protection of foods sensitive to deterioration due to radiation.

Fig. 34 shows the results of the mechanical properties of the films. The TS results were 9.04 ± 0.76 , 8.87 ± 0.23 , 7.71 ± 0.10 , and 4.07 ± 0.30 MPa for GF, MGF1, MGF2.5, and

MGF5, respectively. These results demonstrate that the addition of 2.5 or 5% betanin microcapsules resulted in a significant reduction in TS. In the case of EAB, the results did not differ for GF ($59.91 \pm 2.43\%$) and MGF1 ($62.52 \pm 3.62\%$). However, the EAB was higher for MGF2.5 ($69.46 \pm 2.59\%$) and MGF5 ($79.01 \pm 1.76\%$). In general, the TS is related to the mechanical resistance of the films associated with the cohesion forces between the polymer chains, and the EAB represents the ability of the films to extend until rupture (Tavares et al., 2021). The reduction in TS observed in MGFs was expected due to the presence of microcapsules that can reduce network formation and strengthen the film. As shown in Table 12 (sample D), the microcapsules used in the production of the MGFs had a high oil content, which was approximately 2.7 times higher than the wall material. Some portion of the oil may have been partially released due to the shear stress produced by the ultraturrax, thus influencing the reduction in TS and the increase in EAB. Oils can interfere with chain-to-chain polymer interactions and provide flexible domains within the film, thus acting as plasticizers (Gul et al., 2018; Limpisophon et al., 2010).

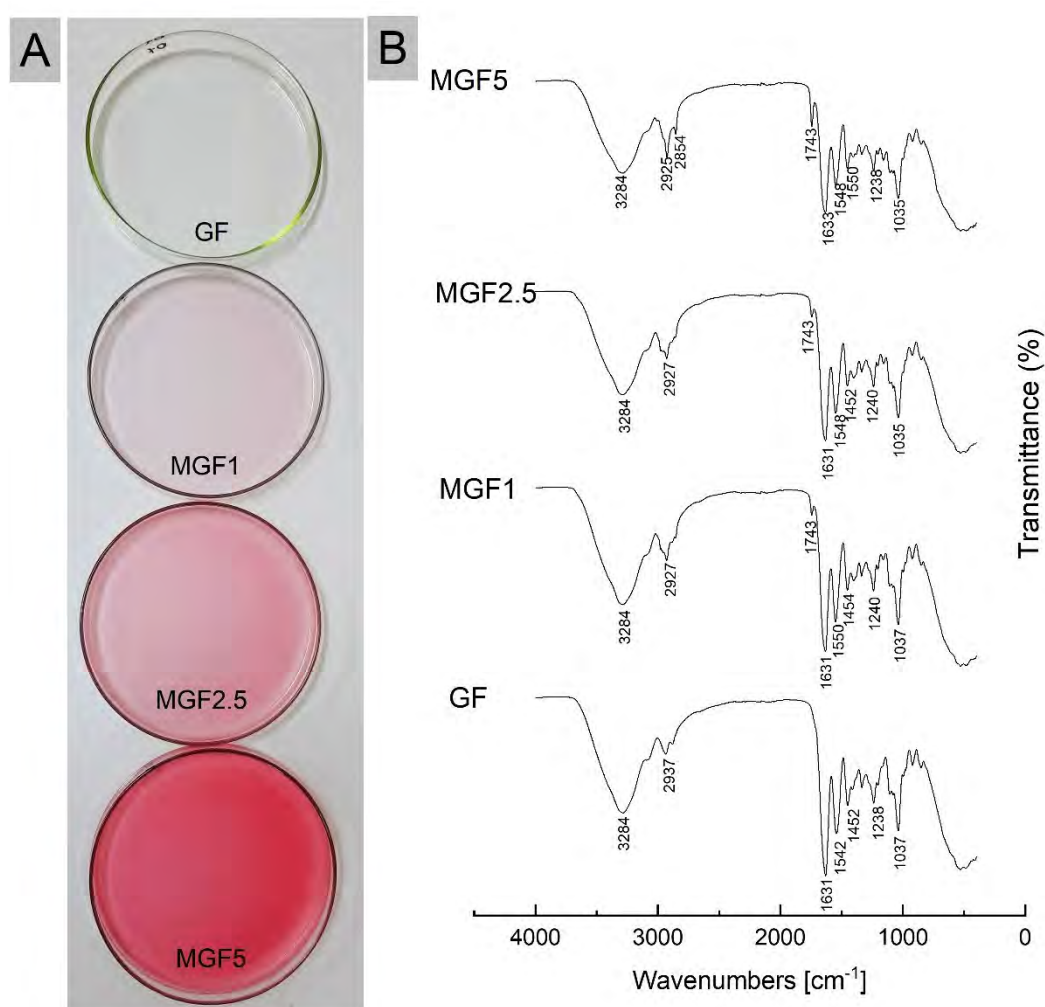


Figure 32. (A) control gelatin film (GF), gelatin film with 1% of betanin microcapsules (MGF1), gelatin film with 2.5% of betanin microcapsules (MGF2.5), and gelatin film with 5% of betanin microcapsules (MGF5). (B) Images of GF, MGF1, MGF2.5 and MGF5.

Table 13. Results of the physicochemical analyzes of the films

Film	Thickness	Opacity
GF	0.16 ± 0.01 ^a	0.23 ± 0.01 ^a
MGF1	0.17 ± 0.01 ^a	1.06 ± 0.05 ^b
MGF2,5	0.22 ± 0.02 ^b	1.87 ± 0.01 ^c
MGF5	0.27 ± 0.03 ^c	2.11 ± 0.06 ^d

GF is gelatin film (control), MGF1 is gelatin film with 1% of betanin microcapsules, MGF2.5 is gelatin film with 2.5% of betanin microcapsules, and MGF5 is gelatin film with 5% of betanin microcapsules. The results are the means ± the standard deviation and the superscript letters are the results of Tukey's statistic test and the difference between them means that the samples differ statistically (p<0.05).

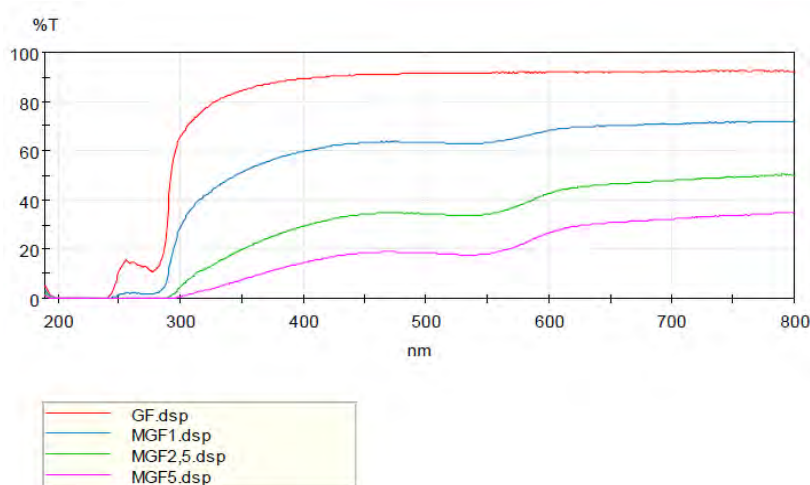


Figure 33. UV-visible light spectra are transmitted through gelatin film (GF) and gelatin film with 1% microcapsule (MGF1), 2.5% microcapsule (MGF2.5), or 5% microcapsule (MGF5).

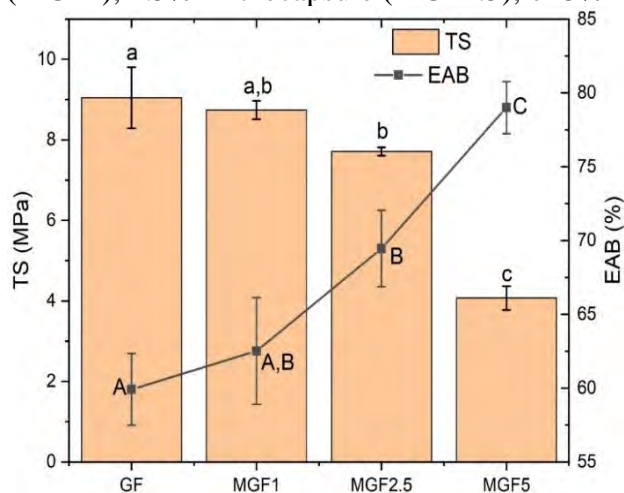


Figure 34. Mechanical properties of simple gelatin film (GF), gelatin films with 1% microcapsules (MGF1), 2.5% microcapsules (MGF2.5), and 5% microcapsules (MGF5). TS is tensile strength and EAB is elongation at break. The error bars represent the standard deviation of the results of three samples. The uppercase and lowercase letters are the results of the Tukey test and, when they are different, they indicate the statistical difference (p < 0.05).

3.3.2 Antioxidant properties of gelatin and betanin composite edible films

The FRAP and ABTS^{•+} antioxidant activity analysis results of GF were 0.34 ± 0.01 and 0.34 ± 0.02 TE ($\mu\text{mol g}^{-1}$), respectively. The FRAP results for MGF1, MGF2.5 and MGF5 were 1.11 ± 0.08 , 2.29 ± 0.13 and 3.52 ± 0.18 TE ($\mu\text{mol g}^{-1}$), respectively. For ABTS^{•+}, the results were 2.03 ± 0.12 , 2.19 ± 0.08 and 3.05 ± 0.10 TE ($\mu\text{mol g}^{-1}$) for MGF1, MGF2.5 and MGF5, respectively. The addition of microcapsules to the film promoted an increase in antioxidant activities, which was accompanied by an increase in its concentration. SIO and betanin were the two components of the microcapsules that were likely present in the highest proportions in the ethanol extract obtained for the FRAP and ABTS^{•+} analyses since they are soluble in ethanol (Nouairi, Freha & Bellil, 2021; Rodríguez et al., 2021). As discussed in the Introduction, betanin has prominent antioxidant activity compared to ascorbic acid, rutin, and catechin (Esatbeyoglu et al., 2015). SIO has antioxidant activities due to the presence of tocopherols (Rodríguez et al., 2021). Therefore, the combination of SIO and betanin may have created synergies and increased the antioxidant capacities (FRAP and ABTS^{•+}) observed in MGFs.

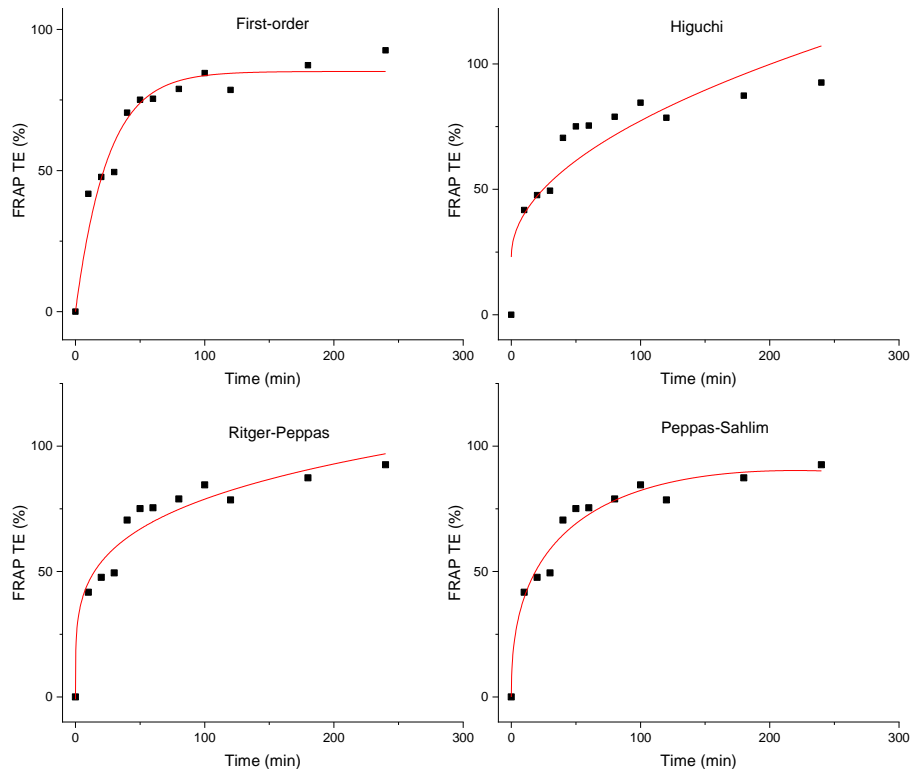


Figure 35 Models of antioxidant activity released from gelatin film with 5% of betanin microcapsules. FRAP TE means ferric reducing antioxidant potential equivalent to Trolox.

The release kinetics of the antioxidant present in films as a function of time are presented in Fig. 35, from which we can observe that approximately 40% of the antioxidants of MGF were released in the first 10 min, after which the release continued, gradually increasing up to 93% at 240 min. The FRAP method and MGF5 were chosen for analysis because they presented higher TE antioxidant concentrations compared to ABTS^{•+} and MGF1 or MGF2.5, respectively. Table 14 shows the results of the parameters and constants of the models used to fit the data on the release of antioxidants from MGF5. The release kinetics data of antioxidant concentrations were better fitted with the Peppas-Sahlim model, as they presented higher values of adjusted R^2 (0.96) and MSC (2.11). Values of MSC between 2 and 3 indicate a good fit (Zhang et al., 2010). In this sense, the release of antioxidants from MGF5

can be described as a combination of Fickian diffusion ($m = 0.45$) and case II relaxation. The m coefficient is related to the n coefficient of the power-law (Ritger-Peppas), which can be given for films, cylinders, and spheres. In case II relaxation, the release rate of antioxidants corresponds to zero-order release kinetics, and the mechanism that conducts its release is the swelling or relaxation of the polymeric chains of the film (Bruschi, 2015). In addition, through constants k_1 and k_2 , it is possible to understand which is the predominant mechanism. Therefore, if $k_1 > k_2$, Fickian diffusion is the main release factor. However, when $k_2 > k_1$, the relaxation of polymer chains is predominant (Freire et al., 2017). Our results reveal the predominance of Fickian diffusion (positive values for k_1) in the relaxation of polymer chains. Similarly, works such as those reported by Aguirre et al. (2021), Farrag et al. (2018;) and Mehran et al. (2020) observed that different bioactive substances were released from films obeying Fickian diffusion and case II relaxation.

Table 14. Parameters of the mathematical models obtained after fitting the results of the release profile of antioxidants in the gelatin film with 5% microcapsules.

Model	adjusted R ²	MSC	k	k1	k2	m	n
Peppas-Sahlim	0.96	2.11	-	16.03	-0.71	0.45	-
Ritger-Peppas	0.94	1.55	23.22	-	-	-	0.27
Higuchi	0.78	0.46	6.11	-	-	-	-
First-order	0.83	0.71	0.02	-	-	-	-

k , k_1 , k_2 , m , and n are the constants of the models; MSC is the Model Selection

4 Conclusion

In the present research, we studied the formation of complex coacervates API-U/CMC to microencapsulate betanin and its application in edible films. The complex coacervates API-U/CMC were formed at pH 3 in the proportion of 2.6/1. Through ITC, it was possible to conclude that the reaction was spontaneous, being enthalpically favorable and entropically unfavorable. The complex coacervates obtained were able to encapsulate up to 87% betanin, guaranteeing its protection from the action of heat and its release in the intestines during the in vitro simulation of digestion. When the microcapsules were added to the edible gelatin films, they improved the flexibility, reduced light transmission, and increased the antioxidant activity of the films. The release of antioxidants present in films occurred through Fickian diffusion and case II relaxation. In this sense, we can conclude that the betanin microcapsules formed by the API-U/CMC complex coacervates can be used to produce edible films capable of protecting food sensitive to light and agents that promote food oxidation.

5 References

- Aguirre, G., Taboada, P., & Billon, L. (2021). Spontaneously self-assembled microgel film as co-delivery system for skincare applications. *Pharmaceutics*, 13(9), 1422. <https://doi.org/10.3390/PHARMACEUTICS13091422/S1>
- Amjadi, S., Ghorbani, M., Hamishehkar, H., & Roufegarinejad, L. (2018). Improvement in the stability of betanin by liposomal nanocarriers: Its application in gummy candy as a food model. *Food Chemistry*, 256, 156–162. <https://doi.org/10.1016/j.foodchem.2018.02.114>
- Amjadi, S., Nazari, M., Alizadeh, S. A., & Hamishehkar, H. (2020). Multifunctional betanin nanoliposomes-incorporated gelatin/chitosan nanofiber/ZnO nanoparticles

- nanocomposite film for fresh beef preservation. *Meat Science*, 167(January), 108161. <https://doi.org/10.1016/j.meatsci.2020.108161>
- ASTM Standard. (2002). ASTM (D882-02) Standard test method for tensile properties of thin plastic sheeting.
- Aztatzi-Ruggerio, L., Granados-Balbuena, S. Y., Zainos-Cuapio, Y., Ocaranza-Sánchez, E., & Rojas-López, M. (2019). Analysis of the degradation of betanin obtained from beetroot using Fourier transform infrared spectroscopy. *Journal of Food Science and Technology*, 56(8), 3677–3686. <https://doi.org/10.1007/s13197-019-03826-2>
- Barbucci, R., Magnani, A., & Consumi, M. (2000). Swelling behavior of carboxymethylcellulose hydrogels in relation to cross-linking, pH, and charge density. *Macromolecules*, 33(20), 7475–7480. <https://doi.org/10.1021/ma0007029>
- Brodkorb, A., Egger, L., Alminger, M., Alvito, P., Assunção, R., Ballance, S., Bohn, T., Bourlieu-Lacanal, C., Boutrou, R., Carrière, F., Clemente, A., Corredig, M., Dupont, D., Dufour, C., Edwards, C., Golding, M., Karakaya, S., Kirkhus, B., Le Feunteun, S., ... Recio, I. (2019). INFOGEST static in vitro simulation of gastrointestinal food digestion. *Nature Protocols*, 14(4), 991–1014. <https://doi.org/10.1038/s41596-018-0119-1>
- Bruschi, M. L. (2015). Strategies to Modify the Drug Release from Pharmaceutical Systems. Elsevier (Chapter 5). <https://doi.org/10.1016/B978-0-08-100092-2.00005-9>
- Cai, Y., Sun, M., & Corke, H. (2003). Antioxidant Activity of Betalains from Plants of the Amaranthaceae. *J Agric Food Chem*, 51(8), 2288–2294. <https://doi.org/10.1021/jf030045u>
- Cai, Y., Sun, M., Wu, H., Huang, R., & Corke, H. (1998). Characterization and Quantification of Betacyanin Pigments from Diverse Amaranthus Species. *Journal of Agricultural and Food Chemistry*, 46(6), 2063–2070. <https://doi.org/10.1021/JF9709966>
- Chen, X., McClements, D. J., Wang, J., Zou, L., Deng, S., Liu, W., Yan, C., Zhu, Y., Cheng, C., & Liu, C. (2018). Coencapsulation of (–)-Epigallocatechin-3-gallate and Quercetin in Particle-Stabilized W/O/W Emulsion Gels: Controlled Release and Bioaccessibility, 66(14), 3691–3699. <https://doi.org/10.1021/acs.jafc.7b05161>
- Coelho, L. M., Silva, P. M., Martins, J. T., Pinheiro, A. C., & Vicente, A. A. (2018). Emerging opportunities in exploring the nutritional/functional value of amaranth. *Food & Function*, 9(11), 5499–5512. <https://doi.org/10.1039/C8FO01422A>
- Comunian, T. A., Thomazini, M., Alves, A. J. G., de Matos Junior, F. E., de Carvalho Balieiro, J. C., & Favaro-Trindade, C. S. (2013). Microencapsulation of ascorbic acid by complex coacervation: Protection and controlled release. *Food Research International*, 52(1), 373–379. <https://doi.org/10.1016/j.foodres.2013.03.028>
- Constantino, A. B.T., & Garcia-Rojas, E. E. (2020). Modifications of physicochemical and functional properties of amaranth protein isolate (*Amaranthus cruentus* BRS Alegria) treated with high-intensity ultrasound. *Journal of Cereal Science*, 95, 103076. <https://doi.org/10.1016/j.jcs.2020.103076>
- Constantino, A. B. T., & Garcia-Rojas, E. E. (2022a). Proteins from pseudocereal seeds: solubility, extraction, and modifications of the physicochemical and techno-functional properties. *Journal of the Science of Food and Agriculture*. 95, 103076. <https://doi.org/10.1002/JSFA.11750>
- Constantino, A. B.T., & Garcia-Rojas, E. E. (2022b). Vitamin D3 microcapsules formed by heteroprotein complexes obtained from amaranth protein isolates and lactoferrin:

- Formation, characterization, and bread fortification. *Food Hydrocolloids*, 129, 107636. <https://doi.org/10.1016/J.FOODHYD.2022.107636>
- Duhoranimana, E., Yu, J., Mukeshimana, O., Habinshuti, I., Karangwa, E., Xu, X., Muhoza, B., Xia, S., & Zhang, X. (2018). Thermodynamic characterization of Gelatin–Sodium carboxymethyl cellulose complex coacervation encapsulating Conjugated Linoleic Acid (CLA). *Food Hydrocolloids*, 80, 149–159. <https://doi.org/10.1016/j.foodhyd.2018.02.011>
- El Ghazzaqui Barbosa, A., Constantino, A. B. T., Bastos, L. P. H., & Garcia-Rojas, E. E. (2022). Encapsulation of sacha inchi oil in complex coacervates formed by carboxymethylcellulose and lactoferrin for controlled release of β -carotene. *Food Hydrocolloids for Health*, 2, 100047. <https://doi.org/10.1016/j.fhfh.2021.100047>
- Esatbeyoglu, T., Wagner, A. E., Schini-Kerth, V. B., & Rimbach, G. (2015). Betanin—A food colorant with biological activity. *Molecular Nutrition & Food Research*, 59(1), 36–47. <https://doi.org/doi:10.1002/mnfr.201400484>
- Farrag, Y., Ide, W., Montero, B., Rico, M., Rodríguez-Llamazares, S., Barral, L., & Bouza, R. (2018). Starch films loaded with donut-shaped starch-quercetin microparticles: Characterization and release kinetics. *International Journal of Biological Macromolecules*, 118, 2201–2207. <https://doi.org/10.1016/J.IJBIOMAC.2018.07.087>
- Fernández-López, J. A., Angosto, J. M., Giménez, P. J., & León, G. (2013). Thermal Stability of Selected Natural Red Extracts Used as Food Colorants. *Plant Foods for Human Nutrition*, 68(1), 11–17. <https://doi.org/10.1007/S11130-013-0337-1/FIGURES/4>
- Freire, M. C. L. C., Alexandrino, F., Marcelino, H. R., Picciani, P. H. de S., e Silva, K. G. de H., Genre, J., de Oliveira, A. G., & do Egito, E. S. T. (2017). Understanding Drug Release Data through Thermodynamic Analysis. *Materials*, 10(6), 651. <https://doi.org/10.3390/MA10060651>
- Gomez-Estaca, J., Comunian, T. A., Montero, P., Ferro-Furtado, R., & Favaro-Trindade, C. S. (2016). Encapsulation of an astaxanthin-containing lipid extract from shrimp waste by complex coacervation using a novel gelatin–cashew gum complex. *Food Hydrocolloids*, 61, 155–162. <https://doi.org/10.1016/j.foodhyd.2016.05.005>
- Gul, O., Saricaoglu, F. T., Besir, A., Atalar, I., & Yazici, F. (2018). Effect of ultrasound treatment on the properties of nano-emulsion films obtained from hazelnut meal protein and clove essential oil. *Ultrasonics Sonochemistry*, 41, 466–474. <https://doi.org/10.1016/J.ULTSONCH.2017.10.011>
- Herbach, K. M., Stintzing, F. C., & Carle, R. (2006). Betalain Stability and Degradation? Structural and Chromatic Aspects. *Journal of Food Science*, 71(4), R41–R50. <https://doi.org/10.1111/j.1750-3841.2006.00022.x>
- Huang, Y., Lin, J., Tang, X., Wang, Z., & Yu, S. (2021). Grape seed proanthocyanidin-loaded gel-like W/O/W emulsion stabilized by genipin-crosslinked alkaline soluble polysaccharides-whey protein isolate conjugates: Fabrication, stability, and in vitro digestion. *International Journal of Biological Macromolecules*, 186, 759–769. <https://doi.org/10.1016/J.IJBIOMAC.2021.07.062>
- Kanha, N., Surawang, S., Pitchakarn, P., & Laokuldilok, T. (2020). Microencapsulation of copigmented anthocyanins using double emulsion followed by complex coacervation: Preparation, characterization and stability. *LWT*, 133, 110154. <https://doi.org/10.1016/J.LWT.2020.110154>
- Kowalczyk, D., Szymanowska, U., Skrzypek, T., Basiura-Cembala, M., Łupina, K., & Biendl, M. (2021). Edible films based on gelatin, carboxymethyl cellulose, and their blends as carriers of potassium salts of iso- α -acids: Structural, physicochemical and antioxidant

- properties. *Food Hydrocolloids*, 115, 106574.
<https://doi.org/10.1016/J.FOODHYD.2020.106574>
- Lan, Y., Ohm, J. B., Chen, B., & Rao, J. (2020). Phase behavior and complex coacervation of concentrated pea protein isolate-beet pectin solution. *Food Chemistry*, 307, 125536.
<https://doi.org/10.1016/J.FOODCHEM.2019.125536>
- Lan, Y., Ohm, J. B., Chen, B., & Rao, J. (2021). Microencapsulation of hemp seed oil by pea protein isolate–sugar beet pectin complex coacervation: Influence of coacervation pH and wall/core ratio. *Food Hydrocolloids*, 113, 106423.
<https://doi.org/10.1016/J.FOODHYD.2020.106423>
- Limpisophon, K., Tanaka, M., & Osako, K. (2010). Characterisation of gelatin–fatty acid emulsion films based on blue shark (*Prionace glauca*) skin gelatin. *Food Chemistry*, 122(4), 1095–1101. <https://doi.org/10.1016/j.foodchem.2010.03.090>
- Mehran, M., Masoum, S., & Memarzadeh, M. (2020). Microencapsulation of *Mentha spicata* essential oil by spray drying: Optimization, characterization, release kinetics of essential oil from microcapsules in food models. *Industrial Crops and Products*, 154, 112694. <https://doi.org/10.1016/J.INDCROP.2020.112694>
- Montoya-Rodríguez, A., Mejía, E. G., Dia, V. P., Reyes-Moreno, C., & Milán-Carrillo, J. (2014). Extrusion improved the anti-inflammatory effect of amaranth (*Amaranthus hypochondriacus*) hydrolysates in LPS-induced human THP-1 macrophage-like and mouse RAW 264.7 macrophages by preventing activation of NF- κ B signaling. *Molecular Nutrition & Food Research*, 58(5), 1028–1041.
<https://doi.org/doi:10.1002/mnfr.201300764>
- Nouairi, M. E., Freha, M. & Bellil, A. (2021). Study by absorption and emission spectrophotometry of the efficiency of the binary mixture (Ethanol-Water) on the extraction of betanin from red beetroot. *Spectrochimica Acta Part A: Molecular and Biomolecular Spectroscopy*, 260, 119939. <https://doi.org/10.1016/j.saa.2021.119939>
- Orsini Delgado, M. C., Nardo, A., Pavlovic, M., Rogniaux, H., Añón, M. C., & Tironi, V. A. (2016). Identification and characterization of antioxidant peptides obtained by gastrointestinal digestion of amaranth proteins. *Food Chemistry*, 197, 1160–1167.
<https://doi.org/10.1016/j.foodchem.2015.11.092>
- Pagano, A. P. E., Khalid, N., Kobayashi, I., Nakajima, M., Neves, M. A., & Bastos, E. L. (2018). Microencapsulation of betanin in monodisperse W/O/W emulsions. *Food Res Int*, 109, 489–496. <https://doi.org/10.1016/j.foodres.2018.04.053>
- Rocha-Selmi, G. A., Bozza, F. T., Thomazini, M., Bolini, H. M. A., & Fávaro-Trindade, C. S. (2013). Microencapsulation of aspartame by double emulsion followed by complex coacervation to provide protection and prolong sweetness. *Food Chemistry*, 139(1–4), 72–78. <https://doi.org/10.1016/j.foodchem.2013.01.114>
- Rodríguez, G., Squeo, G., Estivi, L., Quezada Berru, S., Buleje, D., Caponio, F., Brandolini, A., & Hidalgo, A. (2021). Changes in stability, tocopherols, fatty acids and antioxidant capacity of sacha inchi (*Plukenetia volubilis*) oil during French fries deep-frying. *Food Chemistry*, 340, 127942. <https://doi.org/10.1016/J.FOODCHEM.2020.127942>
- Rufino, M. do S., Alves, R. E., de Brito, E. S., de Moraes, S. M., Sampaio, C. de G., Pérez - Jiménez, J., & Saura - Calixto, F. D. (2007). Metodologia científica: determinação da atividade antioxidante total em frutas pela captura do radical livre ABTS^{o+}. In Embrapa Agroindústria Tropical. Comunicado técnico (Vol. 128). Fortaleza: Embrapa Agroindústria Tropical.
- Rufino, M. do S. M., Alves, R. E., Brito, E. S. de, Moraes, S. M. de, Sampaio, C. de G., Pérez-Jiménez, J., & Saura-Calixto, F. D. (2006). Metodologia científica: determinação da

atividade antioxidante total em frutas pelo método de redução do ferro (FRAP). In Embrapa Agroindústria Tropical. Comunicado técnico (Vol. 125). Fortaleza: Embrapa Agroindústria Tropical.

- Rutz, J. K., Borges, C. D., Zambiazzi, R. C., Crizel-Cardozo, M. M., Kuck, L. S., & Noreña, C. P. Z. (2017). Microencapsulation of palm oil by complex coacervation for application in food systems. *Food Chemistry*, 220, 59–66. <https://doi.org/10.1016/j.foodchem.2016.09.194>
- Sabbione, A. C., Nardo, A. E., Añón, M. C., & Scilingo, A. (2016). Amaranth peptides with antithrombotic activity released by simulated gastrointestinal digestion. *Journal of Functional Foods*, 20, 204–214. <https://doi.org/10.1016/j.jff.2015.10.015>
- Schmitt, C., & Turgeon, S. L. (2011). Protein/polysaccharide complexes and coacervates in food systems. *Advances in Colloid and Interface Science*, 167(1–2), 63–70. <https://doi.org/10.1016/J.CIS.2010.10.001>
- Seki, Y., Altinisik, A., Demircioğlu, B., & Tetik, C. (2014). Carboxymethylcellulose (CMC)-hydroxyethylcellulose (HEC) based hydrogels: Synthesis and characterization. *Cellulose*, 21(3), 1689–1698. <https://doi.org/10.1007/S10570-014-0204-8/FIGURES/10>
- Sengupta, D., Mondal, B., & Mukherjee, K. (2015). Visible light absorption and photosensitizing properties of spinach leaves and beetroot extracted natural dyes. *Spectrochimica Acta Part A: Molecular and Biomolecular Spectroscopy*, 148, 85–92. <https://doi.org/10.1016/J.SAA.2015.03.120>
- Shaddel, R., Hesari, J., Azadmard-Damirchi, S., Hamishehkar, H., Fathi-Achachlouei, B., & Huang, Q. (2018). Double emulsion followed by complex coacervation as a promising method for protection of black raspberry anthocyanins. *Food Hydrocolloids*, 77, 803–816. <https://doi.org/10.1016/j.foodhyd.2017.11.024>
- Souza, C. J. F., & Garcia-Rojas, E. E. (2017). Interpolymeric complexing between egg white proteins and xanthan gum: Effect of salt and protein/polysaccharide ratio. *Food Hydrocolloids*, 66, 268–275. <https://doi.org/10.1016/j.foodhyd.2016.11.032>
- Suárez, S., & Añón, M. C. (2019). Amaranth proteins emulsions as delivery system of Angiotensin-I converting enzyme inhibitory peptides. *Food Hydrocolloids*, 90, 154–161. <https://doi.org/10.1016/j.foodhyd.2018.11.046>
- Tavares, L., Souza, H. K. S., Gonçalves, M. P., & Rocha, C. M. R. (2021). Physicochemical and microstructural properties of composite edible film obtained by complex coacervation between chitosan and whey protein isolate. *Food Hydrocolloids*, 113(October 2020), 106471. <https://doi.org/10.1016/j.foodhyd.2020.106471>
- Tesoriere, L., Allegra, M., Butera, D., & Livrea, M. A. (2004). Absorption, excretion, and distribution of dietary antioxidant betalains in LDLs: potential health effects of betalains in humans. *The American Journal of Clinical Nutrition*, 80(4), 941–945. <https://doi.org/10.1093/ajcn/80.4.941>
- Timilsena, Y. P., Akanbi, T. O., Khalid, N., Adhikari, B., & Barrow, C. J. (2019). Complex coacervation: Principles, mechanisms and applications in microencapsulation. *International Journal of Biological Macromolecules*, 121, 1276–1286. <https://doi.org/10.1016/j.ijbiomac.2018.10.144>
- Vergara, C., Saavedra, J., Saenz, C., Garcia, P., & Robert, P. (2014). Microencapsulation of pulp and ultrafiltered cactus pear (*Opuntia ficus-indica*) extracts and betanin stability during storage. *Food Chem*, 157, 246–251. <https://doi.org/10.1016/j.foodchem.2014.02.037>

- Vicente, J., de Souza C. T., Pereira, L. J. B., da Rocha, E. P., Sá, G. R., Gamallo, O. D., de Carvalho, M. G., & Garcia-Rojas, E. E. (2017). Microencapsulation of sacha inchi oil using emulsion-based delivery systems. *Food Research International*, 99, 612–622. <https://doi.org/10.1016/j.foodres.2017.06.039>
- Wang, H., Li, M., Dong, Z., Zhang, T., & Yu, Q. (2021). Preparation and Characterization of Ginger Essential Oil Microcapsule Composite Films. *Foods*, 10(10), 2268. <https://doi.org/10.3390/FOODS10102268>
- Wang, S., Xia, P., Wang, S., Liang, J., Sun, Y., Yue, P., & Gao, X. (2019). Packaging films formulated with gelatin and anthocyanins nanocomplexes: Physical properties, antioxidant activity and its application for olive oil protection. *Food Hydrocolloids*, 96(February), 617–624. <https://doi.org/10.1016/j.foodhyd.2019.06.004>
- Xiong, W., Ren, C., Tian, M., Yang, X., Li, J., & Li, B. (2017). Complex coacervation of ovalbumin-carboxymethylcellulose assessed by isothermal titration calorimeter and rheology: Effect of ionic strength and charge density of polysaccharide. *Food Hydrocolloids*, 73, 41–50. <https://doi.org/10.1016/j.foodhyd.2017.06.031>
- Yan, C., & Zhang, W. (2014). Coacervation Processes. In A. G. Gaonkar, N. Vasisht, A. R. Khare, & R. Sobel (Eds.), *Microencapsulation in the Food Industry* (pp. 125–137). Elsevier. <https://doi.org/10.1016/B978-0-12-404568-2.00012-1>
- Zhang, Y., Huo, M., Zhou, J., Zou, A., Li, W., Yao, C., & Xie, S. (2010). DDSolver: An add-in program for modeling and comparison of drug dissolution profiles. *AAPS Journal*, 12(3), 263–271. <https://doi.org/10.1208/s12248-010-9185-1>
- Zielińska-Przyjemska, M., Olejnik, A., Kostrzewa, A., Łuczak, M., Jagodziński, P. P., & Baer-Dubowska, W. (2012). The Beetroot Component Betanin Modulates ROS Production, DNA Damage and Apoptosis in Human Polymorphonuclear Neutrophils. *Phytotherapy Research*, 26(6), 845–852. <https://doi.org/doi:10.1002/ptr.3649>

**CAPÍTULO VI. MICROENCAPSULATION OF BETA-CAROTENE BY
COMPLEX COACERVATION USING AMARANTH
CARBOXYMETHYL STARCH AND LACTOFERRIN FOR
APPLICATION IN GUMMY CANDIES**

Subentido na Food Chemistry em junho de 2022

Abstract

Beta-carotene (β -C) is a natural pigment with the potential to combat vitamin A deficiency but is unstable in light, high temperatures, oxygen, and humidity. The objective of this research was to microencapsulate β -C by complex coacervation of amaranth carboxymethyl starch (CMS) and lactoferrin (LF) for application in gummy candies. The results indicated that high affinity electrostatic attraction between CMS and LF can occur at pHs between 3.5 and 5.5 for complex coacervates formation. About 98% of β -C was microencapsulated in CMS/LF complex coacervates, at pH=5. The microcapsules presented spherical morphology, and good photolytic and thermal stabilities. About 70% of β -C was released in the intestines, 86% was released in soybean oil, and only 19% in 50% ethanol. The addition of β -C microcapsules in gummy candies reduced its hardness and allowed 22% bioaccessibility. These results indicate that microencapsulate β -C in CMS/LF complex coacervates can be used for gummy candies fortification.

Key-words: carboxymethylation, food fortification, controlled release, amaranth starch, lactoferrin

1 Introduction

Beta-carotene (β -C) is the most common and stable natural pigment found in nature and can be extracted from different plants, fungi, and algae. In the human body, β -C can be converted into vitamin A, which acts as an antioxidant and anticancer; it can also maintain the proper functioning of the eyes and the gastrointestinal, the immune, and the reproductive systems (Barbosa et al., 2022; L. Wang et al., 2021; Olson, 1989). Therefore, β -C may be useful in combating vitamin A deficiency, which is considered one of the most common nutritional disorders in the world, affecting more than 250 million of children. This deficiency is the leading cause of blindness for approximately 350,000 preschool-age children each year (Priyadarshani, 2017). Supplementation with β -C through fortification of foods (such as gummy candies) commonly consumed by people in this age group can be an alternative to meet the nutritional needs of vitamin A. Gummy candies are characterized by being soft sweets with gelatinized structures. They are part of the fastest-growing group of products in the confectionery industry, attracting the attention of many consumers due to their unique texture, appearance, and taste (Gunes et al., 2022). However, the addition of β -C directly in gummy candies formulation may not be feasible due to its chemical characteristics. β -C is a fat-soluble compound that has a linear and rigid structure, with conjugated double bonds. Its polyene structure makes it a chemical highly reactive compound, with degradation susceptibility in the presence of light, high temperatures, humidity, oxygen, and extreme pHs (Andrés-Bello et al., 2013; Barbosa et al., 2022). However, the microencapsulation technology is useful for overcoming these limitations (Constantino & Garcia-Rojas, 2022; Rutz et al., 2017).

Among several microencapsulation methods, complex coacervation process is highlighted due to its non-use of high temperatures and organic solvents, ensuring high integrity of the wall material and excellent controlled release properties (Bastos et al., 2018; Constantino & Garcia-Rojas, 2022). The process of microencapsulation by complex coacervation can be done in three steps. In the first, an emulsion is formed using preferably a solution containing protein and oil enriched with compounds with biological properties. In the second step, another polymer is added, and the pH is adjusted to optimal conditions that allow the electrostatic attraction (Yan & Zhang, 2014). Depending on the concentration of the biopolymers, the proportion between them, the presence of salts, the pH, and other factors, the system is destabilized allowing the solution separation into two distinct phases: one rich in polymers and oil and the other poor (Timilsena et al., 2019; Yan & Zhang, 2014). In the last step, the formed microcapsules may require crosslinking to strengthen the wall material, followed by drying (Yan & Zhang, 2014).

Lactoferrin (LF) and amaranth starch are proposed in this research as wall material. LF is a globular protein, it has a molar mass between 80 and 84 kDa, and its isoelectric point is between 8 and 8.5. LF is a single polypeptide chain folded into two symmetrical globular lobes (N and C lobes). Each lobe can bind with iron, although it can also bind copper, zinc, and manganese (Bastos et al., 2018; Constantino & Garcia-Rojas, 2022). LF also has biological activities, including antiviral and antibacterial (B. Wang et al., 2017). Amaranth starch is a neutral polysaccharide with low amylose content (less than 14%) and high amylopectin content, thus presenting a dense packing inside its granule. Although it has better stability and high transition temperatures, this structural organization limits its solubility in water and its swelling power, which makes its use in some technological applications difficult (Kong et al., 2010; Zhu, 2017). Therefore, chemical modifications such as carboxymethylation can extend its application, since this method introduces negative charges in the starch molecular structure, improves its solubility, and its gelling properties (Xie et al., 2021; Zhu, 2017).

The objective of the present work was to introduce anionic charges into amaranth starch molecules through carboxymethylation to use it with lactoferrin for beta-carotene microencapsulation by complex coacervation and apply the microcapsules in the formulation of gummy candies.

2 Materials and methods

2.1 Materials

Amaranth grains was purchased from Relva Verde Alimentos EIRELI (São Paulo, Brazil). Soybean oil was purchased in the local market (Volta Redonda, Brazil). Beta-carotene (code 1001584749), α -amylase (code A3403), porcine pepsin (code P6887), porcine pancreas pancreatin (code P7545), and porcine bile extract (code B3883) were purchased from Sigma-Aldrich (St. Louis, USA). Lactoferrin with 95% purity (Vivinal® Lactoferrin) was donated by Friesland Campina (Amersfoort, Netherlands). Ultrapure water with a conductivity of 0.05 μ S/cm (Master System R&D, Gehaka, Brazil) and P.A. reagents were used in all assays.

2.2 Isolation and carboxymethylation of amaranth starch

Amaranth starch was isolated according to the methodology described by Perez et al. (1993), with minor modifications. The amaranth grains were impregnated in a 0.25% NaOH solution in the proportion of 1/10 (w/v) for 24 hours. Then, the grains were washed (3 times), ground in a blender, and filtered through a 53 μ m sieve. The marc was resuspended in water and filtered again. This process was repeated 3 times. Then, a centrifugation (Digicen 21 R, Orto Alresa, Spain) of the resulting filtrate was performed at 6,000 rpm for 20 min. The precipitate was resuspended in water and centrifuged again, repeating the process 5 times until white starch sediment was obtained. The obtained starch was dried overnight in an oven with air circulation (SSDr, Mylbor, Brazil) at 40°C, followed by sieving at 183 μ m. The moisture content of the starch ($15.60 \pm 0.24\%$) was determined according to the AOAC (2005) protocols, method 945.15. The determination of the percentage of amylose was carried out by the iodine binding assay according to the methodology described by He et al. (2012), without modification.

2.2.1 Synthesis of amaranth carboxymethyl starch

The amaranth carboxymethyl starch (CMS) was synthesized according to the Bhattacharyya et al. (1995) methodology, with minor modifications. Twenty grams of amaranth starch, 30 g of monochloroacetic acid, 22 g of NaOH, and 150 mL of isopropyl alcohol were mixed in an Erlenmeyer and allowed to stir on thermostatic magnetic stirrer (C-MAG HS 7, IKA, Germany) at 30°C for 1 h. Then the mixture was taken to a shaker incubator (SL 222, SOLAB, Brazil) and allowed to react for another 3 h at 40°C and shaking at 150 rpm. The synthesized CMS was neutralized with glacial acetic acid, followed by 5 washes with 200 mL of methanol (80%, v/v) and one wash with absolute methanol. Drying of the synthesized CMS was carried out as described above (section 2.2.). The degree of substitution (DS) of the CMS was estimated according to Equation 1, as described by Quadrado & Fajardo (2020) without modification.

$$DS = (162 * (V_b - V) * C_{HCl} * 4) / (m - (58 * (V_b - V) * C_{HCl} * 4)) \quad (1)$$

where V_b (mL) and V (mL) are the volumes of HCl used for titration of blank and CMS samples, respectively; C_{HCl} (mol/L) is the concentration of the standard HCl solution; number 4 refers to the ratio between the total volume of the solution (100 mL) and the volume

of the aliquot collected for titration (25 mL); 162 (g/mol) is the molar mass of the glucose unit, while 58 (g/mol) is the increment in the molar mass of the glucose unit due to substitution by a carboxymethyl group, and m (g) is the dried mass of the CMS sample.

2.2.2 Determination of the average molecular weight by viscometry of amaranth carboxymethyl starch

For the intrinsic viscosity measurements, the Cannon Fenske Opaque viscometer (Schott-Gerate, Germany) was used. The size 75 capillary was immersed in the thermostatic bath (Schott-Gerate, CT-52, Germany) at a temperature of 25 ± 0.1 °C. CMS samples were solubilized in water at concentrations ranging from 0.90×10^{-3} to 5×10^{-3} g/L. The density of the solvent and samples were determined using a pycnometer. The viscosimetric average molecular mass (M_v) of the CMS was calculated from the intrinsic viscosity ($[\eta]$) according to the empirical equation of Mark-Houwink (Eq. 2), described by MILLARD et al. (1997):

$$[\eta] = 0.59 * [M_v]^{0.29} \quad (6.02)$$

2.3 Study of the formation of complex coacervates of carboxymethyl amaranth starch and lactoferrin

2.3.1 Solutions preparation

Lactoferrin (LF) and CMS were weighed on an analytical balance (Shimadzu, AY220, Philippines). Then, 0.1% (w/w) aqueous stock solutions were prepared. LF was solubilized for 1 h and the CMS was solubilized at room temperature overnight, using a magnetic stirrer (NT101, Nova Técnica, Brasil.). The obtained solutions were then filtered at 0.20 μm for further analysis.

2.3.2 Zeta potential

The Zetasizer Nano ZS90 (Malvern Instruments, UK) was used to determine the zeta (ζ) - potential of the CMS (ZP1) and LF (ZP2) solutions. An automatic titrator (MTPT-2, Malvern Instruments, UK) was used to adjust the pH of the CMS and LF solutions, with the aid of 0.5 mol/L HCl, 0.25 mol/L NaOH or 0.025 mol/L NaOH. The titration was carried out from pH 2.0 to 9.0, with an increment of 0.5 ± 0.1 . The reading of ζ -potential was performed three times at room temperature (25 ± 1 °C). The strength of the electrostatic interaction (SEI) was calculated to identify the best conditions for the formation of complex coacervates, according to the Equação 3:

$$SEI (mV^2) = |ZP_1| \times |ZP_2| \quad (3)$$

2.3.3 Phase diagram

A phase diagram was constructed after the determination of SEI for the investigation of the influence of proportions (1/ 2, 1/ 1, 2/ 1, 3/ 1, 4/ 1, 5/ 1 and 10/ 1, LF/ CMS) and total concentrations of biopolymer (0.1, 0.5, 1.0, 1.5, 2.0 and 4.0%, w/w) in complex coacervate formation. For this, the stock solutions were solubilized as described above (section 2.3.1.) with concentrations equal to the analyzed total concentrations of biopolymer (TC). Sodium azide (0.02%) was added to these solutions to prevent the growth of microorganisms. Then, the solutions were weighed, mixed, and stirred for 5 min, the pH was adjusted to 4.5 and the mixtures were left to rest at 4°C for 24 h for visual observation of phase separation.

2.3.4 Isothermal titration calorimetry

Isothermal titration calorimetry (ITC) was performed on the Nano-ITC equipment (TA Instruments, USA). LF (0.325 mM) and CMS ($1,625 \times 10^{-4}$ mM) solutions were prepared in 10 mM citrate buffer at 25°C, pH 4.5, and then were dialyzed using 3.5 kDa membranes (Sigma – Aldrich, Midi 3500, USA), followed by degassing. In total, 250 μ L of LF were injected into the sample cell containing 1200 μ L of CMS. 10 μ L were injected into the sample cell every 150 seconds, with a stirring of 300 rpm. The thermodynamic parameters (described in section 3.2.2.) were obtained using the TA Nano Analyze program[®].

2.4 Beta-carotene microencapsulation

The β -C microencapsulation was carried out by varying the pH (4.0, 4.5, 5.0, and 5.5), varying the core/wall ratio (1/ 1, 1/ 2, and 1/ 4), and the TC was fixed at 1.5% (w/w), as described in Table 16. The dissolutions of CMS in water and β -C (5%, w/w) in soybean oil were made overnight, while LF was dissolved in water for 1 h. In the two biopolymer solutions, 0.02% of sodium azide was added. After dissolution, the pHs of the biopolymer solutions were adjusted to 4.0 using 10% (v/v) acetic acid. To form a simple oil-in-water emulsion, LF and β -C solutions were weighed together, followed by homogenization with an ultraturrax (T25D, IKA, Germany) at 10,000 rpm for 3 min. The CMS solution was added to the formed emulsion dropwise, followed by adjusting the pH to the desired value (4.0-5.5), using 0.5 mol/L NaOH. The formed microcapsules were allowed to stir on a magnetic stirrer for another 3 min. Then, the samples were placed at 4°C for 24 hours. After this period, the supernatant was discarded, and the precipitate was frozen in liquid nitrogen and then lyophilized (Enterprise I, Terroni, Brazil) for 48 hours. In the end, the microcapsules were stored (in a desiccator containing silica) at room temperature until further use.

2.4.1 Beta-carotene encapsulation efficiency

The β -C encapsulation efficiency (EE) was determined according to the methodology previously described by Constantino & Garcia-Rojas (2022), with some modifications. Five milliliters of hexane/acetone mixture (1/1, v/v) were added to 0.05 g of the lyophilized microcapsules, followed by vortexing for 2 min. The suspensions were placed in an ultrasound bath (Branson 2510 DTH, Sonitech, Brazil) for 20 min. Samples were centrifuged at 4,000 rpm for 10 min. The supernatant was collected and measured in a UV-vis spectrophotometer (Biomate 3S, Thermo Scientific, USA) at a length of 450 nm to quantify β -C, using a calibration curve ($Y = 0.0094X - 0.0089$, $R^2 = 0.9936$) constructed with the β -C dissolved (1 to 150 μ g/mL) in the hexane/acetone mixture. The theoretical percentage of β -C (OT) was calculated using Equation (4), and the percentage of loaded β -C (LC) was given by Equation (5). The percentage of EE was calculated by Equation 6:

$$OT (\%) = 100x(WId/WIc) \quad (4)$$

$$LC (\%) = 100x(WFd/WFc) \quad (5)$$

$$EE (\%) = 100x(LC(\%)/OT(\%)) \quad (6)$$

where WId is the initial mass (g) of β -C added to the system and WIc is the total initial mass (g) of the weighted components (soybean oil containing β -C, LF, and CMS) at the time of microencapsulation. The β -C content in the oil was measured in the spectrophotometer, weighing 0.01g of the oil after its solubilization. WFd is the β -C content (g) after

encapsulation and WFc is the final mass (0.05 g) of the β -C microcapsules used in the analysis after lyophilization.

2.4.2 Fourier transform infrared spectroscopy

Native amaranth starch, CMS, LF, soybean oil, β -C, and lyophilized β -C microcapsules were analyzed by Fourier Transform Infrared Spectroscopy (FTIR) (Bruker, Ver-tex 70, Germany). The spectra were observed in the wavenumbers between 400 to 4000 cm^{-1} .

2.4.3 Particle sizes of beta-carotene microcapsules, amaranth carboxymethyl starch, and lactoferrin

Zetasizer nano ZS90 was used to determine the hydrodynamic diameter in nanometer (d.nm) of 0.1% (w/w) of CMS and LF solutions, and β -C microcapsules diluted 5X in water before lyophilization. The pH of all solutions was maintained at 5.0, and the analysis was performed in triplicate using DLS (Dynamic Light Scattering) at 25 °C.

2.4.4 Optical microscopy of beta-carotene microcapsules

The optical microscope K220 (Kasvi, Brazil) coupled with a 5MP Moticam camera (Kasvi, Brazil) was used to determine the morphology of the β -C microcapsules. The images were captured at 10 and 40x magnification.

2.4.5 Study of thermal and photolytic stability of beta-carotene microcapsules

The study of the thermal stability of the β -C microcapsules was carried out at 50°C. For this, 1.5 mL were placed in a hermetically sealed container and placed in Shaker incubator SL 222. For comparison purposes, a solution of free β -C was prepared by dissolving 0.00565 g in the hexane/acetone mixture (1/1, v/v), and 1.5 mL of this solution was added to the hermetically sealed container. Samples were read on days 1, 2, and 3. Photolytic stability was studied using a darkroom (AG-DC-02, ACS Gold, Brazil) with ultraviolet (UV) light at 360 nm for 8 h. Samples were read every hour. The free β -C solutions were also exposed to UV light.

Aliquots of 0.5 mL were taken from the samples for each experiment, then 2.5 mL of the hexane/acetone mixture (1/1, v/v) was added to the solutions, mixed by vortex for 2 min, and allowed to stand for 1 min, followed by the determination of β -C concentrations as described in section 2.4.1.

2.4.6 The in vitro Simulation of gastrointestinal digestion of beta-carotene microcapsules

The gastrointestinal digestion was simulated in vitro according to the INFOGEST 2.0 model (Brodkorb et al., 2019). Briefly, 0.2 g of lyophilized β -C microcapsule samples was mixed with 0.5 mL of water. Then, 0.7 mL of simulated salivary fluid (pH 7.0) containing 0.75 U/mL of salivary amylase in the final oral solution. In the gastric phase digestion, 1.39 mL of the simulated gastric solution (pH 3.0) was added to the mixture from the oral digestion, containing pepsin (2,000 U/mL) in the final gastric solution, then the pH was adjusted to 3 with 0.01 mL 6 mol/L HCl. For intestinal digestion, 2,785 mL of simulated intestinal fluid (pH 7.0) was added, containing in the final intestinal solution 100 U/mL of pancreatin and 10 mmol/L of bile salts. Then the pH was adjusted to 7.0, using about 0.015 mL of 6 mol/L NaOH. All fluids were preheated before the experiment, which was carried out in agitation (95 rpm) in the shaker incubator (TE- 424, Technal, Brazil) at 37 °C, for 2 min for the oral phase, 2 h for each of the gastric and intestinal phases. At determined time intervals, aliquots of 0.2 mL were taken from each phase to determine the β -C concentrations, as described in

the efficiency section (2.4.1). The compositions of the fluids used in each stage of digestion are described in table 15.

Table 15. Electrolytes (1.25x of Concentrations) of fluids used during the in vitro simulated gastrointestinal digestion according to INFOGEST 2.0 protocol (Brodkorb et al., 2019).

Salts	Concentration* in millimole per liter for		
	Saliva stimulation fluid (SSF)	Simulated gastric fluid (SGF)	Simulated intestinal fluid (SIF)
KCl	15.1	6.9	6.8
KH ₂ PO ₄	3.7	0.9	0.8
NaHCO ₃	13.6	25	85
NaCl	-	47.2	38.4
MgCl ₂ (H ₂ O) ₆	0.15	0.12	0.33
(NH ₄) ₂ CO ₃	0.06	0.5	-
HCl	1.1	15.6	8.4
CaCl ₂ (H ₂ O) ₂	1.5	0.15	0.6

*These concentrations are for stock solutions; just before use, they are mixed with the necessary quantities of enzyme and finally diluted to a 1x concentration working solution (i.e., 4 parts of electrolyte solution +1 part consisting of enzymes and water results in 1x concentration of the digestion fluids). The INFOGEST also provide online (link below) template with the calculation of the electrolyte solution and enzymes.

2.4.1 Simulation of the in vitro beta-carotene release kinetics in food matrices

The analysis of beta-carotene release kinetics was performed following the methodology described by Barbosa et al. (2021), with minor modifications. Therefore, 10 mL of soybean oil or 50% aqueous (v/v) ethanol was added to 0.1 g of lyophilized microcapsules. The simulation was made with a shaker incubator TE-424 at 25°C, with agitation at 100 rpm for 2 h. Aliquots of 0.2 mL were taken at defined time intervals, in their place 0.2 mL of soybean oil or 50% ethanol was placed. Then, 1.8 mL of the hexane/acetone mixture (1/1, v/v) was added to the collected aliquots and the absorbance was read to quantify the β-C content, as described in section 2.4.1.

2.5 Application of beta-carotene microcapsules in gummy candies formulation

Gummy candies were prepared according to the formulation described by Amjadi et al. (2018), with minor modifications. Therefore, 8% w/w gelatin, 34% w/w sucrose, 31% w/w glucose syrup, 0.3% w/w citric acid, and 5.77 mL of non-lyophilized β-C microcapsules were used in total gummy candies preparation. The amounts of β-C microcapsules corresponded to the recommended daily amount of β-C (vitamin A equivalent), which is 3592.81 μg for adults (Brazil, 2005). To prepare the gummy candies formulations, glucose syrup, sugar and water were mixed and cooked until complete dissolution. The gelatin was dissolved in water for 30 min at 60°C. The microcapsules were added to the gelatin solution and homogenized at 120 rpm for 5 min. This mixture was added to the sugar. Then the citric acid was added to the mixture, which was stirred (120 rpm) until reaching 70°C in a water thermostatic bath. The mixtures were placed in a silicone mold (2.5 cm high, 2.5 cm long, and 2.5 cm wide), kept in the refrigerator for 24 h, then was removed from the molds and kept in a desiccator (48 h) containing a saturated solution of magnesium nitrate (50% moisture). Gummy candies without microcapsules were also produced to serve as a control.

2.5.1 Beta-carotene stability after gummy candies production

The β -C stability analysis during the production of gummy candies was carried out by measuring its recovery content. For this, 16 g of the gum was mixed with 16 ml of ultrapure water and placed in an ultrasound bath at 40°C for 1 hour. After this period, 5 ml of the hexane/acetone mixture (1/1) were added, followed by vortexing for 1 min. Then, 5 mL of absolute ethanol was added to the mixture, followed by vortexing for 10 seconds. The samples were centrifuged at 8,000 rpm for 10 min and the organic phase in the supernatant was collected for absorbance reading and determination of β -C recovery content as described above (section 2.4.1.).

2.5.2 Texture analysis of gummy candies

Texture analysis of gummy candies was performed with a TA-XTPlus texturometer (Stable Micro Systems, Surrey, United Kingdom) at room temperature ($25 \pm 1^\circ\text{C}$). Hardness, adhesiveness, elasticity, cohesion, gumminess, and resilience were evaluated. For each sample, two measurements with three replicates were performed using a cylindrical probe (P/40). The time between two compressions (50%) applied to the samples was set at 3 seconds. In texture analysis, pre-test, test, and post-test speeds were set at 2, 1, and 1 mm/s, respectively (Kurt et al., 2022).

2.5.3 Bioaccessibility of microencapsulated beta-carotene incorporated in gummy candies

The β -C bioaccessibility (B^*) incorporated into the gummy candies through β -C microcapsules was determined after the *in vitro* simulation of the gastrointestinal digestion of 4 g of the gummy candies. The experiment was carried out using proportionally the contents of oral, gastric, and intestinal fluids as described in the previous section (6.2.4.7). The B^* of the β -C in the gummy candies candy was calculated by Equation 7 and was compared to the B^* of the β -C of the microcapsules.

$$B^* = 100 * (C_{micelle}/C_{digeste}) \quad (7)$$

where $C_{micelle}$ and $C_{digeste}$ are the concentrations of β -C in the micellar and digest phase (in the intestinal phase) after the *in vitro* simulation of gastrointestinal digestion. The micelle was obtained according to the methodology described by Constantino & Garcia-Rojas (2022) without modification.

2.6 Statistical analysis

All experimental measurements were performed in triplicate and data was expressed as mean \pm standard deviation. Statistical analysis was performed using the Origin 8.0 software. One-way analysis of variance (ANOVA) was performed and Tukey's test at the level of significance $\alpha = 0.05$ was used to determine the existence of significant differences between populations.

3 Results e Discussion

3.1 Synthesis of amaranth carboxymethyl starch

The CMS DS and M_v results were 0.27 ± 0.01 and $2.36 \pm 0.07 \times 10^7$ g/mol, respectively. Our DS results are similar to those reported by Bhattacharyya et al. (1995), who also modified amaranth starch by carboxymethylation. High DS values of a modified starch can mean the presence of more anionic binding sites with positively charged molecules. Furthermore, high DS can improve the solubility of starch in water. However, to achieve a high DS of amaranth starch Bhattacharyya et al. (1995) needed to pass it through two steps of carboxymethylation, which can change the granular structure and gelatinize the starch. By losing this native structure, some physicochemical properties (such as thermal stability) could be at stake, since it can be useful in technological applications that use high temperatures. Therefore, the DS of amaranth starch obtained in this work was considered adequate for further steps. The high M_v value obtained in the present study can be explained by the fact that the starch is waxy (higher amylopectin content) since the amylose content determined in the present work was 7.31 ± 0.35 %. Our results agree with findings in the literature, where the molecular weight of amaranth amylopectin can range from approximately 1 to 70×10^7 g/mol (Marfil et al., 2018).

Fig. 36A shows the results of the FTIR analysis of CMS and native amaranth starch. The spectra of the two starches show the presence of OH groups (at 3305 cm^{-1}), CH_2 groups (at 2979 cm^{-1}), C-O vibration of glycosidic units, and the pyranoid ring (band around 1010 cm^{-1}). Furthermore, the band at 1641 cm^{-1} of native starch can be attributed to the scissor vibration mode of the absorbed water molecules (Quadrado & Fajardo, 2020). However, the CMS spectrum presented new peaks at 1594 , 1413 , and 1251 cm^{-1} , which correspond to the elongation of the C-O bond of the carboxylic acid (RCO-O-), the C-C aromatic bond, and the elongation of the C-O bond of carboxylic acid. This result shows that carboxylic groups were inserted into amaranth starch. A ζ -potential analysis (Fig. 37) confirmed a higher density of negative charges for CMS compared to native starch, which is the result of the presence of the anionic carboxylic group in an aqueous solution.

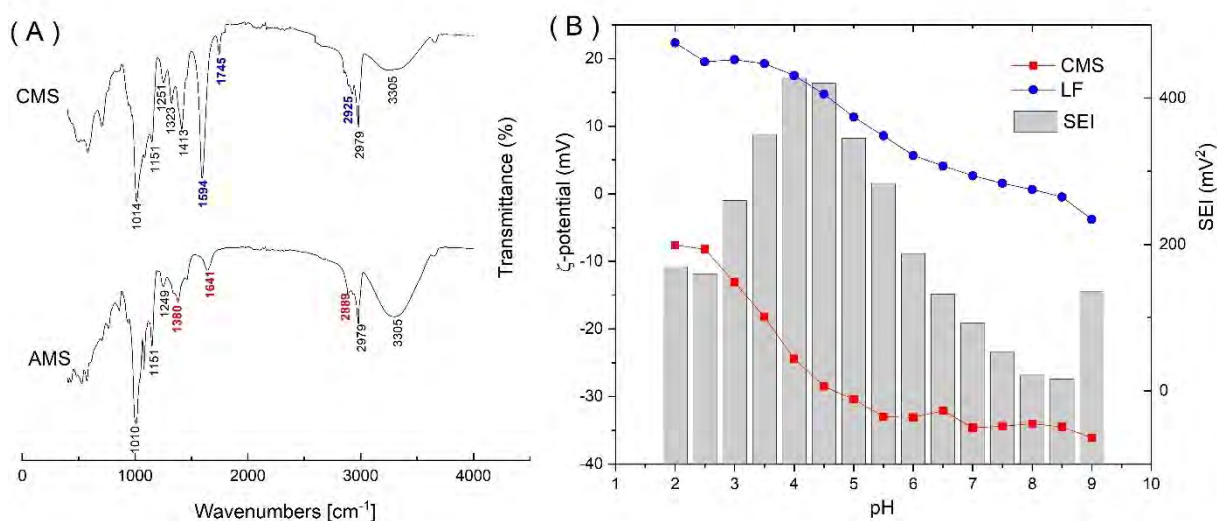


Figure 36. (A) FTIR spectra of carboxymethyl (CMS) and native amaranth (AMS) starches. (B) Results of the ζ -potential and electrostatic interaction force (SEI) of lactoferrin (LF) and carboxymethyl amaranth starch (CMS).

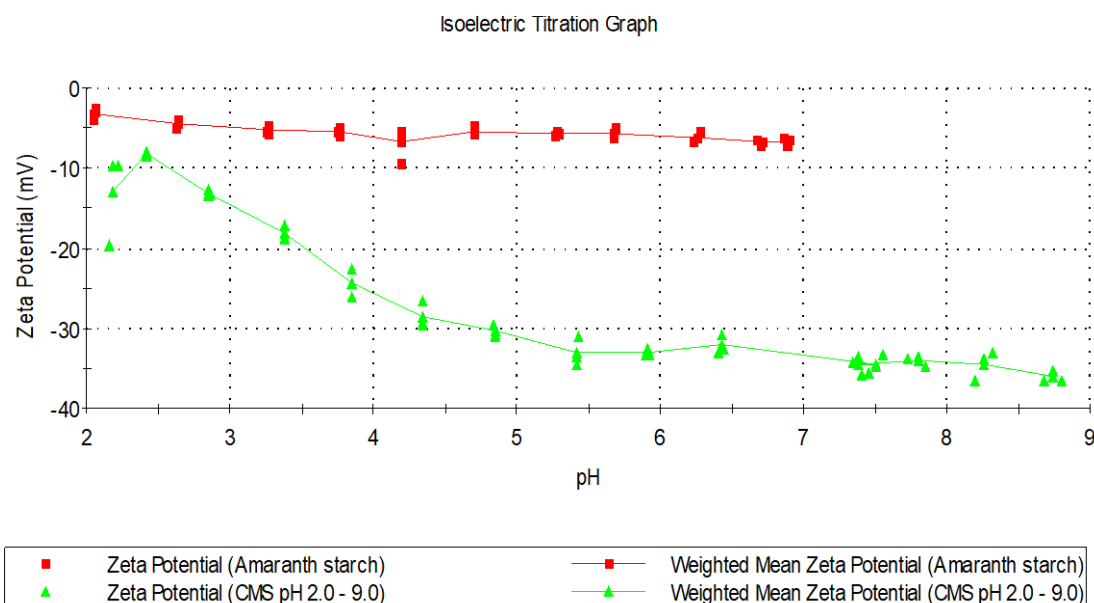


Figure 37. Zeta potentials of native amaranth starch (red) and carboxymethylated amaranth starch (green).

3.2 Formation of amaranth carboxymethyl starch and lactoferrin complex coacervates

3.2.1 Influence of pH and mass ratio amaranth carboxymethyl starch and lactoferrin complex coacervates

The ζ -potential and SEI results of the CMS and LF are shown in Fig. 36B. LF showed an isoelectric point around $\text{pH}=8.34$, while negative charges were observed in the CMS at practically all pHs studied (2-9). The SEI results were highest at pHs 4 and 4.5, followed by 3.5 and 5, with the respectively following SEIs values of 427, 420.38, 350.35, and 345.04 mV^2 . These results indicates that CMS and LF can form complexes with possible highest electrostatic attraction, mainly at pHs 4.0 and 4.5. However, the pK_a of the carboxylic groups is around 4.2 (Nita et al., 2020), consequently is not advisable to study the formation of complexes below this pH due to a possible CMS protonation (Barbosa et al., 2018). In this sense, pH 4.5 was used to investigate the best conditions for the formation of CMS/LF complex coacervates.

Studies of the complex coacervates formation using only ζ -potential and/or turbidimetric analysis may have some limitations, especially when studying high TC that are generally used for encapsulation. In these cases, a phase diagram study can be useful to identify the optimal pH, as conditions identified using low TC can shift to other pHs or even other ratios when TC are high (Lan et al., 2018). Fig. 38 presents the results of the phase diagram of the interaction of CMS and LF in different proportions and TC (%), at pH 4.5. Due to the presence of opposite charges of CMS and LF at this pH, in all conditions of the experiment, there was the formation of complexes (soluble (■) or coacervates) (Fig. SA). In the case of complex coacervates, was identified three systems: (i) solution with smaller volume, precipitate, and clear supernatant (○); (ii) solution with larger volume, precipitate, and clear supernatant (●); (iii) and solution with precipitate and cloudy supernatant (□). The first and second cases were observed in all samples with TC (%) from 0.1 to 1.5%, for the proportions 2/1 and 1/1 (LF/CMS), respectively. Coacervate formation conditions changed to higher proportions (3/1 and 2/1, LF/CMS) in samples with TC (%) greater than 2%. However, we can consider that the 2/1 ratio can form complex coacervates in all TC (%) studied.

Complex coacervates with precipitate and cloudy supernatant may have soluble complexes and/or excess biopolymers which didn't interact (Lan et al., 2018)

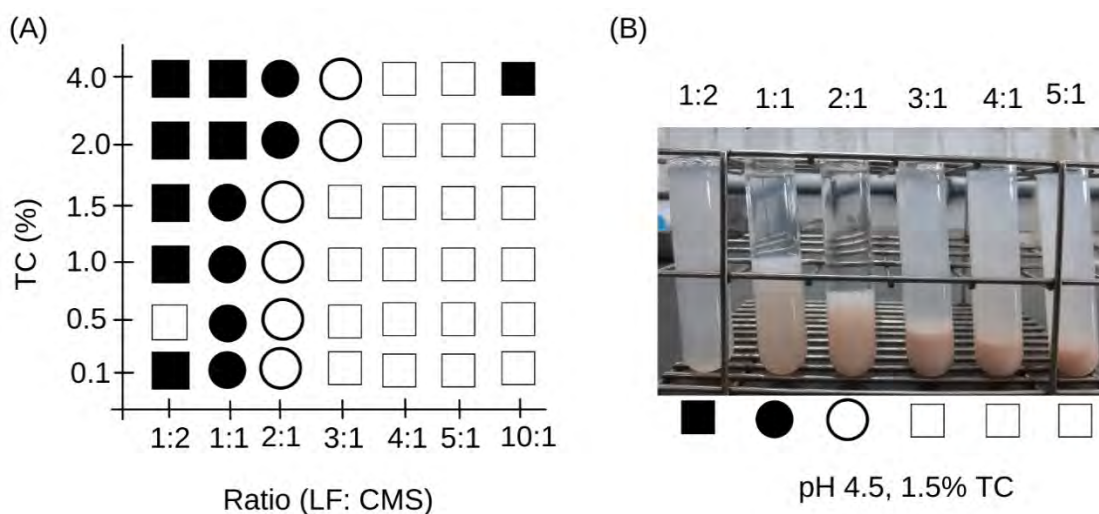


Figure 38. (A) State diagram of complexes formed by lactoferrin (LF) and carboxymethyl amarant starch (CMS) in different proportions and total concentration of biopolymers (CT) at pH 4.5. (B) Visual representation of CMS/LF complexes formed after 24 h, □ represents cloudy solution with precipitate, ■ represents cloudy solution, ○ represents solution with lower volume precipitate, and ● represents solution with higher volume precipitate and slightly cloudy.

3.3 Isothermal titration calorimetry of lactoferrin in amarant carboxymethyl starch

Fig. 39A shows a typical thermogram of the heat rate versus time, obtained during the titration of LF in the CMS, at pH 4.5 and 25°C. The titration profile was exothermic, and its peaks steadily decreased from the sixth until the fourteenth injection, indicating that the binding sites in the CMS were saturated by LF. The exothermic profile was also reported for complex coacervates formation of LF/sodium alginate (Bastos et al., 2018), and pea protein isolate/beet pectin (Lan et al., 2020). The binding isotherm (Fig. 39B) was fitted from the thermogram using the "one independent binding site" since two or more inflection points in the binding isotherm were not observed (Lan et al., 2020). The thermodynamic parameters obtained by this model were dissociation constants ($K_d = 9.23 \pm 3.24 \times 10^{-7}$ mol/L), binding sites ($n = 204.4$), enthalpy variation ($\Delta H = -28.51 \pm 1.55$ kcal/mol), Gibbs free energy change ($\Delta G = -8.23$ kcal/mol), and entropy change ($\Delta S = -68.01$ cal/mol.K). This result indicates that the formation of LF/CMS complex coacervates has a high affinity because the K_d value was above 106 (Bastos et al., 2018; Constantino & Garcia-Rojas, 2022). Negative values of ΔH and ΔS indicate that the reaction was enthalpically favorable and entropically unfavorable for LF/CMS complex formation. Although hydrogen bonds, electrostatic interactions, and hydrophobic interactions may have contributed to the formation of the complexes, electrostatic interactions may be the ones that governed the process due to the presence of opposite charges of the biopolymers during the titration (Bastos et al., 2018; Constantino & Garcia-Rojas, 2022; Lan et al., 2020).

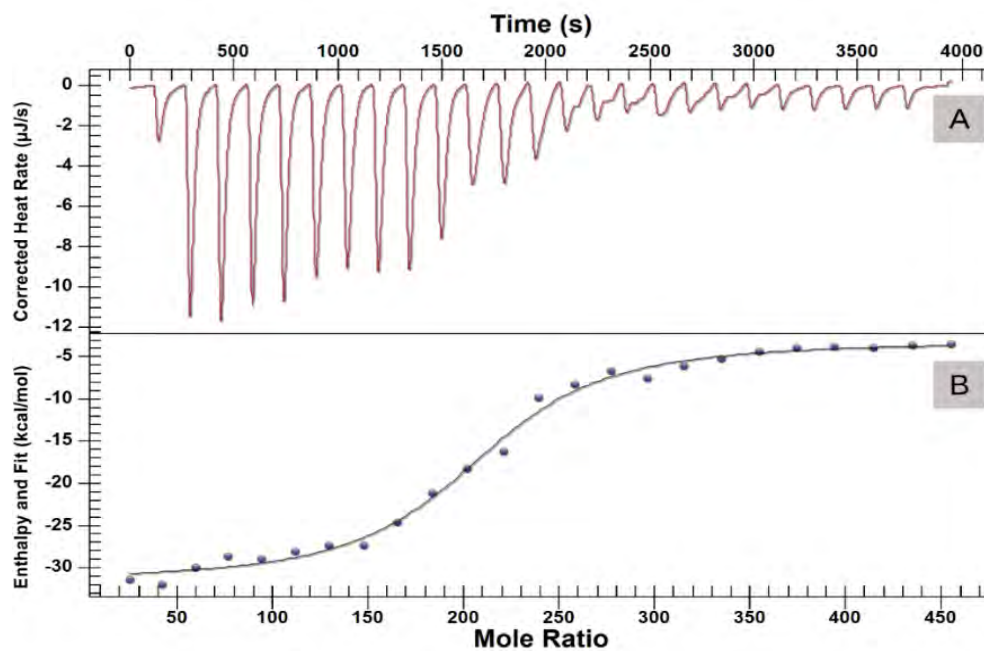


Figure 39. (A) Heat flow thermogram ($\mu\text{cal/s}$) as a function of time (s), obtained during the titration of 0.325 mmol/L of lactoferrin (LF) and 1.625×10^{-4} mmol/L of amaranth carboxymethyl starch (CMS) in citrate buffer (10 mmol/L, pH 4.5) at 25 °C. (B) Graphic representation of the integrated peak areas (kcal/mol) as a function of the molar ratio of LF/CMS ($p < 0.05$).

3.4 Beta-carotene microcapsules obtained by complex coacervates of amaranth carboxymethyl starch and lactoferrin

3.4.1 Beta-carotene encapsulation efficiency

Fig. 40 shows β -C encapsulation systems. The systems with the 1/1 ratio (wall/core) showed an oil layer on the surface. This phenomenon was also observed for encapsulation systems at pH 4.0. The encapsulation systems at pH 4.5 presented clear supernatant, as well as the encapsulation systems at pH 5.0 for the proportions 1/1 and 2/1. The systems at pHs 5.0 and 5.5 showed a more pronounced coloration compared to other pHs. All encapsulation systems at pH 5.0 had higher volumes compared to others. The presence of oil on the surface in encapsulation systems where the core/wall ratio is equal may indicate insufficient protein to encapsulate oil. The more pronounced coloration observed at pHs 5 and 5.5 may be related to the stability of β -C, which tends to be less stable at very acidic pHs (Andrés-Bello et al., 2013). In their research, Lan et al. (2021) observed that the encapsulation of hemp seed oil using beet pectin and pea protein isolate at pH 2.5 (with higher coacervate volume) showed higher EE (%) compared to pH 3.5. However, the oxidative stability of hemp seed oil was better at pH 3.5 due to the strong electrostatic interaction of the biopolymers used, which did not allow the microcapsules to break and thus the loss of encapsulated content during the spray drying process. Thus, it can be understood that, in addition to the core to wall ratio and TC (%), the EE (%) can be influenced by factors such as pH and stability of the compound to be encapsulated. Therefore, we sought to study how the EE (%) of β -C would be affected by both the pH and the core/wall ratio of lyophilized microcapsules.

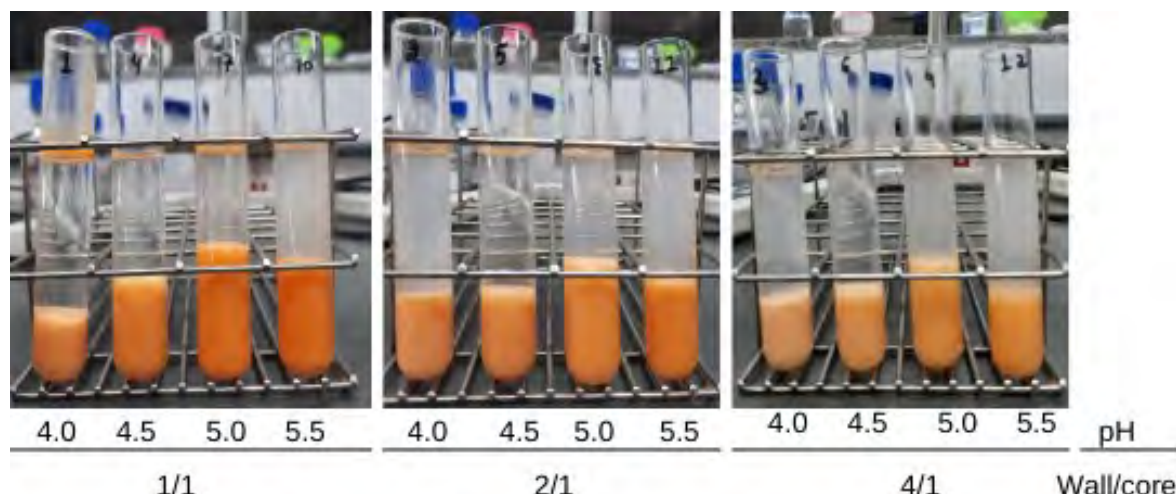


Figure 40. Systems of beta-carotene microencapsulation by complex coacervation of amaranth carboxymethyl starch and lactoferrin.

According to Table 16, the β -C encapsulation efficiency was high ranging from 85 to 98%. The pH and the core/wall ratio influenced the EE (%). As expected, the core/wall encapsulation systems of 1/4 and pH 5.0 or 5.5 presented the highest values of EE (%), although they did not show statistical difference with all other systems, except for the A2 system. This is related to enough protein to interact with the oil added. Many authors have reported that systems with higher wall content in relation to the core can encapsulate oils better (Lan et al., 2021). In the case of pH 5.0 and 5.5, this fact is related to the good stability of β -C and, therefore, no loss during the encapsulation process. High β -C EE (%) was also reported in different complex coacervates systems. For example, Jain et al. (2016) obtained an EE (%) of $79.36 \pm 0.541\%$ using casein and gum tragacanth. In another study, Thakur et al. (2017) obtained $65.95 \pm 5.33\%$ EE (%) when encapsulating β -C using casein and guar gum.

Table 16. Encapsulation efficiency (EE), loading capacity (LC), and initial β -C added (OT) of the microcapsules in different formulations.

Sample	core/wall	pH	LF (g)	CMS (g)	Wall (g)	Core (g)	β -C (g)	Total solids	OT (%)	LC (%)	EE (%)
A1	1/1	4.00	0.30	0.15	0.45	0.450	0.0225	0.90	2.28 ± 0.01	2.00 ± 0.10	$87.53 \pm 4.36^{a,b}$
A2	1/2	4.00	0.30	0.15	0.45	0.225	0.0113	0.68	1.53 ± 0.02	1.32 ± 0.02	85.86 ± 2.25^a
A3	1/4	4.00	0.30	0.15	0.45	0.113	0.0056	0.56	0.93 ± 0.02	0.87 ± 0.03	$93.31 \pm 4.65^{a,b}$
A4	1/1	4.50	0.30	0.15	0.45	0.450	0.0225	0.90	2.27 ± 0.01	2.02 ± 0.08	$88.57 \pm 3.68^{a,b}$
A5	1/2	4.50	0.30	0.15	0.45	0.225	0.0113	0.68	1.53 ± 0.01	1.42 ± 0.07	$92.77 \pm 4.04^{a,b}$
A6	1/4	4.50	0.30	0.15	0.45	0.113	0.0056	0.56	0.94 ± 0.02	0.90 ± 0.02	$95.95 \pm 0.86^{a,b}$
A7	1/1	5.00	0.30	0.15	0.45	0.450	0.0225	0.90	2.29 ± 0.02	2.02 ± 0.08	$88.22 \pm 2.91^{a,b}$
A8	1/2	5.00	0.30	0.15	0.45	0.225	0.0113	0.68	1.66 ± 0.04	1.58 ± 0.02	$95.33 \pm 3.03^{a,b}$
A9	1/4	5.00	0.30	0.15	0.45	0.113	0.0056	0.56	0.97 ± 0.03	0.95 ± 0.02	98.47 ± 0.97^b
A10	1/1	5.50	0.30	0.15	0.45	0.450	0.0225	0.90	2.27 ± 0.01	2.11 ± 0.10	$92.62 \pm 3.82^{a,b}$
A11	1/2	5.50	0.30	0.15	0.45	0.225	0.0113	0.68	1.51 ± 0.02	1.40 ± 0.07	$92.53 \pm 3.57^{a,b}$
A12	1/4	5.50	0.30	0.15	0.45	0.113	0.0056	0.56	0.96 ± 0.03	0.94 ± 0.03	98.20 ± 1.88^b

EE (%), OT (%), and LC (%) were calculated from Equation (4) and Equation (3), respectively. LF is lactoferrin, CMS is amaranth carboxymethyl starch, and β -C is beta-carotene. The same letters in the same column do not differ significantly by Tukey's test with a probability of 5%. The symbol \pm is the standard deviation, n=3.

In this study, sample A9 was used for further analysis because. As explained, the sample had a higher volume in the phase diagram, high EE (%) and the pH 5.0 that was encapsulated had a higher SEI value compared to pH 5.5. These factors favor the manufacture of β -C microcapsules with good physicochemical characteristics, including thermal or photolytic stability.

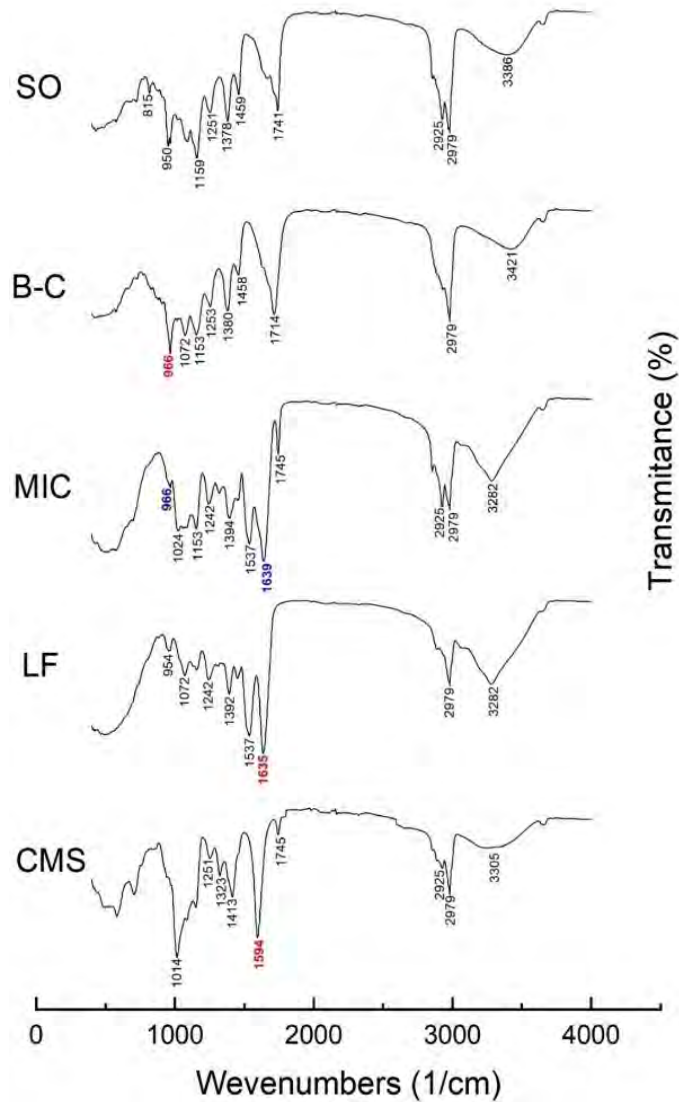


Figure 41 Espectros FT-IR da lactoferrina (LF), amido nativo de amaranto (MAS) amido de carboximetilado (CMS), complexos coacervados CMS/LF (COM), betacaroteno (β -C), óleo de soja (SO) e microcápsulas de betacaroteno (MIC).

3.4.2 Fourier transform infrared spectroscopy

The FTIR results of CMS, LF, soybean oil, β -C, and microcapsules (sample 9) are shown in Fig. 41. CMS spectra were discussed in section 3.1. LF spectra showed characteristic peaks for amide I, II, and III at 1635, 153.7, and 1242 cm^{-1} respectively. The peak at 3282 cm^{-1} present in the LF spectra is from the -OH groups of free amino acids (Constantino & Garcia-Rojas, 2022; Bastos et al., 2018). In the soybean oil spectra, the C-O and C=O signals of the ester groups were observed at 1159 and 1741 cm^{-1} , while the presence of methylene groups

was confirmed by peaks at 1378, 1459, and 2926 cm^{-1} (Bach et al., 2019). In the β -C spectra, the band at 966 cm^{-1} represents the deformation mode of the trans conjugated alkene -CH=CH- out-of-plane, and the peaks at 2979 cm^{-1} represent a CH stretch of the alkane group, 1458 cm^{-1} indicates the C-C elongation in the aromatic ring. The other peaks at 1714 cm^{-1} indicate C=O stretching vibrations (Kaur et al., 2019). In the spectra of the microcapsules, many peaks are superimposed, but the peak corresponding to amide I of the LF shifted from 1635 to 1639 cm^{-1} , and the peak at 1594 cm^{-1} of the CMS does not appear in the spectrum. The peak shift can be attributed to the electrostatic interaction of CMS carboxylic groups and LF amides. Different authors have reported the same phenomenon when studying the complex coacervation of proteins and polysaccharides (Bastos et al., 2018; Lan et al., 2020, 2021). Furthermore, the presence of β -C was observed at 966 cm^{-1} . Therefore, these results confirm the microencapsulation of β -C by complex coacervation using CMS and LF as wall material.

3.4.3 Particle sizes and optical microscopy of beta-carotene microcapsules

The particle size (z-average) results of LF, CMS, and β -C microcapsules (sample A9) were 10.83 ± 0.14 , 191.0 ± 1.31 , and 4247.0 ± 316.54 d.nm, respectively. The particle sizes of the microcapsules were larger compared to those of the LF and CMS together. This can be explained by the fact that encapsulation involves the formation of an emulsion in which the positively charged protein surrounds the oil droplets and with the addition of CMS with negative charges they attract each other, thus forming larger particles. The images obtained by the optical microscope (Fig. 42) shows a well-defined spherical structure of these microcapsules, indicating the preservation of oil droplets during the encapsulation process by complex coacervation. Similar results were observed by Constantino & Garcia-Rojas (2022).

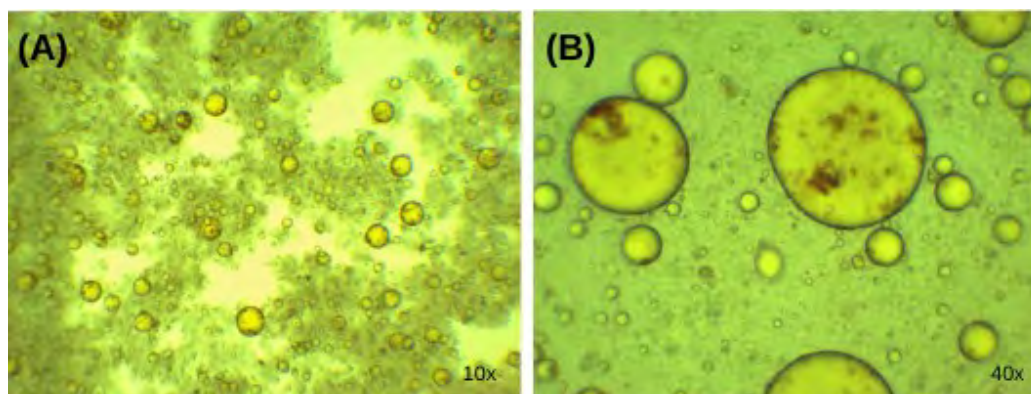


Figure 42. Imagens microscópicas das microcápsulas de betacaroteno tiradas pelas objetivas de 10x e 40x.

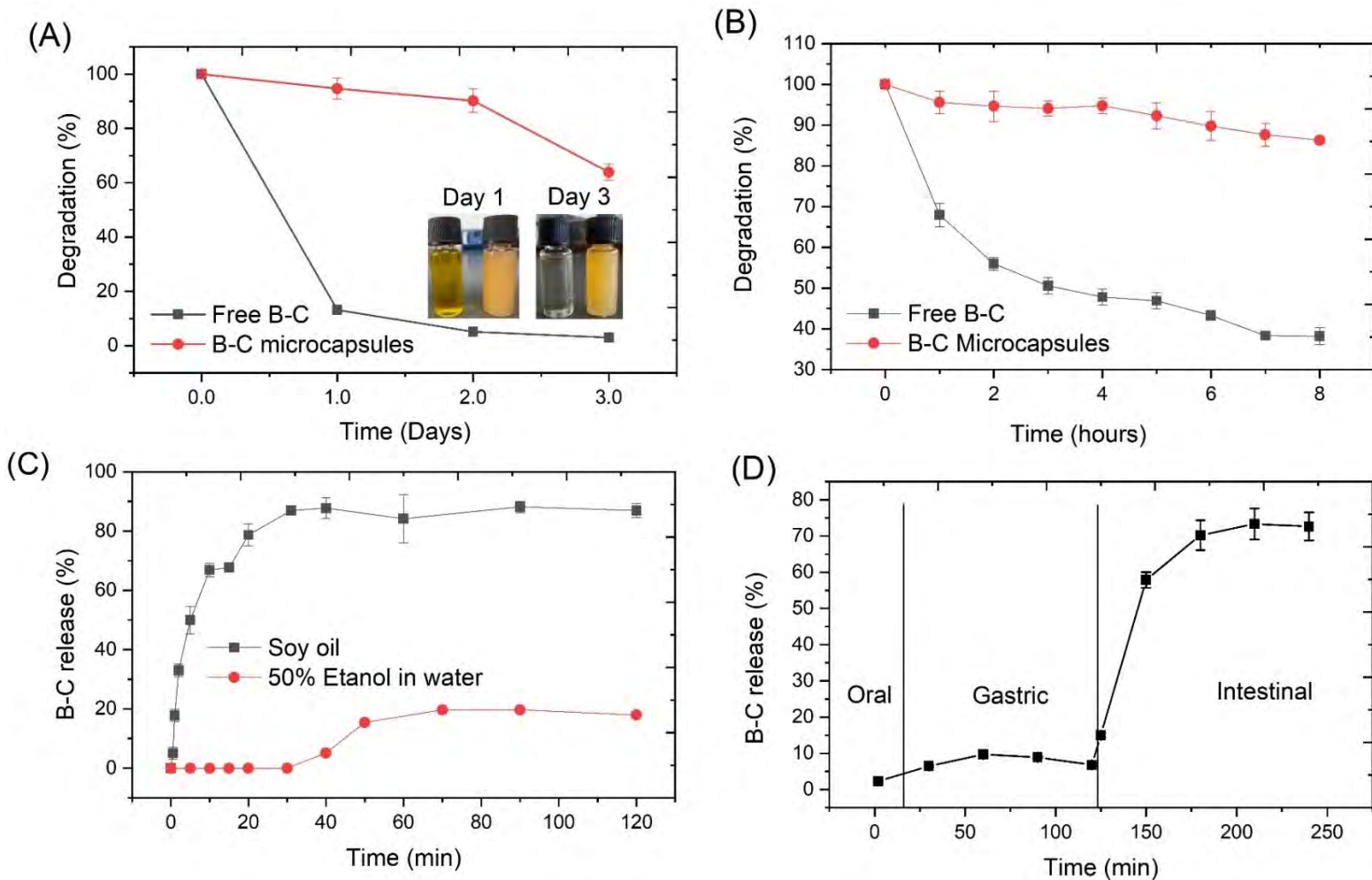


Figure 43. (A) Estabilidade do betacaroteno (β -C) livre e microencapsulada a 50°C por 3 dias. (B) Estabilidade do β -C livre e microencapsulada na radiação ultravioleta por 8 horas. (C) Perfil de liberação do β -C microencapsulado no óleo de soja e em etanol 50%. (D) Perfil de liberação do β -C durante a simulação *in vitro* da digestão das microcápsulas de B-C.

3.4.4 Stability of microencapsulated beta-carotene

The results of the stability of β -C encapsulated are presented in Fig. 43. According to Fig. 43A, heating free β -C at 50°C led to a drop in its concentration to 13.16 ± 0.13 % on the first day and, on the third day, this value dropped to about 2.98 ± 0.14 %. In the case of encapsulated β -C, on the first day 94.62 ± 3.96 % of the β -C was preserved and on the third day, there was still 63.84 ± 2.90 % of β -C. These results indicate that the wall material formed by LF/CMS complex coacervates presents a good ability for β -C protection at this temperature. Furthermore, data on the stability of β -C during exposure to UV radiation (Fig. 43B) show a rapid degradation (31%) of free β -C in the first hour of exposure. Degradation continued gradually until reaching about 62% at the end of 8h. In the case of microencapsulated β -C, only 4.4% of the β -C was lost in the first hour and at the end of the experiment, 14% of the β -C was degraded. The microcapsules showed the ability to protect β -C against the action of UV radiation. This may have occurred due to the presence of LF, as proteins tend to absorb UV radiation (Constantino & Garcia-Rojas, 2022). Some authors have shown that microcapsules produced by complex coacervates tend to protect different compounds with biological activities, including β -C (Barbosa et al., 2021; Constantino & Garcia-Rojas, 2022; Jain et al., 2016; Thakur et al., 2017).

3.4.5 The in vitro simulation of gastrointestinal digestion of beta-carotene microcapsules

The results of the simulation of the in vitro gastrointestinal digestion of β -C microcapsules (sample A9) are shown in Fig. 43D. The Digestion in the oral and gastric phases showed a low β -C release rate (below 10%). This may be attributed to rapid (2 min) digestion in the mouth, while in the stomach, the pH=3.0 allowed the electrostatic interaction between CMS and LF according to the ζ -potential results (section 3.2.). Furthermore, CMS may protected LF against pepsin action (Barbosa et al., 2021). During the intestinal digestion, about 15% of β -C was released in the first 5 min, this release rate gradually increased until reaching 73% at the end of digestion. The increase in β -C release in the intestinal phase may be related to the weak electrostatic interaction between CMS and Lf at pH 7.0, and to the presence of digestive enzymes (pancreatin, trypsin, chymotrypsin, and membrane peptidases) (Barbosa et al., 2021, Santos et al., 2021).

3.4.6 Release kinetics of microencapsulated beta-carotene in food matrices

Fig. 43C shows the results of the release kinetics of microencapsulated β -C in soybean oil and 50% ethanol. The β -C release in soybean oil was rapidly reaching about 50% in the first 5 min, and reached approximately 86% after 30 min. This final concentration remained constant until the end of the experiment. In contrast, the β -C release in 50% ethanol was slower and took approximately 40 min to occur. Also, the β -C release in 50% ethanol was lower and reached approximately 19% in 70 min. This concentration remained constant until the end of the experiment. These results indicate that in highly oily food matrices these microcapsules can release β -C more quickly, compared to systems containing water and relatively low oil concentration. Table 17 presents the results of the mathematical models used to analyze the microencapsulated β -C release in food matrices. According to the adjusted- R^2 values, the data of β -C release in soybean oil was best-fitted with the first-order model (adjusted- $R^2 = 0.979$). This result indicates that Fickian diffusion governs the β -C release in this matrix. While the data of β -C release in 50% ethanol was best fitted with the Peppas-Sahlim model (adjusted- $R^2 = 0.998$), indicating a contribution from Fickian diffusion and case II relaxational. Although Fickian diffusion is predominant ($k_1/k_2 > 1$) (Mehran et al., 2020; Bruschi, 2015), it is necessary consider that the swelling of the microcapsules and relaxation of the chains of the

biopolymers used in the microencapsulation influenced the release. Similarly, Mehran et al. (2020) observed that Peppas-Sahlim was the mechanism of release of microencapsulated peppermint essential oil in complex coacervates of inulin/gum arabic in 50% ethanol. These results suggest that the application of β -C microcapsules obtained by complex coacervation of CMS and LF may be favorable in aqueous food matrices because their release was slow and lower and can keep β -C protected.

Table 17. Fitting results of beta-carotene release in foods matrices

Food matrices	First order			Ritger-Peppas			Higuchi		Peppas-Sahlim			
	Fmax	k1	R ^{2*}	kkp	n	R ^{2*}	kh	R ^{2*}	k1	k2	m	R ^{2*}
Soy oil	84.73	0.170	0.979	31.784	0.245	0.869	11.371	0.558	250.122	-1.685	0.479	0.968
Etanol 50% (v/v)	19.14	0.136	0.969	13.729	0.080	0.904	2.221	0.388	7.217	-0.653	0.453	0.998

*Is the adjusted-R²

3.5 Gummy candies containing beta-carotene microcapsules

Two gummy candies were obtained: (i) without microcapsules (GC) and (ii) with β -C microcapsules (GCM). Compared to GC, GCM showed a yellowish color which can be attributed to the β -C presence (Fig. 44). After the production of gummy candies, the β -C recovery was 66.53 ± 5.46 %. This reduction of β -C concentration in final gummy candies may be related to the production process, mainly to the temperature in the mixture with the gelatin (60°C), and subsequent mixing with the sugars (from approximately 110 to 70°C). As discussed in section 6.3.3.4., β -C has poor stability at high temperatures. Du et al. (2019) observed a drop in β -C concentration to zero after heating at 60°C for 10 hours. Furthermore, as discussed in the encapsulation efficiency (section 6.3.3.1.), the pH (below 4) of gummy candies production may have contributed to this reduction in the β -C content.

Gummy candies

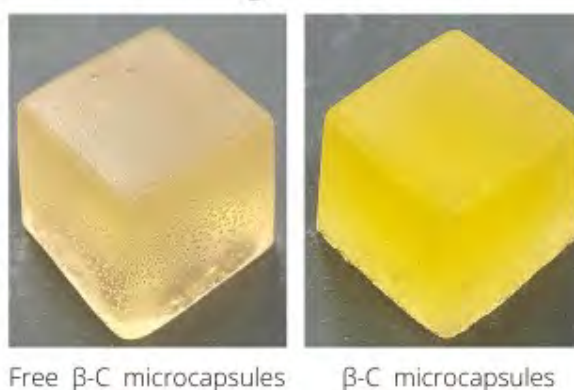


Figure 44 Photographs of gummy candies with and without beta-carotene (β -C) microcapsules.

Table 18 presents the results of the texture analysis of GC and GCM. The hardness, gumminess, and chewiness were reduced after the addition of the microcapsules. While the adhesiveness, elasticity, and resilience were not affected. The reductions in the cited properties may be related to the addition of microcapsules (about 5% of the formulation) which contained an extra amount of water. According to Gunes et al. (2022), higher hydrocolloid content and lower water content lead to harder candies. Kurt et al. (2022) found a reduction in the hardness of gummy candies by reducing the total gelatin content. In the

other study, Amjadi et al. (2018) also found a reduction in hardness and gumminess when adding more betanin liposomes from 5% to 10% in gummy candies.

Table 18. Texture analysis of simple (GC) and beta-carotene microcapsules (GCM) candies gummy

Sample	Hardness (g)	Adhesiveness (g.s)	Elasticity (mm)	Cohesiveness	Gumminess (g)	Chewiness (g.mm)	Resilience
GC	3594.35 ^b ± 3.47	-12.87 ^a ± 3.42	0.96 ^a ± 0.01	0.96 ^a ± 0.01	3439.31 ^b ± 120.49	3316.89 ^b ± 121.40	0.75 ^a ± 0.02
	3084.16 ^a ± 11.23	-17.57 ^a ± 6.05	0.97 ^a ± 0.02	0.95 ^a ± 0.01	2887.44 ^a ± 275.36	2791.95 ^a ± 266.48	0.76 ^a ± 0.04

The results are the means ± standard deviation obtained by the analysis of 4 independent samples. The subscribed letters are the results of the Tukey test at the significance level of 5%.

The β-C bioaccessibility after the in vitro simulation of the gastrointestinal digestion of the microcapsules was 27.92 ± 1.40%, while the microcapsules added to the gummy candies were 22.44 ± 0.64 %. The health or nutritional benefits of compounds with biological activities present or added to foods can be estimated through their bio accessibility. This is because the physiological conditions of the gastrointestinal tract, such as pH and enzymes, can reduce the bioaccessibility of vitamins and other bioactive compounds (Ilyasoglu & El, 2014). However, microencapsulation can protect and deliver these bioactive compounds to the small intestine without being degraded. Therefore, our results show that β-C microencapsulated was protected during the in vitro gastrointestinal digestion. The differences in the bioaccessibility of the pure microcapsule and those added in the gummy candies can be explained by several factors, including the complexity that a food matrix can present, making it difficult to properly digest the microcapsules incorporated in them. Other studies that encapsulated fat-soluble vitamins or compounds obtained results like this study. For example, Barbosa et al. (2021) obtained in vitro about 33% of β-C bioaccessible. Ilyasoglu & El (2014) and Santos et al. (2021) also obtained bioaccessibility close to 30% for docosahexaenoic acid and vitamin D3, respectively.

4 Conclusion

The present study showed that LF and CMS can interact with high affinity and thus form complex coacervates. As a wall material, LF/CMS microencapsulated up to 98% β-C. The pH and the core to wall ratio determined the encapsulation process and influenced its efficiency. The microcapsules protected β-C against the effects of UV radiation, the temperature of 50°C, and gastrointestinal conditions. The β-C microencapsulated was shown to have a slow and low release rate in food matrix with aqueous characteristics (such as 50% ethanol) compared to oily matrices. Furthermore, the microcapsules allowed the addition of β-C (lipid-soluble compound) in the gummy candies (produced in an aqueous medium). They also protected about 66% of the β-C during processing, where temperatures reached over 100°C. Gummy candies-containing microcapsules showed good bioaccessibility of β-C, in addition to improving texture properties (such as hardness, gumminess, and chewiness). Therefore, these results reveal that β-C microcapsules produced by LF/CMS complex coacervates as a wall material can be applied in the fortification of gummy candies and thus serve for supplementation of people at risk or with vitamin A deficiency.

5 References

- Amjadi, S., Ghorbani, M., Hamishehkar, H., & Roufegarinejad, L. (2018). Improvement in the stability of betanin by liposomal nanocarriers: Its application in gummy candy as a food model. *Food Chemistry*, 256, 156–162. <https://doi.org/10.1016/j.foodchem.2018.02.114>
- Andrés-Bello, A., Barreto-Palacios, V., García-Segovia, P., Mir-Bel, J., & Martínez-Monzó, J. (2013). Effect of pH on Color and Texture of Food Products. *Food Engineering Reviews*, 5(3), 158–170. <https://doi.org/10.1007/s12393-013-9067-2>
- AOAC. (2005). Official method of Analysis (18th ed.). Association of Officiating Analytical Chemists.
- Bach, Q. V., Vu, C. M., Vu, H. T., Hoang, T., Dieu, T. V., & Nguyen, D. D. (2019). Epoxidized soybean oil grafted with CTBN as a novel toughener for improving the fracture toughness and mechanical properties of epoxy resin. *Polymer Journal* 2019 52:3, 52(3), 345–357. <https://doi.org/10.1038/S41428-019-0275-3>
- Barbosa, A. E. G., Bastos, L. P. H., & Garcia-Rojas, E. E. (2021). Complex Coacervates Formed between Whey Protein Isolate and Carboxymethylcellulose for Encapsulation of β -Carotene from Sacha Inchi Oil: Stability, In Vitro Digestion and Release Kinetics. *Food Biophysics*, 1–13. <https://doi.org/10.1007/s11483-021-09670-2>
- Bastos, L. P. H., de Carvalho, C. W. P., & Garcia-Rojas, E. E. (2018). Formation and characterization of the complex coacervates obtained between lactoferrin and sodium alginate. *International Journal of Biological Macromolecules*, 120, 332–338. <https://doi.org/10.1016/j.ijbiomac.2018.08.050>
- Bhattacharyya, D., Singhal, R. S., & Kulkarni, P. R. (1995). A comparative account of conditions for synthesis of sodium carboxymethyl starch from corn and amaranth starch. *Carbohydrate Polymers*, 27(4), 247–253. [https://doi.org/10.1016/0144-8617\(95\)00083-6](https://doi.org/10.1016/0144-8617(95)00083-6)
- Brazil, Ministério da Saúde, & Agência Nacional de Vigilância Sanitária. (2005). Resolução nº 269, de 22 de setembro de 2005. Aprova o regulamento técnico sobre a ingestão diária recomendada (IDR) de proteína, vitaminas e minerais. *Diário Oficial da República Federativa do Brasil*.
- Brodkorb, A., Egger, L., Alminger, M., Alvito, P., Assunção, R., Ballance, S., Bohn, T., Bourlieu-Lacanal, C., Boutrou, R., Carrière, F., Clemente, A., Corredig, M., Dupont, D., Dufour, C., Edwards, C., Golding, M., Karakaya, S., Kirkhus, B., Le Feunteun, S., ... Recio, I. (2019). INFOGEST static in vitro simulation of gastrointestinal food digestion. *Nature Protocols*, 14(4), 991–1014. <https://doi.org/10.1038/s41596-018-0119-1>
- Bruschi, M. L. (2015). *Strategies to Modify the Drug Release from Pharmaceutical Systems*. Elsevier. <https://doi.org/10.1016/C2014-0-02342-8>
- Constantino, A. B. T., & Garcia-Rojas, E. E. (2022). Vitamin D3 microcapsules formed by heteroprotein complexes obtained from amaranth protein isolates and lactoferrin: Formation, characterization, and bread fortification. *Food Hydrocolloids*, 129, 107636. <https://doi.org/10.1016/j.foodhyd.2022.107636>
- Delgado-Vargas, F., Jiménez, A. R., & Paredes-López, O. (2000). Natural Pigments: Carotenoids, Anthocyanins, and Betalains — Characteristics, Biosynthesis, Processing, and Stability. *Crit Rev Food Sci Nutr*, 40(3), 173–289. <https://doi.org/10.1080/10408690091189257>

- Du, Y., Bao, C., Huang, J., Jiang, P., Jiao, L., Ren, F., & Li, Y. (2019). Improved stability, epithelial permeability and cellular antioxidant activity of β -carotene via encapsulation by self-assembled α -lactalbumin micelles. *Food Chemistry*, 271, 707–714. <https://doi.org/10.1016/j.foodchem.2018.07.216>
- Gunes, R., Palabiyik, I., Konar, N., & Said Toker, O. (2022). Soft confectionery products: Quality parameters, interactions with processing and ingredients. *Food Chemistry*, 385, 132735. <https://doi.org/10.1016/J.FOODCHEM.2022.132735>
- He, J.-F., Goyal, R., Laroche, A., Zhao, M.-L., & Lu, Z.-X. (2012). Water stress during grain development affects starch synthesis, composition and physicochemical properties in triticale. *Journal of Cereal Science*, 56(3), 552–560. <https://doi.org/10.1016/j.jcs.2012.07.011>
- Ilyasoglu, H., & El, S. N. (2014). Nanoencapsulation of EPA/DHA with sodium caseinate–gum arabic complex and its usage in the enrichment of fruit juice. *LWT - Food Science and Technology*, 56(2), 461–468. <https://doi.org/10.1016/j.lwt.2013.12.002>
- Jain, A., Thakur, D., Ghoshal, G., Katare, O. P., & Shivhare, U. S. (2016). Characterization of microcapsulated β -carotene formed by complex coacervation using casein and gum tragacanth. *International Journal of Biological Macromolecules*, 87, 101–113. <https://doi.org/https://doi.org/10.1016/j.ijbiomac.2016.01.117>
- Kaur, P., Ghoshal, G., & Jain, A. (2019). Bio-utilization of fruits and vegetables waste to produce β -carotene in solid-state fermentation: Characterization and antioxidant activity. *Process Biochemistry*, 76, 155–164. <https://doi.org/10.1016/J.PROCBIO.2018.10.007>
- Kong, X., Kasapis, S., Bertoft, E., & Corke, H. (2010). Rheological properties of starches from grain amaranth and their relationship to starch structure. *Starch - Stärke*, 62(6), 302–308. <https://doi.org/doi:10.1002/star.200900235>
- Kurt, A., Bursa, K., & Toker, O. S. (2022). Gummy candies production with natural sugar source: Effect of molasses types and gelatin ratios. *Food Science and Technology International*, 28(2), 118–127. <https://doi.org/10.1177/1082013221993566>
- Lan, Y., Chen, B., & Rao, J. (2018). Pea protein isolate–high methoxyl pectin soluble complexes for improving pea protein functionality: Effect of pH, biopolymer ratio and concentrations. *Food Hydrocolloids*, 80, 245–253. <https://doi.org/10.1016/j.foodhyd.2018.02.021>
- Lan, Y., Ohm, J. B., Chen, B., & Rao, J. (2020). Phase behavior and complex coacervation of concentrated pea protein isolate-beet pectin solution. *Food Chemistry*, 307, 125536. <https://doi.org/10.1016/J.FOODCHEM.2019.125536>
- Lan, Y., Ohm, J. B., Chen, B., & Rao, J. (2021). Microencapsulation of hemp seed oil by pea protein isolate–sugar beet pectin complex coacervation: Influence of coacervation pH and wall/core ratio. *Food Hydrocolloids*, 113, 106423. <https://doi.org/10.1016/J.FOODHYD.2020.106423>
- Marfil, P. H. M., Paulo, B. B., Alvim, I. D., & Nicoletti, V. R. (2018). Production and characterization of palm oil microcapsules obtained by complex coacervation in gelatin/gum Arabic. *Journal of Food Process Engineering*, 41(4). <https://doi.org/10.1111/jfpe.12673>
- Mehran, M., Masoum, S., & Memarzadeh, M. (2020). Microencapsulation of *Mentha spicata* essential oil by spray drying: Optimization, characterization, release kinetics of essential oil from microcapsules in food models. *Industrial Crops and Products*, 154, 112694. <https://doi.org/10.1016/J.INDCROP.2020.112694>

- Millard, M. M., Dintzis, F. R., Willett, J. L., & Klavons, J. A. (1997). Light-Scattering Molecular Weights and Intrinsic Viscosities of Processed Waxy Maize Starches in 90% Dimethyl Sulfoxide and H₂O. *Cereal Chemistry*, 74(5), 687–691. <https://doi.org/doi:10.1094/CCHEM.1997.74.5.687>
- Nita, L. E., Chiriac, A. P., Rusu, A. G., Ghilan, A., Dumitriu, R. P., Bercea, M., & Tudorachi, N. (2020). Stimuli Responsive Scaffolds Based on Carboxymethyl Starch and Poly(2-Dimethylaminoethyl Methacrylate) for Anti-Inflammatory Drug Delivery. *Macromolecular Bioscience*, 20(4), 1900412. <https://doi.org/10.1002/MABI.201900412>
- Olson, J. A. (1989). Provitamin A Function of Carotenoids: The Conversion of β -Carotene into Vitamin A. *The Journal of Nutrition*, 119(1), 105–108. <https://doi.org/10.1093/jn/119.1.105>
- Perez, E., Bahnassey, Y. A., & Breene, W. M. (1993). A Simple Laboratory Scale Method for Isolation of Amaranth Starch. *Starch - Stärke*, 45(6), 211–214. <https://doi.org/doi:10.1002/star.19930450605>
- Priyadarshani, A. M. B. (2017). A review on factors influencing bioaccessibility and bioefficacy of carotenoids. *Critical Reviews in Food Science and Nutrition*, 57(8), 1710–1717. <https://doi.org/10.1080/10408398.2015.1023431>
- Quadrado, R. F. N., & Fajardo, A. R. (2020). Microparticles based on carboxymethyl starch/chitosan polyelectrolyte complex as vehicles for drug delivery systems. *Arabian Journal of Chemistry*, 13(1), 2183–2194. <https://doi.org/10.1016/j.arabjc.2018.04.004>
- Rutz, J. K., Borges, C. D., Zambiasi, R. C., Crizel-Cardozo, M. M., Kuck, L. S., & Noreña, C. P. Z. (2017). Microencapsulation of palm oil by complex coacervation for application in food systems. *Food Chemistry*, 220, 59–66. <https://doi.org/10.1016/j.foodchem.2016.09.194>
- Santos, M. B., Geraldo de Carvalho, M., & Garcia-Rojas, E. E. (2021). Carboxymethyl tara gum-lactoferrin complex coacervates as carriers for vitamin D₃: Encapsulation and controlled release. *Food Hydrocolloids*, 112, 106347. <https://doi.org/10.1016/j.foodhyd.2020.106347>
- Thakur, D., Jain, A., Ghoshal, G., Shivhare, U. ., & Katare, O. . (2017). Microencapsulation of β -Carotene Based on Casein/Guar Gum Blend Using Zeta Potential-Yield Stress Phenomenon: an Approach to Enhance Photo-stability and Retention of Functionality. *AAPS PharmSciTech*, 18(5), 1447–1459. <https://doi.org/10.1208/s12249-017-0806-1>
- Timilsena, Y. P., Akanbi, T. O., Khalid, N., Adhikari, B., & Barrow, C. J. (2019). Complex coacervation: Principles, mechanisms and applications in microencapsulation. *International Journal of Biological Macromolecules*, 121, 1276–1286. <https://doi.org/10.1016/j.ijbiomac.2018.10.144>
- Wang, B., Timilsena, Y. P., Blanch, E., & Adhikari, B. (2017). Lactoferrin: Structure, function, denaturation and digestion. <https://doi.org/10.1080/10408398.2017.1381583>, 59(4), 580–596. <https://doi.org/10.1080/10408398.2017.1381583>
- Wang, L., Liu, Z., Jiang, H., & Mao, X. (2021). Biotechnology advances in β -carotene production by microorganisms. *Trends in Food Science & Technology*, 111, 322–332. <https://doi.org/10.1016/J.TIFS.2021.02.077>
- Xie, L., Shen, M., Wang, Z., & Xie, J. (2021). Structure, function and food applications of carboxymethylated polysaccharides: A comprehensive review. *Trends in Food Science & Technology*, 118, 539–557. <https://doi.org/10.1016/J.TIFS.2021.09.016>

- Yan, C., & Zhang, W. (2014). Coacervation Processes. In A. G. Gaonkar, N. Vasisht, A. R. Khare, & R. Sobel (Eds.), *Microencapsulation in the Food Industry* (pp. 125–137). Elsevier. <https://doi.org/10.1016/B978-0-12-404568-2.00012-1>
- Zhu, F. (2017). Structures, physicochemical properties, and applications of amaranth starch. *Critical Reviews in Food Science and Nutrition*, 57(2), 313–325. <https://doi.org/10.1080/10408398.2013.862784>

CONCLUSÃO GERAL

A utilização dos pseudocereais e seus produtos derivados (como o amido e proteína) pode promover um importante crescimento econômico e social em alguns países produtores. Em particular, produtos alimentícios à base de isolados proteicos de amaranto, do trigo sarraceno e da quinoa podem ser uma alternativa aos derivados de proteína animal devido às suas propriedades nutricionais e vários benefícios à saúde. Embora existam algumas limitações ao uso dessas proteínas, é possível utilizar tecnologias de modificações de baixo custo, como o uso de ultrassom de alta intensidade (HIUS) e a glicosilação, para melhorar suas propriedades físico-químicas. Por exemplo, a solubilidade e propriedades emulsificantes da proteína isolada do amaranto (API) foi melhorada significativamente após um tratamento com HIUS. Desta forma o API modificado com HIUS (API-U) pode ser utilizado com hidrocolóides para microencapsular compostos bioativos hidrossolúveis e lipossolúveis.

API-U e lactoferrina (LF) formaram complexos de alta afinidade que permitiu a encapsulação de 90% da VD₃. Os complexos API-U/LF protegeram a VD₃ da degradação térmica e fotolítica. Durante a simulação da digestão gastrointestinal *in vitro*, foi obtida uma alta bioacessibilidade da VD₃. As microcápsulas protegeram 86% do VD₃ da degradação térmica (200 °C), e a digestão intestinal mostrou que aproximadamente 90% da VD₃ foi liberado por difusão Fickiana. O API-U também apresentou alta afinidade ao interagir eletrostaticamente com a carboximetilcelulose (CMC). Complexos coacervados API-U/CMC foram formados espontaneamente no pH 3. Os complexos coacervados API-U/CMC foram capazes de encapsular 87% de betanina e garantiu sua proteção da ação térmica e uma bioacessibilidade 84%. Quando as microcápsulas foram adicionadas aos filmes de gelatina comestível, melhoraram a flexibilidade, reduziram a transmissão de luz e aumentaram a atividade antioxidante dos filmes. Os filmes contendo microcápsulas da betanina foram capazes de liberar os seus compostos antioxidantes.

A carboximetilação do amido do amaranto (CMS) permitiu sua utilização para microencapsulação do beta-caroteno (β -C) pelo processo da coacervação complexa. CMS e LF apresentaram alta afinidade para interagirem em pHs entre 4-5. Portanto, foi observada nesta faixa de pH alta eficiência de encapsulamento (EE), especificamente no pH=5 (com 98% de EE). As microcápsulas protegeram o β -C da degradação térmica e fotolítica e, após a digestão gastrointestinal, permitiram sua liberação nos intestinos. As microcápsulas permitiram a adição de β -C (composto lipossolúvel) nas balas gomosas (produzidas em meio aquoso), mostrou uma bioacessibilidade de β -C de 22%, além de melhorar as propriedades de textura (como dureza, gomosidade e mastigabilidade).

Neste sentido, conclui-se que a proteína e o amido isolados do amaranto são biopolímeros que podem ser utilizados para microencapsular compostos bioativos e permitir sua proteção de fatores que o degradam, aumentando assim sua vida útil e estendendo sua aplicação na produção de diferentes tipos de alimentos. Também podemos concluir que as microcápsulas obtidas por coacervação complexa podem sim ser utilizadas para fortificação de alimentos e produção de embalagens comestíveis. No entanto, o teor das biomoléculas microencapsuladas adicionadas em alimentos devem obedecer à quantidade de ingestão recomendada de acordo com legislações as específicas. Pesquisas futuras poderiam focar na utilização desses biopolímeros na formação de complexos solúveis com intuito de encapsular compostos bioativos para fortificação de bebidas.

ANEXOS

ANEXO A. Pedido de depósito de patente de filmes comestíveis composto por microcápsulas de betanina e gelatina



**SOLICITAÇÃO DE
SERVIÇOS AO NIT**



**Ao
Núcleo de Inovação Tecnológica da UFRRJ/NIT-UFRRJ
Rodovia BR 465, Km 07, 2º andar, Sala 109 – Prédio Principal
Campus Seropédica/RJ - CEP 23.897-000**

Prezados Senhores,

Eu, **Augusto Bene Tomé Constantino, 20181008900**, lotado e com exercício no **PPGCTA do Departamento de Ciência e Tecnologia de Alimentos**, encaminho a este Núcleo os documentos abaixo relacionados, a fim de dar início à avaliação de pertinência do pedido de depósito da Patente de Invenção denominada **“filmes comestíveis composto por microcápsulas de betanina e gelatina e preparação do mesmo”**

Relação de documentos anexos:

	Material	Nº de páginas
()	Relatório de Invenção	
()	Desenhos, se necessário	
()	Publicações relacionadas ao presente invento	
()	Cópia de material de divulgação e/ou atestados de participação em eventos e/ou cópia de anais, onde o invento tenha sido divulgado/apresentado.	
()	Cópia do contrato de Direitos de Propriedade Industrial firmado entre a UFRRJ e Empresa (s) participante (s), quando for o caso.	
()	Outros documentos julgados pertinentes: -	

O PROCESSO FOI SUBMETIDO A ALGUMA AGÊNCIA DE FOMENTO (EX.: FAPERJ, CNPQ, FINEP, OUTROS)? () Sim (x) Não

Seropédica/RJ, 15 de junho de 2022.

Atenciosamente,

Augusto Bene Tomé Constantino
(Assinatura do solicitante)

Recebido no NIT-UFRRJ em ____/____/____

ANEXO B. Pedido de depósito de patente de bala de goma de gelatina fortificada com microcápsulas de betacaroteno.



**SOLICITAÇÃO DE
SERVIÇOS AO NIT**

NIT-UFRRJ
NÚCLEO DE INOVAÇÃO
TECNOLOGICA

Ao
Núcleo de Inovação Tecnológica da UFRRJ/NIT-UFRRJ
Rodovia BR 465, Km 07, 2º andar, Sala 109 – Prédio Principal
Campus Seropédica/RJ - CEP 23.897-000

Prezados Senhores,

Eu, **Augusto Bene Tomé Constantino, 20181008900**, lotado e com exercício no **PPGCTA do Departamento de Ciência e Tecnologia de Alimentos**, encaminho a este Núcleo os documentos abaixo relacionados, a fim de dar início à avaliação de pertinência do pedido de depósito da Patente de Invenção denominada **“Bala de goma de gelatina fortificada com microcápsulas de betacaroteno e o preparo da mesma”**

Relação de documentos anexos:

	Material	Nº de páginas
(x)	Relatório de Invenção	
(x)	Desenhos, se necessário	
(x)	Publicações relacionadas ao presente invento	
(x)	Cópia de material de divulgação e/ou atestados de participação em eventos e/ou cópia de anais, onde o invento tenha sido divulgado/apresentado.	
()	Cópia do contrato de Direitos de Propriedade Industrial firmado entre a UFRRJ e Empresa (s) participante (s), quando for o caso.	
()	Outros documentos julgados pertinentes: -	

O PROCESSO FOI SUBMETIDO A ALGUMA AGÊNCIA DE FOMENTO (EX.: FAPERJ, CNPQ, FINEP, OUTROS)? () Sim (x) Não

Seropédica/RJ, 15 de junho de 2022.

Atenciosamente,

Augusto Bene Tomé Constantino
(Assinatura do solicitante)

Recebido no NIT-UFRRJ em ____/____/____
